DESIGN AND ANALYSIS OF REVERSIBLE

SOLID OXIDE CELL SYSTEMS FOR

ELECTRICAL ENERGY STORAGE

by

Christopher H. Wendel

A thesis submitted to the Faculty and the Board of Trustees of the Colorado School of Mines in partial fulfillment of the requirements for the degree of Doctor of Philosophy (Mechanical Engineering).

Golden, Colorado

Date _____

<div style="text-align: right;">

Signed: _____
Christopher H. Wendel

Signed: _____
Dr. Robert J. Braun
Thesis Advisor

</div>

Golden, Colorado

Date _____

<div style="text-align: right;">

Signed: _____
Dr. Gregory S. Jackson
Professor and Head
Department of Mechanical Engineering

</div>

ii

ABSTRACT

Electrical energy storage is projected to be a critical component of the future world energy system, performing load-leveling operations to enable increased penetration of renewable and distributed generation. Reversible solid oxide cell (ReSOC) technology has the potential to play a major role in stationary electrical energy storage markets. ReSOCs operate in two distinct modes: fuel producing (electrolysis mode) and power producing (fuel cell mode). A stand-alone energy storage system is realized from this technology by coupling the two operating modes with intermediate storage of reactant and product species. In this dissertation, ReSOC energy storage systems are designed and analyzed with computational modeling to establish suitable system configurations and operating conditions that achieve high roundtrip efficiency.

A critical feature of the ReSOC system that enables high roundtrip efficiency is that the ReSOC is operated at conditions where methane is generated in electrolysis mode to offset the typically endothermic conversion process. Methanation is promoted by low temperature and high pressure conditions, meaning that intermediate-temperature ReSOCs ($<700°$ C) are important to achieving high system performance. Doped lanthanum gallate (LSGM)-electrolyte ReSOC characteristics are leveraged in this study.

The results include thermodynamic analysis of ReSOC systems, physically-based calibrated modeling of intermediate temperature ReSOCs, steady-state system simulation at distributed (100 kW) and bulk (>10 MW) scales, and bottom-up system costing. System modeling results suggest that dc roundtrip energy storage efficiency of 65-74% are achieved for a 100 kW system. Maximum efficiency is achieved when the tanked species are maintained in the vapor phase to mitigate the energetic requirement of steam generation; although the energy density suffers within this configuration. The bulk scale system achieves 74% roundtrip efficiency at optimal stack operating conditions of 680° C, 20 bar, and 70%

fuel utilization. Economic calculations estimate bulk-scale (250 MW / 500 GWh) storage cost of 1.7 ¢/kWh based on the system capital cost. This storage cost is lower than compressed air and battery technologies and comparable to pumped hydro, but improvements in cell technology and additional system simulation and hardware selection must be addressed before commercialization.

TABLE OF CONTENTS

LIST OF FIGURES

LIST OF TABLES

LIST OF SYMBOLS

LIST OF ABBREVIATIONS

Anode functional layer . . . . AFL

Area specific resistance . . . . ASR

Balance of plant . . . . BOP

Chemical Engineering Plant Cost Index . . . . CEPCI

Combined heat and power . . . . CHP

Compressed air energy storage . . . . CAES

Continuously stirred tank reactor . . . . CSTR

Control volume CV

Electrical energy storage . . . . EES

Electrochamical impedance spectroscopy . . . . EIS

Fuel electrode . . . . FE

$Gd_{0.1}Ce_{0.9}O_{1.95}$ . . . . GDC

Heat exchanger . . . . HX

Hydrogen to carbon ratio . . . . HTCR or H/C

Interconnect IC

Lanthanum strontium manganite . . . . LSM

Lower heating value . . . . LHV

$La_{0.6}Sr_{0.4}Fe_{0.8}Co_{0.2}O_{3-\delta}$ . . . . LSCF

Membrane electrode assembly . . . . MEA

Open circuit voltage . . . . OCV

ACKNOWLEDGMENTS

The effort put forth to complete this dissertation has not solely been my own, but rather reflects the contributions of many both to the technical content of my education as well as my growth as an individual. First, I would like thank the educators who have helped guide me. The members of my committee, Drs. Kee, Decaluwe, O'Hayre and Dean for their feedback and expert guidance on the technical challenges of this work. I also thank Neal Sullivan and Jahi Simbai, for helping me realize that Mines was the right place to complete my graduate studies. And my advisor, Robert Braun for helping me find direction in my research endeavors and technical contributions.

The love and support of my family and friends allowed me to see this work through to completion. I thank my mother for believing in me and always knowing the right balance between support and expectation, I thank my father for passing to me his capability and interest in problem solving and all things technical, and my sister for always being there for me. Special thanks to Sarah, for your the timely reminders that I am not failing and your understanding and encouragement that got me through the hardest times.

CHAPTER 1

INTRODUCTION

Large-scale energy storage development is envisioned as a key requirement in being able to both increase the flexibility of and modernize the electric grid by temporally decoupling energy production and consumption. Electrical energy storage (EES) is expected to play a critical role in the development of advanced grid-energy management systems including large-scale penetration of intermittent renewable resources, such as wind and solar [1–7]. A reversible solid oxide cell (ReSOC) is a scalable electrochemical conversion device capable of meeting future EES demands. A ReSOC is physically similar to, and benefits from previous development of, both solid oxide fuel cells (SOFC) and solid oxide electrolysis cells (SOEC) which employ similar electrode-electrolyte material sets and operating condition ranges. However, unique implementation and operational challenges exist for ReSOC systems that require independent consideration.

Realizing the potential of ReSOCs for electrical energy storage requires research and development at both the cell and system levels. This dissertation details the design and analysis of energy storage systems utilizing ReSOCs. It will address system design decisions related to configuration, operating conditions, and application scale through system and Re-SOC cell-stack modeling validated by experimental performance results. This introductory chapter explains the motivation for the research, describes how ReSOCs are envisioned to operate as energy storage devices, and states the overall research objectives.

1.1 Motivations

The motivation for this research can be summarized by the following statements: (1) the market opportunity for EES is unfulfilled by current commercial technologies, (2) Re-SOCs have the potential to provide cost effective and scalable energy storage, (3) several of the technical advancements in SOFC technology uniquely benefit ReSOC energy storage

systems, for example lowering the operating temperature, and (4) the characteristics and design of novel ReSOC systems require individual consideration separate from SOFC and SOEC systems which has not been addressed in the present literature.

1.1.1 The benefits and applications for electrical energy storage

A variety of centralized- and distributed-scale applications are projected to benefit from electrical energy storage. These applications are generally categorized as either energy management applications, which have a high energy-to-power capacity ratio, or power management applications, which have a low energy-to-power capacity ratio. Energy management applications require long-duration, high efficiency, and low cost energy storage, and include energy arbitrage, transmission and distribution upgrade deferral, and end user benefits, such as peak shaving. Alternatively, power management applications require fast dynamics and high reliability, and include voltage and frequency regulation and end-user power quality management. Each specific energy storage application has unique design specifications depending on the operating requirements and economic benefit [1, 8–10]. A ReSOC energy storage system is well suited for energy management applications because such a system can operate over a wide range of energy-to-power ratios by sizing the energy and power ratings independently and is expected to have high energy storage efficiency and energy capacity suitable for storage duration on the order of hours to days.

Efforts to developing efficient and inexpensive energy storage technologies have seen a recent resurgence due to increased penetration of renewable energy resources and public renewables portfolio standards at the state (e.g., California [11]; Colorado [12]) and national levels (German Renewable Energy Act, 2010; Denmark [13]; European Union [14]). Fluctuating power generation from wind and solar energy sources can be stabilized by use of energy storage devices. Figure 1.1 demonstrates the variability of wind-based power generation and the capability of electricity storage to control power output to the grid. In this example, and arbitrary energy storage system is charged during times of excess generation and discharged when demand for electricity is high.
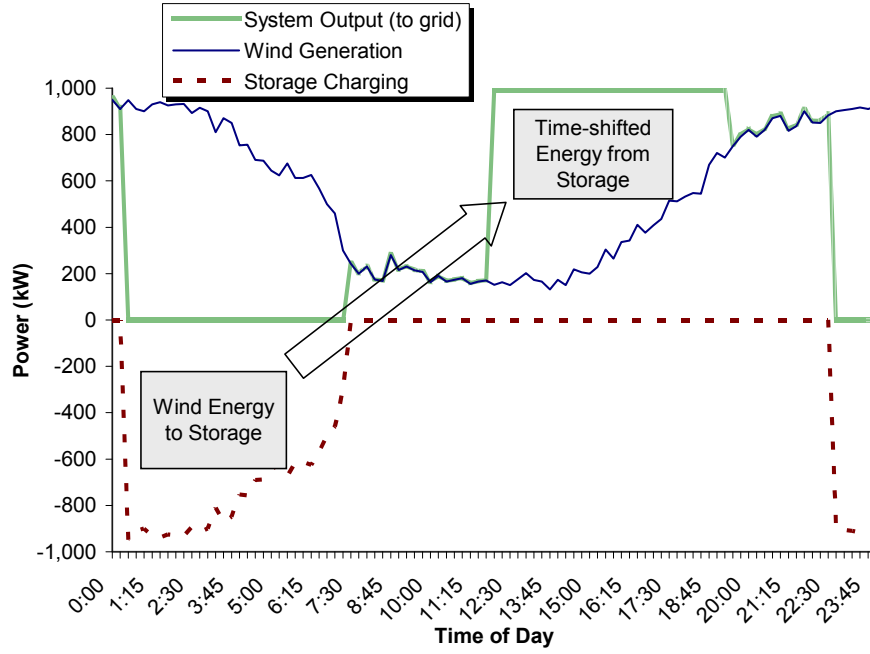
Figure 1.1: Variability of a renewable wind resource and the capability of energy storage to stabilize the power output [8].

Various energy storage technologies are represented in Figure 1.2 and categorized based on their respective power or energy management capabilities. Technologies that are currently advancing toward meeting the technical requirements for energy management applications include compressed air energy storage (CAES), pumped hydro storage (PHS), conventional batteries (e.g., lead-acid, nickel-cadmium), advanced batteries (e.g., lithium ion, sodium-beta alumina, redox flow batteries), and energy management flywheels. However, these technologies face unique development challenges such that the requirements for highly efficient, durable, and cost-effective EES have not yet been met [6, 9, 10]. For example, PHS presently accounts for 95% of worldwide electrical energy storage, but requires a geographically suitable site to be implemented effectively. Furthermore, because a range of applications, and thus operating requirements, are expected from EES devices, a portfolio of technology solutions will be beneficial [1, 6–8, 15–18].

Assessing the technical and economic design requirements for energy storage systems is an area of active research [1, 6, 8, 9]. The relevant performance metrics for stationary

Energy Storage Technologies for Distributed Energy Resources, Presented by EPRI PEAC & Sandia Labs
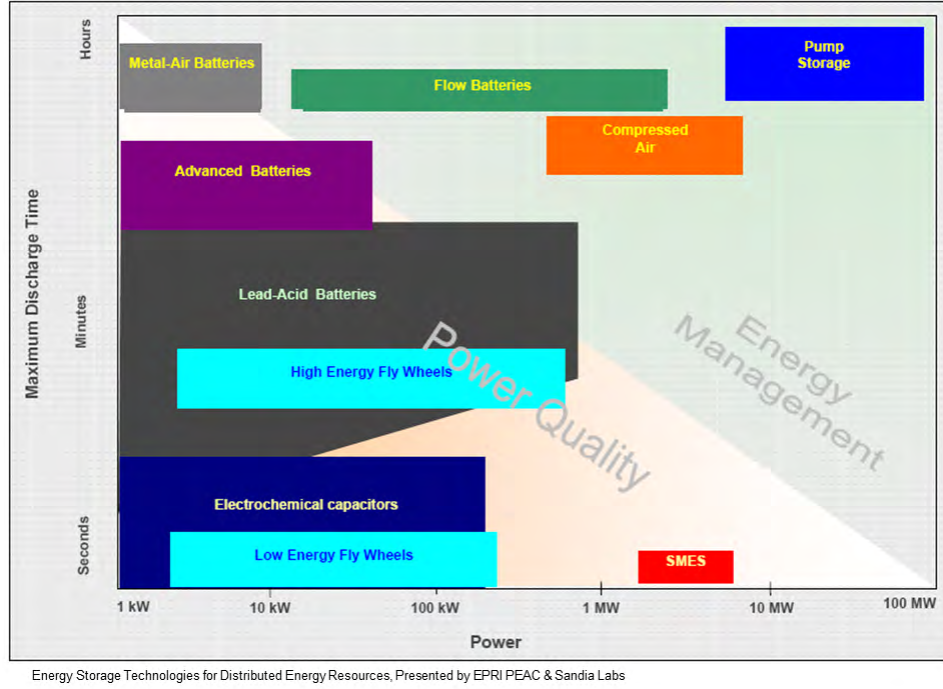
Figure 1.2: Different energy storage technologies and their respective power and energy capacities [19].

energy storage include roundtrip efficiency, energy density, capital cost, and levelized cost. However, estimating the performance required for economically feasible implementation of an EES technology is complicated because many of the projected energy storage applications are not presently being practiced, such as those associated with highly intermittent renewables penetration and micro-grids. Furthermore, energy storage devices will often be capable of fulfilling multiple energy storage applications simultaneously such that the economic benefits may "stack". This dissertation uses recently published targets from the U.S. Department of Energy (DOE) as performance targets including short-term goals of 75% efficiency, 250 $/kWh capital cost, and 20 ¢/kWh-cycle levelized cost, and long-term goals of 80% efficiency, 150 $/kWh capital cost, and 10 ¢/kWh-cycle levelized cost [1]. The modeling results and analysis presented through this dissertation will help establish whether ReSOC technology is capable of meeting these goals.

1.1.2 Solid oxide cells: Continued progress and present state of technology

The market opportunity for novel energy storage solutions, such as using reversible solid oxide cells, exists because present technologies have not been able to meet the requirements for grid-energy storage applications; however, fuel cell technologies have historically been slow to gain market share for commercial application. A fuel cell is a solid-state electro-chemical conversion devices that produces electrical power directly from the chemical energy stored in fuel species (e.g., hydrogen, syngas, natural gas, fuel reformate, carbon, gasified coal). The benefits of fuel cells over conventional combustion based power generation include significantly higher thermal efficiencies, lower emissions, fuel flexibility, and scalability. These benefits have ultimately not been realized because of problems in durability over extended operating periods, high production costs, and costly balance of plant (BOP) required for fuel processing and thermal management. These problems are not insurmountable and fuel cells are continually advancing with low temperature proton exchange membrane (PEM) fuel cells [20–24] and high temperature solid oxide fuel cells [25–27] receiving the most academic and commercial focus.

An electrolysis cell performs the opposite function of a fuel cell by electrochemically producing fuel from an oxidized feedstock (e.g., H_2O, CO_2) and electricity [28]. Electrolysis cells are physically and operationally similar to fuel cells, although they are operated with opposite electrode polarity. Efficiently producing hydrogen from renewable sources is an important step toward decarbonizing the world energy system and electrolysis technologies such as electrolysis cells will contribute to this effort. Because of their potential as an integral part of the future energy system, solid oxide [29–32], alkaline [33–35], and PEM electrolysis cells [36, 37] are currently being pursued. Alkaline and PEM electrolysis are presently commercial technologies [38–41], although hydrogen production by this method is costly compared with steam reforming of natural gas which accounts for 95% of worldwide hydrogen production [42]. Many of the commercialization challenges experienced by SOFCs are also barriers to commercialization of SOECs, however the electrolysis cells are less mature

and face additional durability challenges including delamination at the anode-electrolyte interface [43–45]. High temperature electrolysis is considered a promising alternative to the more mature low-temperature processes, particularly because of the possibility to supply a portion of the energy requirement from high grade thermal energy available from nuclear [32] or solar sources [46, 47].

In addition to advancement of SOFC and SOEC technologies toward widespread commercialization, some research effort has been dedicated to developing reversible solid oxide cells that can operate cyclically as either a fuel cell or an electrolyzer [48–51]. Because of the physical similarity between the devices, ReSOCs benefit from improvement and cost reduction of SOFCs which makes ReSOC systems practical in the near future. Many of the strategies to reduce cost and improve performance of SOFC and SOEC devices are uniquely suited to benefit ReSOC energy storage systems. For example, one advantage of ReSOCs over other fuel cell technologies is the ability to use various reactant compositions such as natural gas or fuel reformate in SOFCs (i.e., internal reforming) and simultaneous reduction of H_2O and CO_2 to produce syngas in SOECs (i.e., co-electrolysis). This "fuel-flexibility" increases the utility of these devices within the present energy infrastructure and has the additional benefit of increasing the energy density of an energy storage application by storing a synthetic hydrocarbon mixture rather than hydrogen.

Intermediate temperature SOFC operation (i.e., <800°C) has been a long sought solution to increase efficiency, increase durability, and reduce costs of balance of plant components, stack interconnects, and sealing materials [25, 52]. The difficulty in reducing the operating temperature of ReSOCs is in finding stable electrolyte materials with high oxygen ion conductivity at reduced temperature and electrode catalysts with high activity. These problems have been addressed by implementing alternative electrolyte materials operating in the temperature range of 500-650°C. Such intermediate-temperature ionic conductors were reviewed by Goodenough [53] including stabilized zirconia, doped ceria, stabilized δ-Bi_2O_3, pyrochlores, and doped lanthanum gallate. Alternative manufacturing methods such as inter-

mediate temperature catalyst impregnation help reduce performance losses associated with reaction kinetics [54]. Pressurized SOFC and SOEC operation has also been explored as a way to increase electrochemical efficiency and system efficiency through synergistic combinations with other processes (e.g., SOFC-gas turbine or SOEC-Fischer Tropsch) [55–59]. Both low temperature and high pressure ReSOC operation are instrumental to the integrated system thermal management strategy of the energy storage systems explored in the present work. This approach relies on exothermic methanation during electrolysis operation, which is thermodynamically favored at high pressure and low temperature. This thermal management strategy is explained further in Section 1.3 and detailed in Chapter 2.

Reversible solid oxide cell design and operation is uniquely challenging because of the need to operate in both fuel cell and electrolyzer modes, including durability issues associated with galvanic cycling and selecting electrode materials that are stable in both oxidizing and reducing environments [50, 51, 60]. However, the performance improvement and cost reduction of SOFC, SOEC, and ReSOC technology are leading to increased likelihood of implementing ReSOC energy storage systems in the near future which makes the proposed system design and analysis research highly relevant.

1.1.3 Advancing from a promising technology to a practical energy storage system

The general idea of using ReSOCs for energy storage has been suggested in published literature as early as 1987 [61], although the present research is motivated by the scarcity of publications on specific implementations of such systems. The few studies that have addressed system-level considerations are reviewed in Chapter 3. A ReSOC system will draw heavily from the developments of SOFC and SOEC systems; however, such a system should perform both power production and fuel production functions using the same physical components — in the same way that a heat pump / air conditioning system performs both heating and cooling functions. Thus, ReSOC system design requires independent consideration with regard to system configuration and operating conditions.

Academic and industrial research and development has led to established system configurations and operating strategies for both SOFC power systems and gas turbine SOFC hybrid systems, which establish the current state-of-the-art performance and focus research objectives to advance these systems toward widespread commercialization [58, 62–65]. Similarly, SOEC system design for non-fossil production of hydrogen, syngas, and hydrocarbon based products has been considered [55, 66, 67], although to a lesser extent than SOFC systems. This research will contribute to the limited, but expanding, body of work addressing the design and analysis of ReSOC systems for energy storage applications.

1.1.4 Informing materials development and cell performance targets

A final motivation for this research is to integrate ReSOC energy storage system design with cell-stack materials development. Materials development is a critical component of realizing ReSOC energy storage systems. In particular, ReSOCs must perform galvanic cycling not required by SOFC and SOEC applications. Furthermore, the efficiency of the system implementation considered in this work is shown to be highly dependent upon ReSOC operating conditions—notably temperature, pressure, and reactant composition. Thus, integrating system design with materials development enables iterative and collaborative design to target operating ranges that suit both system and stack performance.

The lofty efficiency and cost targets for energy storage systems also suggest that cost reduction in ReSOCs may be required to achieve high efficiency at suitable stack power densities. System techno-economic analysis can inform the cell performance and cost goals while accounting for the effects of system operation. In other words, early-stage system analysis can help predict what portion of system cost can be attributed to the ReSOC stack. Taken further, the system analysis can determine what cell performance is required for competitive implementation of ReSOC systems. This work includes models calibrated to represent present cell performance as well as models to represent improved cells.

1.2 Introduction to reversible solid oxide cells

A reversible solid oxide cell is a solid-state, ceramic-based, electrochemical device that is physically similar to solid oxide fuel cells and solid oxide electrolysis cells, but differs in that it can operate in both current directions. ReSOCs have also been referred to as regenerative solid oxide fuel cells or solid oxide regenerative fuel cells. High temperatures (500-1000°C) are required for efficient ReSOC operation to allow mobility of oxygen ions in the solid electrolyte. Depending on the cell polarity, the ReSOC can operate either as a fuel cell (SOFC mode) to electrochemically oxidize fuel species and generate electricity, or as an electrolysis cell (SOEC mode) to electrochemically reduce reactant species while consuming electrical energy. The two modes of operation are depicted in Figure 1.3. The membrane electrode assembly (MEA), is a laminated ceramic and metal structure composed of a porous fuel electrode (anode in SOFC mode, cathode in SOEC mode), a thin solid electrolyte, and a porous oxygen electrode (cathode in SOFC mode, anode in SOEC mode). A variety of material sets have been considered for each of the layers of the MEA with the most common being a nickel-yttria stabilized zirconia (YSZ) cermet fuel electrode, YSZ electrolyte, and lanthanum strontium manganite (LSM) oxygen electrode. However, this conventional material set is limited to high operating temperatures >750°C [68–70]. This dissertation focuses on intermediate temperature ReSOC material sets based on strontium- and magnesium-doped lanthanum gallate (LSGM)-electrolytes which achieve high performance at reduced operating temperature ($<$ 650°C) [71–74].

During operation, reactant species flow through the fuel channel adjacent to the fuel electrode (see Figure 1.3). In SOFC mode, these reactant species can include hydrogen, syngas (i.e., H_2 + CO), natural gas (reformed or not), or reformate from other gaseous, liquid, or solid fuels. In SOEC mode the reactant species are H_2O and/or CO_2. If steam is the lone reactant, the process is typically referred to as electrolysis, while co-electrolysis refers to simultaneous reduction of H_2O and CO_2 to produce syngas. The oxygen electrode requires an oxygen supply during SOFC mode operation to act as a reactant in the electrochemical
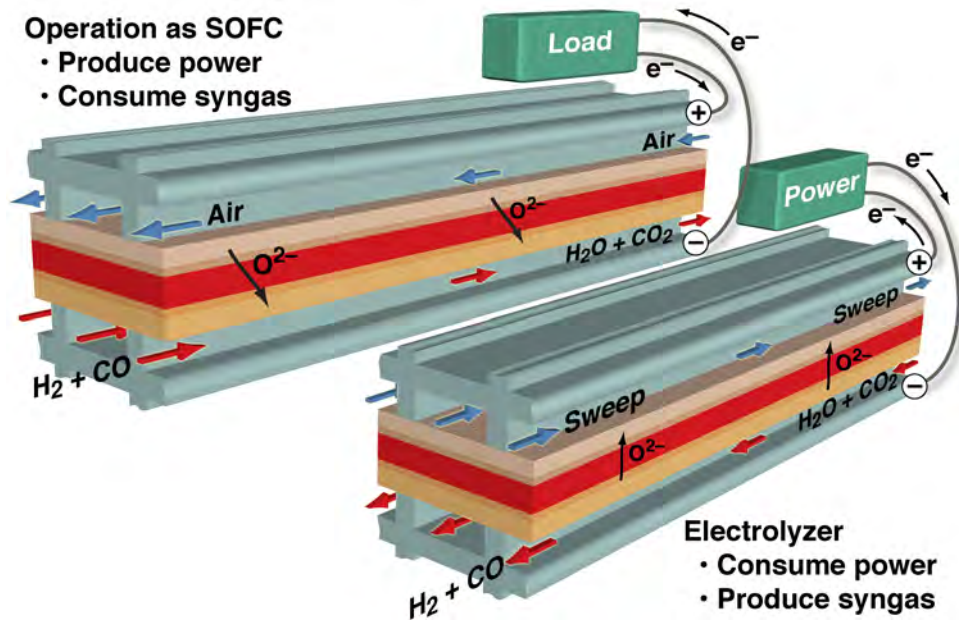
Figure 1.3: Channel level schematic of a reversible solid oxide cell operating in either power-producing fuel cell or fuel-producing electrolysis mode. Figure supplied courtesy of Dr. Robert Kee.

conversion. The oxygen is typically supplied as either air or oxygen. In SOEC operation, oxygen is produced at the oxygen electrode and an efficiency benefit is achieved by flowing air, or a different sweep gas, through the oxygen channel to improve transport of the produced oxygen away from the reaction site.

A single ReSOC typically operates between 0.5 and 2.0 V and cell stacking is required to achieve useful voltage output from the device. Cell stacking introduces the need for electronically conductive interconnect materials and sealing to prevent gas-crossover or leaking from the stack. For high temperature devices, cell stacking is further complicated because of the potentially varying thermal expansion behavior of the various materials used to construct the ReSOC stack. Because of the structural integrity of ReSOCs, several geometric cell configurations are possible including planar, tubular, and segmented-in-series [75]. Planar ReSOCs benefit from improved power density, while tubular and segmented in series configurations can simplify challenges associated with sealing.

The electrochemical oxidation reactions occurring during SOFC operation are exothermic such that excess cooling airflow is typically provided to the stack to remove excess heat. Internal reforming reactions can also act as a thermal energy sink. Alternatively, the reduction reactions in SOEC mode are endothermic and maintaining the cell operating temperature requires additional heat, typically either from an external source or by operating the cell less efficiently such that waste-heat generation overcomes the thermal energy deficit. The difference in thermal behavior in each operating mode presents a significant challenge in system design of an integrated ReSOC system. In an effort to improve system efficiency, a thermal management strategy is used in this work which involves selecting the ReSOC stack operating conditions (temperature, pressure, reactant composition) to promote the exothermic methanation reaction in the ReSOC stack. By promoting exothermic methanation, the SOEC mode stack can operate more efficiently and still maintain the high temperature required for effective electrochemical conversion.

Many of the unique characteristics of ReSOCs that distinguish them from other types of electrochemical cells result from the high operating temperature. Some of the advantages of high temperature include: (1) ability to use carbonaceous reactants without risk of CO catalyst poisoning, (2) precious metal catalysts are not required for the oxidation or reduction reactions, (3) even without precious metal catalysts the activation losses are relatively small which is particularly important for reversible energy storage applications, and (4) high system efficiencies are possible for combined heat and power generation (CHP). There are also several disadvantages of high temperature operation including: (1) material durability issues with thermal expansion compatibility and durability in an extreme operating environment, (2) expensive balance of plant components to handle high temperature gas processing, and (3) high temperature heat must be provided to a solid-oxide electrolyzer to allow higher efficiency. As noted in the motivation section, intermediate temperature (500-750°C) operation eliminates many of the disadvantages, while retaining the advantages. Extensive discussion of the operating characteristics of ReSOCs is given in Chapter 2.

1.3 Using reversible solid oxide cells for energy storage

As explained in the previous section, reversible solid oxide cells can operate cyclically as either a fuel cell or an electrolysis cell. An electrical energy storage system is realized from this technology by coupling the two modes of operation with intermediate storage of "fuel" and "exhaust" species. This device has also been referred to as a "Solid Oxide Flow Battery" because it shares the advantage of redox flow batteries of independently sizing power and energy capacity by the size of the electrochemical conversion device (e.g., ReSOC stack) and storage tank volume, respectively.
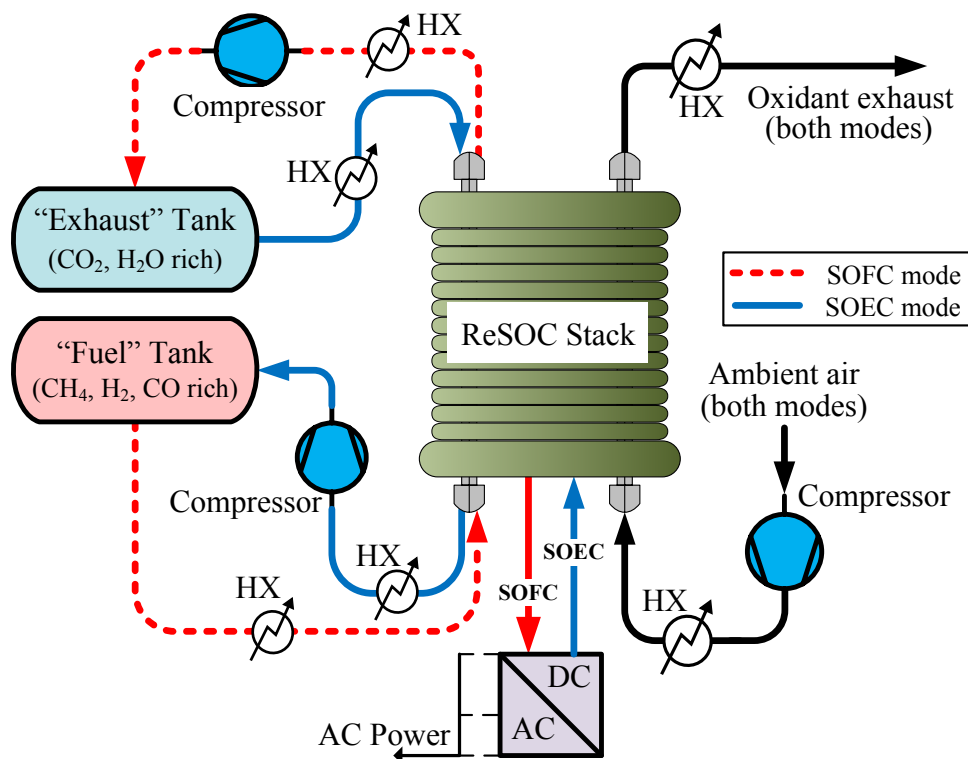
Figure 1.4: Simple reversible solid oxide cell system schematic showing operation in both modes with storage tanks and BOP components.

Figure 1.4 shows a simplified schematic of the proposed energy storage system. The energy storage device is charged by operating the ReSOC stack as an electrolyzer (SOEC mode). In this mode reactant species are delivered to the stack from the exhaust storage tank where they are electrochemically reduced to form fuel species (i.e., H_2, CO, CH_4)

with a supply of electricity from a renewable source, for example. The produced fuel is compressed and stored in a fuel tank for later use. In SOFC mode, the device is discharged as fuel species are delivered to the stack from the fuel tank where they are electrochemically oxidized to generate electrical power. The exhaust species, which are primarily H_2O and CO_2 with some unspent fuel, are compressed and stored in the pressurized exhaust tank. Air flow is delivered to the ReSOC stack in both modes of operation. In SOFC mode, air provides oxygen for the global electrochemical oxidation reactions; while in SOEC mode, air acts as a sweep gas to reduce the partial pressure of generated oxygen from steam/CO_2 electrochemical reduction, thereby increasing the efficiency of fuel production and avoiding potential deleterious materials issues.

While Figure 1.4 presents the basic operation of such an energy storage system, it neglects the specific component selection and integration required to transport reactant and product species between the storage tanks and the ReSOC stack, as well as the thermal management required in coupling a high temperature conversion device (i.e., ReSOC) with lower temperature storage. System design and analysis is required to establish how the storage and conversion functions are coupled, particularly concerning thermal management. Many different system configurations are possible to fill in the balance of plant components in between the storage tanks and the ReSOC stack including various arrangements of heat exchangers, condensers, evaporators, auxiliary reactors, valves, pipes, compressors, and turbines. A bulk of this research effort requires establishing suitable system configurations such that the energy storage system maintains the theoretically high conversion efficiency of the ReSOC stack.

1.4 Thesis objectives

The overall objective of this dissertation is to design and analyze stand-alone reversible solid oxide cell energy storage systems. These systems are novel, so a bulk of the research effort is dedicated to developing ReSOC system concepts for different application scales, determining key design variables, developing methods and strategies for system integration, and

formulating a procedure to simulate ReSOC systems. These efforts are essential in providing context to the specific research objectives described below which aim to evaluate the performance of ReSOC technology in energy storage applications. To that end this dissertation will evaluate stand-alone electrical energy storage systems based on roundtrip efficiency, capital cost, and levelized cost. These system performance metrics will be compared with targets and projections of energy storage technologies and applications such as the long-term U.S. DOE target of 80% system efficiency, <\$150/kWh capital cost, and 10¢/kWh-cycle levelized cost. Estimation of these performance metrics will be achieved by technical and economic modeling of ReSOC systems; however, because no prior system integration studies have been published, it is necessary to first establish a system that accurately represents the capabilities of ReSOC technology for energy storage. Such a system design effort must consider the unique characteristics of ReSOCs as well as the unique design requirements of energy storage applications such that the most suitable system may be quite unlike established systems that appear initially similar (e.g., SOFC power systems, SOEC hydrogen production systems, or redox flow batteries). There are many system design considerations that will influence the system performance including:

- *Stack operating conditions*: temperature, pressure, reactant composition, reactant conversion.

- *Storage conditions*: composition, temperature, pressure.

- *System configurations*: gas processing configurations (e.g., heat exchanger and turbomachinery networks), product recycle, oxidant storage vs. fresh air delivery, condensable reactant/product management (i.e., steam), storage configuration (i.e., above ground tanks or geological reservoirs).

Exploration of each of these operating conditions and configurations through system modeling is necessary to understand the often complex impacts on system efficiency. For example, it is known that high temperature ReSOC stack operation is required for efficient transport

14

of oxygen ions across the solid electrolyte, however lower temperature operation is expected to improve system efficiency by promoting exothermic methane formation in the electrolysis mode. Development of intermediate temperature ReSOC material sets has extended the possible range of ReSOC operation to 600-1000°C, but the balance of plant parasitic power will also change over this wide range of stack operating temperature. Furthermore, design of energy conversion systems commonly involves tradeoffs between efficiency and capital cost, and determining the most suitable configuration for this novel system must consider the efficiency vs. capital cost balance specific to energy storage application. For example, efficiency may be improved by including turbines to generate power from expanding the reactant gas stream from the storage pressure to the stack operating pressure, however at the expense of increased capital cost. The benefit of these turbines depends on the pressure ratio between the ReSOC stack and storage tank such that the operating conditions and configuration design are highly interconnected.

The following sub-objectives will be addressed to systematically accomplish the global objective of evaluating ReSOCs for energy storage:

1. Establish the system thermodynamics with particular focus on ideal operation and maximum efficiency.

2. Determine favorable system configurations and operating conditions based on efficiency and energy density for both distributed (100 kW) and grid-scale applications (>10 MW).

3. Perform sensitivity analysis to show how system performance may improve with advances in ReSOC technology

4. Evaluate system capital and levelized cost.

The first sub-objective addresses the energetic limitations of ReSOC systems with specific focus toward determining the maximum theoretical roundtrip efficiency of a ReSOC energy

storage system. Furthermore, thermodynamic analysis can be used as a first approximation for identifying desirable operating conditions of the ReSOC stack including temperature, pressure, and reactant compositions.

The second sub-objective progresses the analysis a step further by addressing how far actual system performance deviates from the ideal case. Thus, technical performance must be assessed through integrated system modeling for a variety of possible system configurations and across a range of operating conditions to elucidate system trade-offs and optimal operating points. The system configurations and operating conditions considered in this study are detailed in Section 2.5 including discussions of the expected effect of each design decision on system performance. For example, operating the ReSOC stack at elevated pressure is expected to increase stack efficiency by promoting exothermic methane formation during electrolysis; however, the increased parasitic load required to compress ambient air oxidant or sweep gas to a highly pressurized ReSOC stack can be detrimental to roundtrip efficiency. This parasitic compressor load could be mitigated with alternate configuration approaches such as using an oxidant tank to store air, enhanced air, or oxygen near the stack operating pressure, or using oxidant turbines for the ReSOC stack exhaust to recuperate power expended in the air compressors. Furthermore, because energy storage applications are projected from the kW to GW scale, this analysis will address two scales of application which will have different operating characteristics and must therefore be considered independently.

The third sub-objective utilizes sensitivity analysis to consider the possibility of improving the performance of the ReSOC system with future improvements in ReSOC technology. With increased research and development of ReSOCs, higher market penetration, and economies of scale production, cost and performance are expected to become more favorable in the future. Therefore, in order to accurately demonstrate the possibility of using such a technology for energy storage, performance should be assessed for future scenarios with improved ReSOC cost and cell characteristic (i.e., efficiency). This sensitivity analysis contributes to the overall iterative design process of ReSOC systems by providing information to researchers

focusing on materials development as to what performance may be required for competitive implementation.

Addressing the objectives described above requires technical modeling of a ReSOC stack and systems to quantify the technical and economic performance with fidelity capable of capturing sensitivity to various operating conditions and system parameters. System component models will be required including turbomachinery (compressor, turbine) and gas and liquid processing (heat exchangers, boilers, condenser, recycle ejector, storage tanks). Much of the technical modeling can be achieved with thermodynamically based models of the system components, however to accurately capture the subtleties of operating conditions variation on the ReSOC stack, a channel-level model is required. This level of modeling fidelity captures the performance effect of variations in key parameters including temperature, pressure, reactant compositions, and flow configuration. Thus, another objective of this work is to develop a ReSOC model and system component models that can accurately predict performance over the desired range of operating conditions. Specifically, this requires calibrating a ReSOC model to represent performance of next-generation intermediate temperature cells.

1.4.1 What is not addressed in this work

For a system modeling study of this nature, it is important to realize that there are many aspects that cannot be addressed in the scope of a single dissertation. Dynamic operation is inherent in energy storage systems for load following, mode switching, start-up, and shutdown; however, this research will not address dynamic system operation. The configurations and operating conditions of this novel system must be fundamentally understood before the utility of dynamic modeling is required to address control strategies and higher fidelity economic feasibility considerations. Additionally, because the energy storage applications being targeted operate in a primarily steady manner outside of mode switching, steady-state modeling analysis will provide a sound estimation of the system performance.

There are several system configurations that have been proposed, or are potentially feasible with ReSOCs that will not be considered in this work. System configurations such

as those with alternate storage and thermal management strategies are reviewed in Chapter 3, but not considered for analysis in this dissertation. Additionally, while much of the technical work of this dissertation is related to determining the most suitable system configurations and operating conditions, formal optimization is not included. For system analysis, optimization procedures are highly computationally intensive and often applied to relatively mature systems. For this novel system an understanding of the most suitable operating conditions can be achieved through parameter variation and engineering analysis, while formal optimization procedures can be employed in the future based on the systems developed from this work.

1.5 Thesis outline

The remaining chapters of this dissertation are organized to address the objectives described above. First, Chapter 2 provides additional background information on the energy storage market, theory of operation and working principles of ReSOCs, and discussion of the challenges and characteristics of ReSOC energy storage systems. Chapter 3 presents a literature review focused on the most relevant previously published ReSOC system studies. The literature review also notes important experimental results enabling ReSOC operation under the conditions suggested by the modeling results. Chapter 4 analyzes ReSOCs based on thermodynamic performance. This chapter describes a useful methodology for analyzing ReSOC systems based on the thermodynamic potentials (i.e., thermoneutral and reversible voltages) to highlight desirable operating conditions and establish the limits of theoretical roundtrip efficiency. Chapter 5 details the assumptions, equations, and methodology used in the stack and system-level modeling studies. This also includes a description of the calculation procedure required to simulate roundtrip operation of reversible systems. A significant focus of the model description is the implementation and calibration of the intermediate temperature channel-level ReSOC model. This calibrated model is used to generate results in the following chapters.

Chapter 6 presents the results of a cell and stack level modeling study to analyze the performance of the ReSOC stack in energy storage applications independent of the supporting system. In particular, design decisions related to the current density, flow configuration, and reactant compositions are considered as to their impact on roundtrip efficiency and stack thermal management. Chapter 7 presents a system configuration analysis for a distributed-scale application (100 kW discharge power). The configurational variations include whether to store reactant and product gases in a vapor state or condense water out of the process streams for separate storage. The analysis focuses on the impact of preheating loads and BOP auxiliary power to determine roundtrip efficiency and energy density performance metrics. Chapter 8 considers implementation of large systems (>10 MW). The configuration is dictated by practical engineering limitations of implementing a bulk-scale system, so the analysis is centered on parametric studies of key operating conditions including stack temperature, pressure, and fuel utilization. The final results section, Chapter 9 presents economic analysis for selected systems from Chapters 7 and 8. A bottom-up costing method is employed to estimate levelized and capital cost as a summation of the cost of each system component as well as labor and operating expenses. The conclusions given in Chapter 10 synthesize the results in the previous chapters. Particular attention is given to future work in an effort to guide additional research efforts on this topic.

CHAPTER 2

BACKGROUND

The results and discussions in this dissertation draw from various technical disciplines ranging from electrochemical and thermodynamic considerations of solid oxide cell performance to system design and energy storage applications. This chapter provides background information to support the novel contributions to reversible solid oxide cell system development. First, the applications and benefits of energy storage are explained with a focus on those applications that can be effectively serviced with ReSOC systems. Next the working principles and theory of operation of ReSOCs are detailed. The current-voltage characteristic is highlighted to explore the effect of different operating conditions on cell performance.

The working principles of ReSOCs highlight many favorable characteristics of using this technology for energy storage; although hurdles also arise, particularly in regard to system thermal management. The system thermal management is critical to maintaining high roundtrip efficiency, and the selected approach of using heterogeneous reactions of the carbonaceous gases for thermal management is explicitly outlined here. This chapter also includes a discussions of why intermediate temperature ReSOCs are a favorable option for energy storage applications by comparing their characteristics to those of low temperature PEM cells and conventional high temperature solid oxide cells. This chapter concludes by outlining the challenges associated with implementing ReSOCs in an energy storage system. Achieving a high roundtrip energy storage efficiency is a central challenge of this work, which is impacted by the cell-stack operation as well as system balance of plant component selection and integration. These impacts are described qualitatively here.

2.1 Energy storage applications and technology requirements

Energy storage is considered to be a critical component of the future electric grid to enable high penetration of intermittent renewable resources, increase efficiency, and reduce

environmental impact. Several publications and reports have detailed the expected applications for energy storage technologies [1, 8, 18, 76–78], although most of these applications are not widely used because present-day energy storage systems cannot meet the technical performance and cost standards required to make energy storage implementation fiscally attractive. As the need for electrical energy storage increases (e.g., with increased share of wind and solar power generation) and electricity storage technologies improve, implementation will become more attractive. However, methods alternate to electricity storage can also satisfy some of the projected applications. For example, demand-side management or "smart-grid" solutions [79], where power consumption is regulated to meet generation profiles (rather than vice-versa) by appliances [80], industries [81] or electric vehicles [82]. Thermal energy storage is another approach with the potential for high impact, either at low temperature with building heating/cooling [83] or high temperature as in concentrating solar power plants [84]. Finally, peaking power plants currently provide the service of some energy storage applications, and may continue to do so in the absence of suitable energy storage technologies. In fact, in a recent DOE report, energy storage cost standards for different applications are compared against the cost of installing increased capacity of peaking combined cycle power plants [8]. In the following subsections, energy storage applications are explained from the perspective of economic benefit and energy storage system requirements. Chapter 1 explained that ReSOC systems are suited for energy management, rather than power management, applications; however, several factors other than energy and power capacity must be considered when designing a system for certain applications including startup time, dynamic capabilities (i.e., ramping rate), and cost. Taking these selected applications together with published performance targets leads to initial design requirements for a ReSOC system.

2.1.1 Energy management applications

In a 2010 report from the U.S. Department of Energy [8], the total market potential for electricity storage in the United States was estimated to be as high as 200 billion US$. This

estimate is formulated by calculating an economic benefit ($/kW) of various energy storage applications and projecting the potential storage power capacity (MW). Additional benefits are expected from widespread energy storage that are not included in this report, such as pollution reduction from increased grid efficiency and reduced wear on baseload generation from lower ramping requirements.
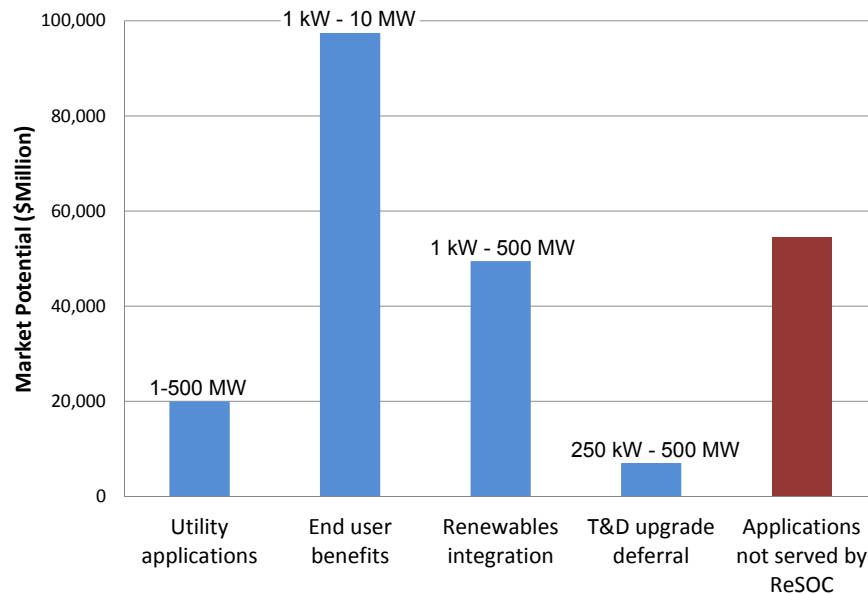
Figure 2.1: The 10-year economic potential for energy storage applications and individual application power capacity ranges. Data from Reference [8].

Several electrical energy storage applications are considered to be infeasible with ReSOC systems because of fast startup time, short discharge duration, or high ramping requirements. On the other hand, a majority of the projected energy storage capacity is in energy management services, many of which have scheduled operating periods, long discharge durations, and low ramping requirements well suited for ReSOC systems. Figure 2.1 shows the market potential of the different application categories that can be served by ReSOCs. Based on the technical operating requirements, greater than 75% of the market potential for EES may be reached by a competitive ReSOC system. Although, some of the applications that meet the operating characteristics of ReSOC systems may not be achievable with such a system because the cost of implementation is too high. The application categories are described below.

Utility applications

The two utility-scale applications are both related to electricity supply and include electric energy time-shift and electric supply capacity. Electric energy time-shift involves purchasing inexpensive energy from the wholesale electricity market during times of low demand to charge a storage system. The storage system may be discharged to re-sell the stored electricity to the wholesale market at times of high demand, or mitigate electricity purchases during peak-demand periods. This service may be performed by either a regulated utility or non-utility merchant. Efficiency and variable operating costs are particularly important performance metrics for technologies performing time-shift because the instances where time-shift is economically beneficial increase with increased efficiency and reduced operating cost. Electric supply capacity represents the opportunity to use an energy storage system in place of increased generation capacity. In this way, construction of a new power plant that would supply peaking capacity at a relatively low capacity factor is mitigated. The cost of these services is estimated to be 359–710 \$/kW and the application scale can range from 1–500 MW [8].

End user benefits

End user benefits include energy cost management within a time-dependent electricity cost structure (i.e., time-of-use energy pricing) and peak-shaving to reduce a maximum capacity charges. Time of use (TOU) electricity pricing prescribes off-peak and on-peak electricity price fluctuations that can exceed 100% daily and seasonally. Peak demand charges apply a cost to the maximum power draw from a customer for different supply periods (i.e., on-peak, part-peak, or off-peak). By charging an on-site electrical storage system during periods of low power-draw or inexpensive demand charge and discharging during high demand charge periods, the customer achieves economic savings. The economic benefit of TOU energy cost management and peak shaving are estimated as 1226 and 582 \$/kW,

respectively. However, these applications are synergistic in that peak electricity use often coincides with on-peak pricing. Thus, operating a single electricity storage system can achieve the benefits of both TOU energy cost management and peak-shaving.

The high market potential for end user benefits shown in Figure 2.1 is attributed to both high economic benefit and high market capacity. Furthermore, the application scale of < 10 MW suggests that these benefits may be well served by first generation ReSOC systems preceding widespread adoption of the technology required to support large-scale systems. These end user applications motivate the system configurations for 100 kW, distributed-scale systems given in Chapter 7.

Renewables integration

Renewables integration applications for energy storage include renewable energy time shift and renewable capacity firming [8]. Other studies have combined the renewable energy time shift with the utility application energy time shift described above because the applications are operationally very similar [1, 18]. However, the economic benefit is calculated differently by Eyer [8], based on the lost capacity factor of a renewable resource, meaning that the benefit is lower for time-shifting renewable energy (233-389 $/kW) compared with wholesale energy arbitrage (400-700 $/kW). Renewables capacity firming aims to "fill-in" power production when the output from a renewable resource is lost due to variations in weather. These variations can be rapid, meaning that the ramping rates required to provide this service may be difficult for a ReSOC system.

Transmission and distribution upgrade deferral

Transmission and distribution (T&D) upgrade deferral is achieved with energy storage systems by supplying storage capacity downstream of an overloaded or near-capacity transmission node. Typically, the electricity distribution infrastructure operates at an average capacity of 50% [85]. Including electricity storage can increasing the usage of the T&D in-

frastructure to a more economically favorable capacity [18]. It should be noted that there is significant price variation in the estimates of upgrading T&D capacity. In fact, 85% of the potential power capacity predicted for T&D services has the lowest cost benefit of any storage application (Transmission congestion relief, 31-141$/kW). Thus, while the technical requirements for T&D upgrade deferral match those expected from a ReSOC system, the cost is likely to be a barrier, particularly for early ReSOC systems. As seen in Figure 2.1, the T&D upgrade deferral is a small portion of the total economic benefit possible with ReSOCs.

Applications not served by ReSOC

The energy storage applications that are considered infeasible with a ReSOC system are eliminated from considerations based on fast time-to-online (< 10 min.), short discharged duration (<30 min.), or high ramping requirements. The applications that are eliminated for the above reasons are primarily associated with power quality management or backup reserves and include: electric supply reserve capacity, voltage support, transmission support, area regulation, electric service reliability, electric service power quality, short duration wind generation integration, and substation on-site power [8].

2.1.2 System design requirements

Based on the projected electrical energy storage application benefits [8] and DOE performance targets [1], initial performance requirements can be formulated for a ReSOC system. Table 2.1 shows the design requirements proposed here for the ReSOC system at two application scales. The power capacity normalized life cycle cost is taken from the average of high and low projection from Reference [8] for utility applications (bulk scale) and end-user benefits (distributed scale) and adjusted for a 20 year system life by scaling the present worth factor [8]. Long-term efficiency and cost metrics are used here because the ReSOC systems are presently immature and the long-term targets are intended for 2020. The energy capacity for the distributed scale system is designed to allow 10-hour discharge duration, satisfactory for the daily energy management services described above. However, seasonal storage with

bulk scale systems may require discharge durations on the order of months, indicating much higher energy capacity [86].

Table 2.1: System design specifications for distributed and bulk-scale systems.

Design specification	Distributed scale	Bulk scale
Power capacity	100 kW	> 10 - 250 MW
Energy capacity	1 MWh	100 MWh - 500 GWh
Roundtrip efficiency (%) [1]	80%	80%
10 year life cycle cost ($/kW) [8]	1340	820
Levelized cost (¢/kWh-cycle) [1]	10	10
Capital cost ($/kWh) [1]	150	150
Cycle life [1]	5000	5000

2.2   Reversible solid oxide cell working principles

The ReSOC operating characteristics has a significant impact on the performance of the energy storage systems explored in this work. Thus, to inform later discussions on stack and system modeling results in Chapters 6–8, the theory of operation of ReSOCs in both operating modes is explained here. The principles of ReSOC operation are analogous to often more familiar SOFC operation, although the necessity of considering both operating modes in reversible systems warrants distinction. The following subsections discuss the operating principles related to ReSOC reaction chemistry, current-voltage relationship, and reactant gas compositions.

2.2.1   Reaction chemistry

Global reaction chemistry within ReSOCs includes electrochemical fuel oxidation (or reduction), fuel reforming (or methanation), and water-gas shift (or reverse shift) processes. Reaction equations 2.1–2.3 summarize these primary reactions that occur in a ReSOC where the Δh given is the molar heat of reaction at 650℃. As written, the forward reactions typically occur when the ReSOC is operated in fuel cell mode and the reverse reactions occur during electrolysis; although it is possible, for example to have both water-gas shift

26

and reverse water-gas shift reactions occur at different locations within the ReSOC in a single operating mode depending on the reactant compositions and axial temperature profile.

$$H_2 + {}^{1}\!/_2 O_2 \leftrightarrow H_2O \quad \Delta h = \text{-247 kJ/mol} \tag{2.1}$$
$$CH_4 + H_2O \leftrightarrow 3H_2 + CO \quad \Delta h = \text{224 kJ/mol} \tag{2.2}$$
$$H_2O + CO \leftrightarrow H_2 + CO_2 \quad \Delta h = \text{36 kJ/mol} \tag{2.3}$$
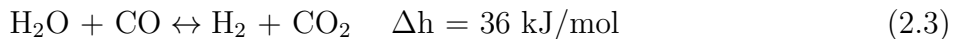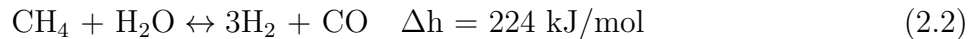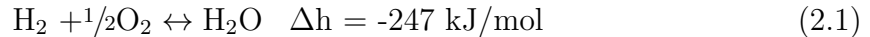
Figure 2.2 shows the reactions 2.1–2.3 occurring within the ReSOC in each mode of operation, that is, charging during electrolytic operation and discharging during fuel cell operation. In SOFC mode, hydrogen is consumed and water vapor is produced at the fuel side electrode-electrolyte interface as a result of the fuel cell electrochemical oxidation reaction (2.1). If carbon-containing species (CO, CO_2, CH_4) are present in the anode feed gas, steam-methane reforming (2.2) and water-gas shift (2.3) reactions may also take place in the fuel electrode compartment depending on the operating conditions and material sets employed. Endothermic steam-methane reforming (2.2) is promoted as a result of H_2 depletion and H_2O production (from 2.1), and under low pressure and high temperature cell conditions. This reaction helps to mitigate the excess oxidant cooling typically required during power producing SOFC mode. However, the steam-reforming reaction rate over Ni-YSZ electrodes is rapid and can create large temperature gradients within the cell.

The reverse of reactions 2.1–2.3 occurs when the cell is operated in SOEC mode as shown in Figure 2.2. The electrolytic reduction reaction (reverse of 2.1) proceeds when a cell voltage greater than the open-circuit voltage is applied across the electrodes thereby reversing the flux of oxygen through the solid electrolyte. The methanation reaction (reverse 2.2) is promoted by production of H_2, consumption of H_2O, and lower temperature and higher pressure operating conditions. The exothermic methanation reaction helps to offset the thermal energy consumed by the endothermic electrolysis reaction (reverse 2.1), which is important in maintaining the high temperature required for the ReSOC to operate. Direct oxidation and reduction of CO and CO_2, respectively, are known to occur in ReSOCs [87],
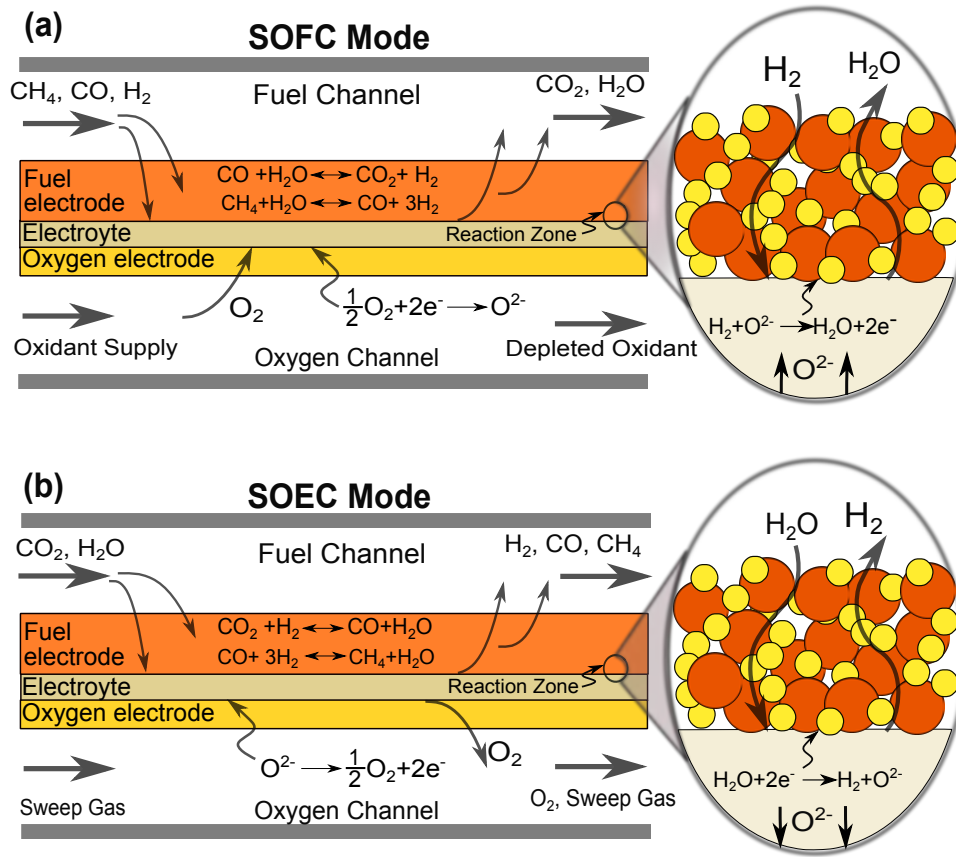
Figure 2.2: Reversible solid oxide cell channel schematic showing gas flow channels, MEA structure, species diffusion, and reaction chemistry in (a) SOFC and (b) SOEC modes

although the water-gas shift and reverse shift reactions are typically assumed to be the dominant reaction pathways for these species. This assumption has been questioned in recent publications as discussed in Section 5.1.5.

2.2.2 Reactant gas compositions

The simplified system concept depicted in Figure 1.4 includes two gas compositions associated with the "fuel" and "exhaust" storage tanks, however it is not immediately clear which compositions are most suitable. Furthermore, because this is a closed system, the reactant compositions are not determined by a feedstock input, such as natural gas in an SOFC power system or some ratio of steam and CO_2 in a co-electrolysis process. Rather, the gas occupying the "exhaust" tank is produced during SOFC mode where its composition is

established from the SOFC stack operating conditions including temperature, pressure, and fuel utilization. Similarly, the composition of the gas in the fuel tank is established from the fuel channel product stream when the system is operated in SOEC mode at its respective operating conditions.
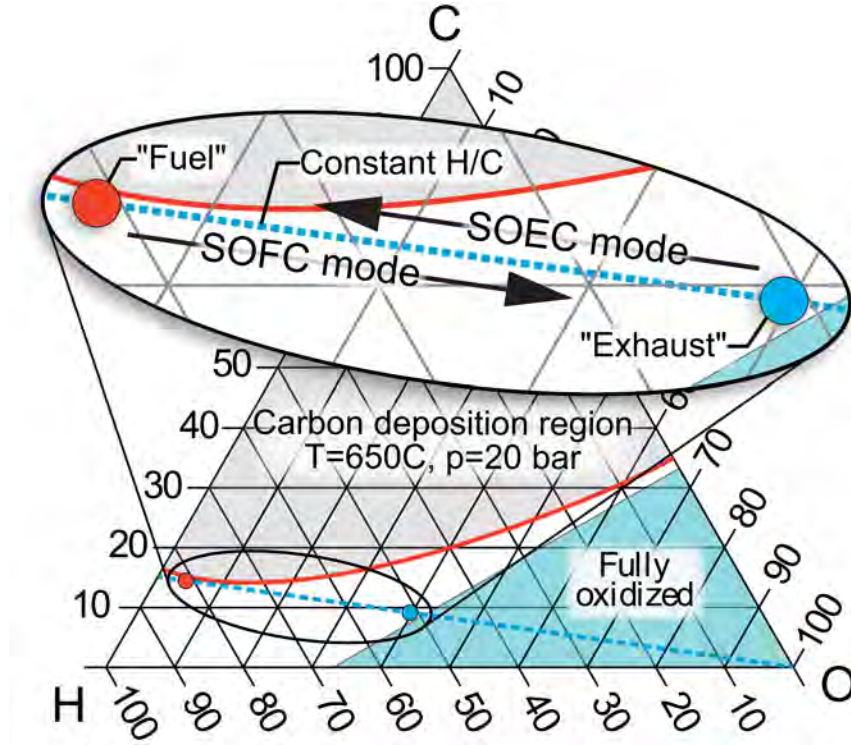
Figure 2.3: Ternary C-H-O diagram indicating carbon deposition region boundary (red line), carbon deposition region (grey), and fully oxidized region (blue)

The two compositions are conveniently depicted on the C-H-O ternary diagram as shown in Figure 2.3. They have equivalent hydrogen-to-carbon ratios (HTCR or H/C), but the oxygen content changes with the addition of oxygen during SOFC mode and removal of oxygen during SOEC mode. The possible compositions are bounded by the fully oxidized region and carbon deposition region. Solid carbon deposition causes irreversible damage in ReSOCs (i.e., catalyst poisoning, increased mass transport resistance in the gas diffusion electrode, etc.) and its formation depends on many factors including temperature, pressure, and mixture composition. The thermodynamic carbon deposition boundary is determined

by equilibrium calculations assuming solid carbon forms graphite on the ReSOC [88–90]. It is a function of temperature and pressure alone and can be used to estimate deleterious operating conditions. The deposition boundary is calculated by minimizing the free energy of a gas mixture made up of relevant C-O-H molecules. The method used here is described in Reference [89] and considers the 6 common species in SOFC systems (i.e., H_2, CO, CH_4, H_2O, CO_2, and C). The method is implemented using thermodynamic properties available in Engineering Equation Solver [91].

Methane-fueled SOFC systems often use steam-to-carbon ratios > 2 to reduce coking potential, but validated safe operating ranges have not yet been established for the conditions considered here. Thus, the carbon deposition boundary is used as a starting point to select appropriate compositions. Overall, the criteria for selecting viable gas compositions include mitigating carbon deposition, ensuring sufficient methane for thermal management, and allowing high fuel energy density for increased energy storage capacity. Thus, it is desirable to operate with a highly carbonaceous composition (i.e., low hydrogen-to-carbon ratio) that does not exceed the carbon deposition boundary.
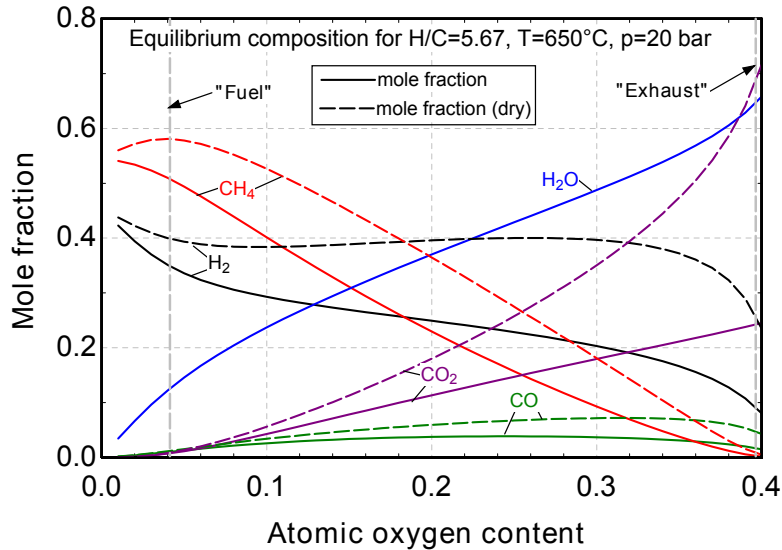
Figure 2.4: Species constitution vs. atomic oxygen content spanning the "fuel" and "exhaust" compositions as indicated in Figure 2.3.

Figure 2.4 shows the equilibrium mole fractions calculated for varying oxygen content based on the transition between the "fuel" and "exhaust" points in Figure 2.3 at 650°C and 20 bar. The fuel composition is rich in methane (nearly 60% dry) and hydrogen. The exhaust has high water content (65%) and the remainder is primarily carbon dioxide and hydrogen.

2.2.2.1 Utilization parameter definitions

A utilization parameter (i.e., fuel utilization or reactant utilization) quantifies the fraction of reactant delivered to the stack which is electrochemically converted. For a reversible system, it is also useful to consider the utilization in terms of oxygen transport across the electrolyte. Thus, the utilization parameters are used to mathematically relate the "fuel" and "exhaust" compositions.

In the case of fuel cell mode, the fuel utilization is defined as the ratio of the molar rate of electrochemical hydrogen consumption to the equivalent molar flow of hydrogen supplied to the fuel channel of the SOFC mode stack:

$$U_F = \frac{\dot{N}_{H2,consumed}}{(\dot{N}_{H2} + \dot{N}_{CO} + 4\dot{N}_{CH4})_{SOFC,inlet}} \tag{2.4}$$

where $\dot{N}_i$ is the molar flow of species i and $\dot{N}_{H2,consumed}$ is the molar rate of hydrogen consumption at the fuel electrode.

Alternatively, reactant utilization for electrolysis operation can be defined as the ratio of oxygen generated at the oxygen electrode to the total oxygen available in the reactant species entering the fuel channel:

$$U_R = \frac{\dot{N}_{O2,produced}}{2(\dot{N}_{H2O} + 2\dot{N}_{CO2} + \dot{N}_{CO})_{SOEC,inlet}} \tag{2.5}$$

This definition suggests that complete electrochemical reduction of the reactant species (i.e., $U_R = 1$) includes reducing CO. In practice, the presence of heterogeneous side-reactions at the fuel electrode offers other chemical formation pathways, such as CH_4 formation via methanation, making this definition especially useful for lower temperature, pressurized sys-

tems.

Despite Equations 2.4 and 2.5 being defined for SOFC and SOEC operation, respectively, each parameter also influences the opposite operating mode for a reversible system. For example, the fuel utilization affects SOEC mode operating parameters. Specifically, in a closed energy storage system, oxygen is either transferred to or removed from the fuel electrode and the utilization term is a measure of this. In turn, the magnitude of the utilization affects the tank composition for the subsequent mode switching operation. Because the ReSOC system must ensure continuous reversible operation, the storage tanks must eventually return to their original state of charge (i.e., respective composition or oxygen content). In other words, the mass flows and conversion rates associated with a prescribed SOFC mode fuel utilization define the operating conditions (i.e., reactant utilization) required in SOEC mode such that the system is recharged to the original state exhibited by the storage tanks. To recharge the system in this way, the value of reactant utilization (U_R) is not necessarily equivalent to the value of the fuel utilization (U_F) because the reactant utilization measures the extent of reduction of a gas mixture, while the fuel utilization measures the extent of oxidation of a different gas mixture. Additionally, a given fuel utilization does not indicate a specific reactant utilization which will return the system to its original state because the two parameters are not explicitly related.

2.2.3 Current-voltage relationship

The relationship between current and voltage in a ReSOC is a determining characteristic of the cell efficiency. The open circuit voltage (OCV) is estimated by the reversible potential, calculated as:

$$E_N = -\frac{\Delta g}{nF} \tag{2.6}$$

where Δg is the Gibb's free energy, F is Faraday's constant, and n is the number of electrons transferred per reaction. The Nernst equation is revealed from 2.6 by expanding the entropy

component of the Gibb's Free energy and assuming the hydrogen redox reaction:

$$E_N = E_0 - \frac{RT}{nF} \ln \frac{x_{\text{H2O}}}{x_{\text{H2}}x_{\text{O2}}} + \frac{RT}{2nF} \ln \frac{p}{p_0} \tag{2.7}$$

where E_N is Nernst potential, E_0 is standard equilibrium potential calculated at cell temperature and standard pressure, and the species mole fractions, temperature, pressure, Faraday constant and universal gas constant are represented by x_i, T, p, F and R, respectively. The number of electrons transferred per reaction is $n = 2$ for reaction 2.1.
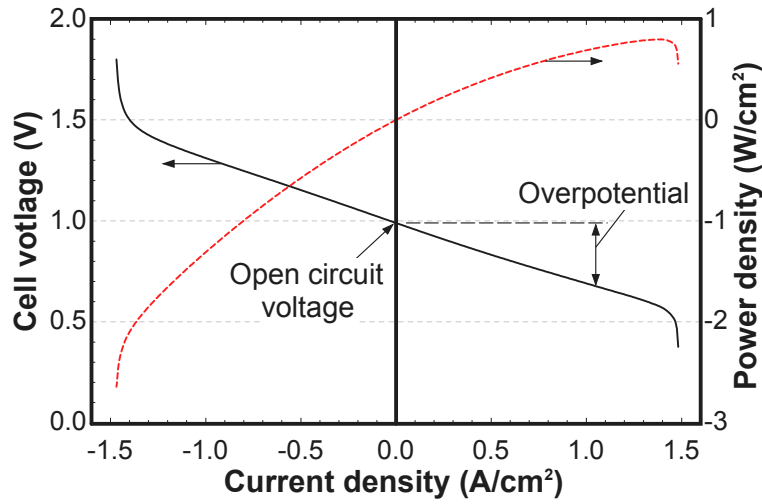
Figure 2.5: Representative current-voltage characteristic.

The cell voltage in each mode of operation is calculated as a deviation from OCV by a current-dependent overpotential. A representative voltage-current plot for a ReSOC is shown in Figure 2.5 where the current is positive in SOFC mode and negative in SOEC mode. An intermediate fidelity cell model was employed to generate Figure 2.5 which is described in Chapter 5. For high temperature (800-1000°C) ReSOCs, activation overpotential is relatively small compared to low temperature electrochemical cells, particularly in the electrolysis mode of operation. However, under intermediate temperature conditions (550-800°C), the activation overpotential is more significant, particularly at low current density [92]. Ohmic overpotential increases linearly with current density and is attributed to the resistance to electron and ion transport in the MEA. The majority of ohmic resistance is attributed to ion

transport in the electrolyte and interfacial contact resistances between cell components and layers. Concentration overpotential due to reactant depletion at the electrode-electrolyte interface arising from diffusion limitations in the porous electrodes occurs at both the fuel and oxygen electrodes.

Inefficiency (i.e., overpotential) increases with increased current density; however, it is essential to operate at reasonably high current density in order to achieve an economically high stack power density. Utilizing a unitized stack for reversible operation requires balancing design considerations for both modes of operation. For example, heat generation associated with cell-stack inefficiency helps to offset the endothermic reduction reaction (reverse reaction 2.1) in electrolysis mode, but can cause excessive heat generation in fuel cell mode. The current-voltage relationship is influenced by the cell operating conditions (e.g., T, p, x_i) and these effects must be considered when determining suitable operating conditions for energy storage. The following subsections consider the influence of different operating conditions on the current voltage characteristic all generated with the channel-level model described in Chapter 5. These results are modeled assuming the cell-stack interconnect is isothermal to represent laboratory conditions.

Pressurized operation

The effect of pressure on the current voltage performance is given in Figure 2.6, which indicates that pressurized operation has advantages for enhancing ReSOC performance, particularly in SOFC mode where the ratio of power produced to power consumed in SOEC mode at a given magnitude current density is higher. Increasing the pressure also changes the cell thermal behavior, for example by promoting the exothermic methanation reaction. The cell temperature at a given current density is relatively higher if the methanation reaction occurs inside the fuel channels. Therefore, pressurized operation allows more efficient (i.e., lower overpotential) operation for a practical system when methanation occurs in the fuel channel.
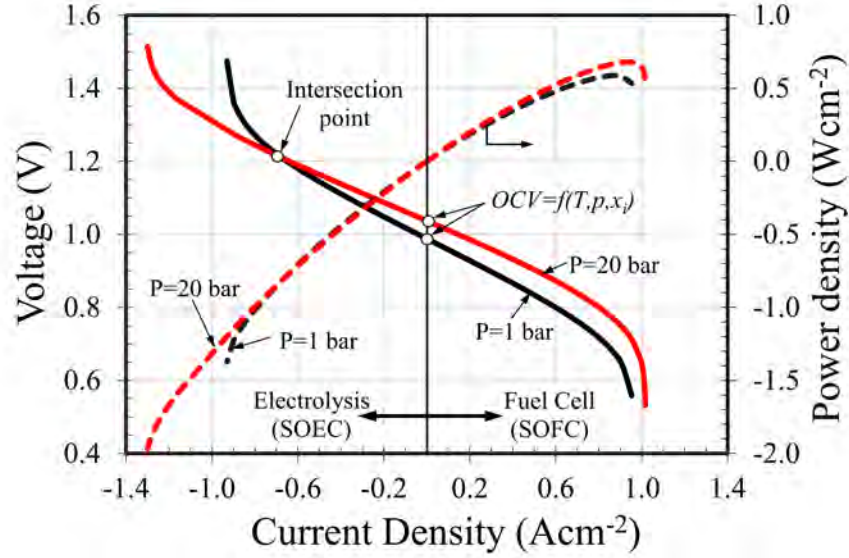
Figure 2.6: Voltage and power density vs. current density for a ReSOC under atmospheric (black) and pressurized (red) conditions.

Pressurized operation has two distinct effects on the cell electrochemical performance: (1) increased OCV and (2) reduced losses associated with the activation and concentration polarizations. The third term in the right side of Equation 2.7 represents the pressure dependence of the Nernst potential. As the cell pressure increases, this term rises from 0 (at 1 bar) to larger values, resulting in increased Nernst potential at each current density. With an increase in E_N, the SOFC power production and efficiency also increases. Although, pressurized operation has the opposite effect in electrolysis mode at low magnitude current densities (i.e., it increases the cell power consumption because the applied voltage must be higher for a given current density). At high current density (i.e., past the intersection point in Figure 2.6) the pressurized SOEC has better performance compared to atmospheric because the increased Nernst potential is offset by reduced activation and concentration losses. Indeed, pressurized operation significantly reduces the concentration losses and enhances the charge-transfer reaction kinetics in both modes of operation as has been reported previously [92].

Despite increased SOEC mode power consumption at elevated pressure in the low current density regime, increased power production in fuel cell mode results in a net benefit for roundtrip storage efficiency (see the roundtrip efficiency definitions in Section 2.5.1). The combined effects of the phenomena described above indicate that pressurization increases the overall performance of the cell in both operating modes. Thus, the present work considers pressurized ReSOC systems as a practical approach to improve system performance.

Influence of reactant composition

The pressurized and ambient current-voltage characteristics shown in Figure 2.6 are produced with the same feedstock gas composition in both fuel cell and electrolysis modes, resulting in a continuous curve as the cell moves through polarity switching at zero current. This result is representative of constant fuel flow, cell-level laboratory testing practices. However, for the proposed energy storage application, the reactant gas compositions in each mode will not be the same and it is therefore necessary to explore the implications of different compositions on the cell characteristic. Figure 2.7 shows predicted voltage-current curves considering unique reactant compositions in SOFC and SOEC modes for both constant fuel flow and constant fuel utilization. As can be seen from the constant fuel flow case, the curves associated with each composition have distinctly different OCV values. Comparing the constant fuel flow results presented in Figure 2.6 and Figure 2.7 shows that the ReSOC performance increases when the feedstock gas compositions are not the same. For example, with more hydrogen (reactant) and less water (product) in the feedstock gas composition in SOFC mode, the Nernst potential, and consequently power output, increases. Alternatively, since water is the main reactant in the SOEC mode, high amounts of water in the SOEC mode feedstock gas composition decrease the Nernst potential and consequently reduce the cell power consumption for a given current density.

To consider the implications of the voltage-current characteristic in the context of system level operation it is re-emphasized that for a practical system, the inlet composition in
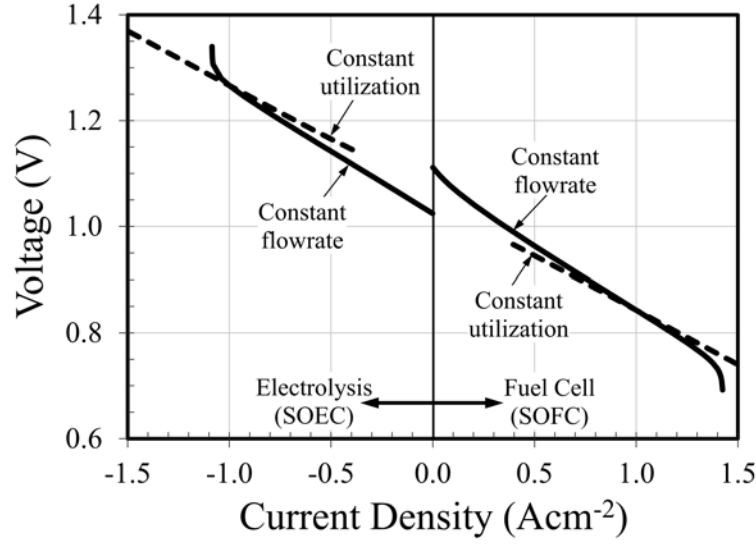
Figure 2.7: Voltage vs. current with different reactant compositions in each mode with either constant fuel flow or constant fuel utilization

one mode of operation is determined based on the exhaust gas conditions established from operation in the opposite mode (see Section 2.2.2). For the constant fuel flow V-j curve in Figure 2.7, the feedstock composition in SOEC mode is produced from the stack in SOFC mode only at a specific current density which corresponds to 70% fuel utilization (i.e., at 1 A/cm² where the constant fuel flow and constant utilization curves cross). Because of the interdependence of the two feedstock compositions, roundtrip operation in the proposed system will follow a V-j characteristic more closely represented by constant fuel utilization than constant fuel flow. In both operating modes, the cell performance is worse for the constant utilization case compared to constant fuel flow at current density magnitudes < 1 A/cm² because of higher reactant consumption and associated changes in OCV. Beyond 1 A/cm², the constant fuel flow case exhibits higher fuel utilization (> 70%), resulting in lower cell performance compared to the constant utilization case. The constant utilization curves are not shown near OCV because portions of the cell become inactive at low current density when high fuel utilization is maintained.

2.3 System thermal management

The previous sections described many of the operating features of a reversible solid oxide cell. Chief among these features is the discrepancy in thermal behavior between the two operating modes. For the stand-alone energy storage systems considered here, it is important that the stack is operated to be net exothermic so that reactant preheating can be satisfied by stack tail-gases that have increased in temperature as they flow through the stack. Thus, a particular challenge is the endothermic electrolysis reactions which must be overcome with a heat supply. Operating at overpotential high enough to achieve a net exothermic process is prohibitively inefficient for most energy storage applications. Alternatively, in this work the stack is operated to intentionally promote exothermic methanation reactions during electrolysis operation. The extent of methanation will dictate how much additional heat is required in the stack to satisfy system preheating requirements. From a basic interpretation, LeChatlier's principle indicates that increasing pressure and lowering temperature of the ReSOC stack will benefit methane formation. Other stack operating conditions including reactant composition and utilization also have a significant influence on the thermal performance as explained in Chapter 4.

2.4 Low, intermediate, and high temperature electrochemical cells

Reversible solid oxide cells are less mature than PEM or alkaline electrochemical cells, however the ReSOCs are critical to the implementation of the systems modeled in this dissertation due to several unique operating characteristics. In particular, the thermal management approach described in the previous section is not possible with low temperature PEM cells because they are irreversibly damaged by the presence of carbon monoxide and the operating temperature is not suitable for reforming and fuel-synthesis chemistry. Another detriment of low temperature cells in energy storage applications is depicted in Figure 2.8, which compares the polarization curves for PEM and ReSOC operated on steam-hydrogen reactant mixtures. The large polarization at low current density for the PEM cell is attributed

to kinetic limitations. These losses lead to significantly higher power required to generate hydrogen and somewhat lower power generated in fuel cell mode. Conversely, the ReSOC shows a relatively flat profile at open circuit voltage, which indicates that only slightly more power is required to generate hydrogen compared to the electricity recovered.
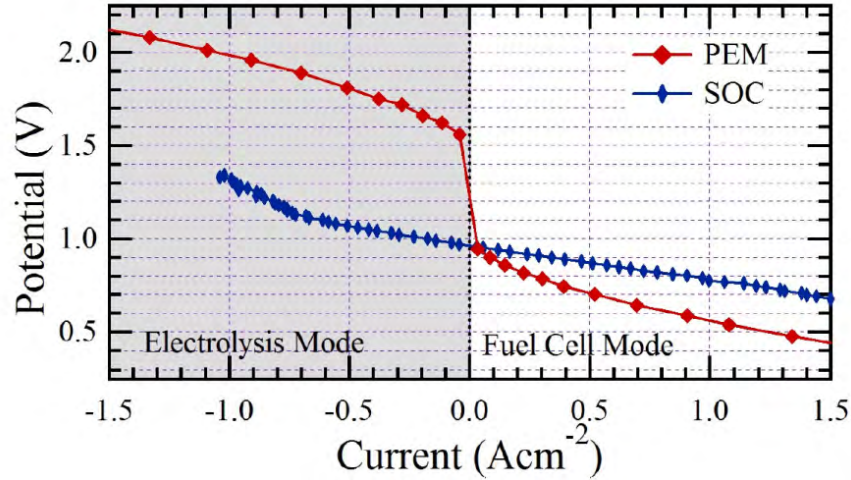
Figure 2.8: Comparison of current-voltage characteristics for low temperature PEM [93] and high temperature SOC [94]. Figure supplied courtesy of Dr. Scott Barnett.

The above discussion illustrates the necessity of solid oxide cells for high efficiency energy storage applications. Furthermore, intermediate temperature solid oxide cells are targeted in this work because of their capacity for high performance in operating regimes that coincide with methane formation. Figure 2.9 shows model-generated roundtrip stack efficiency results as a function of temperature for two different calibrated models. The high temperature YSZ-electrolyte model [92] achieves the targeted 80% efficiency at 850°C, but efficiency declines rapidly at lower temperature due to increased serial resistance and polarization losses. Alternatively, the LSGM-electrolyte cell model (described in Chapter 5) achieves > 80% roundtrip efficiency at temperatures as low as 650°C, which is a more favorable temperature for methane formation.
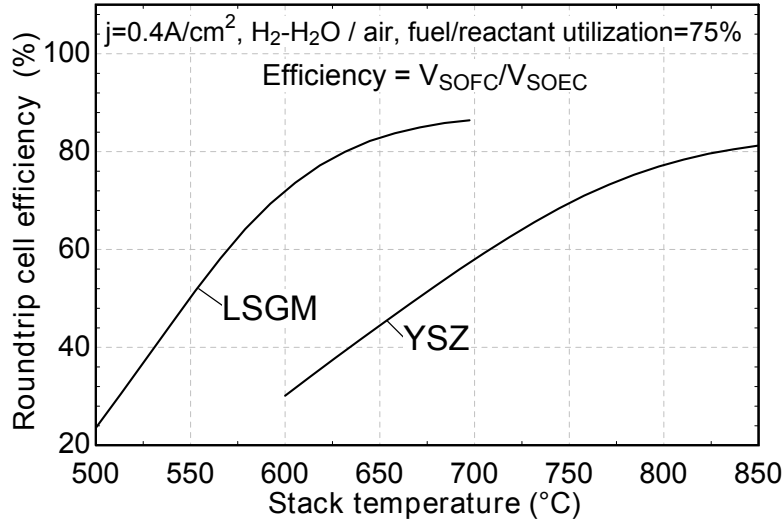
Figure 2.9: Roundtrip stack efficiency vs. temperature for high temperature YSZ-electrolyte and intermediate temperature LSGM-electrolyte cells for steam-hydrogen reactants at constant current density and utilization

2.5 Reversible solid oxide cell system design considerations

Some unique challenges arise in designing ReSOC systems, including: (1) overcoming the thermal disparity between fuel cell (typically exothermic) and electrolysis (typically endothermic or near thermoneutral) operation using a unitized cell-stack and common hardware, (2) selecting configurations and operating conditions (T, p, utilization, composition) that promote high efficiency in both operating modes, and (3) thermal integration between high temperature stack operation and lower temperature, pressurized storage. Furthermore, because stack reaction products are tanked for use in the opposite mode of operation, they must be processed to enable compression to storage pressure with minimal energetic cost. These design challenges can be overcome by careful selection and thorough understanding of system configurations and operating conditions. The remainder of this chapter is dedicated to outlining the key operating parameters and system design decisions that are evaluated in the following modeling results. Typically the system design requires balance two or more competing trends (e.g., stack efficiency vs. system efficiency or system efficiency vs. capital cost). Evaluating these design tradeoffs is a primary focus of this dissertation. Before the

system integration considerations are addressed, it is important to define the roundtrip efficiency parameters to help explain the implications of different design decisions on system technical performance.

2.5.1 Roundtrip efficiency considerations

The efficiency of a ReSOC system for energy storage depends on both the efficiency of the ReSOC and the auxiliary power required by the balance of plant. The roundtrip system efficiency, $\eta_{\text{RT,system}}$, is defined as the quotient of the net energy generated in SOFC mode to the total energy supplied in SOEC mode:

$$\eta_{\text{RT,system}} = \frac{V_{\text{SOFC}}q_{\text{SOFC}} - E_{\text{BOP,SOFC}}}{V_{\text{SOEC}}q_{\text{SOEC}} + E_{\text{BOP,SOEC}}} \qquad (2.8)$$

where V_{SOFC} and V_{SOEC} are the operating nominal cell voltages, q_{SOFC} and q_{SOEC} are the total charge transferred across the electrolyte, and $E_{\text{BOP,SOFC}}$ and $E_{\text{BOP,SOEC}}$ are the total BOP energy required during SOFC mode and SOEC mode, respectively. The BOP energy includes parasitic power loads from components, such as compressors, power produced from turbines, and energy entering the system in the form of fuel or process streams. As the definition implies, for achieving high roundtrip efficiency, it is desirable to operate at high cell voltage in SOFC mode and low applied voltage in SOEC mode (i.e., operate at low overpotential), as well as to have low BOP energy consumption in both modes of operation.

It is convenient to define the efficiency in terms of energy (rather than power) to allow different operating durations in SOFC and SOEC modes. However, for repeatable and self-sustaining operation, the system must be returned to the initial state of charge (i.e., charged state) by operating in SOEC mode. Depending on the energy storage application and operating strategy, the charged state may be achieved, for example, daily, weekly, or seasonally. The state of charge is defined as the hydrogen equivalence of the gas stored in the SOFC tank, which is proportional to the charge transfer required to completely oxidize the stored fuel. Thus, to ensure repeatable operation, the total charge transferred during SOEC mode must be equal to the charge transferred while discharging the system in SOFC

mode: $q_{SOFC} = q_{SOEC}$.

The roundtrip stack efficiency, $\eta_{RT,stack}$ is calculated by neglecting the BOP energy required in both modes such that Equation 2.8 is simplified to:

$$\eta_{RT,stack} = \frac{V_{SOFC}}{V_{SOEC}} \tag{2.9}$$

The roundtrip stack efficiency is useful for understanding system performance by quantifying the efficiency impact of the ReSOC stack and the BOP independently.
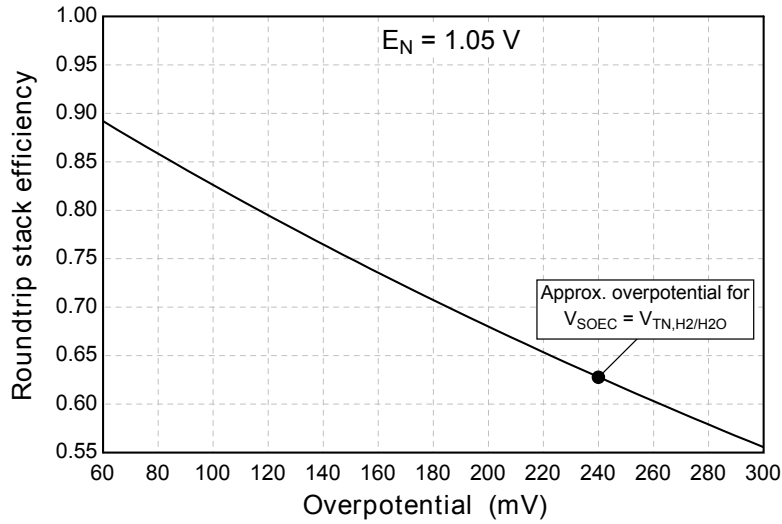
Figure 2.10: Roundtrip stack efficiency vs. overpotential assuming constant overpotential in both operating modes and open-circuit voltage of 1.05 V.

Operating at the high overpotential required to generate net heat in a steam-hydrogen electrolyzer is prohibitively inefficient for an energy storage application. More specifically, the overpotential require to reach the thermoneutral voltage is approximately 240 mV for steam electrolysis at 800℃ and 1 atm, which limits the roundtrip stack efficiency to 63% (see Figure 2.10). To achieve higher efficiency, the electrolyzer must operate at lower overpotential. For example, in Figure 2.10, an overpotential of 117 mV is the maximum allowed to achieve 80% stack efficiency. To allow some axuiliary power consumption from, e.g., compressors, a more realistic target is 85 mV, corresponding to a stack efficiency of 85%. This simple analysis reiterates the necessity of operating within the thermal management strategy

described in Section 2.3, where low overpotentials are enabled by exothermic fuel-synthesis chemistry in the ReSOC.

2.5.2 System configurations

Figure 2.11 shows a schematic of the baseline system implementation. The features of this system configuration include storage tanks for the two gas compositions (fuel & exhaust), a product compressor to compress the stack products to the storage pressure, an air compressor to compress ambient air to the stack operating pressure, heat exchangers to recuperate thermal energy from the oxidant and product streams for preheating, and valves to throttle streams to lower pressure and aid in mode-switching. The system in Figure 2.11 indicates the opportunity to utilize many of the system components in both modes of operation, such as compressors and heat exchangers, favorably reducing capital cost. Analysis of the component loads and operating ranges is required to validate the feasibility of this approach.
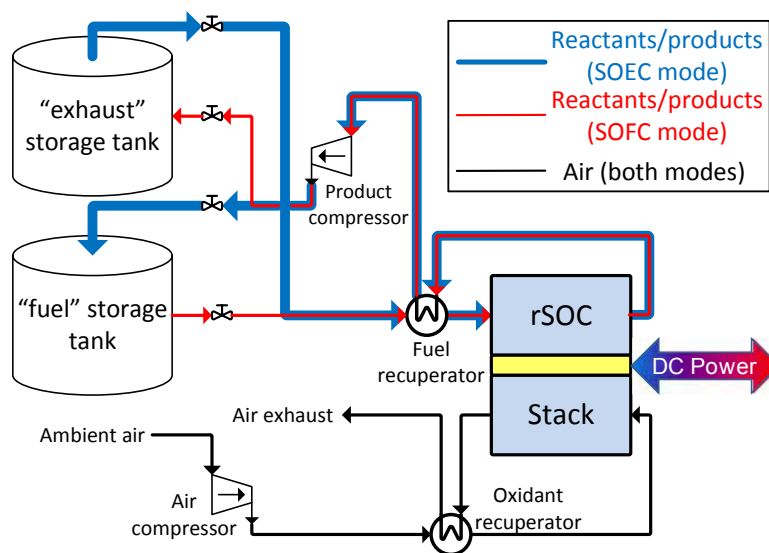
Figure 2.11: Baseline system schematic.

Two primary operating concerns are notable from the baseline system shown in Figure 2.11. First, storing the fuel and exhaust directly from the stack outlet requires storage of condensible species, particularly H_2O. At the high operating temperature of the ReSOC

stack, H_2O is gaseous even at elevated pressures; however, H_2O can condense in the tanks for storage near ambient temperature. Storing a two-phase mixture has implications for operation of the storage system and requires additional thermal energy to evaporate the liquid water when it must be used is a reactant. The exhaust composition can include, for example, greater than 75 mol% H_2O. Condensation in the tanks can be mitigated by lower pressure and higher temperature storage conditions, which are unfavorable from an energy density standpoint. Furthermore, maintaining high temperature storage suggests highly insulated or heated storage tanks, thus either increasing the capital cost or energy consumption of the system. Implementations where high temperature storage is used to prevent condensation of stored gases will be referred to as the stored vapor case, although alternate system configurations are discussed below to avoid this potentially unfavorable strategy. The energy management applications targeted with ReSOC energy storage system require storage on the order of hours to days, such that maintaining high temperature (e.g., 200°C) gaseous storage may be impractical.

The second operational concern for the baseline system is the potential for excessive compressor power consumption. The compressor power is determined by the flowrate, pressure ratio and compressor inlet temperature. For the baseline configuration, high inlet temperature (e.g., 200°C) is required for the product compressor to maintain gas phase of all species throughout the compression process. Furthermore, the high flowrate and pressure ratio for the air compressor can cause detrimentally large power consumption for the expected stack operating pressure (e.g., greater than 10 bar).

Advanced system configuration implementations address the operational challenges of the baseline system described above and can improve performance in other ways. The configurations considered in this research are depicted in the system schematic in Figure 2.12. The configurational modifications include: (1) active water management with a condenser and evaporator to separately store liquid water, (2) recycle of stack products and air/oxidant exhaust, (3) tanked oxidant storage, (4) expansion turbines, and (5) auxiliary methanation

and/or steam-methane reforming reactors. These system modifications are described below.
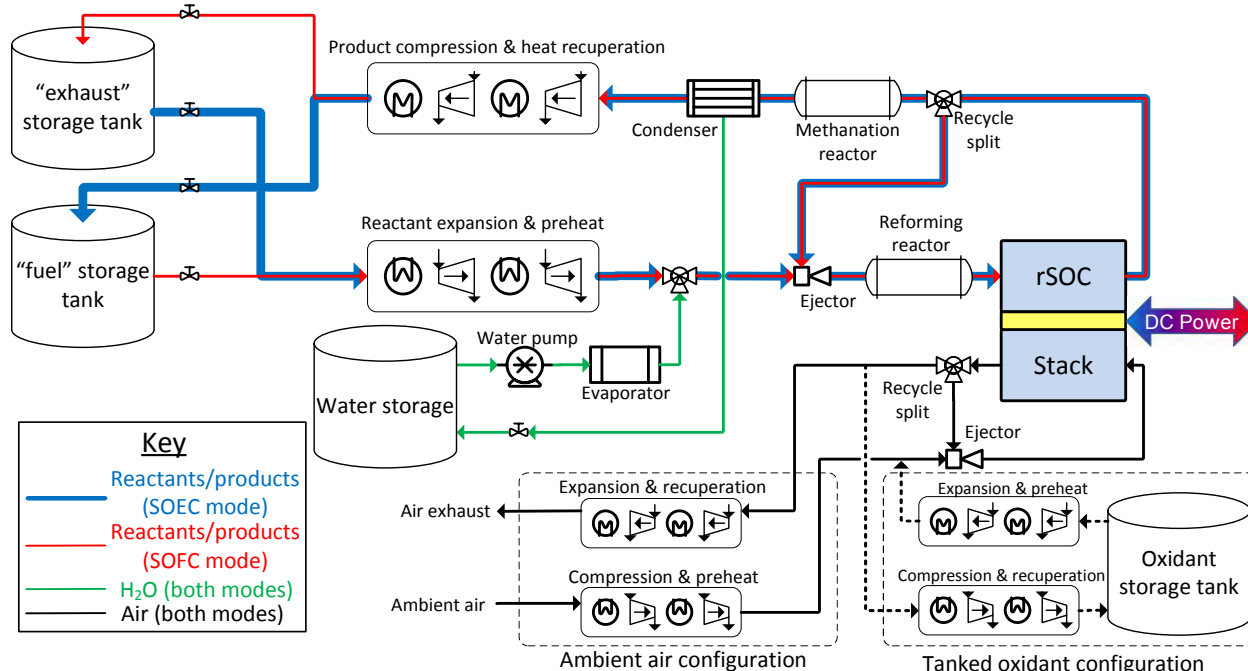
Figure 2.12: Advanced system schematic.

Active water management (e.g., water separation)

Active water management refers to the controlled separation of water from the product stream prior to compression and storage of the other product species. Implementing active water management requires additional components including evaporator, condenser, water pump, extra valves and piping, and potentially a water storage vessel. By removing the water prior to compressing the product gases to storage pressure, the remaining product gases can be compressed at a lower temperature, thus reducing the power requirement. Additionally, the gases can be stored at higher pressure and lower temperature without concern for water condensation, favorably reducing the required storage vessel volume. However, additional thermal energy is required to evaporate the reactant water in both modes of operation. For a stand-alone system the thermal energy required by the evaporator is ultimately provided by inefficiencies in the ReSOC stack, so a greater thermal load required by the BOP suggests

lower roundtrip stack efficiency. The energy required for evaporation is particularly detrimental in SOEC mode where water is a majority reactant. Power consumed by the water pump is negligible compared to the gas compressors because it acts on high density liquid water.

Stack product recycle

Recycle of products from both the fuel channel and oxidant channel has the potential to improve system performance. Recycle typically relies on high-temperature ejector components to entrain the recycle flow without needing to first cool the recycled stream. The ejector implementation requires slightly increased compression of the driving flow (i.e., "fresh oxidant"). Oxidant recycle is a well-established operating strategy in SOFC systems as a method to reduce the size and cost of gas processing components such as compressor and heat exchangers. Although, oxidant recycle results in an unfavorable depletion of the oxygen partial pressure in the ReSOC oxidant channel if air is used as the oxidant, reducing the Nernst potential.

Electrolysis systems typically operate with a sweep gas (e.g., air) to reduce the partial pressure of generated oxygen in the oxidant channel, but typical SOEC operating conditions are such that cooling is not a primary function of the sweep gas. However, the system proposed for this research relies on the electrolysis mode stack operating exothermically such that cooling the stack is a primary function of the sweep gas flow. Sweep-gas recycle can be employed for a similar benefit as in SOFC mode. Oxygen is concentrated in the sweep gas (air) as a result of recycle which causes the Nernst potential to increase unfavorably. Although, similar to SOFC mode this performance penalty may be compensated by reduced power consumption of the compressors.

Recycle of products from the fuel channel has more complicated impacts on system performance than oxidant recycle because it can impact the ReSOC thermal characteristic, electrical characteristic, and reactant composition in addition to compressor and heat ex-

changer loads. One common reason for implementing SOFC stack recycle is to provide steam at the stack inlet to reduce the likelihood of coke formation with a hydrocarbon fuel. This reduces the thermal load that would otherwise be required to evaporate steam. Product recycle is not as commonly employed in SOEC systems, although it will impact stack and system efficiency through changes to the thermal and electrical characteristic. Ultimately model simulations can be used to demonstrate the dominant effects of recycle in each mode and assess its utility as an operating strategy.

The performance benefit from recycling a portion of the gas streams exiting the stack is often optimized for a given recycle ratio, which is defined as the mass flow of the recycled stream compared to the total mass flow leaving the stack. Thus, the recycle ratio of both the oxidant and fuel channel streams will be considered as a system operating parameters in the proposed studies.

Oxidant storage

Tanked oxidant storage has the potential to reduce the BOP power consumption for pressurized stack systems by storing oxidant at a pressure near the stack operating pressure. Rather than compressing oxidant to the stack pressure, oxidant is expanded from the storage pressure and oxidant or sweep gas exiting the oxidant channel must be compressed back to the storage pressure. Tanked oxidant storage has the potential to significantly reduce the load on the oxidant compressor by reducing the pressure ratio. For example, if the stack operating pressure of 20 bar is assumed, compressing ambient air from atmospheric pressure requires a pressure ratio of about 20, while tanked storage at 100 bar requires a pressure ratio of only 5.

An additional benefit of tanking the oxidant is realized if the stored gas is either pure oxygen or enhanced air. Higher concentration of oxygen in the oxidant improves ReSOC efficiency by both reduced activation and concentration losses at the oxygen electrode and increased Nernst potential. It should be noted, however, that activation and concentration

losses are also drastically reduced for pressurized operation such that ohmic overpotential is likely to dominate cell performance. Increasing the Nernst potential is beneficial in SOFC mode as it leads to increased power density, although increased Nernst potential in SOEC mode requires increased power for the electrochemical conversion. The benefit of increased Nernst potential in SOFC mode outweighs the increased power requirement in SOEC mode such that using pure oxygen in both modes is desirable when compared to ambient air. The benefit of using pure oxygen as the oxidant is enhanced when oxidant recycle is implemented because the depletion and concentration of oxygen associated with ambient air recycle in SOFC and SOEC modes, respectively does not occur. An additional consideration for tanked oxidant is the safety of storing highly purified oxygen.

Reducing the oxidant compressor power consumption, for example by tanking oxidant, has the potential to drastically reduce the total system BOP power consumption. Power consumption from the oxidant compressor may be as much as an order of magnitude larger than the product compressor due to higher volumetric gas flowrate and pressure ratios.

Expansion turbines

Another configuration with the potential to improve system efficiency is including expansion turbines to reduce the net BOP power consumption. This implementation is, in a sense, recuperating some of the power expended in the gas compression processes to improve system efficiency at increased capital cost. Turbine expansion of exhausted oxidant from stack pressure to ambient is expected to be the most beneficial implementation because the oxidant stream has a relatively large flowrate and exits the stack at high temperature. It must also be considered, however, that the gas streams leaving the stack are required for preheating processes such that not all of the energy is available for recovery in turbines. Turbine expansion of the reactant species discharged from pressurized storage tanks can also be considered as a strategy to generate electrical power from the balance of plant.

Multi-stage expansion and compression

Implementation of the compressors and expansion processes noted above must be integrated with the heat exchange processes. This also allows for possible performance enhancement with multiple expansion and compression stages. For example, multi-stage compression with intercooling can be utilized to reduce compression power for large pressure ratios when using ambient air. Similarly, partially expanding pressurized gas streams exhausted from the stack through a turbine, and then extracting heat for preheating processes prior to a second stage of expansion increases turbine power generation by expanding gases at high temperatures.

2.5.3 Stack operating conditions

The operating conditions of the ReSOC stack influence the system efficiency through the electrochemical characteristic, thermal characteristic, and BOP operation. The relevant considerations for stack temperature, pressure, and gas compositions are explained here.

Stack temperature

The stack temperature is a primary factor in determining the electrochemical performance because of its influence on the ohmic resistance of the solid electrolyte and the kinetics of the charge-transfer reactions. However, various stack materials have been explored to show high efficiency operation over a wide temperature range (600-1000°C). The open-circuit voltage as predicted by the Nernst equation is also influence by temperature and increases with decreased temperature. The stack temperature impacts the thermal characteristic of the stack based on its influence on the thermochemical reactions (i.e., reforming and methanation). Finally, the stack temperature influences the balance of plant operation by, for example, establishing the preheating requirements and the temperature of the gas streams leaving the stack. Typically gas streams enter the stack at 100-200°C below the average stack operating temperature and are heated by convection from the MEA structure. The stack temperature

can be characterized by the average MEA temperature when accounting for axial temperature variations, although large thermal gradients and high temperature can degrade stack performance from mechanical stress and catalyst sintering.

Stack pressure

Pressurizing a ReSOC favorably reduces both the activation and concentration overpotentials by concentrating reactant species in both the fuel and oxidant channels. Furthermore, increasing the reactant partial pressure increases the open circuit voltage which is expected to increase roundtrip storage efficiency. Pressurization is seen as a key component of the thermal management strategy of promoting methanation to overcome endothermic electrolysis reactions.

Pressurized stack operation has a positive effect on stack performance, although the system performance may suffer from high pressurization based on excessive BOP power consumption. That is to say, the compressor power required to deliver oxidant to the stack increases with pressurization if the oxidant is ambient air. The previous section noted the possibility to mitigate this issue with alternate system configurations including oxidant stored in a pressurized tank or expansion turbines. However, the additional capital cost incurred with these configurations may not be necessary if the stack is operated at an intermediate pressure (e.g., around 5 bar).

Reactant composition

The prior composition discussion explained that thermal management, carbon deposition mitigation, and energy density are the important composition considerations and concluded that it is desirable to select a reactant composition that is highly carbonaceous (i.e., low hydrogen-to-carbon ratio), but does not exceed the carbon deposition boundary. Because the carbon deposition boundary is a function of temperature and pressure, more carbonaceous compositions can be used without deleterious effects at higher pressure and lower

temperature. Also, higher HTCR implies higher steam content in both the "fuel" and "exhaust" compositions which has additional impacts on system level operation related to the storage and balance of plant operation. For example, if a "stored vapor" approach is used, then higher H_2O content requires either higher temperature or lower pressure storage, both of which increase the required tank volume. Similarly a higher compression temperature is necessary when there is more H_2O in the gas stream. If active water management is employed to separately store liquid water, more energy is needed to evaporate the increased amount of reactant steam if the reactant requires a higher HTCR to mitigate carbon deposition.

The reactant utilization parameters (i.e., fuel utilization and reactant utilization) also affect system performance through the ReSOC thermal characteristic, electrical performance, and system balance of plant performance. Electrochemical performance is improved at lower utilization because of reduced reactant depletion. The thermal ReSOC characteristic is influenced by utilization which is demonstrated through analysis of the thermoneutral voltage (see Chapter 4). Utilization also impacts the balance of plant performance because, for example, at lower utilizations a larger flowrate of reactant and product species is transported between pressurized storage tanks and the ReSOC stack. This can lead to a larger influence of BOP operation on system performance due to higher turbomachinery power.

2.5.4 Storage operating conditions

The relevant storage operating conditions include temperature, pressure, and composition, although stored composition is determined from ReSOC stack operating conditions and is not considered an independent design parameter. The storage tank temperature impacts the volume required to store a given volume of gas. The storage temperature is also related to storage composition in the case of "stored vapor" in that a higher storage temperature is required to prevent condensation. When water is separately stored through active water management the storage temperature of the gas storage tanks (i.e., "fuel" and "exhaust") can be near-ambient to eliminate the need for complicated tank heating or cooling configu-

rations (e.g., for liquefied storage of CO_2 or CH_4). The storage pressure has implications on system performance similar to storage temperature in its impact on tank size and relationship to the stored gas composition. However, the tank pressure also has a significant impact on BOP power by defining the pressure ratio across the associated compressors and possibly turbines. The tradeoff between power consumption from the compressors and storage tank volume will be an important design decision illuminated by this work.

2.5.5 Configurations not considered in this work

The above discussion outlined the configurations and operating conditions that will be considered in the proposed system, however it is important to also note the configurations that are excluded from this research to maintain a practical scope. The excluded configurations can be generally categorized as relating to the storage configurations, alternate thermal management strategies such as coupled external heat sources or thermal energy storage, and auxiliary reactors.

Alternate storage configurations

Various storage configurations are possible for the hydrogen, syngas, or synthetic natural gas fuel compositions considered for fuel cell energy storage systems. In particular, the literature review in Chapter 3 will highlight the possibilities to store hydrogen in a magnesium-hydride material, metal red-ox, and store hydrogen in a sealed fuel-channel stack in constant contact with the ReSOC fuel electrode. An additional storage strategy that might be particularly complimentary with the thermal management strategy used in this research is to utilize the existing natural gas pipeline infrastructure for storage of fuel species. These storage configurations should be researched to assess feasibility, although this dissertation considers only gaseous and/or liquid storage in vessels (i.e., tanks or underground caverns).

Various implementations of tanked storage can also be considered which influence system cost and performance, although these are particularly relevant for dynamic system operation which is not considered in this proposed work. For example, rigid storage tanks necessarily

introduce a dynamic element to the system as the temperature and pressure of the stored gases drop while the tank is discharged. Variable volume storage can help to mitigate this dynamic variation. One possible fuel storage design has been proposed which consists of a single rigid tank that is divided into two chambers by a movable piston (or partition). One chamber discharges gases to the stack while the other chamber is filled with stack outlet gases to be used in the opposite mode of operation. Thus, the chambers within the fuel storage tank more closely approximate a variable-volume, constant pressure operating characteristic. Alternatively, it may be possible to use a single tank which contains a mixture of both "fuel" and "exhaust" compositions, although several characteristics of this approach are expected to lead to reduced efficiency such as reactant depletion and increased auxiliary compressor power.

External heat source

This research relies on the thermal management strategy of utilizing carbonaceous reactant compositions and selecting operating conditions which promote methanation in the electrolysis mode. The following literature review explains the possibility to use phase change materials for thermal energy storage between modes or couple the system with an industrial process that generates waste heat or solar-thermal source. System efficiency can benefit by using the waste heat in the electrolyzer to preheat reactant streams and evaporate water, allowing the ReSOC stack to operate more efficiently.

Auxiliary reactors

Auxiliary chemical reactors including methanation and steam-methane reforming reactors allow additional chemical conversion outside of the ReSOC stack. For example, a methanation reactor can be employed downstream of the stack in SOEC mode to increase the conversion of methane. The nickel catalyst in the ReSOC fuel electrode has good activity for methane formation and conversion approaches near to equilibrium. However, the ReSOC

must operate at relatively high temperatures for efficient electrochemical conversion, while methane formation is promoted at low temperature. An auxiliary reactor can operate at different conditions than the ReSOC stack so that the methane content of the stored "fuel" is not thermodynamically limited by the conditions of the ReSOC stack.

If the stored fuel is converted to a methane-rich mixture in an auxiliary methane reactor it might be unsuitable for direct feed into the ReSOC in SOFC mode. Thus a steam-methane reforming reactor can be utilized to partially reform the methane-rich "fuel" gas and steam mixture prior to electrochemical conversion in the ReSOC. Partial external reforming of natural gas is a typical system implementation for SOFC power systems to improve electrochemical performance and durability by mitigating coke formation and extreme temperature gradients from rapid reforming at the cell inlet. Additionally, both methanation and steam-methane reforming reactions are catalyzed by nickel, such that it may be possible to utilize the same reactor for both processes, favorably reducing capital cost. A separate study has considered the use of an auxiliary methanation reactor in ReSOC energy storage systems [95].

CHAPTER 3

LITERATURE REVIEW

Developing energy storage systems with ReSOC technology requires research attention toward both cell development and system design and integration. This literature review summarizes past work in both of these areas that has informed the following system design and analysis. First, a brief historical review of fuel cell energy storage is given.

The concept of generating hydrogen as a practical energy storage medium has be credited to J.S. Haldane in 1923 [96] in his paper read at Cambridge University [97]. In this paper, Haldane describes the future energy system in which metallic windmills supply the majority of total electricity demand. Surplus power from the windmills is supposed to electrolytically generate oxygen and hydrogen from water, which are stored in underground reservoirs and used to generate electricity during times of deficit power using "explosion motors" or "oxidation cells" [97]. This concept of electricity storage by means of hydrogen generation was again presented by Erren and Campbell in 1933 [98] as a way to utilize off-peak power and reduce coal imports. Several patents were also published in the early to mid 20th century pertaining to use of hydrogen as an electricity storage method with electrochemical cells [99–102].

More recent reviews of energy storage technologies describe fuel cell energy storage processes [2, 4, 16, 18, 78, 103], meaning the coupling of fuel cells and electrolysis cells with hydrogen and oxygen storage; although, the literature primarily associates this technology with use of low temperature reversible PEM or alkaline cells. However, these low temperature systems have limited roundtrip efficiency of 20-55% [104–106]. The so called "power-to-gas" method in which hydrogen or synthetic natural gas are generated by electrolysis is being used in Germany [107]. While power-to-gas and other similar approaches achieve the same energy storage function sought by the systems explored in this dissertation (i.e., mitigating renew-

ables curtailment), they are not reviewed here. Rather, this review focuses on stand-alone reversible systems that use high temperature solid oxide cells and integrate fuel synthesis, storage, and production functions into a single integrated system.

To the authors knowledge, the concept for using solid oxide cells in energy storage applications was initially indicated in a 1984 patent [108]. Shortly thereafter in 1987, D.J. Bents of NASA published a system study analyzing a regenerative solid oxide cell system intended to maintain constant power supply during space missions where the primary energy source is a photovoltaic array [61]. Following this initial system analysis, relatively little research and development effort was directed toward ReSOC systems; however, there has been a resurgence in the past 5 years including several patents related to ReSOC systems [109–113]. The following section describes the most relevant publications related to ReSOC energy storage system design and analysis.

3.1 System integration studies

Integrated energy storage systems using reversible solid oxide cells have been studied by academic and industry research groups. Most of the prior work is limited to computational modeling studies except for one laboratory scale prototype system. The studies encompass a range of modeling fidelities, thermal management strategies, and intended applications (e.g., scales and functions). One significant variation among the prior system studies is the method by which heat is provided to the stack during electrolysis operation to offset the endothermic electrochemical reactions. These systems also differ by the composition of the generated fuel (e.g., hydrogen, syngas, hydrocarbons), and the storage medium (e.g., tanks, geological features, metal hydrides, closed-stack). The most relevant studies are summarized in Table 3.1.

Bents [61] proposed a solid oxide regenerative fuel cell intended to provide back-up power supply in tandem with a photovoltaic array for space applications. The system converts pure hydrogen and oxygen to water to generate electricity in the fuel cell and produces hydrogen and oxygen from water in the reverse mode of operation. The thermal load required to

evaporate water and overcome the endothermic electrolysis reaction is provided from waste heat generated by operating the electrolyzer at a high voltage (i.e., lower efficiency). The study notes that overpotential of 220-400 mV is required to provide the required waste heat, depending on the system operating pressure. This high overpotential results in a relatively low roundtrip efficiency of about 40% estimated from system modeling.

Guan et al. [114] analyzed a reversible solid oxide cell system operating in either hydrogen production mode or dual-mode, where the system used natural gas to produce power during times of high electricity demand. The system was evaluated based on the cost of hydrogen production and found that operating in dual mode reduced to overall cost of hydrogen to $3.70/kg and $2.68/kg for a distributed and central station, respectively. The electrolysis system analysis found that hydrogen cost is minimized at a cell voltage of 1.2 V (i.e., below the thermoneutral voltage) where excess heat is supplied by burning natural gas. Roundtrip energy storage for peak-shaving and arbitrage applications was also analyzed and found to be beneficial if the electricity price difference was sufficiently high (i.e., 0.15 ¢/kWh vs. 0.21 ¢/kWh for centralized peak-shaving). Roundtrip efficiency was not reported.

McElroy et al. [115] developed a bench-scale (1 kW) ReSOC system that stores the excess heat generated during exothermic fuel cell operation (SOFC mode) in a phase change material (PCM), specifically lithium fluoride with a melting temperature of 848°C. The hot PCM then provided thermal energy to the stack during electrolysis (SOEC mode). The study used a 1 kW rated stack and determined that about 450 W of thermal energy could be transferred from the exothermic fuel cell stack to the PCM, but 490 W of resistive heating was required to maintain the PCM temperature because of heat loss to the environment. The excessive heat loss from the test-scale system was expected to be reduced for larger systems and improved insulation, although further publications from this research have not been found.

Bierschenk et al. [116] investigated promoting exothermic methanation in a ReSOC to offset the thermal energy requirements associated with the endothermic electrolysis reac-

tions. This method requires a carbonaceous reactant composition and employs the reverse of the chemical reactions observed in a solid-oxide fuel cell with internal steam-methane reforming. By carefully selecting the operating conditions include stack temperature and pressure, thermodynamic calculations show that the roundtrip energy storage efficiency is improved because the net thermal energy consumption in the electrolyzer is reduced. The analysis shows that high pressure (10atm) and/or low temperature (600°C) operation is necessary to promote the methanation reaction to the extent required for highly efficient energy storage.

Ren et al. [117] modeled a ReSOC storage system utilized bronze with a melting temperature of 1010°C as a thermal storage PCM to store excess heat from SOFC mode to help maintain high temperature operation during SOEC mode. Furthermore, this study employed a novel ReSOC stack design which has a sealed fuel chamber containing a mixture of hydrogen and steam. Modeling results indicate energy storage efficiencies of 42% and 64% at current densities of 0.649 and 0.325 A/cm^2, respectively. The ReSOC stack model utilizes pure oxygen as the oxidant delivered at an operating pressure of 70bar. Parasitic load and thermal management associated with the oxidant system is not discussed.

Akikur et al. [46] proposed a ReSOC system where electrical input is provided solely by an integrated photovoltaic (PV) array and used computational modeling to estimate system efficiency and cost of electricity. The proposed system uses excess electricity from the PV source to electrolyze steam and store the generated hydrogen. Electrolysis efficiency is enhanced by heat supplied from a parabolic trough solar collector to overcome endothermic electrolysis processes including preheating and evaporating stored water. When additional electricity is required (e.g., at night), the stored hydrogen is used to generate electricity in the SOFC. The study considers three modes of operation: (i) electricity produced from PV and hydrogen produced from electrolysis, (ii) electricity produced from PV and electricity produced from fuel cell, and (iii) power produced from fuel cell only. The reported CHP efficiencies for each operating mode are 20%, 23%, and 83.6%, respectively. Over a year of

operation, the annual cost of electricity for this system is estimated to be 0.068 \$/kWh.

Shiraki et al. [118] presented modeling results from a ReSOC system which includes hydrogen storage with a Mg-based metal hydride which is exothermic when absorbing hydrogen at 300°C with a heat release of 74 kJ/mol of absorbed hydrogen. The results show that the electrolysis efficiency is improved from 94% to 107% when the hydrogen storage system is implemented because the exothermic storage provides thermal energy to preheat and vaporize reactant steam. Release of hydrogen in SOFC mode requires an equivalent heat to the storage device, which is expected to be available from SOFC stack waste heat, although the efficiency in the power producing mode is not reported. Furthermore, parasitic losses from balance of plant, for example, are not mentioned in the efficiency calculation.

Al-musleh, et al. [119] presented modeling results for an electricity storage system using ReSOCs which converts between stored liquid hydrocarbon fuels and liquefied carbon dioxide. Reported roundtrip efficiencies are 55–59% and the storage of liquid reactants and products supposes to make gigawatt-hour storage feasible. The analysis considers both methane and methanol fuels synthesized from hydrogen produced in a solid oxide electrolysis cell and stored CO_2. The solid oxide cell is operated at the thermoneutral point in both modes (i.e., to supply heat for the electrochemical reactions in SOEC mode and supply heat to the fuel reformer in SOFC mode).

Er-rbib et al. [120] analyzed a reversible power-to-gas system in which hydrogen and carbon monoxide are produced by co-electrolysis in a solid oxide electrolysis cell and used to form methane in a Sabatier process. The system uses the natural gas network as a storage medium and is intended to generates power in the solid oxide fuel cell from reformed natural gas during times of electricity deficit. The system design is focused on optimizing reactor stages and product recycle in the methanation process to supply high purity methane to the natural gas pipeline (99.1 mol.% after three adiabatic reactor stages). Roundtrip efficiency and cost metrics are not reported.

Table 3.1: Summary of the system integration literature review.

Reference	System description	Analysis method	Key results
Bents, D.J., 1987 [61]	10 kW monolithic stack, tanked liq. H_2O with H_2, tanked O_2, variable pressure system (5-100 atm), external radiative cooling loop	Steady state computational system-level model, component sizing	40% roundtrip efficiency, higher energy density compared to established battery technologies
McElroy, J.F. et al., 2004 [115]	1 kW bench-scale system, steam-hydrogen conversion, LiF phase change material for thermal management	Bench-scale prototype experimental performance	63% roundtrip voltage efficiency, stack is not thermally self-sustained at this power rating
Guan, J., et al., 2006 [114]	Natural gas fueled fuel cell mode, heater-assisted H_2 production electrolysis mode	Steady-state computational system-level model, techno-economic performance	Dual-mode operation reduces cost of electricity, lowest cost of hydrogen production at 1.2 V/cell
Bierschenk, D.M., et al., 2011 [116]	Tanked synthetic fuel and exhaust gases, highly simplified system representation	Thermodynamic calculations, cell-level experimental results showing methane synthesis in SOEC	Roundtrip efficiency > 80% possible by operating at 600°C and 10 atm with carbonaceous reactants
Al-musleh, E.I., et al., 2014 [119]	Closed cycle between liquid CO_2 and liquid carbon fuels, SOEC hydrogen production followed by synthetic fuel synthesis reactors	Computational system-level model, steady-state, exergy analysis	Roundtrip efficiency of 55-59%, various C1 and C2 fuels have good properties for the proposed system

The studies reviewed above and summarized in Table 3.1 illustrate the various possible thermal management strategies that have been considered for implementing energy storage with ReSOCs. The scarcity of studies exploring any single thermal management strategy suggests that additional research is required to clarify the advantages and disadvantages of each approach. Furthermore, comprehensively evaluating ReSOCs for energy storage applications requires first establishing which thermal management strategies are most promising. The dissertation proposed in this document explores the strategy proposed by Bierschenk et

al. [116] of operating a ReSOC with carbonaceous reactant compositions at conditions which favor the methanation reaction as a significant component of an overall thermal management strategy. Successful implementation of this proposed system requires operating the cell under conditions that are somewhat different than typical solid oxide cells including galvanic cycling, intermediate temperature, and elevated pressure. A brief review of the capabilities of ReSOCs under these conditions is provided next.

3.2 ReSOC research and development critical to energy storage applications

Along with the system level considerations associated with ReSOC energy storage systems, cell-level challenges persist relating to durability and operating ranges. Cell development is not a focus of this research, although understanding performance capabilities of the technology is vital in accurately representing ReSOC systems through computational modeling. Much of the literature is based on individual mode operation (i.e., either fuel cell or electrolysis operation only); however, motivated by more recent interest in using ReSOCs for energy storage some studies consider cyclic operation of a ReSOC in both modes.

Xu et al. [50] proposed a device in which the ReSOC is coupled with a metal red-ox hydrogen storage unit. Experimental results indicate a high roundtrip efficiency of 91.5%, although the kinetics of the red-ox storage method limit the operating current density to 50 mA/cm^2. Furthermore, this study presents results from 10 charge/discharge cycles of 10 minutes each which shows stable operation in both modes. Several additional publications from the same research group have explored durability and performance of ReSOCs for storage applications including intermediate temperature operation [121, 122], additional considerations related to the iron-based red-ox storage process [123], and computational modeling of the proposed device [124].

Zhang et al. [125] developed an experimental testing rig to evaluate performance of ReSOCs in both modes. Durability tests were performed for 100-4000 hours on cells provided by MSRI, Ceramatec, St. Gobain, and SOFCPower which had been developed for use as solid oxide fuel cells. During electrolysis mode testing, the Ceramatec button cell showed

performance improvement, while the MSRI test showed low degradation, and the St. Gobain and SOFCPower cells showed rapid degradation. This report notes that cells developed specifically for SOFC applications are not necessarily directly applicable for use as electrolysis cells or ReSOCs.

Hughes et al. [51, 126] evaluated LSM-YSZ | YSZ | LSM-YSZ symmetrical cells under galvanic cycling conditions. No measurable performance degradation was recognized for current densities below 0.5 A/cm^2, although rapid increase in both ohmic and polarization resistance was observed for current densities of 1.5 A/cm^2. Another study [60] also shows no degradation at 0.5 A/cm^2 for 1000 hours of cyclic operation and further attributes the degradataion at 1.5 A/cm^2 to delamination of the electrode. The degradation rate decreases with decreased current density and decreased cycle duration.

Wonsyld et al. [127] reported durability performance of 10- and 20-cell ReSOC stacks operating on under steam-electrolysis, co-electrolysis, and syngas-fueled power producing modes. No degradation was observed over the course of 113 2-hour cycles for the 10-cell stack, while the 20-cell stack operating at higher temperature showed low degradation rates of 1.44 and 0.10 mΩ/cm^2-cycle were shown in electrolysis and fuel cell modes, respectively. The degradation rate is suggested to be low in the temperature range of 760–790°C.

The systems modeled in this dissertation rely on operating ReSOCs under conditions which are not typical in state-of-the-art SOFCs or SOECs, specifically at intermediate temperature and high pressure. However, significant research attention has been devoted to these operating conditions to improve efficiency and reduce cost (see Section 1.1.2). Alternative electrolyte materials are considered with higher conductivity than YSZ at low-to intermediate-temperatures [31, 128, 129], for example Sr- and Mg-doped lanthanum gallate [73], Sm- or Gd-doped ceria (SDC or GDC) [130–132], and Sc-stabilized zirconia (SSZ) [133]. This review is not intended to comprehensively detail the present state of reduced temperature solid oxide cell research. Rather, it provides some context to show that efficient ReSOC operation has been demonstrated and is being improved over a wide temperature

range of 500-1000°C. Operating characteristics of LSGM-electrolyte ReSOCs are the focus of this dissertation and some additional details on these promising intermediate temperature cells is included in Chapter 5.

Pressurized ReSOC operation has been widely considered to improve cell and system efficiency. Pressurized operation reduces kinetic and concentration overpotentials and increases the open-circuit voltage (most favorable for SOFC mode operation). Various studies have shown the results of pressurization at the cell level both experimentally [59, 134–137] and theoretically [56, 57, 138], and at the system level [55, 63, 65]. Most of the research on pressurized cells explores pressures below 20 bar.

CHAPTER 4

THERMODYNAMIC CONSIDERATIONS

Thermodynamic analysis is useful in determining theoretical performance of any thermochemical system. For ReSOC energy storage systems, thermodynamics can predict the theoretical maximum roundtrip efficiency by considering the energetics of both fuel cell and electrolysis processes. Another benefit of analyzing the system thermodynamics is to understand the performance impact of key operating conditions. For the system under consideration, which operates with carbonaceous reactant mixtures, the energy conversion process in the ReSOC stack involves both electrochemical and heterogeneous reactions, making the thermodynamic analysis more complicated than for a single reduction-oxidation reaction. In this chapter, thermoneutral and reversible (i.e., open-circuit) voltage parameters are defined, which represent the total energy and electrical energy associated with an electrochemical conversion process, respectively. The thermoneutral voltage has been used previously in water electrolysis applications to understand energetic system requirements, but here it is defined more broadly to account for the carbonaceous compositions used in the present system. By analyzing these voltage parameters over a range of conditions, the performance impact of ReSOC operating temperature, pressure, reactant composition, and utilization is understood. Conclusion gleaned from these parametric studies help to explain the effect of these operating parameters on system level studies in the following chapters.

4.1 Ideal ReSOC operation for energy storage applications

Before exploring the effect of operating conditions on ReSOC thermodynamics, it is important to consider ideal operation of ReSOCs for energy storage. Here, ideal operation is considered to be maximum roundtrip efficiency with considerations for both stack and system efficiency loss. In the following subsections, the theoretical roundtrip stack efficiency is defined. Next, the theoretical roundtrip efficiency is considered for electrochemical reactions

64

including steam/hydrogen, CO/CO_2, and methane red-ox. Finally, the thermoneutral and reversible voltage parameters are defined and their utility in determining desirable operating conditions is explained from the viewpoint of stack and system operation.

4.1.1 Theoretical roundtrip stack efficiency

For roundtrip energy storage in reversible solid oxide cells, the theoretical maximum roundtrip stack efficiency is defined as the maximum electrical energy generated in fuel cell mode divided by the minimum total energy required in electrolysis mode.

$$\eta_{\text{RT,thermo}} = \frac{\text{max energy generated by fuel cell}}{\text{min energy required by electrolysis cell}} \tag{4.1}$$

In most red-ox reactions, for example steam/hydrogen or CO_2/CO, the magnitude of the enthalpy change is larger than the magnitude of the Gibbs free energy change and the thermodynamic roundtrip efficiency is defined as:

$$\eta_{\text{RT,thermo,}\Delta\text{S}<0} = \frac{\Delta G}{\Delta H} \tag{4.2}$$

where the maximum work generated in fuel cell mode is the change in Gibbs free energy, ΔG and the total energy required in electrolysis mode is the change in enthalpy, ΔH. However, this definition is only applicable when the change in entropy, ΔS is negative for the oxidation (i.e., fuel cell) process. In other words, if the value of ΔS is positive, Equation 4.2 suggests efficiency exceeding 100% because ΔH and ΔG are both negative values and $\Delta H = \Delta G + T\Delta S$.

Here, ΔH and ΔG represent the change in the thermodynamic property of an oxidation process; although, the property change of the reduction process is simply the negative of the oxidation process. In other words, the represented processes may be, for example, H_2 + $1/2O_2$ $\leftrightarrow$ H_2O or "fuel" $\leftrightarrow$ "exhaust", where the given ΔH and ΔG are for the forward direction (i.e., oxidation) and reduction is represented by the reverse processes.

For the case of positive entropy change of oxidation (i.e., $\Delta S > 0$), the efficiency definition is:

$$\eta_{\text{RT,thermo,}\Delta S>0} = \frac{\Delta H}{\Delta G} \tag{4.3}$$

where the maximum energy generated by the fuel cell is equal to the enthalpy change. A positive entropy change indicates that the electrochemical oxidation reaction has a deficit of thermal energy, which must be supplied by either heat or electricity (i.e., increased overpotential). Said differently, the fuel cell process can generate net energy equal to the enthalpy change, which is smaller than the maximum work output (i.e., Gibbs free energy change) because the endothermic process must be overcome by supplying the difference, $T\Delta S$. This is analogous, but opposite, to typical steam electrolysis where a portion of the energy required for hydrogen generation can be supplied as heat (i.e., up to a value of $T\Delta S$). The denominator in Equation 4.3 suggests that the electrolysis process requires an electricity input equal to ΔG, although the generated fuel only has an energy content equal to ΔH. The excess electricity supplied to the electrolysis process (i.e., $T\Delta S$) is converted to waste heat because the electrochemical reaction is net exothermic.

It is important to note that oxidation processes with a positive entropy change are uncommon (e.g., complete oxidation of carbon to carbon monoxide), and the theoretical roundtrip efficiency of most red-ox reactions is described by Equation 4.2. That being said, the following results will show that for carbonaceous mixtures under certain operating conditions, the overall entropy change of the process (i.e., "fuel" $\rightarrow$ "exhaust") is positive, due to high rates of in-situ fuel reforming coupled with electrochemical oxidation.

Finally, in the case of $\Delta S = 0$, the thermodynamic roundtrip efficiency is 100%. In other words, both fuel cell and electrolysis processes are thermoneutral, meaning that all electricity input to the electrolyzer can theoretically be converted to chemical energy of the produced fuel, and all chemical energy stored in the fuel molecules can theoretically be recovered as electricity.

The theoretical efficiency definitions above assume that all energy conversion occurs in the ReSOC stack, which is not strictly true under configurations where auxiliary reactors and/or turbomachinery interact in the system BOP. For example, including a stack tail-gas expander can recuperate electrical energy from waste heat in the electrochemical conversion, allowing the roundtrip system efficiency to potentially exceed theoretical roundtrip stack efficiency as defined in Equation 4.1. Because the energy recovered from waste heat is limited by the waste heat available, the theoretical system efficiency is ultimately still limited to <100%.

4.1.2 Pure red-ox reaction thermodynamics

The thermodynamic efficiencies defined in the previous subsection are now used to compare the theoretical roundtrip performance of different red-ox chemistries, including steam-hydrogen (H_2 + $1/2O_2$ ↔ H_2O), carbon dioxide-carbon monoxide (CO + $1/2O_2$ ↔ CO_2), and methane (CH_4 + $2O_2$ ↔ $2H_2O$ + CO_2). The ΔH, ΔG, and theoretical efficiency for these three reactions are given as a function of temperature in Figure 4.1 - Figure 4.3. The thermodynamic quantities are converted to voltage units by dividing by the charge transfer associated with the red-ox reaction (i.e., "nF"), where n is the number of electrons transferred in each reaction (e.g., n=2 for steam-hydrogen and carbon monoxide-carbon dioxide, and n=8 for methane red-ox). Notably these reactions all have a negative entropy change for oxidation, so the efficiency is calculated by Equation 4.2.

For the steam-hydrogen case (see Figure 4.1), the maximum roundtrip efficiency decreases with increased temperature because more waste heat ($T\Delta S$) is generated during fuel cell operation. The electrical energy requirement for electrolysis is equivalent to the maximum electricity generation in fuel cell mode (ΔG), although the additional energy ($T\Delta S$) must be provided as either heat or electricity (i.e., via increased overpotential). The theoretical maximum efficiency for the steam-hydrogen case falls below 80% at 625°C. The CO/CO_2 red-ox shows a similar trend to steam-hydrogen (see Figure 4.2), although has slightly worse performance compared with the steam-hydrogen case due to higher entropy change. Operating temperature below 400°C is required to achieve >80% roundtrip efficiency. The
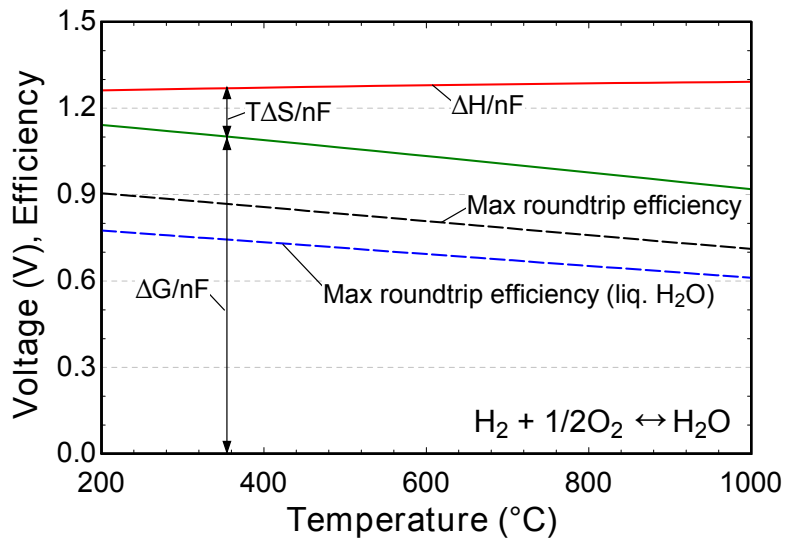
Figure 4.1: Thermodynamic performance of steam-hydrogen red-ox for gaseous and liquid reactants as a function of temperature.
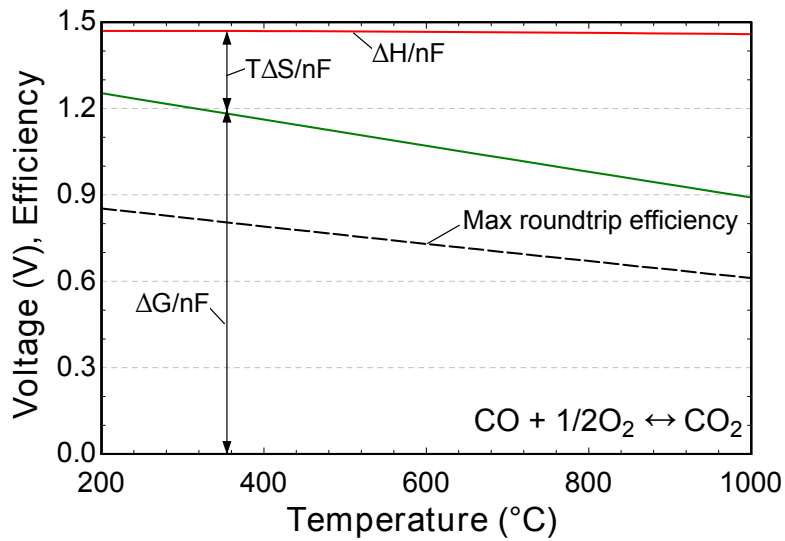
Figure 4.2: Thermodynamic performance of carbon monoxide-carbon dioxide red-ox for gaseous reactants as a function of temperature.
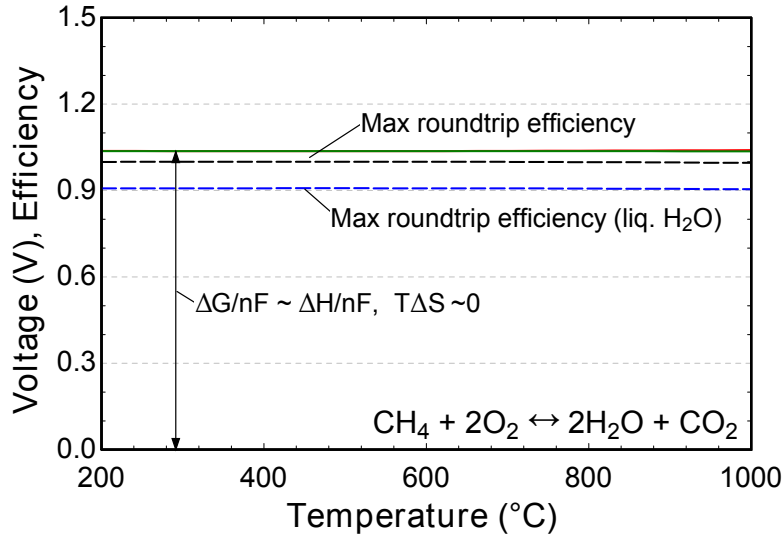
Figure 4.3: Thermodynamic performance of methane red-ox for gaseous and liquid reactants as a function of temperature.

thermodynamic performance of the methane red-ox reaction is shown in Figure 4.3. For this reaction, the $T\Delta S$ term is nearly zero, indicating almost complete reversibility, and nearly 100% theoretical efficiency independent of operating temperature.

The thermodynamic results in Figure 4.1 and Figure 4.3 also include the maximum roundtrip efficiency when the reactant water is considered to be in the liquid phase by including the latent heat of water vaporization in the reaction enthalpy. This calculation indicates the efficiency penalty associated with needing to boil water, which is around 10 percentage points, and motivates system designs where H_2O is maintained in a vapor phase during storage to achieve higher roundtrip efficiency.

Because of several practical operating limitations, including the inability to directly electrochemically convert or produce CH_4, the ideal case of methane red-ox cannot be executed. However, the operating conditions and catalytic activity of ReSOC material sets enable indirect methane red-ox reactions. Carbon deposition and reactant utilization limitations also require that the ReSOC reactants and products are not pure or in stoichiometric ratios as indicated by the reaction equation in Figure 4.3. In fact, the tanked gases will be some mixture of syngas and exhaust species falling somewhere in between the pure hydrogen, carbon

69

monoxide, and methane oxidation cases. The thermodynamics of the practical operating case can be assessed by assuming equilibrium of reactants and products; this method is described in Section 4.2 and results presented in Section 4.4. First, the next subsections define the thermodynamic voltage parameters and explain additional thermodynamic considerations from the alternate viewpoint of system operation as opposed to the reaction chemistry.

4.1.3 Thermoneutral voltage

The thermoneutral voltage, V_{TN} (also referred to as thermal-neutral voltage or reaction voltage) is a useful parameter for quantifying the heating and/or cooling requirements of a ReSOC and has been employed previously in the literature in the context of thermal management for steam electrolysis and co-electrolysis studies [30, 32, 56, 67, 139–142]. The thermoneutral voltage is typically defined as the change in enthalpy (i.e., heat of reaction) associated with the electrochemical reaction per unit of charge transferred:

$$V_{TN,\mathrm{rxn}} = -\frac{\Delta h_{\mathrm{rxn}}}{nF} \tag{4.4}$$

where Δh_{rxn} is the enthalpy of an electrochemical oxidation reaction. The thermoneutral voltage for the steam-hydrogen electrochemical red-ox reaction (Equation 2.1) is $V_{TN,\mathrm{H2/H2O}}$ = 1.29V at 800°C as shown in Figure 4.1.

Figure 4.4 shows $V_{TN,\mathrm{H2/H2O}}$ on a typical current-voltage plot and the operating regions (voltages) where heat is generated or consumed. In fuel cell mode, net heat is generated at all current densities because the energy generated by the exothermic fuel cell reaction is greater than the energy removed from the stack as electric power. Thus, the heat generation region in SOFC mode corresponds with cell voltages below the thermoneutral voltage (i.e., $V_{\mathrm{SOFC}} < V_{TN}$). If the ReSOC temperature is too high it may be irreversibly damaged and become unsafe, so the net exothermic process must be offset. Solid oxide fuel cell stacks are cooled by excess oxidant flow and/or internal heat sinks, such as endothermic fuel reforming.

In contrast, an electrolyzer must be operated at a cell voltage greater than the thermoneutral voltage ($V_{\mathrm{SOEC}} > V_{TN}$) to generate net heat. When this condition is satisfied, the
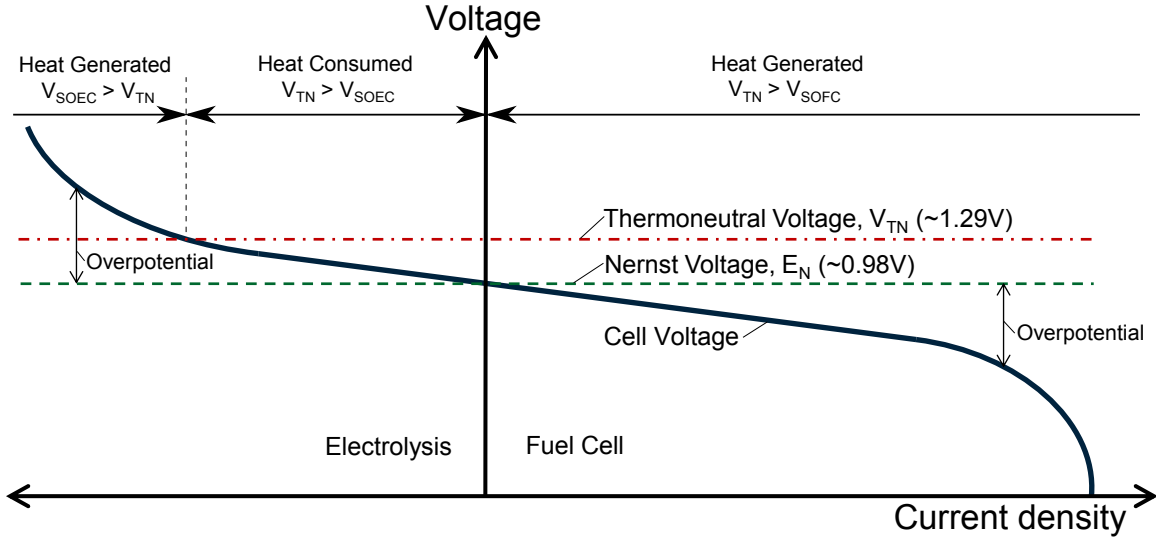
Figure 4.4: Representative current-voltage characteristic showing regions of excess heat generation and heat deficit.

electrical energy supplied to the stack is greater than the thermal energy required by the endothermic electrolysis reaction.

To generate net heat in both modes of operation without an external heat source, the following condition must be met:

$$V_{\text{SOEC}} > V_{TN} > V_{\text{SOFC}} \qquad (4.5)$$

This condition can be satisfied with reasonably low overpotential if the thermoneutral voltage is reduced. Motivated by increasing interest in co-electrolysis of H_2O and CO_2, some studies have broadly defined the thermoneutral voltage to include the thermal impact of all chemical and electrochemical reactions occurring within an SOEC stack. By defining thermoneutral voltage in this way, its value can be manipulated by careful selection of the operating conditions. For example, Bierschenk et al., [116] have explored the dependence of thermoneutral voltage on operating temperature and pressure in the context of a ReSOC energy storage system in which tail-gases are captured and tanked (i.e., similar to that shown in Figure 1.4). Sun et al., [56] have shown the effect of operating temperature, pressure, fuel utilization, and fuel composition on thermoneutral voltage in the context of synthetic

71

hydrocarbon fuel production via co-electrolysis.

4.1.3.1 Deriving the thermoneutral voltage

A general definition of the thermoneutral voltage is the cell voltage at which the net heat consumed by all of the cell reactions (both electrochemical and chemical) exactly balances the heat generated by the passage of current through the internal cell resistance, thereby resulting in no net heat evolution from the cell. In other words, it is the voltage at which the ReSOC operates both isothermally and adiabatically. This definition is particularly useful when considering carbon-containing feedstocks in which either electro-oxidation or electro-reduction and thermal reforming reactions occur. In practice, a ReSOC with internal thermal reforming reactions will not be strictly isothermal because of temperature gradients associated with the finite reaction rates. For these cases, the thermoneutral voltage has been previously defined as the cell voltage that causes the gas temperature at the cell outlet to equal the temperature of the gases entering the cell [143].
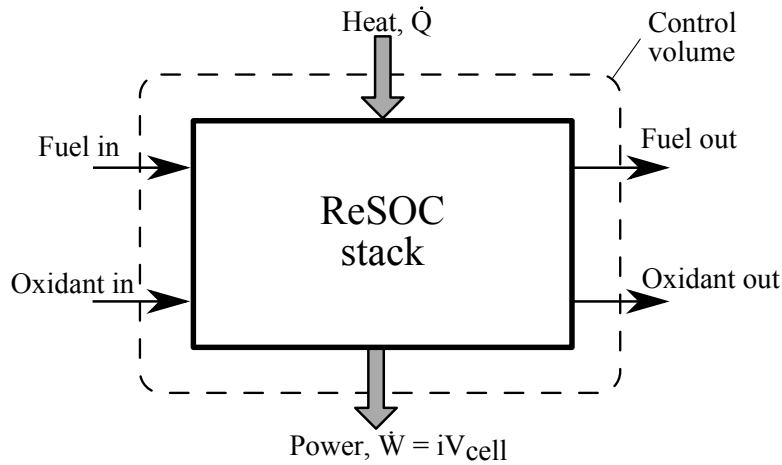
Figure 4.5: Control volume and associated gas stream and energy flows for a ReSOC stack.

A mathematical definition for V_{TN} is developed from a steady-state energy balance on the ReSOC stack shown in Figure 4.5:

$$\dot{Q} - \dot{W} = (\dot{H}_{\text{fuel,out}} + \dot{H}_{\text{ox,out}}) - (\dot{H}_{\text{fuel,in}} + \dot{H}_{\text{ox,in}}) \qquad (4.6)$$

where $\dot{Q}$ is the net heat transferred to the ReSOC from the environment, $\dot{W}$ is the electric power generated, and $\dot{H}$ is the enthalpy rate of each of the gas flow streams. The electric power is further defined as $\dot{W} = iV_{\text{cell}}$ where i is the current and V_{cell} is the cell voltage (i.e., V_{SOFC} or V_{SOEC}). When the ReSOC is operated adiabatically ($\dot{Q} \to 0$) and isothermally, the thermoneutral voltage definition is satisfied such that the cell voltage becomes the thermoneutral voltage ($V_{\text{cell}} \to V_{TN}$). Applying these conditions to Equation 4.6, the thermoneutral voltage is revealed as:

$$V_{TN} = -(\Delta \dot{H}_{\text{fuel}} + \Delta \dot{H}_{\text{ox}})/i \qquad (4.7)$$

To more easily interpret the general definition given in Equation 4.7, the change in enthalpy of the flow streams, $\Delta \dot{H}$ can be expressed alternatively as the enthalpy change associated with the reactions occurring within the ReSOC:

$$V_{TN} = -\left(\frac{r_{\text{redox}}}{i}\Delta h_{\text{redox}} + \frac{r_{\text{reforming}}}{i}\Delta h_{\text{reforming}} + \frac{r_{\text{shift}}}{i}\Delta h_{\text{shift}}\right) \qquad (4.8)$$

where r_k and Δh_k are the rate and enthalpy of reaction k as represented by reaction Equations 2.1–2.3. The above substitution is specific to a cell in which the reactants are limited to the 6-species involved in Equations 2.1–2.3. Additional reaction equations must be added to Equation 4.8 when other reactive species are present (e.g., carbon, ethane, propane, etc.).

In Equation 4.8, V_{TN} is reduced by increasing $r_{\text{reforming}}$ (methane-reforming / methanation) and reducing r_{shift} (water-gas shift / reverse shift). V_{TN} is most significantly affected by changes to $r_{\text{reforming}}$ because $\Delta h_{\text{reforming}}/\Delta h_{\text{shift}} \approx 6.5$. This mathematical interpretation affirms that promoting endothermic steam-methane reforming in SOFC mode and exothermic methanation in SOEC mode reduces the thermoneutral voltage.

The derivation for Equations 4.8 is independent of whether the ReSOC is operated in fuel cell or electrolysis mode; the current and each of the reaction rates have opposite signs if the polarity is switched. Additionally, consider that for a fuel stream with no carbon containing species (CO, CO_2, CH_4), $r_{\text{reforming}}$ and r_{shift} equal zero. For this special case, Equation 4.8 is equivalent to Equation 4.4 because of the relationship between the current

and the electrochemical reaction rate, $i = r_{\text{redox}} n F$.

4.1.3.2 Quantifying thermal requirements using the thermoneutral voltage

The thermoneutral voltage can be used to quantify the amount of excess heat generated by an isothermal ReSOC. By combining Equations 4.6 and 4.7, net heat consumed by an isothermal stack is calculated as:

$$\dot{Q} = i(V_{\text{cell}} - V_{TN}) \tag{4.9}$$

Net heat is generated by the stack if $\dot{Q} < 0$. Significant differences between V_{cell} and V_{TN} result in large magnitude $\dot{Q}$ which may negatively impact system roundtrip efficiency through increased BOP power consumption. For example, if there is a large amount of heat generated by the ReSOC, an increased oxidant flow is required to cool the stack leading to increased compressor power. On the other hand, in designing a distributed energy storage technology it is important that the system generate enough heat for the system processes (e.g., preheating stack inlet steams) as well as to account for losses to the environment.

The thermoneutral voltage may be further understood by exploring the relationship between the net heat consumption of a ReSOC and the thermodynamics of a red-ox reaction. For example, consider a pure red-ox reaction such that the thermoneutral voltage is calculated by Equation 4.4. By substituting Equations 2.6 and 4.4 into Equation 4.9 and recognizing that $V_{\text{cell}} = E_N - \eta$, the net heat consumed by the ReSOC is calculated as:

$$\dot{Q} = i(-\frac{\Delta g}{nF} - \eta + \frac{\Delta h}{nF}) = i(\frac{T \Delta s}{nF} - \eta) \tag{4.10}$$

where Δs is the entropy change of the reaction. When the cell is operated at the thermoneutral voltage, no net heat is consumed by the cell, leading to:

$$\eta_{TN} = \frac{T \Delta s}{nF} \tag{4.11}$$

where η_{TN} is the overpotential required to reach the thermoneutral voltage. For the hydrogen oxidation reaction, for example, the change in entropy is negative, such that a negative overpotential is required to operate at the thermoneutral voltage. This implies drawing

power from a fuel cell that is operated above open-circuit voltage, which is not a physically realistic result. It does, however, highlight the exothermic nature of the oxidation reaction at any overpotential (see also Figure 4.4). Alternatively, when considering the steam electrolysis reaction, Δs is positive and the overpotential required to reach the thermoneutral voltage is equivalent to the thermal energy required by the reaction ($T\Delta s$) per unit of charge transferred.

4.1.4 Reversible voltage

The reversible voltage was previously defined for a single red-ox reaction in Section 2.2.3 as the change in Gibb's free energy divided by the charge transfer. For the same reasons discussed in the previous section to broaden the definition of the thermoneutral voltage, here the reversible voltage, E_N is defined as the change in Gibb's free energy of the isothermal and isobaric process depicted in Figure 4.5:

$$E_N = -(\Delta \dot{G}_{\text{fuel}} + \Delta \dot{G}_{\text{ox}})/i \tag{4.12}$$

where E_N represents the maximum voltage of the oxidation process and the minimum voltage required in electrolysis mode for a general roundtrip electrochemical conversion. Importantly, the reversible voltage definition in Equation 4.12 simplifies to Equation 2.6 for a single red-ox reaction with pure inlet streams. However, this broader definition captures additional affects that are neglected when a single red-ox reaction is assumed, for example the effects of reactant incomplete conversion and dilution.

4.1.5 Approach to selecting desirable ReSOC operating conditions

An energy storage system based on ReSOC technology has several unique attributes, and achieving high roundtrip efficiency necessitates balancing what are essentially competing effects in each mode of operation. In particular, selecting operating conditions that are typically attractive when operating in forward, power producing mode (i.e., SOFC operation), such as at elevated pressure or temperature, generally do not produce a similarly

favorable performance enhancement when the cell is operated in reverse (i.e., in electrolysis mode). The utility of the thermoneutral voltage as a performance parameter becomes more apparent when trying to resolve these conflicting tendencies in selecting desirable operating conditions.

The discussion in this chapter, as well as Chapter 2 has illustrated the benefits of operating a ReSOC stack at low overpotential (i.e., high V_{SOFC}, low V_{SOEC}) to achieve high round-trip efficiency (Section 2.5.1) and reducing the thermoneutral voltage to reduce the BOP energy requirements (Section 4.1.3.2). To summarize, in SOFC mode, it is desirable to operate the stack at a voltage slightly below V_{TN} to generate heat but with relatively low stack cooling requirements and slightly below E_N for high stack efficiency (i.e., low overpotential). In SOEC mode, it is desirable to operate slightly above the V_{TN} to generate a small amount of heat which can enable self-sustaining thermal operation and slightly above E_N for high stack efficiency. These conditions are achievable when V_{TN} is lowered to near E_N, such that:

$$V_{TN} \approx E_N \tag{4.13}$$

This ideal operating point is consistent with the efficiency definitions in Section 4.1.1, where 100% theoretical efficiency is predicted when $\Delta H = \Delta G$, in that V_{TN} and E_N are calculated from ΔH and ΔG, respectively. Equation 4.13 is used throughout the parametric analysis results in this chapter to assess "desirable" stack operating conditions that are expected to result in high roundtrip system efficiency.

4.2 Calculation procedure for estimating thermodynamic voltages

The thermoneutral and reversible voltages are calculated using Equations 4.7 and 4.12, respectively. Calculating these voltages is complicated for a carbonaceous fuel because the impact of heat generated and consumed by the fuel reforming chemical reactions must be accounted for. The rates of these reactions depend on the change in fuel composition across the stack. Therefore, V_{TN} and E_N can be quantitatively estimated when the fuel compositions

at both the inlet and outlet of the stack are specified and the appropriate molar balances are applied. For this analysis, V_{TN} and E_N are estimated by assuming that the fuel compositions at the stack inlet and outlet are in equilibrium at the stack operating conditions (T, p) and that the ReSOC is isothermal and isobaric.
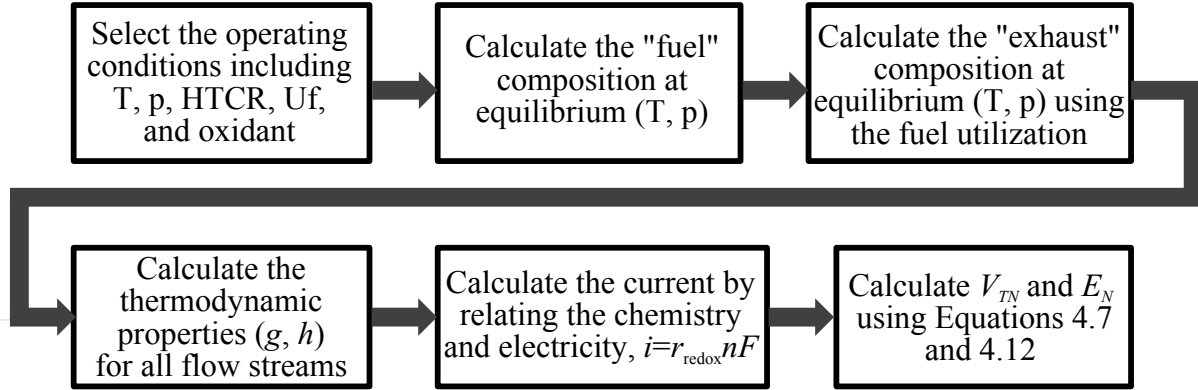
Figure 4.6: Calculation sequence for estimating the thermoneutral and reversible voltages with equilibrium compositions

The calculation sequence for estimating the voltage parameters is shown in Figure 4.6. This procedure involves selecting the ReSOC operating temperature, pressure, fuel utilization, and inlet fuel composition. The species mole fractions in the reactant and product mixtures are calculated from a given hydrogen-to-carbon ratio, fuel oxygen content, and fuel utilization. The considerations for selecting appropriate HTCR and fuel oxygen content are given in Section 4.3. The "fuel" mole fractions (i.e., SOFC inlet composition) are calculated from a selected HTCR and equilibrium conditions. Next, the "exhaust" composition (i.e., SOEC inlet) is calculated at equilibrium from a prescribed fuel utilization. The oxidant / sweep-gas stream flowrate and composition must also be selected to account for the enthalpy and Gibbs free energy change in the oxygen channel. For the results given here, the oxidant / sweep-gas is set to pure oxygen at an arbitrarily large flowrate, which eliminates the effect of dilution when, for example, air is used. However, the formulation of Equation 4.12 is able to capture the effects of oxidant dilution through the mixing entropy in the Gibbs free energy calculation.

The thermodynamic properties of the flow streams are found from the known inlet and outlet gas compositions and an arbitrary flowrate. The current is calculated from the rate of the electrochemical reaction, which can be determined based on a molar balance between the "fuel" and "exhaust" streams. The current could alternatively be calculated by considering the rate of change in atomic oxygen content between the two known gas compositions and the fact that each oxygen atom has an associated charge transfer of 2 electrons. Finally, the thermoneutral and reversible voltages are calculated from Equations 4.7 and 4.12.

Calculating the thermodynamic properties of the inlet and outlet compositions (i.e., "fuel" and "exhaust") requires selecting the inlet flow rate. The selected flow rate is arbitrary when calculating the thermodynamic voltages under the present assumptions because the rates of reactions are proportional to the current. Another way to consider this is that the extensive parameters (current, molar flow rates, reaction rates) scale proportionally.

The thermodynamic voltages are independent of the mode of operation for the assumptions used in this analysis. Specifically, when considering SOEC mode, the rates of reaction and current are the same magnitude as in SOFC mode, but opposite sign. However, V_{TN} and E_N may differ between operating modes for systems where chemical conversion occurs outside of the ReSOC stack (e.g., for systems with auxiliary reforming or fuel synthesis reactors, or when chemical conversion occurs during storage). The equilibrium assumption used here is reasonable for an ReSOC system application because the stack inlet gas composition is equivalent to the stack outlet composition in the opposite mode of operation and near-equilibrium is typically achieved in ReSOCs [144].

4.2.1 Thermodynamic property values

When generating results using the calculation procedure described above, it is essential to use appropriate thermodynamic property formulations and equations of state. A thermodynamic analysis of water electrolysis by Todd et al. [139] revealed that errors of 10% and 22% were observed for thermoneutral and reversible voltages, respectively, if ideal gas was assumed when calculating thermodynamic properties. The errors were calculated by

comparison to thermodynamic properties calculated using a non-dimensional Hemlholtz free energy function based on high fidelity equations of state from, e.g., the International Association of Properties of Water and Steam, National Institute of Standards and Technology, and International Council for Science : Committee on Data for Science and Technology. The error observed from the ideal gas method increases with increased temperature and pressure up to 1000 K and 100 bar.

Here, two thermodynamic property methods are compared. The first uses an ideal gas relationship and Kay's mixing rule with enthalpy and Gibbs free energy properties taken from Engineering Equation Solver, such that the mixture enthalpy and entropy are calculated by:

$$h_{\text{mix}} = \sum x_i h_i(T) \tag{4.14}$$

$$g_{\text{mix}} = \sum x_i (h_i(T) - T s(T, p_i)) \tag{4.15}$$

The second method uses MultiFlash commercial software package (Version 4.3) with Redlich-Kwong-Soave (RKS) equation of state. The results comparing these two methods over a range of temperatures and pressures are given in Figure 4.7. These results indicate that errors less than 1.1% and 0.5% are expected from the ideal gas assumption for the thermoneutral and reversible voltages, respectively. The error increases with increased pressure and $< 0.1\%$ error is observed at 10 bar. The remaining thermodynamic results are calculated using the ideal gas assumption. System modeling presented in the later sections uses real-gas properties as found in Engineering Equation Solver with ideal mixing.

4.3 Gas composition considerations

A discussion of the reactant gas compositions is given in Section 2.2.2 including considerations for carbon deposition, energy density, and thermal management. Here, those considerations are used to inform the selection of compositions to be used in the following thermodynamic calculations. Recall that the system operates with two distinct compositions, referred to as the "fuel" and "exhaust" which have equivalent hydrogen-to-carbon
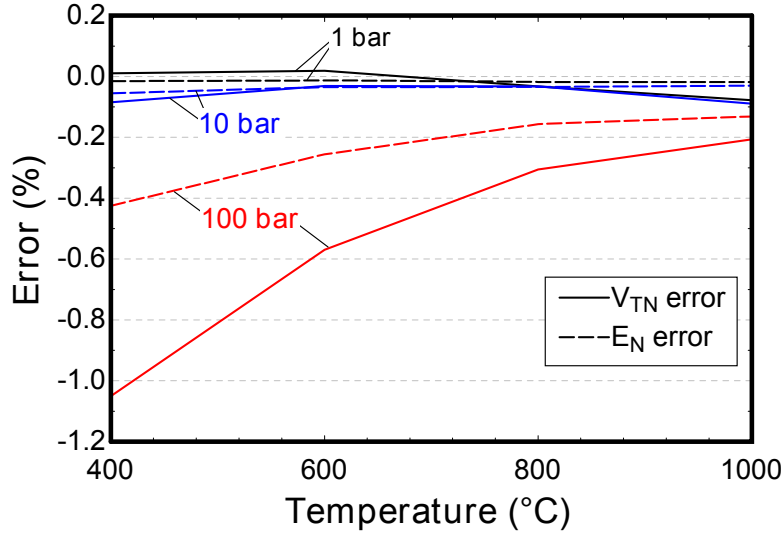
Figure 4.7: Error between ideal gas and Redlich-Kwong-Soave thermodynamic calculations for thermodynamic voltage parameters calculated with equilibrium compositions at HTCR=10, oxygen content of 5% and 60% fuel utilization.

ratio, but different level of oxidation (i.e., atomic oxygen content). The two gas compositions are conveniently represented on the C-H-O ternary diagram given in Figure 4.8. The relevant species for a ReSOC system are H_2, CO, CH_4, H_2O, and CO_2 [145]. The equilibrium mole fractions of these five species can be calculated from the atomic ratios (e.g., hydrogen-to-carbon ratio and oxygen content) for a given temperature and pressure. Solid Carbon should also be accounted for in ReSOC analysis, but the H/C/O ratios are selected in this study such that carbon is not present at equilibrium.

Figure 4.8 shows the fully-oxidized fuel region and the carbon deposition region (where solid carbon deposition is thermodynamically predicted at equilibrium [88–90]). The carbon deposition boundary lines in Figure 4.8 cover a range of possible temperatures and pressures that will be explored as ReSOC stack operating conditions in Section 4.4.

Selection of viable gas compositions must mitigate carbon deposition, ensure sufficient methane for thermal management, and allow high fuel energy density for increased energy storage capacity. To achieve these requirements, the gas composition entering the stack in SOFC mode should be furthest from the fully oxidized region, while not crossing the
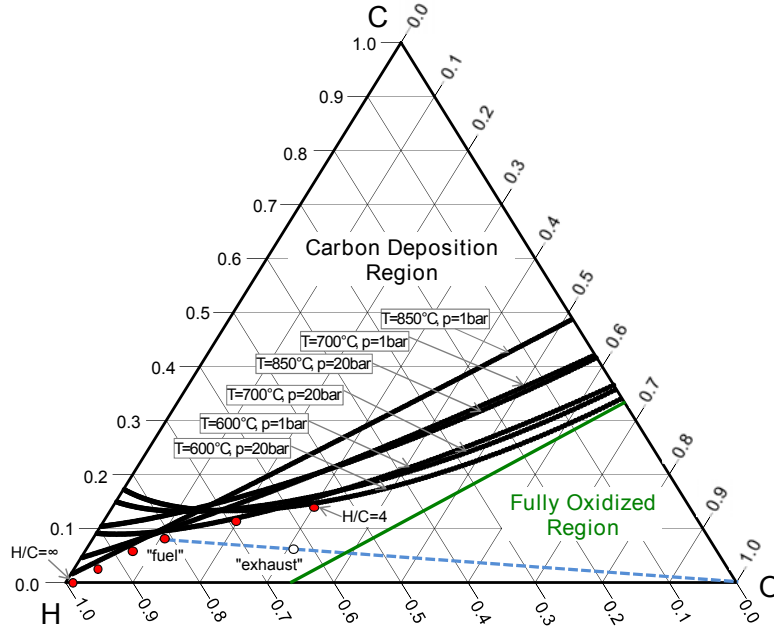
Figure 4.8: C-H-O ternary diagram showing carbon deposition boundaries for a range of temperatures and pressures. Also shown are several selected fuel gas compositions and one example exhaust gas composition

carbon deposition boundary. Table 4.1 lists several possible fuel tank gas compositions which correspond to those shown in Figure 4.8. These fuel compositions are characterized by their hydrogen-to-carbon ratio. When the HTCR is decreased (i.e., more carbon in the fuel), more oxygen is required to mitigate carbon deposition. The HTCR $\to \infty$ case is included for reference to purely steam-hydrogen fuel compositions.

Table 4.1: Potential fuel gas compositions used in the thermodynamic analysis.

HTCR	%C	%H	%O
4	14.0	56.0	30.0
6	11.5	69.0	19.5
10	8.10	81.0	10.9
15	5.80	87.0	7.20
40	2.35	94.0	3.70
∞	0.00	97.0	3.00

Figure 4.9 shows the mole fractions of the fuel tank gas composition as a function of HTCR for equilibrium conditions of 750°C and 10 bar. The methane mole fraction peaks around HTCR=10 because (i) at low HTCR, the high percentage of oxygen required to mitigate carbon deposition leads to high percentages of carbon-containing CO and CO_2, and therefore, less CH_4, and (ii) at high HTCR, the relatively lower amount of carbon leads to less CH_4 and more H_2. As the HTCR increases, CO, H_2O, and CO_2 species concentrations all decrease because less oxygen is required in the fuel composition to prevent carbon deposition. Figure 4.9 also shows the CH_4 mole fraction for a reduced temperature equilibrium composition (600°C). The mole fraction of CH_4 is higher for the low temperature case, particularly at low HTCR.
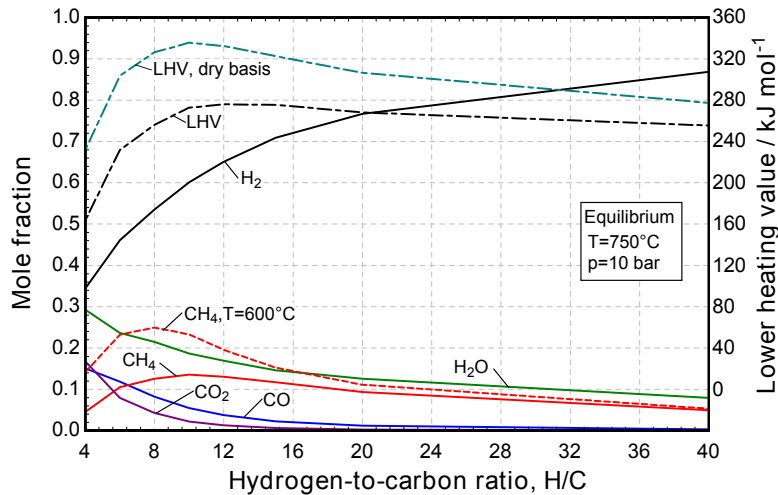
Figure 4.9: Equilibrium composition (left) at 750°C and 10 bar and lower heating value (right) as a function of hydrogen-to-carbon ratio.

The lower heating value (LHV) is an important parameter in assessing the advantages of different fuel compositions. A higher LHV indicates that lower storage volume is required for an equivalent energy of fuel, thereby reducing tank volume and cost. Storage temperature and pressure strongly influence storage volume, but are not considered here. Furthermore, a high LHV fuel requires lower volumetric flow to sustain a given current density and fuel utilization (or fuel energy flow) in the stack. As such, the power requirement of the fuel-side

compressors and heat exchange size is reduced for a fuel with high LHV.

The lower heating value of the fuel composition is strongly correlated with the methane mole fraction (see Figure 4.9). The LHV is also calculated for a dry composition and is about 20% higher than the LHV when H_2O is included. The dry LHV is perhaps more representative of the eventual stored energy density of a ReSOC system because some water knockout is likely to be needed for ease in storage. As a reference, the maximum ReSOC system dry LHV is 42% of the LHV of pure methane and 139% of the value of pure hydrogen.

4.4 The effect of operating conditions on thermodynamic voltage parameters

Attractive operating conditions for ReSOCs are identified through sensitivity studies of thermoneutral and equilibrium voltages to variations in cell pressure, temperature, fuel utilization, and fuel composition with the goal of reducing V_{TN} and/or increasing E_N such that $V_{TN} = E_N$. First, Section 4.4.1 explores the heat-to-power ratio to further validate that $V_{TN} = E_N$ is a desirable operating point. Next, the pressure, temperature, and fuel utilization operating conditions are analyzed as to their effect on V_{TN} and E_N. Finally, a specific example is given to compare the thermodynamics of pressurized and non-pressurized ReSOC stacks.

4.4.1 Heat-to-power ratio

The heat-to-power ratio of the ReSOC stack defines the stack heating or cooling load relative to electrical power. For an SOFC and SOEC stack, the heat-to-power ratio is estimated in terms of thermoneutral voltage by dividing both sides of 4.9 by the electric power, $\dot{W} = iV_{\text{cell}}$, leading to the following equations:

$$(\dot{Q}/\dot{W})_{\text{SOFC}} = V_{TN}/V_{\text{SOFC}} - 1 \tag{4.16}$$
$$(\dot{Q}/\dot{W})_{\text{SOEC}} = 1 - V_{TN}/V_{\text{SOEC}} \tag{4.17}$$

where $(\dot{Q}/\dot{W})_{\text{SOFC}}$ is the ratio of net heat generated to power generated in an SOFC and $(\dot{Q}/\dot{W})_{\text{SOEC}}$ is the ratio of net heat generated to power supplied in an SOEC so that a

positive heat-to-power ratio indicates excess heat generation in both operating modes. The cell voltages are calculated as a simple offset from reversible voltage by $V_{\text{SOFC}} = E_N - \eta$ and $V_{\text{SOEC}} = E_N + \eta$.

Figure 4.10 illustrates how the thermoneutral voltage and heat-to-power ratio are affected by stack operating pressure and compares a carbonaceous reactant composition (H/C=10) to a steam-hydrogen composition (H/C $\rightarrow \infty$). The Nernst potential, cell voltages, and thermoneutral voltage are plotted as a function of pressure in Figure 4.10(a). A constant overpotential of 85 mV is assumed in each mode of operation for a roundtrip stack efficiency of approximately 85% (see Figure 2.10 in Section 2.5.1). The reversible potential increases slightly with pressure as expected from the increased concentration of reactant species. The reversible potential, and thus the cell voltages, are relatively similar for the two compositions. The thermoneutral voltage for the carbonaceous fuel composition decreases significantly with pressure primarily because of increased methanation in SOEC mode and associated steam-methane reforming in SOFC mode. Alternatively, the thermoneutral voltage for the non-carbon case is constant with pressure. The pressure dependences of these voltage parameters are discussed further in Section 4.4.2.

The voltages from Figure 4.10(a) are used to estimate heat-to-power ratios shown in Figure 4.10(b) to reveal the impact of stack pressure on thermal and electrical load. For both compositions, the SOFC mode heat-to-power ratio is positive, meaning that excess heat is generated. This excess heat generation is consistent with SOFC voltage being lower than thermoneutral voltage (see Figure 4.10(a)). With increased pressure, the SOFC mode heat-to-power ratio for the non-carbonaceous composition decreases as the thermoneutral voltage and SOFC voltage converge. This can also be understood as the SOFC operating more efficiently at higher pressure so that less waste heat is generated. An SOFC operating on a carbonaceous composition has an additional heat-sink from methane reforming, resulting in a lower heat-to-power ratio compared to the non-carbonaceous composition. As pressure increases, the heat-to-power ratio for the carbonaceous composition decreases substantially
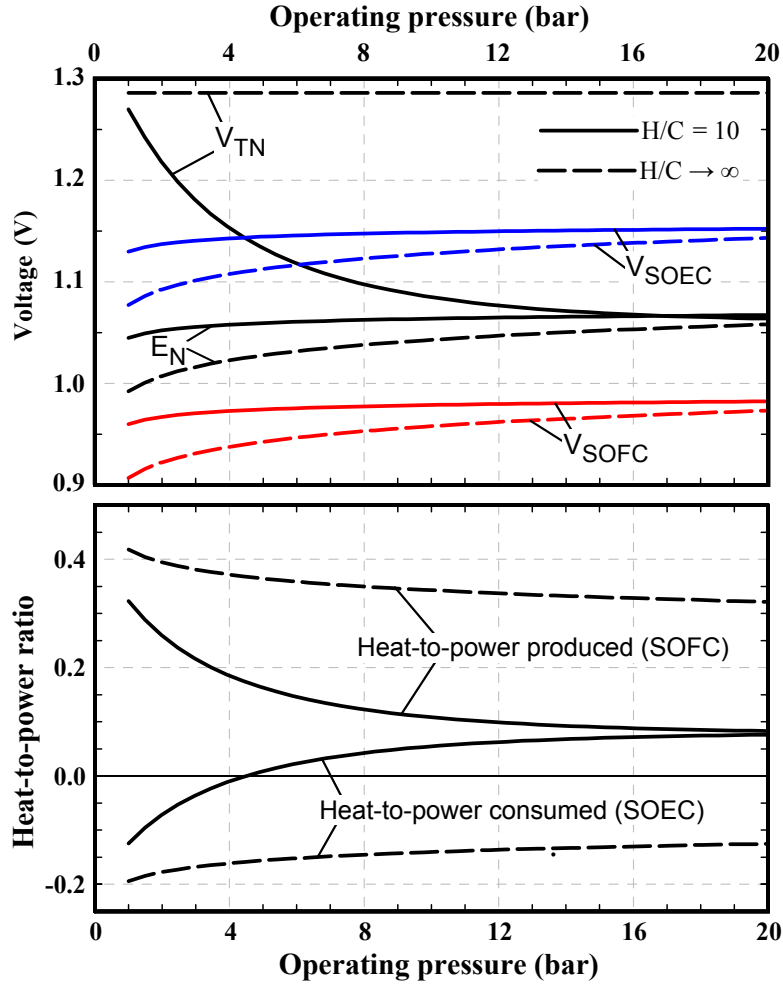
Figure 4.10: (a) Thermoneutral and reversible voltages and cell voltage in both operating modes, and (b) heat to power ratio as a function of pressure for carbonaceous (H/C=10) and non-carbonaceous (H/C$\rightarrow \infty$) compositions at T=750°C, U_F=50%, and constant over-potential in both modes of 85 mV.

because more methane is entering and being reformed in the stack in SOFC mode due to higher production of methane in the pressurized SOEC.

Unlike SOFC operation at elevated pressure, the heat-to-power ratio increases with increasing operating pressure in SOEC mode (see Figure 4.10(b)). At near-ambient pressures, the SOEC operated with carbonaceous reactants requires a net heat input to maintain a 750°C operating temperature (i.e., the heat-to-power ratio is negative), but above 4.5 bar, the stack becomes a net generator of heat. Consistent with the definition of thermoneutral voltage, the adiabatic operating condition occurs when $V_{TN} = V_{\text{SOEC}}$ (see also Fig-

ure 4.10(a)). The heat-to-power ratio increases with pressure in SOEC mode because the exothermic methanation reaction achieves higher conversion at higher operating pressures.

The heat-to-power ratios for the steam-hydrogen case in Figure 4.10 illustrates that there is either a relative excess or deficit of net heat generation for fuel cell and electrolysis operating modes, respectively, when the reactant feed gas is carbonless (or the methanation / reforming reaction is not catalyzed). For the carbonaceous composition, the expected desirable operating point where $V_{TN} = E_N$ is satisfied around 17 bar. At this pressure, a small amount of net heat generation (7-8% of electric power) is estimated, indicating that the thermal characteristic of the stack will be similar in both operating modes — favorable for system operation.

4.4.2 Pressure dependence of the thermodynamic voltages

The operating pressure is analyzed by plotting V_{TN} and E_N as a function of pressure for several hydrogen-to-carbon ratios as given in Figure 4.11. The reversible potential increases with increased HTCR because the partial pressure of H_2 increases and partial pressure of H_2O decreases (see also Figure 4.9). In other words, at higher HTCR, the reversible potential is more representative of the pure steam-hydrogen red-ox reaction, whereas at lower HTCR, the reversible potential is weighted toward lower values by the influence of the methane red-ox reaction (see Section 4.1.2). It is also apparent that E_N increases with increased pressure. The increase in Nernst potential with total pressure is slightly counteracted by the decrease in hydrogen partial pressure as hydrogen is increasingly converted to methane at higher pressure.

The pressure and compositional dependence (i.e., HTCR) of the thermoneutral voltage as depicted in Figure 4.11 is more easily understood by considering the behavior of V_{TN} at a fixed HTCR. For a fixed HTCR, at low pressure V_{TN} decreases with increasing pressure until a minimum is reached, then begins to increase with pressure at higher pressure. As HTCR decreases, the magnitude of the V_{TN} minima decreases and the location of the minima are observed at increasing pressures. For example, V_{TN} for H/C=10 reaches a minimum of 1.07

V at about 24 bar, while the H/C=40 fuel composition shows a minimal V_{TN} of 1.20 V at about 8 bar. One conclusion that can be drawn from Figure 4.11 is that a lower V_{TN} is achievable for a more carbonaceous fuel, but higher pressure is required to realize the full benefit of the higher carbon content. Desirable operating conditions where $V_{TN} = E_N$ exist for H/C=10 (at 17 bar) and H/C=6 (at 25 bar).
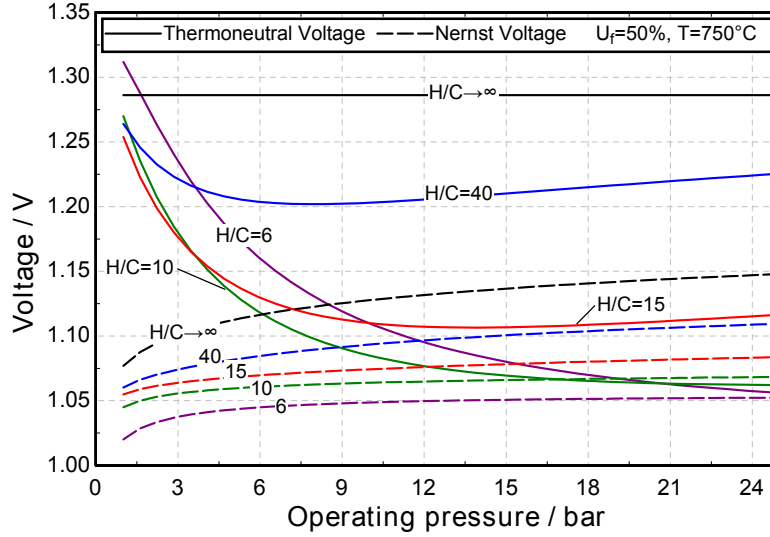
Figure 4.11: Thermoneutral and reversible voltages as a function of pressure for several fuel compositions at U_F=50% and T=750°C.

The difference in methane mole fraction between the ReSOC inlet and outlet is useful for extracting a physical explanation of the thermoneutral voltage trends seen in Figure 4.11. The methane mole fraction in the tanked fuel and exhaust gas compositions are shown in Figure 4.12 as a function of pressure for HTCR=10. The extent of the methane reforming and methanation reactions is directly associated with a difference in CH_4 mole fraction. The methane mole fraction in both of the gas compositions increases with pressure, although the methane content in the fuel composition (i.e., that generated in SOEC mode) begins to level off at high pressure because a majority of the carbon atoms in the fuel mixture already exists as CH_4 rather than CO or CO_2, so increasing the pressure has a lesser effect on increasing the methane content. The minima behavior in Figure 4.11 is attributed to the leveling off of the methane content in the fuel composition, but not in the exhaust.

The pressure dependence of the change in methane mole fraction across the stack is similar to the pressure dependence of V_{TN} for the same conditions, although inverted (see Figure 4.11). Specifically, when the change in methane mole fraction is low (i.e., low rate of methanation / reforming reactions), the thermoneutral voltage is high. The small differences between the pressure dependence of V_{TN} in Figure 4.11 and the pressure dependence of change in methane mole fraction in Figure 4.12 is attributed to both the small thermal influence of the water-gas shift reaction and the change in total number of moles across the ReSOC such that the change in mole fraction is not exactly proportional to the extent of reaction. The SOFC outlet (i.e., exhaust) composition under these conditions (high p, low U_F) contains significantly more methane than a typical SOFC exhaust, which is particularly evident at pressures above 5 bar.
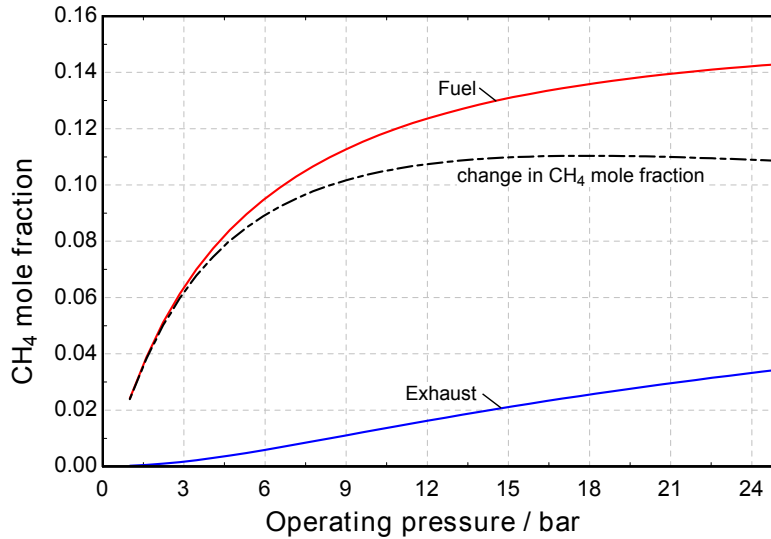
Figure 4.12: Methane mole fraction in the fuel and exhaust gas compositions at equilibrium as a function of pressure at U_F=50% and T=750°C.

4.4.3 Temperature dependence of the thermodynamic voltages

The operating temperature is analyzed by plotting V_{TN} and E_N as functions of temperature for several of the fuel gas compositions listed in Table 4.1 at constant fuel utilization and pressure. In Figure 4.13, the reversible voltage decreases with increasing temperature

due to the combined effect of changes in the hydrogen concentration and in the magnitude of the Gibbs free energy change. The ΔG increases (becomes less negative) with increased in the $T\Delta S$ value, and the partial pressure of hydrogen increases due to the temperature dependence of the steam-methane reforming reaction (i.e., it moves away from methane formation at high temperature). As demonstrated previously, the trend of increasing E_N with increasing HTCR is retained over a range of operating temperatures.
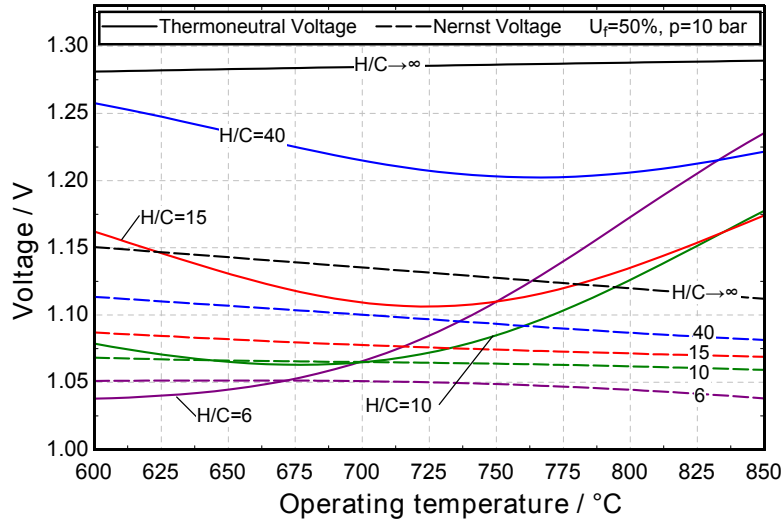
Figure 4.13: Thermoneutral and reversible voltages as a function of temperature for several fuel compositions at U_F=50% and p=10 bar.

The trend lines exhibited in Figure 4.13 can also be understood by recognizing how V_{TN} depends on temperature for a fixed hydrogen-to-carbon ratio. For a fixed HTCR, thermoneutral voltage exhibits a generally concave up behavior where at lower operating temperatures (< 700°C) it first decreases with increasing temperature before increasing again at more elevated temperatures. Interestingly, both the magnitude and location of V_{TN} minima decrease with decreasing HTCR and decreasing temperature. For example, the minimum V_{TN} is 1.20V for H/C=40 and occurs at 765°C while the minimum V_{TN} is 1.06V for H/C=10 and occurs at 675°C. These results demonstrate that while a lower V_{TN} can be reached for more carbonaceous fuel gases, the cell operating temperature must also be lower to realize the full benefit of the higher carbon content. The H/C=6 case reaches a minimum

V_{TN} outside of the temperature range shown in Figure 4.13.

The temperature dependence of thermoneutral voltage is similar to the pressure dependence in that increasing pressure has a similar affect as decreasing temperature. As the HTCR increases, the thermoneutral voltage approaches that of a steam-hydrogen reactant gas (i.e., H/C$\rightarrow \infty$) where the slight increase in $V_{TN,H2/H2O}$ with temperature is a result of the temperature dependence of the enthalpy change.
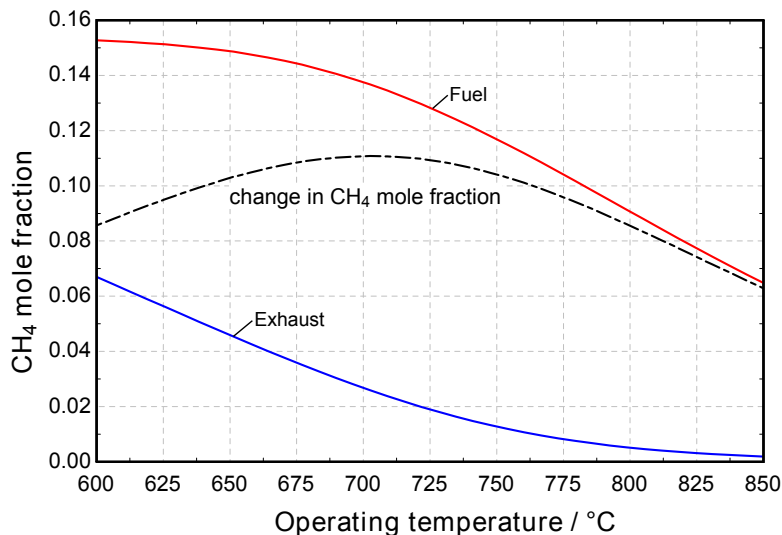
Figure 4.14: Methane mole fraction in the fuel and exhaust gas compositions at equilibrium as a function of temperature at U_F=50% and p=10 bar.

The optima behavior observed for V_{TN} as a function of temperature can be explained similar to the pressure dependence. Figure 4.14 shows the methane content of the fuel and exhaust compositions as a function of temperature. As temperature is reduced, the methane content in both the fuel and exhaust compositions increases; however, the methane content of the fuel reaches a maximum, while that of the exhaust continues increasing. Thus, the minimum V_{TN} is achieved near to where the change in methane content between the fuel and exhaust compositions is maximized. This optimal temperature is also dependent on pressure, fuel utilization, and HTCR, meaning that finding the desirable operating conditions must be viewed as a multi-dimensional optimization problem.

4.4.4 Utilization dependence of the thermodynamic voltages

Figure 4.15 shows the behavior of V_{TN} and E_N as functions of fuel utilization and the HTCR of the feed gas. The well-known behavior of decreasing reversible voltage with increasing fuel utilization is exhibited and arises because of the decrease in partial pressure of fuel species (e.g., hydrogen) in the SOFC mode fuel channel (or fuel species increase in the SOEC mode fuel channel).
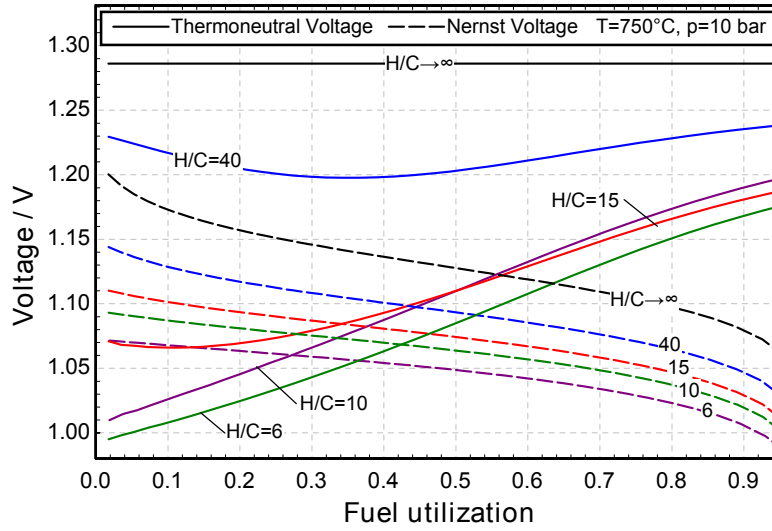
Figure 4.15: Thermoneutral and reversible voltages as a function of fuel utilization for several fuel compositions at T=750°C and p=10 bar.

In contrast, thermoneutral voltage increases with increased fuel utilization. However, this behavior can demonstrate the opposite trend at low utilizations when there is little carbon in the fuel mixture (see the curves for H/C $\geq$ 15). In feed gases with high HTCR, V_{TN} decreases with increases in fuel utilization in low utilization regimes (< 0.4). This trend is a result of the complex equilibrium calculations and the resulting compositional-dependent thermoneutral voltage surface. This phenomenon, while interesting, is not particularly valuable for the present analysis because it occurs at unattractive operating conditions for a ReSOC system concept. The $V_{TN} = E_N$ condition is satisfied for fuel compositions with hydrogen-to-carbon ratios of 6, 10, and 15 at fuel utilizations of 28%, 42%, and 34%, respectively. These low fuel utilizations may be intuitively concerning from an overall system efficiency standpoint.

However, recall that the roundtrip system efficiency is not directly dependent on fuel utilization because the ReSOC concept is a closed system. The BOP parasitic energy load is, however, expected to increase at lower fuel utilizations because a greater volume of fuel must be transported through the system for equivalent stack power capacity.

4.4.5 Pressurized vs. non-pressurized ReSOC systems

The previous subsections explain the dependence of V_{TN} and E_N on relevant ReSOC operating conditions. Now, the thermoneutral voltage is considered in the context of comparing pressurized and non-pressurized systems. Pressurized ReSOC systems may be an attractive option to increase in-situ methane formation, but pressurized stacks are considered less feasible for distributed scale applications (< 1 MW). Development of low- and intermediate-temperature ReSOCs has shown high performance down to 600°C for laboratory scale tests [74, 146]. Thus, for distributed scale systems, sufficient methane formation may be achieved at ambient pressure by reducing the stack operating temperature. For either approach, the reactant compositions and fuel utilization must also be considered.
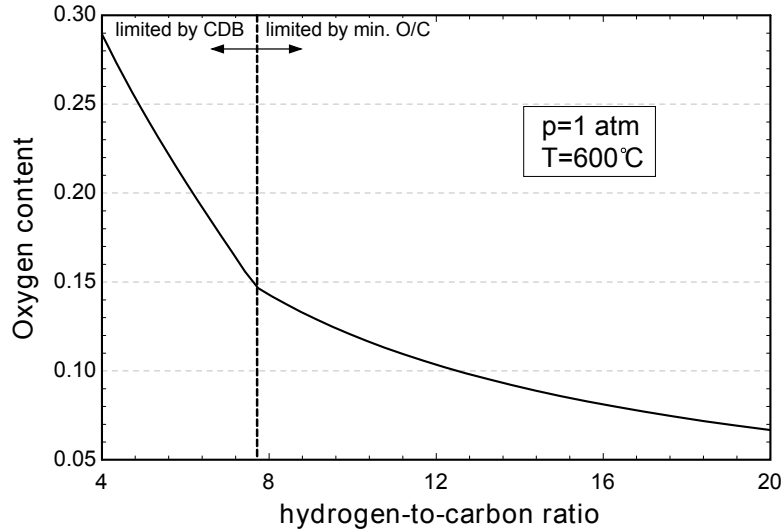
Figure 4.16: Oxygen content as a function of hydrogen-to-carbon ratio for the fuel compositions used in the ambient pressure thermodynamic analysis.

The fuel compositions used for the following examples is different from those given in Table 4.1. Instead, the H-C-O ratio is determined from the carbon deposition boundary for a specified temperature and pressure (rather than multiple overlayed deposition boundaries as in Figure 4.8). For a given HTCR, the oxygen content is selected to be 2% greater than the limiting case as dictated by the carbon deposition boundary and a minimum oxygen-to-carbon ratio of 1.5 is enforced. Based on this methodology, the oxygen content as a function of HTCR is shown in Figure 4.16.

The non-pressurized example considers a ReSOC temperature of 600°C and the thermoneutral and reversible voltages are plotted in Figure 4.17 as a function of hydrogen-to-carbon ratio. Thermoneutral voltage decreases with decreased fuel utilization, and is minimized at HTCR of 7.5. This optimal point correlates with the HTCR at which the oxygen content switches from being constrained by the carbon deposition boundary (at lower HTCR) to being constrained by the minimum oxygen-to-carbon ratio. These minima indicate that the level of oxidation of the fuel mixture has a strong impact on stack thermal behavior caused by reforming chemistry.
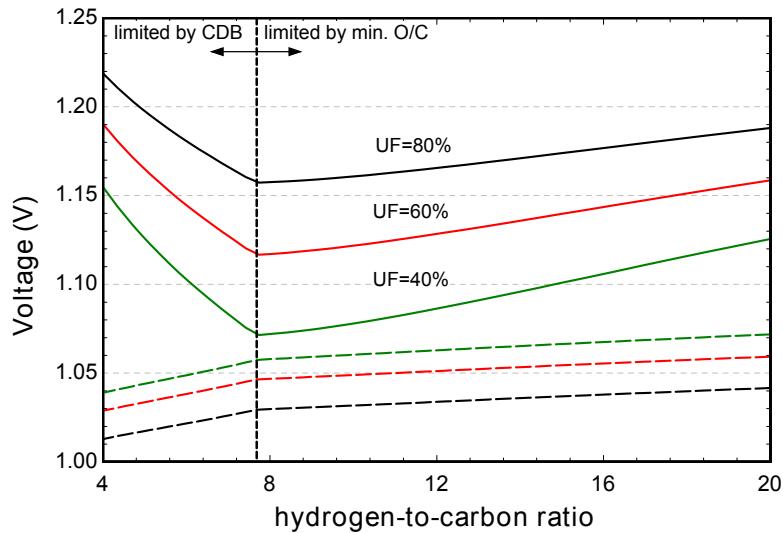
Figure 4.17: Thermodynamic voltages vs. hydrogen-to-carbon ratio for an ambient pressure example at 600°C

It is notable that the non-pressurized example has no operational point where thermoneutral voltage is reduced to the value of the Nernst potential. This highlights the difficulty of operating ReSOC systems efficiently at ambient pressure. However, for a fuel utilization of 40%, the thermoneutral voltage is only 15mV greater than the reversible voltage, meaning that the cell can operate exothermically for realistic overpotential values. Cells with even lower operating temperature ranges may beneficially balance the thermal load between operating modes and/or allow higher fuel utilization for distributed-scale, ambient pressure systems.

The pressurized case considers a stack pressure of 20 bar. Figure 4.18 shows contour plots of the difference between Nernst and thermoneutral voltage (i.e., $E_N - V_{TN}$) at different temperatures. The voltage differences, given in mV, indicate the overpotential required to achieve thermoneutral operation in SOEC mode.

The trends in Figure 4.18 follow those shown in the previous subsection, whereby the thermoneutral and Nernst voltages generally converge with reduced temperature, reduced HTCR, and reduced fuel utilization. For each temperature, the thermoneutral and Nernst voltages are equal at HTCR between 4 and 11, and for fuel utilizations below 75%. Lower operating temperature indicates that a lower HTCR is optimal and allows higher fuel utilization, favorable to storage energy density and reducing BOP power. In fact, at 800°C, the desirable operating point is only achieved at fuel utilization near or below 40%. These contour plots also re-enforce the complex behavior of the thermoneutral voltage, where the desirable operating points appear at different HTCR and fuel utilizations depending on the temperature.

Interestingly, the difference between V_{TN} and E_N is relatively constant over a wide range of fuel utilizations at 600°C. This is in contrast to the higher temperature cases where the difference is strongly influenced by U_F, but relatively constant with HTCR. Thus, the pressurized 600°C operating point may provide more operational flexibility from a control standpoint, although requires continued development in cell materials to achieve efficient
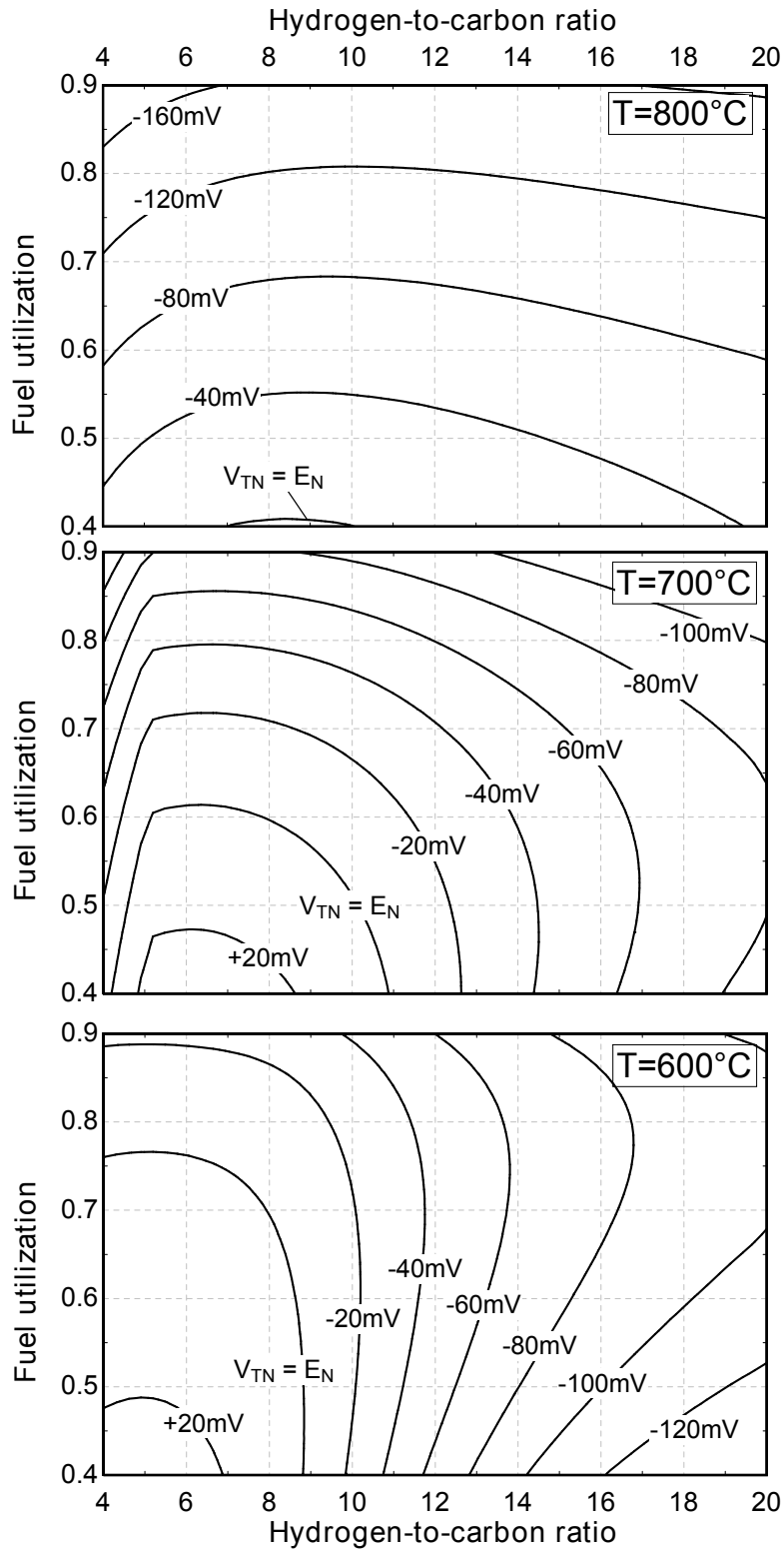
Figure 4.18: Contour plot of the difference between thermoneutral and reversible voltage as a function of fuel utilization and hydrogen to carbon ratio for a pressurized stack (20 bar) at 600, 700, and 800°C.

and cost-effective stacks at $< 650°C$.

4.5   Conclusions from the thermodynamic analysis

Throughout this chapter, various thermodynamic parameters, including individual reaction thermodynamics, heat-to-power ratios, and thermodynamic voltage parameters have been used to highlight one central point: It is desirable to operate a reversible solid oxide cell system at conditions where the thermoneutral and equilibrium voltages are approximately equal so that the stack is mildly exothermic in both operating modes.

The thermoneutral voltage was highlighted as an important system parameter for stack thermal management and achieving high roundtrip system efficiency. This voltage parameter is also helpful in resolving the apparent conflict in identifying mutually beneficial operating conditions for a system that will employ a ReSOC device in both fuel cell and electrolysis modes of operation.The thermoneutral and reversible voltage parameters were derived from control volume analysis. A calculation procedure was described for quantifying these voltages at representative ReSOC operating conditions. The effect of temperature, pressure, fuel utilization, and fuel composition (as described by the hydrogen-to-carbon ratio) on V_{TN} was explored, resulting in the following general conclusions:

- The minimum achievable V_{TN} is lower for feed gas compositions that have lower hydrogen-to-carbon ratios.

- V_{TN} is favorably reduced by high pressure and low temperature operating conditions. This characteristic is made possible by the production of significant methane in SOEC mode when sufficient carbon is present, but the operating conditions must also promote methane formation.

- V_{TN} increases with increased fuel utilization.

- Optimal operating conditions highlighted by the thermoneutral voltage analysis may be significantly altered by changing other stack operating conditions.

These conclusions are particularly relevant to the design and analysis of ReSOC energy storage systems and SOEC fuel synthesis systems where thermal management and heat supply are highly impactful on system performance. Furthermore, it is possible that SOFC system studies, particularly combined heat and power systems, will benefit by using the thermoneutral voltage parameter to provide a unique thermodynamic viewpoint to system thermal management.

Analysis of the thermoneutral voltage shows that both pressurized and ambient pressure ReSOC stacks are feasible for sufficiently reducing V_{TN}. Pressurized systems may operate at a higher fuel utilization compared to ambient pressure systems, but the stack pressure of 20 bar still requires reduced operating temperature to achieve high utilization at the desirable operating point.

The ReSOC stack operating conditions must be selected with strong consideration to optimal cell performance and durability. Specifically, the operating conditions must enable the ReSOC to operate at the low overpotential required to achieve competitive roundtrip system efficiency, while also utilizing a relatively high current density to keep the size of the ReSOC stack economical. The dichotomy between the high temperature required for low resistance operation of existing ReSOCs and the intermediate temperature desired for an efficient energy storage application provides additional motivation for intermediate temperature ReSOC development.

This chapter has shown how ReSOC stack operating conditions are expected to affect system performance based primarily on thermodynamics. The results in the remaining chapters extend these analysis with higher fidelity studies that employ actual voltage-current performance characteristics of ReSOCs to quantify the system efficiency and economics of the proposed system. Before presenting the additional results, Chapter 6 details the modeling approach used in the higher fidelity stack and system-level studies.

CHAPTER 5

STACK AND SYSTEM MODELING APPROACH

The overall objectives of this dissertation must be addressed by formulating models to accurately capture the system technical performance. This chapter describes the assumptions, equations, and modeling methodology used to generate the ReSOC stack and system results presented in the following chapters. A major focus of this work is to establish effective ReSOC operating conditions. Therefore, the ReSOC stack is modeled with a higher fidelity compared to the other system components. A physically based channel-level ReSOC model is developed to capture performance variations to various cell operating strategies and conditions based on experimental performance from next generation LSGM-electrolyte ReSOCs. The other system components are modeled thermodynamically based on energy and entropy balances. Following the component model definitions, this chapter also explains the calculation procedure required to model reversible systems at steady state. This includes considerations for ensuring continued operation of the charge/discharge process and performance of a single system in two distinct operating modes. Lastly, performance metrics are defined to represent the efficiency and energy density performance of the system.

5.1 ReSOC stack model

The ultimate function of the stack model developed herein is to represent performance of a ReSOC stack within a system model. This performance includes electrical power generation (or consumption in electrolysis mode) as well as reactant and product gas stream properties that interface with other system components (e.g., T, x_i). This work follows the approach of previously published solid oxide cell models that focus on the repeating channel-level geometry of a solid oxide cell and extrapolate that performance to represent the stack characteristic [143, 147–149]. These previously developed models are calibrated to represent performance of high temperature cells (i.e., those based on YSZ-electrolyte).

They include conservation equations to represent the thermochemical phenomena occurring within the ReSOC stack and represent the electrochemical processes by calculating individual overpotential contributions associated with ohmic, activation, and concentration polarizations. Chapter 4 concluded that intermediate temperature cells are instrumental to successful implementation of the proposed system. Thus, this ReSOC model used in this work is calibrated to the performance of next generation intermediate temperature cells with an LSGM electrolyte material set optimized to operate between 550 and 650°C. The conservation equations are derived and implemented as in previously published models, but the parameters used in the electrochemical model are modified to represent the performance of LSGM-electrolyte cells. The cell data available for calibration is from button-cell tests and includes variation in temperature and reactant composition. A zero-dimensional button cell model is used to calibrate the electrochemical model parameters to the cell current-voltage performance. The following subsections present the available experimental data including a brief description of the testing conditions and process, describe the zero-dimensional button-cell model and electrochemical model formulation, and derive conservation equations for the channel-level model.

5.1.1 Description of experimental data

The experimental data used for model calibration in this work was collected by researchers at the Northwestern University Department of Material Science and Engineering; additional publications on the testing process and conditions can be found elsewhere [74, 116, 126, 150]. Here a brief summary of the cell fabrication and testing is given.

Button cells with thin $La_{0.8}Sr_{0.2}Ga_{0.8}Mg_{0.2}O_{3-\delta}$ (LSGM) electrolyte on $Sr_{0.8}La_{0.2}TiO_{3-\alpha}$ (SLT) supports and $La_{0.6}Sr_{0.4}Fe_{0.8}Co_{0.2}O_{3-\delta}$ (LSCF) cathode were fabricated by tape casting method. The SLT powder was synthesized by a solid state reaction method, as described previously [74, 150]. The SLT powder was mixed with 30 wt.% graphite (Timcal, Swizerland) by adding an appropriate amount of menhaden fish oil as dispersant and ball milling for 24 h in ethanol and Xylenes mixed solvent. Afterwards, polyvinyl butyral (binder), butylbenzyl

phthalate (plasticizer) and poly alkylene glycol (plasticizer) were added into the mixture, and it was ball milled for another 24 h. The slurry was tape casted to form a membrane through a Richard E. Mistler tape casting machine. The LSGM (Fuel Cell Materials, Ohio)-30 wt.% graphite anode functional layer (AFL) and LSGM electrolyte were tape casted in the same way. The SLT-30 wt.% graphite support layer/AFL/LSGM electrolyte was hot laminated together at 80°C. After punching to circular shape, the cell was fired at 1425°C for 4h. The LSCF (Praxair, Washington)-$Gd_{0.1}Ce_{0.9}O_{1.95}$ (GDC, Nextech, Ohio) (50wt.%) cathode functional layer and LSCF current collector was screen printed on the LSGM side and fired at 1100°C for 2h. A 5 M $Ni(NO_3)_2$ (Fisher Chemicals, New Jersey) solution was infiltrated into the porous SLT support and LSGM functional layer. After calcining at 700°C for 0.5 h, nanostructured NiO covered the SLT and LSGM surface homogeneously. The desired Ni amount was achieved by multiple infiltration cycles.

The cell was sealed onto an alumina tube and tested using a four-probe configuration. The oxygen electrode was exposed to 200 sccm flow air while the fuel electrode was fueled with humidified hydrogen at 100 sccm through a heating bubbler containing H_2O in order to entrain a known partial pressure. For the syngas, H_2, CH_4, CO_2 were flowed through a heated bubbler, while the ratio was controlled by the mass flow rate. Current-voltage curves were recorded using an IM6 electrochemical workstation (ZAHNER, Germany) for cell testing from 650°C to 550°C. Electrochemical impedance spectra (EIS) were also recorded with the frequency range of 100 mHz-100 kHz. The cell structure was examined by scanning electron microscopy (SEM, Hitachi S-4800-II and SU8030) as illustrated in Figure 5.1. The cell yields a structure with a 600-micron nickel infiltrated SLT fuel-electrode support, 50-micron nickel infiltrated LSGM anode functional layer, 16-micron LSGM solid electrolyte, 20-micron LSCF-GDC oxygen electrode functional layer, and 20-micron LSCF current collector.

5.1.2 Zero-dimensional button cell model

A zero-dimensional button cell ReSOC model is used to calibrate electrochemical model parameters to the experimental data. The electrochemical model represents physical phe-
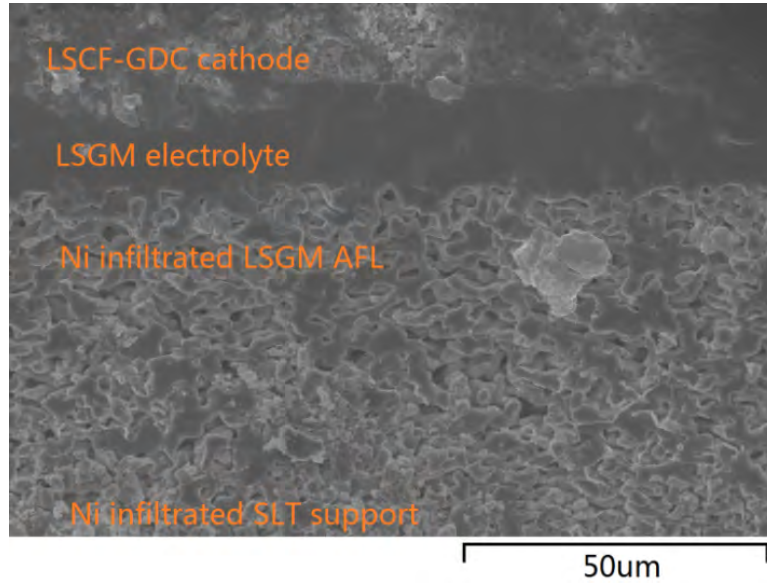
Figure 5.1: Low-magnification scanning electron microscopy overview images of an LSGM-electrolyte button cell after testing.

nomena occurring in the PEN (positive electrode, electrolyte, negative electrode) including the ohmic, activation, and concentration overpotentials using Ohms law, the Butler-Volmer equation, and Fickian diffusion, respectively. The electrochemical model equations are described in Section 5.1.3. Similar button-cell models have been developed previously [151, 152]. The button-cell model includes the following assumptions:

1. Continuously stirred tank reactor (CSTR) species balances at the fuel and oxygen electrode surfaces.

2. Isothermal fuel, air, and PEN structure.

3. Active electrochemical reaction site isolated to the electrode-electrolyte interfaces.

4. No direct electrochemical conversion of CO and CO_2.

5. Equilibrated water-gas-shift reaction (Equation 2.3) and rate based steam-methane reforming (Equation 2.2) from [153].

5.1.3 Electrochemical model

The electrochemical model described here is used in two ways: to calibrate electrochemical model parameters using the button-cell model described in section 5.1.2 and to define the current-voltage relationship in the channel-level model described in 5.1.5. This section describes the electrochemical model including cell voltage and individual overpotential equations and assumptions. The electrochemical model parameters are given in Table 5.1.

Cell and open-circuit voltages

The operating cell voltage, V_{cell} is determined by individually computing the overpotential contributions from ohmic, activation, and concentration losses which cause the cell voltage to deviate from open-circuit voltage. The cell voltage is expressed as:

$$V_{\text{cell}} = E_N - \eta_{\text{ohm}} - \eta_{\text{act}} - \eta_{\text{conc}} - V_{\text{leakage}} \tag{5.1}$$

Where E_N is the open-circuit voltage, η_i are the individual overpotential contributions and V_{leakage} is an experimentally calibrated parameter ranging from 0-30 mV which represents the difference between theoretically calculated and experimentally determined OCV attributed to gaseous and/or electronic leakage. The open-circuit voltage is calculated with the Nernst equation applied to the steam-hydrogen red-ox reaction as given by Equation 2.7.

Ohmic overpotential

The ohmic overpotential results from resistance to ionic and electronic transport through cell layers. The overpotential scales directly with current density by Ohms law:

$$\eta_{\text{ohm}} = i R_{\text{eq,ohm}} \tag{5.2}$$

where i is the cell current and $R_{\text{eq,ohm}}$ is the equivalent ohmic resistance of the cell which is influenced by cell material set, geometry, and operating conditions. The equivalent resistance is calculated as:

$$R_{\text{eq,ohm}} = R_{\text{PEN}} + R_{\text{C}} \tag{5.3}$$

where R_{PEN} represents the resistance to charged species transport through the PEN structure and R_{C} is a correction term used to account for other possible resistance contributions such as interfacial contact between cell layers. The PEN resistance is calculated as a summation of serial resistance contributions from the electrodes and electrolyte:

$$R_{\text{PEN}} = \frac{1}{A_{\text{cell}}} \sum th_i / \sigma_i \tag{5.4}$$

where A_{cell} is the cell active area, th_i and σ_i are the thickness and conductivity, respectively of each layer of the PEN including anode, electrolyte and cathode.

Ionic transport through the electrolyte typically dominates the PEN resistance because electrode materials are selected with high electronic conductivity. Previous studies have measured LSGM ionic conductivity for applications as SOFC electrolytes [72, 154]; however, slight variations in composition and manufacturing process can significantly impact the resistance. For this model, the ohmic resistance was measured from the button-cells using the real-axis intercept of the Nyquist plot generated by electrochemical impedance spectroscopy (see Figure 5.3). The EIS derived ohmic resistance shows similar temperature dependence as the published literature. A modified Arrhenius form is used to represent the temperature dependence of the electrolyte resistance (see Table 5.1).

The anode support material, Ni-SLT has seen less attention in the literature. This thick support layer is included to provided mechanical strength to the cell structure. Also, SLT is favorable in place of an extended LSGM support structure because it is less expensive [74]. Conductivity of SLT has been shown to vary significantly with temperature and the oxygen partial pressure of the testing environment [150, 155, 156]. Furthermore, variations in manufacturing method and material composition cause the conductivity to vary from 10 [156] to 1000 S/cm [155]. The electrode conductivity is further complicated by parallel conduction through the SLT and infiltrated surface-nickel. Oxygen electrode conductivity with the LSCF-GDC material has been reported with LSCF conductivity of 200–400 S/cm between 400 and 800°C [157]. The GDC phase is intended as an ion conductor and electronic conduction is assumed to occur in the LSCF phase. Electronic conductivities of 10 and 300

S/cm are used for the fuel and oxygen electrode, respectively. For comparison, the conductivity of LSGM at 650°C is about 0.036 S/cm [154], meaning that even for electrode thickness an order of magnitude greater than the electrolyte, the PEN resistance is dominated by the electrolyte. The value of R_C is selected as zero by calibrating with the experimental data.

Activation overpotential

The total activation overpotential includes contributions from both the fuel (FE) and oxygen electrodes (OE):

$$\eta_\mathrm{act} = \eta_\mathrm{act,FE} + \eta_\mathrm{act,OE} \tag{5.5}$$

The Butler-Volmer equation is used to estimate kinetic losses associated with the charge transfer reactions at each electrode-electrolyte interface [158]:

$$j = j_{0,i} \left[\exp\left(\frac{nF\alpha_{\mathrm{a},i}}{RT} \eta_\mathrm{act,i} \right) - \exp\left(-\frac{nF\alpha_\mathrm{c,i}}{RT} \eta_\mathrm{act,i} \right) \right] \tag{5.6}$$

where $j_{0,i}$ is the exchange current density and $\alpha_{\mathrm{a},i}$ and $\alpha_{\mathrm{c},i}$ are the anodic and cathodic charge transfer coefficients, respectively. The exchange current density represents the rate of reaction at open-circuit voltage, and can be related to parameters of the PEN structure such as reaction site density and catalyst activity. However, these parameters are difficult to measure and empirical formulations are typically used. For this study, the exchange current densities are represented as in References [159–161]:

$$j_{0,\mathrm{FE}} = j_{0,\mathrm{FE}}^\mathrm{ref} \frac{p_{\mathrm{H}_2}}{p_0}^{n_{\mathrm{H}_2}} \frac{p_{\mathrm{H}_2\mathrm{O}}}{p_0}^{n_{\mathrm{H}_2\mathrm{O}}} \exp\left(\frac{-E_\mathrm{act,FE}}{R} \left(\frac{1}{T} - \frac{1}{T_\mathrm{ref}} \right) \right) \tag{5.7}$$

$$j_{0,\mathrm{OE}} = j_{0,\mathrm{OE}}^\mathrm{ref} \frac{p_{\mathrm{O}_2}}{p_0}^{n_{\mathrm{O}_2}} \exp\left(\frac{-E_\mathrm{act,OE}}{R} \left(\frac{1}{T} - \frac{1}{T_\mathrm{ref}} \right) \right) \tag{5.8}$$

where p_i is the partial pressure of species i at the reaction site, and $j_{0,i}^\mathrm{ref}$, n_i, and $E_{\mathrm{act},i}$ are empirical fitting parameters. Approximate values for the exchange current density activation energy, $E_{\mathrm{act},i}$ were taken from studies on the performance of similar fuel [162] and oxygen electrodes [163]. The present model is not validated against different oxidant compositions

because no data was available for these specific cells. The oxygen partial pressure dependence of the exchange current density, n_{O2} is obtained from Ref. [126].

Table 5.1: Electrochemical model parameters.

Model parameter	Value
Ohmic overpotential parameters	
$\sigma_{\text{electrolyte}}$ (ionic)	5.17E6/T*exp(-93,800/RT) S/cm
σ_{FE} (electronic)	10 S/cm [156]
σ_{OE} (electronic)	300 S/cm [157]
Correction resistance, R_C	0 Ω
Activation overpotential parameters	
$j_{0,\text{FE}}^{\text{ref}}$	15600 A/m^2
$j_{0,\text{OE}}^{\text{ref}}$	2470 A/m^2
$\alpha_{a,\text{FE}}$	0.4
$\alpha_{c,\text{FE}}$	0.6
$\alpha_{a,\text{OE}}$	0.5
$\alpha_{c,\text{OE}}$	0.5
$E_{\text{act,FE}}$	60.0 kJ/mol [162]
$E_{\text{act,OE}}$	162.0 kJ/mol [163]
n_{H_2}	0.50
$n_{\text{H}_2\text{O}}$	0.50
n_{O_2}	0.20 [126]
Concentration overpotential parameters	
FE porosity	0.26 (26%) [74]
OE porosity	0.30 (30%)
FE pore diameter	1 micron
OE pore diameter	1 micron
FE tortuosity	3.0
OE tortuosity	3.0

Concentration overpotential

The concentration overpotential represents the losses due to reactant and product diffusion through the porous electrode structures. Fickian diffusion is used to determine reactant mole fractions at the active site as in Reference [92]. The calculated mole fractions are then

105

used to determine the concentration overpotential:

$$\eta_{\text{conc}} = \frac{RT}{nF} \ln \left[\frac{x_{\text{H}_2,\text{bulk}} x_{\text{H}_2\text{O},\text{TPB}} x_{\text{O}_2,\text{bulk}}^{0.5}}{x_{\text{H}_2,\text{TPB}} x_{\text{H}_2\text{O},\text{bulk}} x_{\text{O}_2,\text{TPB}}^{0.5}} \right] \tag{5.9}$$

where $x_{i,\text{bulk}}$ and $x_{i,\text{TPB}}$ are the mole fractions in the bulk gas above the electrode surface (i.e., CSTR composition) and at the active reaction site, respectively. The influence of species diffusion on activation polarization is considered by using the $x_{i,\text{TPB}}$ values when calculating p_i in Equations 5.7 and 5.8.

The porosity, pore diameter, and tortuosity are physically based model parameters that influence the concentration overpotential. The FE porosity was taken from measurements on similar cells to be 26% [74] and typical values for solid oxide cells are used for the remaining parameters [92].

5.1.4 Model comparison to experimental data

The button cell model is calibrated to represent the performance of LSGM-electrolyte cells by adjusting key electrochemical parameters including R_C, $\alpha_{\text{a},i}$, $\alpha_{\text{c},i}$ $j_{0,i}^{\text{ref}}$, and n_i. Experimental and model-predicted current-voltage curves in Figure 5.2 indicate good agreement. The most notable model deviations occur at high current density. For energy storage applications, the efficiency requirements should limit the magnitude of the operating current density to < 1 A/cm^2. The model also captures effects of reactant composition variation as shown by the syngas-fueled V-j curve in Figure 5.2.

Figure 5.3 presents the Nyquist plots of typical EIS data tested at OCV from the same cell as shown in Figure 5.2. The area specific resistances (ASR) of the cell are 0.18 Ωcm^2 at 650°C, 0.42 Ωcm^2 at 600°C, 1.01 Ωcm^2 at 550°C for the 50%H$_2$/50%H$_2$O cases, and 0.48 Ωcm^2 at 594°C for the syngas case. However, the ASR values are lower when calculated by the negative slope of the chord between cell voltages at -0.5 and 0.5 A/cm^2, as reported in Figure 5.2. The lower ASR value with increased current density is a consequence of the activation polarization behavior, which increases logarithmically with current density. This effect is most evident with decreasing temperature where activation losses are a major
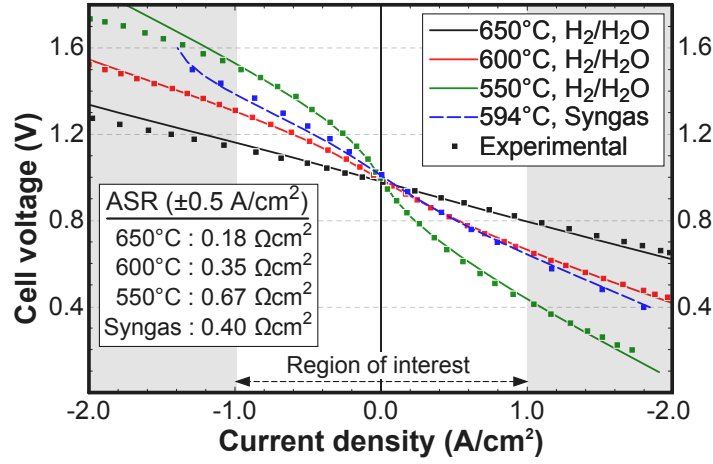
Figure 5.2: Model and experimental current-voltage comparison for LSGM-electrolyte Re-SOC operated at atmospheric pressure with 50 mol.% H_2/H_2O or syngas (25%-H2, 25%-CH4, 38%-H2O, 12%-CO2) flow to the fuel electrode at 100 sccm and air flow to the oxygen electrode at 200 sccm.

contribution to total cell resistance.

5.1.5 Channel-level model

This section documents the development of a reversible solid oxide cell model including geometry definitions, governing conservation equation derivations, and a description of the numerical solution technique. Some unique features of this model include: (i) ability to operate in both forward (SOFC) and reverse (SOEC) modes, (ii) co- and counter-flow configurations, (iii) thermodynamic property calls with ideal gas or higher fidelity models, (iv) 5-specie reactant mixtures. The channel level model includes the following assumptions in addition to those listed in Section 5.1.2:

1. Plug flow in the fuel and air channels.

2. Neglected radiative heat transfer between the PEN and interconnect.

3. Lumped temperature of the solid PEN structure.
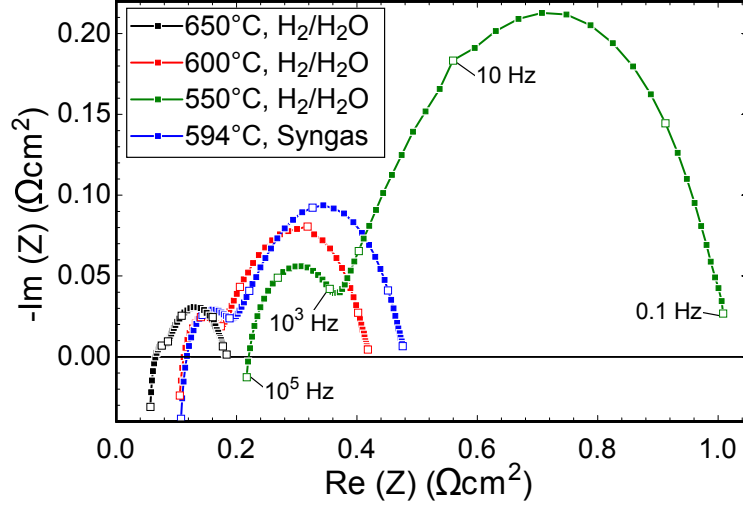
Figure 5.3: Electrochemical impedance spectroscopy Nyquist plot from button-cell tests at the conditions described in Figure 5.2.

4. Fully developed laminar flow in the fuel and air channels, resulting a constant Nusselt number.

5. Neglected conduction and diffusion in the fuel and air gas streams.

6. Constant pressure in the fuel and air channels.

7. Isopotential PEN layer due to high electrical conductivity of the electrode materials.

8. Heterogeneous reaction chemistry occurs at the interface of the flow channel and fuel electrode support.

The electrochemical model described previously assumes no direct electrochemical conversion of carbon monoxide and carbon dioxide. Rather, the pathway for consumption and production of these species is the water gas shift and reverse shift reactions. Recent publications have suggested that it is important to account for the direct electrochemical conversion pathway [164, 165]. On the other hand, solid oxide cells are known to have fast kinetics that achieve near equilibrium within the channel, meaning that product composition should not be significnatly affected by this assumption. The conversion pathway will also impact the

108

electrochemical cell performance through the concentration and activation polarizations. The activation polarization parameters are fit to experimental data through calibration and the cell is not operated under conditions where diffusion losses significantly affect performance. For these reasons, the assumption of only steam and hydrogen electrochemical conversion is maintained in this study and considered suitable for system analysis. However, higher fidelity modeling concerned with cell materials or structure optimization and mechanistic analysis must consider the impacts of direct CO/CO_2 conversion.

Channel geometry

The geometry for the channel-level model is shown in Figure 5.4 including the height and width of the rectangular fuel and air channels and the thickness of cell components including the PEN structure and interconnectors (IC). The PEN thickness is further defined as the sum of the thicknesses of the fuel electrode, oxygen electrode, and solid electrolyte, and support layers. This model will be extrapolated to represent stack performance by further prescribing the number of channels per cell and number of cells per stack.

Species conservation

The general species conservation equation for component j is used as a starting point for the channel level species conservation equations:
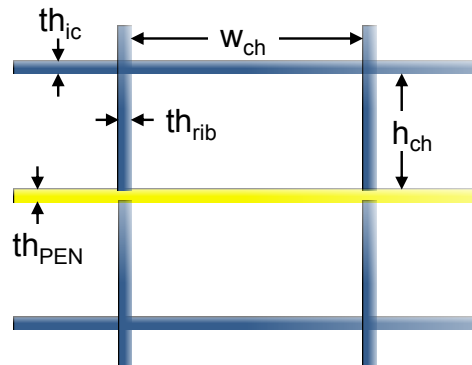
Figure 5.4: Reversible solid oxide channel geometry.

$$\frac{\partial C_j}{\partial t} + \mathbf{v} \cdot \nabla \mathrm{C}_j = D \nabla^2 C_j + R_{vj} \tag{5.10}$$

Simplifying the above equation for steady state, neglecting diffusion, and one-dimensional flow results in:

$$v_x \frac{dC_j}{dx} = R_{vj} \tag{5.11}$$

Concentration is converted to molar flow by $C_j = \frac{\dot{N}}{v_x A_x}$, where A_x is the constant flow-channel cross sectional area. The volume based reaction rate, R_{vj} is converted to a general reaction rate, $r_{j,k}$ in units of moles/second for reaction k and component j.

$$\frac{d\dot{N}_j}{dx} = \frac{A_x}{V_{\mathrm{CV}}} \sum r_{j,k} \tag{5.12}$$

where V_{CV} is the volume of the control volume. The above equation is next discretized for an explicit finite difference scheme with backward differencing.

$$\frac{\dot{N}_{j,i} - \dot{N}_{j,i-1}}{\Delta x} = \frac{A_x}{V_{\mathrm{CV}}} \sum r_{j,k,i} \tag{5.13}$$

Recognizing that the volume, area, and discretized lenght (Δx) terms calcel, the molar flow at node i is solved as:

$$\dot{N}_{j,i} = \dot{N}_{j,i-1} + \sum \nu_{j,k} r_{k,i} \tag{5.14}$$

where $\nu_{j,k}$ is the stoichiometric coefficient for reaction k and species j. The geometry of the reaction area or reaction volume for heterogeneous or homogeneous reaction, respectively must be incorporated into the calculation of $r_{k,i}$. The final discretized species balance given in Equation 5.14 could otherwise be obtained from a finite volume method for a discretized volume shown in Figure 5.5. The finite volume approach is used in deriving the energy conservation equations next.

Energy conservation

Four energy conservation equations are required for the channel level model to calculate the temperature profiles in the fuel gas stream, air gas stream, solid PEN, and solid intercon-

nect. The relevant energy flows are shown in Figure 5.5 determined based on the modeling assumptions. The energy flows include enthalpy flow of the gas streams, thermal conduction in the solids, enthalpy flow associated with gas diffusion between the gas channels and porous electrodes, electrical energy in the PEN, and convection between the gas and solid phases. The energy balances are derived and listed below for the four phases using the finite volume method based on the phase interactions shown in Figure 5.5 and the numerical modeling stencil given in Figure 5.6.
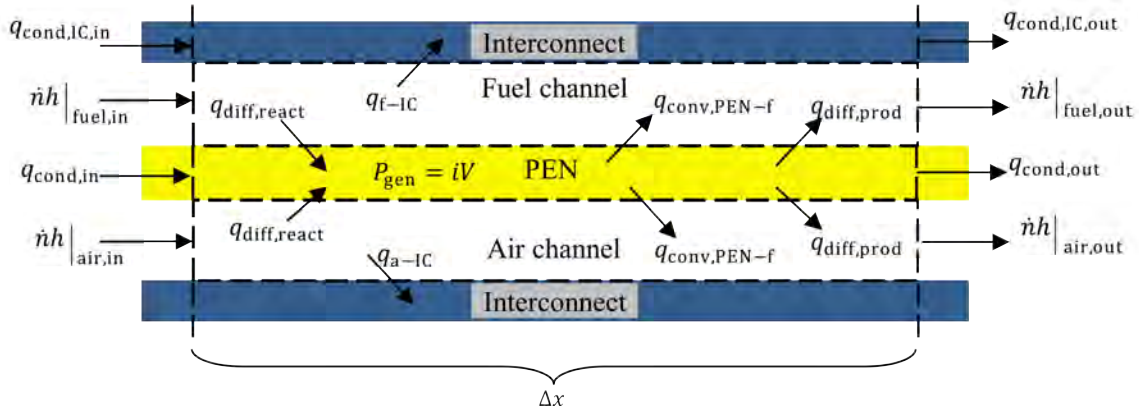
Figure 5.5: Heat flow diagram for a single discretized node in the channel-level model.

- Fuel channel: $(\dot{N}h)_{\mathrm{fuel,out}} - (\dot{N}h)_{\mathrm{fuel,in}} = q_{\mathrm{diff,prod}} - q_{\mathrm{diff,react}} + q_{\mathrm{conv,PEN\text{-}f}} + q_{\mathrm{conv,IC\text{-}f}}$

- Air channel: $(\dot{N}h)_{\mathrm{air,out}} - (\dot{N}h)_{\mathrm{air,in}} = q_{\mathrm{diff,prod}} - q_{\mathrm{diff,react}} + q_{\mathrm{conv,PEN\text{-}a}} + q_{\mathrm{conv,IC\text{-}a}}$

- PEN: $0 = q_{\mathrm{cond,in}} - q_{\mathrm{cond,out}} + q_{\mathrm{diff,react,f}} - q_{\mathrm{diff,prod,f}} + q_{\mathrm{diff,react,a}} - q_{\mathrm{diff,prod,a}} - q_{\mathrm{conv,PEN\text{-}a}} - q_{\mathrm{conv,PEN\text{-}f}} + P_{\mathrm{gen}}$

- Interconnect: $0 = q_{\mathrm{cond,IC,in}} - q_{\mathrm{cond,IC,out}} + q_{\mathrm{conv,f\text{-}IC}} + q_{\mathrm{conv,a\text{-}IC}}$

The individual energy flow terms at node i from the conservation equations above and the geometry defined in Figure 5.4 are calculated as:

- Convection from PEN to fuel gas: $q_{\mathrm{conv,PEN\text{-}f,i}} = h_{\mathrm{conv,f,i}} w_{\mathrm{ch}} \Delta x (T_{\mathrm{PEN,i}} - T_{\mathrm{f,i}})$

- Convection from PEN to air gas: $q_{\text{conv,PEN-a,i}} = h_{\text{conv,a,i}} w_{\text{ch}} \Delta x (T_{\text{PEN,i}} - T_{\text{a,i}})$

- Convection from fuel gas to IC: $q_{\text{conv,f-IC,i}} = h_{\text{conv,f,i}} (w_{\text{ch}} + 2 * h_{\text{ch}}) \Delta x (T_{\text{f,i}} - T_{\text{IC,i}})$

- Convection from air gas to IC: $q_{\text{conv,a-IC,i}} = h_{\text{conv,a,i}} (w_{\text{ch}} + 2 * h_{\text{ch}}) \Delta x (T_{\text{a,i}} - T_{\text{IC,i}})$

- Reactant and product diffusion: $q_{\text{diff,react,i}} + q_{\text{diff,prod,i}} = \sum_k^{N_{\text{rxn}}} r_{j,k,i} \sum_j^{N_{species}} \nu_j h_{j,i}(T,p)$

- PEN conduction forward: $q_{\text{cond,in}} = -\frac{k_{\text{PEN}} th_{\text{PEN}} w_{\text{ch}}}{\Delta x} (T_{\text{PEN},i} - T_{\text{PEN},i-1})$

- PEN conduction backward: $q_{\text{cond,out}} = -\frac{k_{\text{PEN}} th_{\text{PEN}} w_{\text{ch}}}{\Delta x} (T_{\text{PEN},i+1} - T_{\text{PEN},i})$

- IC cond. forward: $q_{\text{cond,in}} = -\frac{k_{\text{IC}}}{\Delta x} [th_{\text{rib}}(h_{\text{ch}} + th_{\text{IC}}/2) + th_{\text{IC}}(w_{\text{ch}} + th_{\text{IC}}/2)] (T_{\text{IC},i} - T_{\text{IC},i-1})$

- IC cond. backward: $q_{\text{cond,in}} = -\frac{k_{\text{IC}}}{\Delta x} [th_{\text{rib}}(h_{\text{ch}} + th_{\text{IC}}/2) + th_{\text{IC}}(w_{\text{ch}} + th_{\text{IC}}/2)] (T_{\text{IC},i+1} - T_{\text{IC},i})$

where $h_{\text{conv,fuel}}$ and $h_{\text{conv,air}}$ are the convection coefficients for the fuel and air channels calculated from a constant Nusselt number, $\text{Nu} = h_{\text{conv}} D_h / k$ of 3.39 for fully-deleveloped laminar flow from [166], where D_h is the hydraulic diameter and k is the gas thermal conductivity calculated using the Mason and Saxena modification [167] for the fuel and air mixtures.
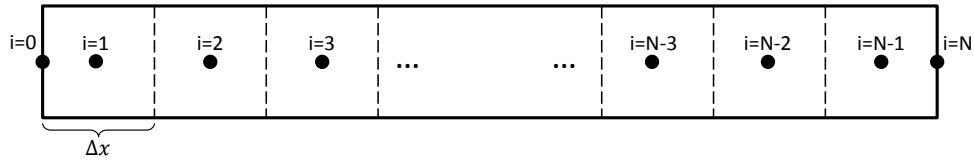
Figure 5.6: Discretization stencil for the channel-level model.

Because the heterogeneous reactions are assumed to occur in the catalyzed fuel-electrode support structure, the gaseous species participating in the reactions must diffuse from the gas channel into the support structure. This phenomena is accounted for by the reactant and product enthalpy flow terms, $q_{\text{diff,react}}$ and $q_{\text{diff,prod}}$, which are calculated based on the local rates of reaction in the cell.

One boundary conditions is required for each of the thermal energy and species conservation equations in the gas channels. The gas channel inlets are assumed to have constant

concentration and temperature, prescribed by the interface with other system components. Two boundary conditions are required for the solid structure thermal energy equations, which are second-order because of the thermal diffusion. The solid PEN and interconnects are assumed to be insulated.

Software implementation

The species conservation, energy conservation, and electrochemical model equations described previously are solved simultaneously to determine the local current, temperatures, and species concentrations, as well as cell voltage. The equation set is solved using two commercial software packages, Engineering Equation Solver [91] and gPROMS [168]. These software packages include built-in thermodynamic and transport property databases used to calculate the stream enthaplies, reaction equilibrium constants, gas thermal conductivity and viscosity.

5.1.6 Stack model adjustments

To more accurately represent cell-stack performance, an additional ohmic resistance is included. Experimental results on 6- and 10-cell YSZ-based stacks show an increased ohmic resistance of about 0.10 Ω cm^2 compared to single-cell tests [29, 169]. The additional resistance is attributed to stack component contact resistances. Thus, in the following, the equivalent ohmic resistance is defined as: $R_{eq,ohm,stack} = R_{eq,ohm,button} + 0.1\ \Omega\ \mathrm{cm}^2/A_{cell}$ (see Equation 5.2). The geometry used in the following model results is taken from these stack studies [29] with 12 x 12 cm cells (9.6 x 9.6 cm active area), and assumed 1 x 2 mm channels [92] and 1 mm thick interconnect. The PEN layer thicknesses are the same as described in Section 5.1.1 except that the fuel-electrode support thickness is reduced to 300 microns to represent a typical planar cell-stack design.

A comparison of the button-cell, planar cell, and planar stack models is provided in Figure 5.7 based on the models described previously in this chapter. The models are all simulated under laboratory conditions, meaning that the button cell is flooded with excess

reactant flow (maximum utilization of 5%) and the interconnects of the channel-level cell and stack models are isothermal to simulate operation within a temperature controlled furnace. The cell and stack models are simulated with constant reactant flowrates selected so that 50% fuel utilization and an excess air ratio of 5 are achieved at current density of 1.2 A/cm^2. The cell model shows slightly worse performance than the flooded button-cell model due to dilution of reactant species as they are utilized along the length of the channel. The performance impact is similar in both operating modes and increases at higher current density. The stack model indicates a substantial performance loss compared to the cell model attributed to additional ohmic resistances in cell-stacking.
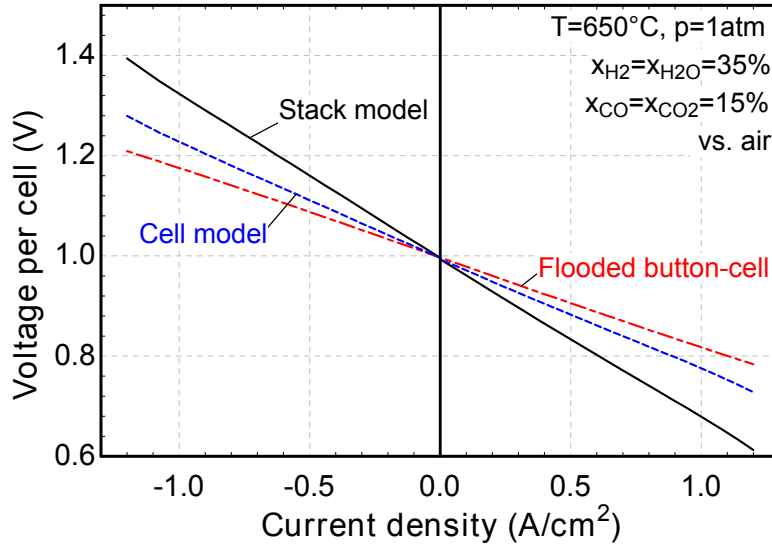
Figure 5.7: Comparison of the button-cell, planar cell, and stack models at 650℃, 1 atm with constant reactant flowrates.

5.2 System component models

The system balance of plant components include heat exchangers, compressors, turbines, ejectors, boiler, and condenser. Primarily, these components are modeled with thermodynamic equations including energy and entropy balances. Turbomachinery components are modeled with a fixed isentropic efficiency to determine the electric load or generation for a given inlet temperature and pressure ratio. A two-stream heat exchanger model determines

the heat transfer rate and one of the four interface temperatures. Similarly, boiler and condenser models dictate the thermal load required to generate steam or condense water out of a vapourous mixture. An important element of the system design is integrating the heat exchange network of these system components. A minimum pinch temperature of 20°C is used for all heat transfer processes.

For some of the system configurations presented here, condenser loads have excess heat rejection requirements not satisfied by system process streams. Air cooled condensers are considered to reject excess heat from the system to the environment with a parasitic power penalty of 0.04 kW_e per kW_{th} of rejected heat and minimum condenser outlet temperature of 50°C. The parasitic load is determined from a simple calculation assuming fan efficiency of 75%, air temperature rise from 30 to 80°C, and pressure change across the fan of 1.5 kPa.

A recycle ejector, or jet-pump, is used in some configurations to recycle oxidant exhausted from the ReSOC air-channel. The ejector performance is described by the following equation which is used to determine the driving flow pressure required by the compressor to entrain the desired flowrate of recycled oxidant [170].

$$\eta_{\text{ejector}} = \frac{\dot{V_2}p_2\ln(\frac{p_3}{p_2})}{\dot{V_1}(p_1 - p_3)} \tag{5.15}$$

where $\dot{V_1}$ and $\dot{V_2}$ are the volumetric flowrates of the primary driving flow and the recycled oxidant flow, respectively, and p_1, p_2, and p_3 are the static pressures of the driving flow, entrained flow (e.g., recycled oxidant), and ejector discharge stream, respectively. The pressure drop across the ReSOC stack air channel significantly impacts ejector performance.

Because this work considers only steady-state modeling results, the tanks (or other storage vessels) are modeled as simple sources and sinks with constant properties. This implications of tanked storage and stored gas property variation with time are highlighted throughout the results discussions. Additional discussion of the tank modeling assumptions is given in Section 5.5.

5.3 Operating parameter constraints

To accurately simulate reversible systems, the charge and discharge operating conditions must be selected so that the system is eventually returned to the original state of charge, thereby allowing continuous operation. The state of charge defined as the total amount of charge that can be delivered by the system at its current conditions is directly proportional to the hydrogen equivalence of the gas mixture stored in the fuel tank. It depends on both the quantity and composition of the stored gas mixtures. As related to the schematic in Figure 1.4, the system must be operated so that the tanks are not depleted of mass or diluted of their respective fuel or exhaust compositions. This section defines the operating constraints and explains how they manifest in the modeling studies by selecting appropriate combinations of current density, reactant gas flow, operating duration, and utilization parameters.

Energy storage is an inherently dynamic process, and the constraints described in this section are framed generally based on cumulative property change over an operating duration (i.e., energy, mass, electrical charge). In practice, this formulation allows a system to return to the original state of charge daily, seasonally, annually, or otherwise, after many complete or partial charge/discharge cycles at varying operating conditions. However, for the steady-state modeling considered here, the conditions are specified on a rate-basis (i.e., power, flow rate, electrical current).

To ensure complete system recharge, the total mass entering and leaving each tank must be equal over some operating duration. For the simple system considered here, the gas flows entering and leaving the tanks also corresponds to flows entering and leaving the stack. For example, the flow discharged from the fuel tank is the same as the flow at the stack inlet in SOFC mode. The mass flow constraints are represented by the following integral equations:

$$\int_0^{t_{\text{charge}}} \dot{m}_{\text{"fuel"},\text{in}}(t) = \int_0^{t_{\text{discharge}}} \dot{m}_{\text{"fuel"},\text{out}}(t) \tag{5.16}$$

$$\int_0^{t_{\text{charge}}} \dot{m}_{\text{"exhaust"},\text{out}}(t) = \int_0^{t_{\text{discharge}}} \dot{m}_{\text{"exhaust"},\text{in}}(t) \tag{5.17}$$

where t_i is the total operating duration and $\dot{m}_{i,j}$ is the mass flowrate into or out of the "fuel" or "exhaust" tank in either SOFC or SOEC mode as a function of time. The above constraints can also be applied in stand-alone reversible stack modeling (i.e., studies that do not consider the balance of plant as in 6). In these cases, the fuel flow into our out of a storage tank is replaced by the matching flow into or out of the stack. For example, the flow out of the "fuel" tank is equivalent to the flow into the stack in SOFC mode, while the flow into the "fuel" tank is equivalent to the flow out of the stack in SOEC mode.

A charge balance constraint ensures that the tanks are not diluted because each transfer of charge in the ReSOC requires an associated oxygen ion transfer. This condition requires that charge transfer in each mode is equal such that the atomic oxygen content of each tank is eventually returned to its original state (i.e., low oxygen content in the fuel tank and oxidized gas mixture in the exhaust tank). This constraint is imposed through the current density as:

$$\int_0^{t_{\text{charge}}} j_{\text{charge}}(t) = -\int_0^{t_{\text{discharge}}} j_{\text{discharge}}(t) \tag{5.18}$$

where j_{charge} and $j_{\text{discharge}}$ are the operating current densities in each mode. For steady state simulation, as in this research, Equations 5.16–5.18 simplify to:

$$\dot{m}_{\text{"fuel"},\text{in}} t_{\text{charge}} = \dot{m}_{\text{"fuel"},\text{out}} t_{\text{discharge}} \tag{5.19}$$

$$\dot{m}_{\text{"exhaust"},\text{in}} t_{\text{discharge}} = \dot{m}_{\text{"exhaust"},\text{out}} t_{\text{charge}} \tag{5.20}$$

$$j_{\text{charge}} t_{\text{charge}} = -j_{\text{discharge}} t_{\text{discharge}} \tag{5.21}$$

The steady-state constraints include the operating duration in each mode, which allows simulating, for example, longer (i.e., slower) charge duration and shorter (i.e., faster) discharge duration to fulfill specific energy storage applications.

The constraints for mass flow and current density are also connected to commonly used utilization parameters in solid oxide cells (see fuel utilization or reactant utilization definitions in Section 2.2.2). As such, two out of three (j, $\dot{m}$, and U_F or U_R) are assigned, which determines the third.

The oxidant utilization is characterized by the excess supplied to the stack as:

$$\lambda_{O2} = \frac{\dot{N}_{O2,\text{supplied}}}{\dot{N}_{O2,\text{transfer}}} \qquad (5.22)$$

where the excess air ratio, λ_{O2} is the ratio of oxygen flow at the inlet of the oxidant channel, $\dot{N}_{O2,\text{supplied}}$ to oxygen electrochemically converted, $\dot{N}_{O2,\text{transfer}}$ (either consumed in SOFC mode or generated in SOEC mode). By this definition, when the excess air ratio and current density magnitude are equal, the oxidant flowrate is also equal in each operating mode. The excess air ratio (or oxygen utilization) is not constrained in relation to recharging the system because the charge balance constraint given in Equation 5.18 ensures that the oxygen production and generation are equal. In configurations that utilize ambient air as oxidant / sweep gas, the air is limitless. However, if a tanked oxidant is used, the tank volume must be sized to allow sufficient oxidant supply for fuel oxidation.

5.4 Calculation procedure for modeling reversible systems

The process for simulating the roundtrip ReSOC operation at steady state is outlined in the computational flow diagram in Figure 5.8. First the simulation parameters are selected including nominal stack temperature, pressure, fuel utilization, excess air ratio, current density, fuel inlet temperature, and operating duration ratio (i.e., $t_{\text{SOFC}}/t_{\text{SOEC}}$). Within this approach, the fuel-channel inlet flowrate is fixed by the current density and fuel utilization, while the oxidant inlet temperature is fixed based on the energy conservation equations to maintain the prescribed average cell temperature. Different parameter selection strategies may be employed so long as the constraints defined in the previous section are satisfied. Some different parameter selection strategies specific to each of the following stack and system level studies are described in the following chapters.

Select simulation operating conditions: T, p, U_f, λ_{O_2}, and j.

→ Determine H-C-O ratios from T, p, and other considerations (see section 6.2).

→ Estimate SOFC inlet composition from equilibrium calculation.

→ Simulate SOFC mode with estimated inlet composition, T, p, U_f, λ_{O_2}, and j.

→ Simulate SOEC mode with T, p, j, U_f, λ_{O_2}, and inlet composition from outlet of SOFC.

→ Calculate roundtrip efficiency and other performance metrics from model results in each mode (e.g. voltage).

Iterate until $x_{SOFC,in,i} = x_{SOEC,out,i}$

Figure 5.8: Calculation sequence for simulating ReSOC systems at steady-state.

After the stack operating parameters are selected, the atomic H-C-O ratios of the stored "fuel" composition (i.e., SOFC mode inlet composition) are selected, which may depend on cell temperature and pressure. This process requires considering carbon deposition, required carbon content for thermal management, and cell efficiency. Thermodynamic calculations as detailed in Chapter 4 are helpful in selecting initial system operating conditions. Based on the H-C-O composition, the SOFC mode inlet mole fractions are estimated from equilibrium at the nominal stack operating conditions. At steady state conditions (i.e., after many charge/discharge cycles), the tanked "fuel" composition will reflect the composition generated from the SOEC operating mode. To represent this steady-state condition, the model is simulated iteratively between SOFC and SOEC mode. During iteration the composition entering one mode is set to the composition generated in the opposite mode until the outlet composition from the SOEC mode stack converges to the inlet compositions of the SOFC mode stack (typically converges after 2-4 iterations). Finally, the roundtrip efficiency and other performance parameters are calculated based on the model results including cell voltage, axial temperature and species profiles in the ReSOC, tanked compositions and properties, and BOP component loads.

5.5 Performance metrics

The roundtrip efficiency metrics have been defined previously in Section 2.5.1. The performance of an energy storage system is determined primarily by the roundtrip efficiency and cost. However, in determining the most suitable ReSOC system, it is important to also consider the system thermal behavior, energy density, and durability.

High system energy density is important to reduce capital investment in storage tanks. The storage temperature and pressure have a major effect on energy density; however, the composition is also important whereby higher proportion of energy dense methane requires smaller tanks for equivalent energy storage capacity. The energy density, ϵ_{st} is estimated here for steady state simulations by the following equation:

$$\epsilon_{st} = \frac{P_{SOFC,net} t_{discharge}}{\sum V_{tank,i}} \tag{5.23}$$

where $P_{SOFC,net}$ is the net power generation during discharging and $V_{tank,i}$ represents any storage tank volumes (i.e., "fuel", "exhaust", and "oxidant"). The numerator in 5.23 is the net energy that can be produced by a ReSOC system including considerations for inefficiency and unused fuel. The amount of energy stored in the "fuel" tank (e.g., fuel heating value) at full charge is necessarily higher than the recoverable energy. For steady state simulation, the tank volumes are estimated by:

$$V_{tank,i} = \frac{v\left(T, p_{max}\right) \dot{N}_{evacuation} t_{evacuation}}{1 - \frac{v(T,p_{max})}{v(T,p_{min})}} \tag{5.24}$$

where $v(T, p)$ is the molar specific volume calculated at temperature T and pressure p, $t_{evacuation}$ and $N_{evacuation}$ are the duration and molar flow during tank discharging, T is the tank temperature and p_i is either the maximum or minimum tank pressure. This formulation is derived assuming constant tank temperature during operation, which is not expected for rigid tanks. However, higher fidelity system simulation is required to capture the effects of dynamic operation on system energy density. During steady-state system simulation, both the "fuel" and "exhaust" tank pressures are assumed to be at the average of maximum and minimum tank pressure. In other words, for a nominal tank pressure of 20 bar, the tank is assumed to vary between 3 and 37 bar during operation.

The cell durability is also considered as it relates to cell temperature gradients and carbon deposition. The ceramic cells are susceptible to mechanical failure from uneven thermal expansion, so it is important to maintain low axial temperature gradients. Operating condition selections including temperature, pressure and H-C-O ratios of the fuel mixture

are constrained by estimated carbon deposition regions and the axial temperature gradient is used as a metric of cell durability.

CHAPTER 6

SIMULATION OF CELLS AND STACKS

Some operating characteristics of the reversible solid oxide cell system can be understood by analysis of the cell and cell-stack itself without integrated system modeling with the supporting balance of plant. Because the stack significantly influences system performance through both its electrical and thermal characteristics, it is relevant to study the stack in more detail. Two benefits are derived from isolated analysis of the cell-stack model: (i) the tradeoffs associated with operating parameter decisions are revealed so that the impact of operating parameters are more easily understood when interpreting system simulation results, and (ii) certain operating parameter decisions are shown to be explicitly beneficial independent of system implementation. Here, the channel-level model described in the previous chapter is used to predict the effect of key operating conditions on roundtrip efficiency, heat generation, and cell durability. In particular, parametric studies are performed to assess the performance impact of current density, reactant composition (i.e., fuel and exhaust), oxidant / sweep gas composition (i.e., air vs. oxygen), stack flow configuration, stack tail-gas recycle, pressurization, and operating temperature. Many of these operating parameters impact both stack and system operation which is discussed. Additionally, the channel-level model computes axial temperature and species profiles within the ReSOC, meaning that durability concerns related to temperature gradients and carbon deposition are quantified to inform operating parameter selection. These stack-level studies follow the calculation methodology described in Sections 5.3 and 5.4. However, some operating parameter selection is specific to these studies which is explained first.

6.1   Operating parameter selection

The following results assess the performance impact of various operating parameters and design decisions including current density, fuel composition, flow configuration, and

oxidant composition. It is useful to determine base case operating parameters preceding the parametric studies. The base case average cell temperature is selected to 650°C to match the best performance shown in cell test results (see Section 5.1.1), although some benefit is expected from further reducing the operating temperature to 600°C as described in 6.2.7. The other base case parameters are listed in Table 6.1 and used in the following studies unless otherwise indicated. The fuel utilization and average current density are model input parameters, which fix the inlet reactant fuel flow in each operating mode. Similarly, the prescribed excess air ratio fixes the inlet oxidant flowrate (see Equation 5.22).

In this chapter, the heat generation is characterized by the temperature increase of the supplied oxidant at fixed excess air ratio, where higher air temperature increase corresponds with increased heat generation. For this approach, a negative air temperature rise means that high temperature air is supplied to heat the cell and maintain the prescribed average cell temperature. For system implementations it is critical that the oxidant stream is heated in the ReSOC stack to then provide system preheating, so a positive air temperature rise is used as a criteria for selecting suitable operating conditions. The gas flow in the fuel channel also acts as a potentially variable heat sink, but is negligible because the flowrate is much smaller than the oxidant and the flowrate and specific heat do not vary drastically for the conditions in this study.

Table 6.1: Stack simulation base case operating parameters.

Parameter	Value
Flow configuration	co-flow in both modes
Average temperature, T	650°C
Stack pressure, p	1 bar
Fuel utilization, U_F	60%
Excess air ratio, λ_{O2}	5.0
Current density, j	0.5 A/cm^2
H/C/O fuel composition	87.7 / 7.3 / 5.0
Fuel channel inlet temperature	600°C
Oxidant composition	21% O_2 / 79% N_2

6.2 Cell-stack operating parameter studies

The following sections detail the parametric study results for the stand-alone stack simulation. Each study includes a discussion of the results and possible implications toward system operation and performance.

6.2.1 Current density

The current density has a major influence on cell efficiency because it impacts overpotential in both operating modes. The roundtrip efficiency decreases nearly linearly with increased current density, as shown in Figure 6.1 for both the stack and cell model characteristics, which differ only by the 0.10 Ωcm^2 ohmic overpotential described in Section 5.1.6. The cell performance indicates that roundtrip efficiency of 80% is achieved at 0.48 A/cm^2; however when the stack characteristic is used, the current density required for 80% efficiency is 0.32 A/cm^2. This result suggests that improvement in stack performance, reducing the internal resistances associated with stacking cells, is necessary to achieve high efficiency with reasonable current density (i.e., > 0.4 A/cm^2).
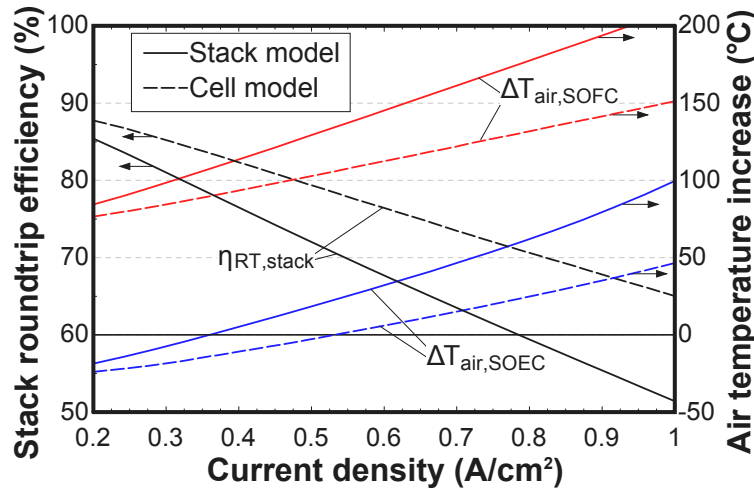
Figure 6.1: Efficiency (left) and air temperature increase (right) vs. current density predicted from both the stack (solid) and cell (dashed) model characteristics.

The cell heat generation is also quantified in each mode by the air temperature increase and reported in Figure 6.1. Under the baseline operation conditions, the stack is net endothermic in SOEC mode at the 80% target efficiency, as shown by the negative air temperature increase at 0.32 A/cm^2 and 0.48 A/cm^2 for the stack and cell models, respectively. The efficiency is therefore limited by thermal management issues at the system level, meaning that while it is important to improve the stack performance for power density and economic reasons, the operating conditions must also be adjusted so that the SOEC mode is exothermic even at high efficiency. The air temperature rise is >75°C in SOFC mode cell (or stack) for the range of current densities shown, meaning that the oxidant-channel exhaust can effectively preheat the oxidant-channel inlet stream. The stack model characteristic is used for the remaining studies.

The axial cell temperature profiles are shown in Figure 6.2 for current densities of 0.25 and 0.75 A/cm^2. For the co-flow configuration used in the base case, the cell temperature increases in the gas flow direction because gas flow cools the cell at the inlet and is then heated by the exothermic chemistry and/or irreversible electrochemical conversion losses along the length of the cell. Larger cell temperature increase and larger axial temperature gradients are observed for more exothermic operation, either by increased current density or operating in SOFC mode versus SOEC mode. The SOEC mode -0.25 A/cm^2 case is nearly isothermal, operating within 5°C of the average temperature over the length of the cell. The cell temperature decrease at the air inlet indicates that the inlet airflow is actually heating the cell. Alternatively, the 0.75 A/cm^2 SOFC mode case shows a temperature difference of nearly 100°C along the cell. The initial cell temperature decrease in this case is caused by a small amount of methanation at the gas flow inlet, when the composition is rapidly brought from the near-equilibrium value at the SOEC outlet (675°C) to the SOFC inlet (610°C).

The temperature profiles in Figure 6.2 do not have the steep gradients and complex profiles typically observed when operating on, for example, direct internal reforming SOFCs. Despite the use of carbonaceous reactant species, the composition entering the stack in

125
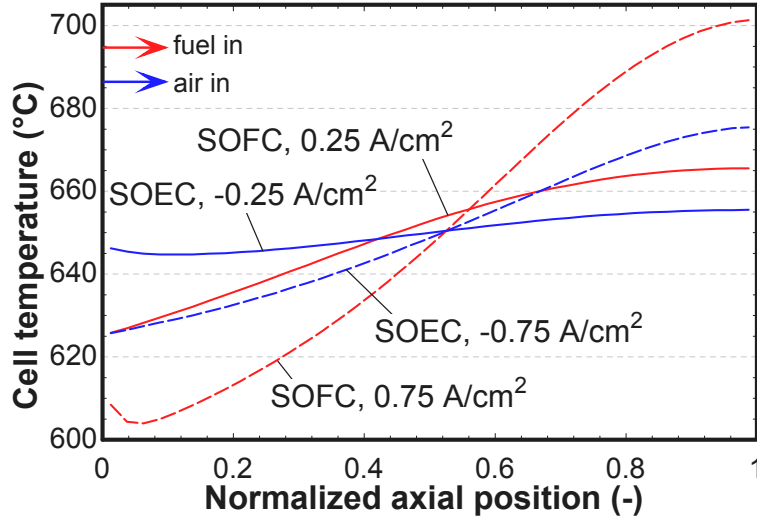
Figure 6.2: Axial temperature profiles for SOFC and SOEC modes at different current densities in co-flow configuration.

either operating mode is already near the equilibrium composition at the stack operating conditions. Axial species profiles are shown in Figure 6.3, where the compositions at either end (zero or unity axial position) represent the stored SOFC or SOEC outlet gases. The gradual species conversion contributes to the relatively stable temperature profiles. The methane content generated in the SOEC is 12 mol.%, and the reactant species are primarily steam and hydrogen.

6.2.2 Reactant composition

Selecting appropriate reactant compositions for the fuel and exhaust tanks requires considering the effects of cell electrical performance, thermal generation, energy density, and durability. Furthermore, because the reactant composition in one mode is ultimately generated from operating in the opposite mode, the compositions are dependent on the stack operating conditions. In the ReSOC stack, the hydrogen-to-carbon ratio of the reactant stream remains constant, while the oxygen content is either increased (SOFC mode) or decreased (SOEC mode).

126
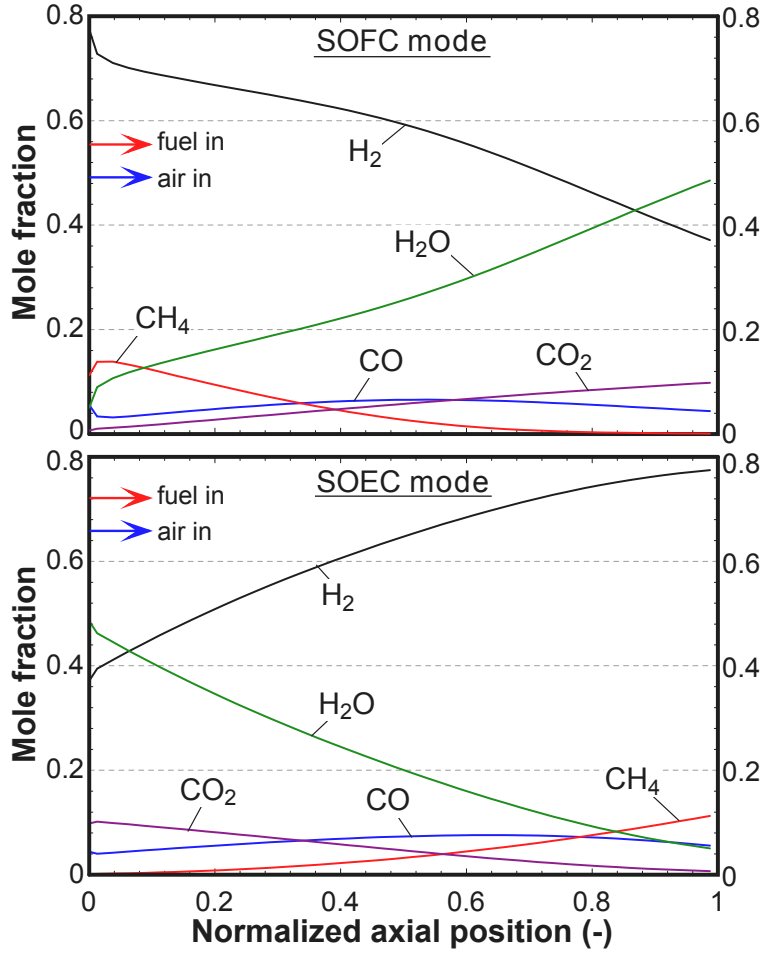
Figure 6.3: Axial species profiles in SOFC and SOEC modes in co-flow configuration.

The C-H-O ternary diagram (see Figure 6.4) is used to define the feasible range of compositions. Conversion in the ReSOC stack is represented by moving either toward or away from the oxygen-vertex on the constant H/C lines. The fully oxidized region is the area where stoichiometry dictates formation of oxygen molecules. The fuel channel composition in SOFC mode may not be oxidized beyond this point because the cell performance declines rapidly (i.e., implies $U_F > 1$). The carbon boundary suggests that coking occurs if there is too much carbon or too little oxygen in the fuel mixture.

The selected fuel composition is near the carbon deposition boundary which enables storing a highly reduced gas mixture to improve storage energy density and fuel cell performance.
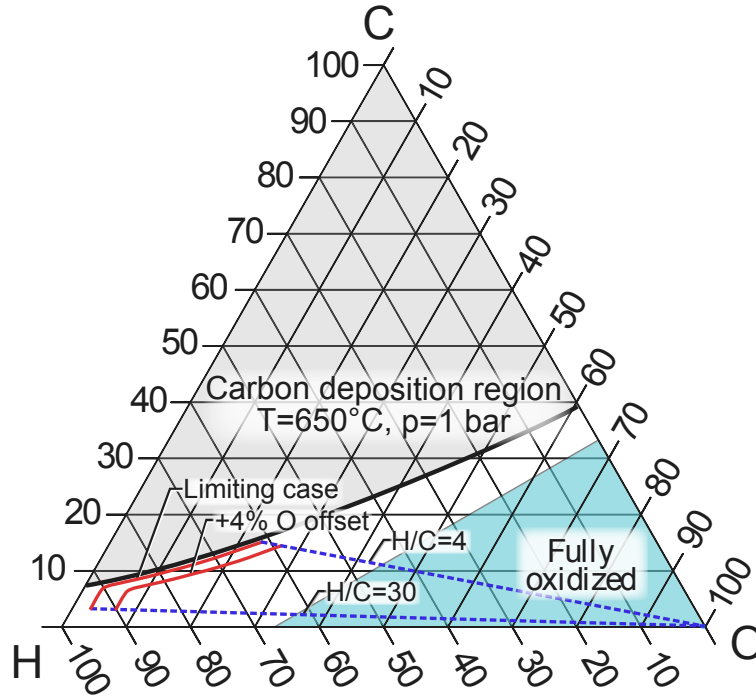
Figure 6.4: C-H-O ternary diagram showing carbon deposition region (grey), fully oxidized region (blue), and possible fuel compositions (red lines).

However, there is a range of H-C-O ratios near the deposition boundary which are indicated by the red lines in Figure 6.4 between HTCR values of 4 and 30. The atomic oxygen content is limited to a minimum of 3% when not constrained by the carbon deposition boundary. Due to local variations in temperature and composition, and non-equilibrated conditions within the porous fuel electrode, the carbon deposition boundary is not a perfect indicator of safe operating conditions, as discussed in Section 2.2.2. Two cases are considered in this study: (1) fuel oxygen content constrained by the carbon deposition boundary, and (2) fuel oxygen content offset from the carbon deposition boundary by 4% atomic oxygen content. The minimum oxygen-to-carbon ratios for these cases are 0.42 and 1.02, respectively.

The cell voltages in each operating mode and roundtrip efficiency are plotted in Figure 6.5(a) as a function of HTCR representing the "limiting case" and "+4% O offset" lines shown in Figure 6.4. For both cases, the roundtrip efficiency is maximized between HTCR of 6 and 8, and minimized at HTCR of about 12.6, where the composition shifts from being

constrained by the carbon deposition boundary to being set by the minimum oxygen constraint (i.e., O=3%). The effect of HTCR on stack roundtrip efficiency is relatively minor, varying by about 1 percentage point over a wide range of compositions.
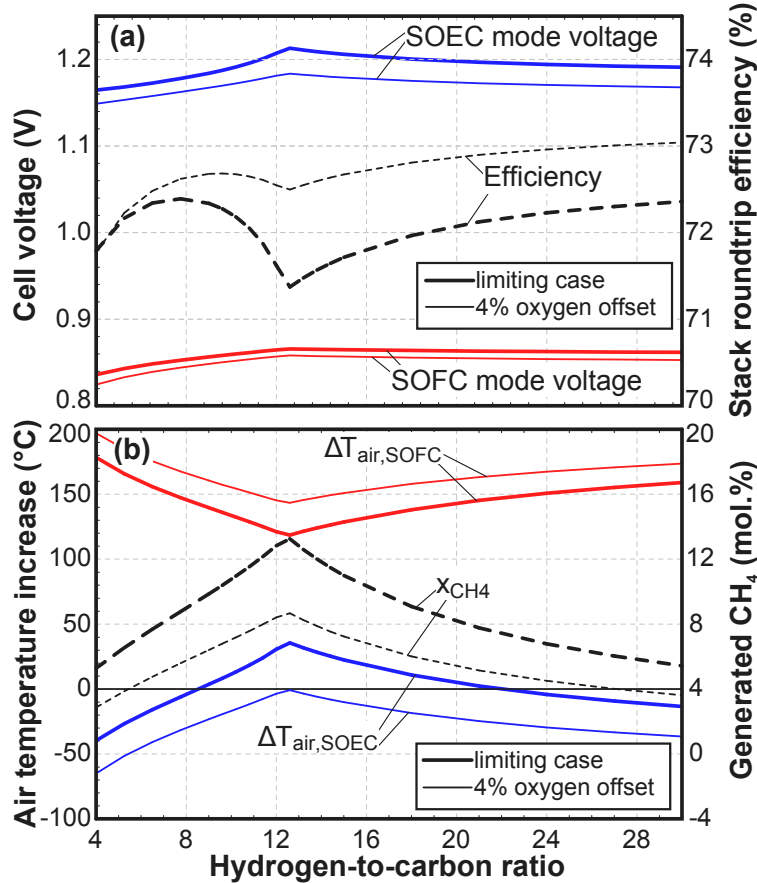
Figure 6.5: Cell performance parameters with the composition limited by carbon deposition boundary and offset by +4% oxygen content, including: (a) cell voltage and roundtrip efficiency, (b) air temperature increase and generated methane mole fraction.

Switching from the limiting case to the offset case results in a roundtrip efficiency increase of about 1 percentage point at HTCR=12.6. Both SOFC and SOEC mode voltages decrease when the fuel oxygen content increases (i.e., offset case); this is explained by decreased OCV when the cell is exposed to a more oxidized gas mixture. However, a net increase in roundtrip efficiency is realized because the SOEC voltage decrease is greater than that experienced by SOFC operation.

Figure 6.5(b) shows the air temperature increase and generated methane mole fraction for varied HTCR. The SOEC mode air temperature increase is negative for most of the range shown, but is maximized for lower oxygen content (i.e., the limiting case, rather than offset case) and at HTCR of 12.6 which corresponds with the point of minimum efficiency. The SOFC mode temperature rise is also minimized at HTCR=12.6, which is favorable for reducing the required cooling airflow and associated compressor load. The maximum SOEC mode air temperature rise is partially attributed to the lower efficiency at this composition. However, normalizing the HTCR=12.6 case to a stack roundtrip efficiency of 72.4% (i.e., equal to efficiency at HTCR=7.75) by reducing the current density to 0.478 A/cm^2 results in an air temperature rise of 32°C, which is higher than the -6°C rise observed for HTCR=7.75 at 0.5A/cm^2. This indicates that the HTCR=12.6 operating point is favorable to system thermal management because of higher SOEC mode heat generation independent of the cell efficiency.

The optimal SOEC heat generation behavior at HTCR=12.6 is explained by increased methane production. The generated methane content shown in Figure 6.5(b) is maximized to a value of 13 mol.% at HTCR=12.6 for the limiting case. The 4% offset case is endothermic for all HTCR. Normalizing the limiting and offset cases to fixed roundtrip efficiency at HTCR=12.6 by increasing the offset case current density to 0.525 A/cm^2 results in higher SOEC mode heat generation for the limiting case (not shown). This result is consistent with higher methane formation for the limiting case and concludes that the best thermal performance is achieved by operating near the carbon deposition boundary. This conclusion highlights the importance of clarifying how close the gas composition can operate to the carbon deposition limit without suffering deleterious coking. The base case H-C-O composition given in Table 6.1 is used as the "fuel" composition in the remaining studies in the remaining studies. It has an oxygen offset of 2% from the limiting case, oxygen-to-carbon ratio of 0.68, and an HTCR of 12, which is near the optimal point from Figure 6.5.

6.2.3 Co- vs. counter-flow configurations

The flow configuration – meaning whether the oxidant and reactant streams are flowing in the same direction, opposite direction, or perpendicular to each other – also impacts the cell and system performance. Typically cross-flow performance falls in between that of co- and counter-flow [171]. The one-dimensional model employed in this study is formulated to simulate either co- or counter-flow operation. Table 6.2 shows performance results for all combinations of flow-configuration in SOFC and SOEC mode.

Table 6.2: Performance summary of co- and counter-flow configurations in both operating modes.

Flow configuration		SOFC mode				SOEC mode				RT efficiency
SOFC	SOEC	V_{cell} mV	dT/dx °C/mm	ΔT_{air} °C	x_{CH4} %	V_{cell} mV	dT/dx °C/mm	ΔT_{air} °C	x_{CH4} %	(%)
co	co	862	1.15	129	0.1	1197	0.43	18	11.2	72.0
cntr	cntr	869	3.07	138	0.7	1194	0.98	21	12.6	72.8
co	cntr	862	1.15	120	0.1	1193	1.04	29	12.8	72.3
cntr	co	869	3.13	147	0.7	1197	0.43	11	11.3	72.6
co/counter, 0.488 A/cm^2		866	1.12	119	0.1	1190	0.99	27	12.7	72.8

The stack roundtrip efficiency is maximized when both modes are operated in counter-flow. This is in agreement with previous studies showing highest electrical performance for counter-flow in SOFCs [147] and SOECs [172]. Perhaps more interesting is the effect of flow configuration on stack heat generation. Operating the SOFC mode in co-flow and/or operating the SOEC mode in counter-flow leads to higher SOEC mode heat generation (see air temperature change, ΔT_{air} in Table 6.2). These trends are explained by the higher change in methane mole fraction from fuel channel inlet to outlet in SOEC mode. Counter-flow operation results in lower fuel-channel outlet gas temperatures because the fuel channel outlet corresponds with the air cooling inlet. Alternatively, co-flow operation leads to higher fuel-channel outlet temperatures. When the SOFC is operated in a co-flow configuration, the higher outlet temperature results in lower outlet methane content when compared to counter-

flow (see Table 6.2). Further, when SOEC mode is operated in counter-flow, the lower outlet temperature results in higher methane content. Thus, when the SOFC is operated in co-flow and SOEC in counter-flow (i.e., co/counter-flow), the amount of exothermic methane formation is largest compared to the other configurations, leading to maximum SOEC air temperature rise of 29°C. This configuration also leads to more methane reforming in the SOFC mode, and an associated minimum SOFC air temperature rise. For practical systems, the 29°C temperature rise is not sufficient to satisfy pinch temperatures in a preheating heat exchanger, so oxidant airflow may be reduced to increase the temperature rise with a minor electrical performance penalty.

The high air temperature increase for the co/counter-flow case is primarily due to increased methanation, but also partially explained by the lower roundtrip efficiency. To quantify this impact, the efficiency of the co/counter-flow case is increased to the value of the counter/counter-flow case (i.e., 72.8%) by reducing the current density to 0.488 A/cm^2. For equivalent efficiency, the heat generation is higher when the stack is operated in co/counter-flow (see Table 6.2). However, the discharge power density at the lower current density is reduced by 3% compared with the counter/counter-flow case.

The cell durability is also an important consideration in choosing the flow configuration, as represented here through the maximum cell temperature gradient. Two trends are observed: (i) higher axial temperature gradient is seen for counter-flow operation, which is consistent with previous SOFC modeling studies [147] and (ii) higher temperature gradient is seen in SOFC mode, compared with SOEC mode. The second trend is explained by the cell net heat generation, as shown in Figure 6.2 where higher heat generation also leads to higher temperature gradients. The high efficiency and near-equilibrium reactant compositions used for this ReSOC application lead to lower axial temperature gradients compared to typical SOFC applications. Thus, the temperature gradients are not critical in selecting the most suitable stack flow configurations.

Other practical design considerations when selecting flow configuration include reducing localized variations in the cell environment between operating modes including local temperature, composition, and current density swings. For the co/counter-flow configuration suggested by the results in Table 6.2, it may be envisioned that the airflow direction is unaltered between operating modes, while the fuel-channel flow switches direction along with mode switching. Axial species, temperature, and current density profiles for the co/counter-flow configuration are shown in Figure 6.6. For this simulation, the air temperature increase is set to 100°C in both operating modes, replacing the excess air ratio parameter assignment in the base case. This approach is more suitable to system simulation to ensure the pinch temperature in the air preheater can be met by the air exhaust stream. However, the excess air ratios are 6.1 and 1.4 for SOFC and SOEC mode, respectively, which reduces the practicality of using the same air blower in both operating modes. Additional parameter adjustment may be employed in system simulations to reduce the difference in airflow rate between operating modes.

In Figure 6.6(a), the composition at a given axial location in the stack varies less than if the reactants entered the fuel channel from the same side in each operating mode. However, system implementation of changing the flow direction in the fuel channel must be addressed. The temperature and current density magnitude profiles are shown in Figure 6.6(b). The cell temperature increases in the fuel-flow direction in both modes, meaning that the cell will undergo localized temperature cycling of up to 50°C. Similarly, the current density profiles show opposite trends throughout the cell, indicating galvanic cycling between 0.49 and -0.27 A/cm^2 at the air inlet, and between 0.43 and -0.65 A/cm^2 at the air outlet. The flow configuration may be selected to either maintain relatively constant gas constitution in the fuel channel (as shown in Figure 6.6), or more constant temperature profiles (if the fuel-channel flow direction is the same in each operating mode).
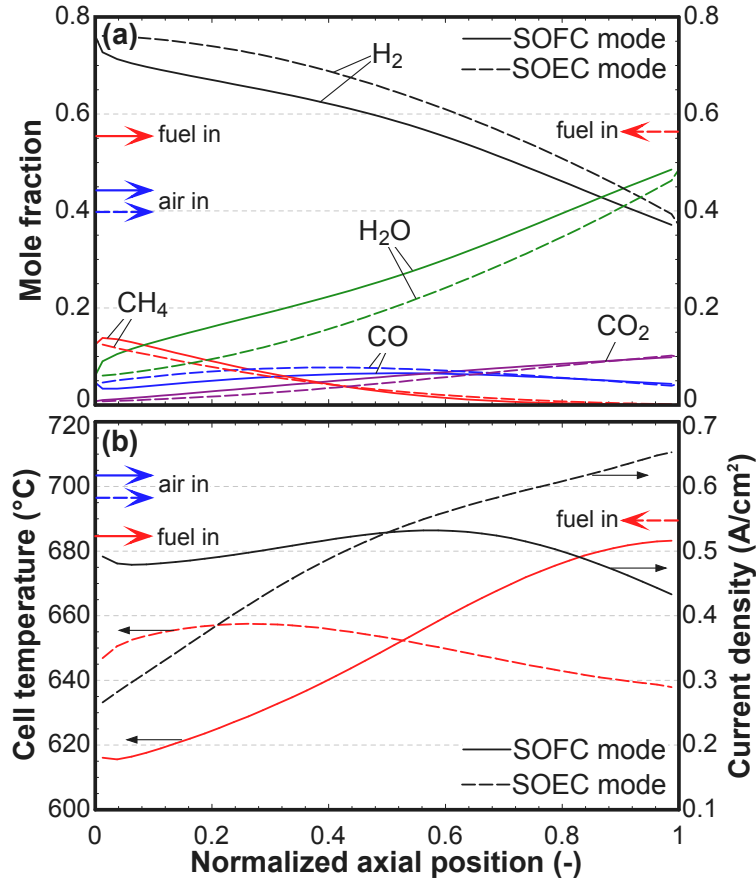
Figure 6.6: Axial profiles for (a) species, (b) temperature and current density magnitude in both SOFC and SOEC mode. Co-flow in SOFC mode and counter-flow in SOEC mode with reversed reactant flow direction and constant airflow direction.

6.2.4 Oxidant composition: air vs. oxygen

A ReSOC energy storage system may be configured to use either ambient air or stored oxidant (i.e., stored oxygen or oxygen enhanced air). In this section, we consider the efficiency and thermal impacts of the oxidant composition. Figure 6.7(a) shows the cell voltage and roundtrip efficiency as a function of oxidant oxygen mole fraction between 21% (air) and 100% (pure oxygen). The stack roundtrip efficiency increases by around 2.5% when the cells are operated with oxygen rather than air. This benefit is attributed primarily to increased SOFC mode operating voltage, which overcomes a slight increase in SOEC mode voltage. In both modes, shifting from air to oxygen increases the OCV and decreases the activation

and concentration overpotentials. In SOFC mode, these two effects are complimentary, both favorably increasing the SOFC mode voltage. In SOEC mode, the two effects act in opposition, where the overpotential is decreased and OCV is increased for a net voltage increase.
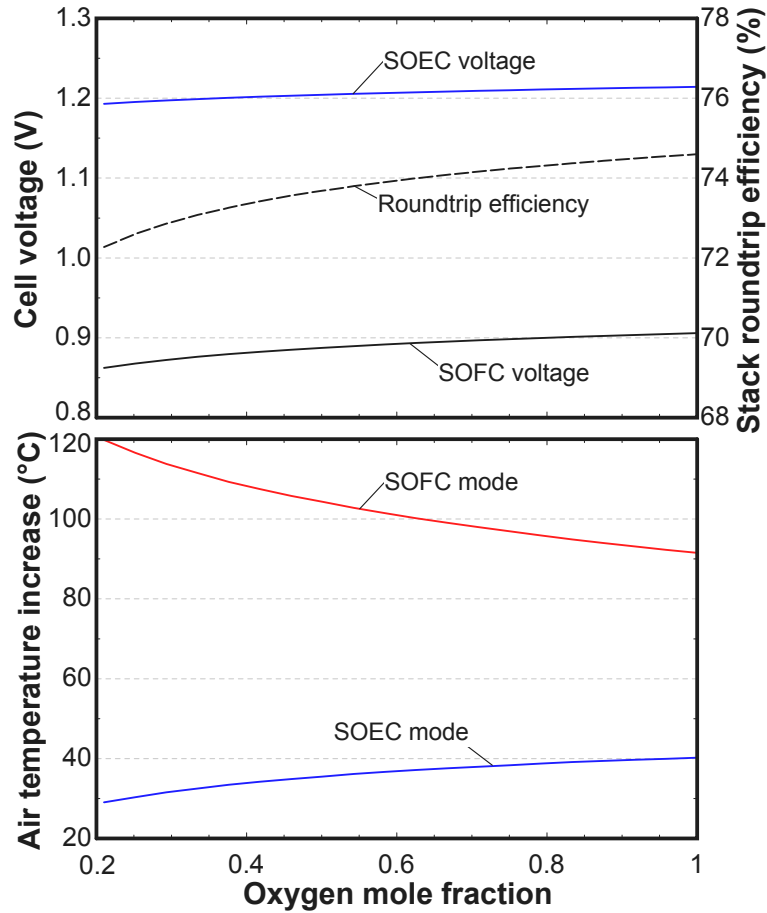
Figure 6.7: Voltage, stack roundtrip efficiency, and air temperature increase vs. oxidant composition.

The thermal impact of using oxygen rather than air is that more heat is generated in SOEC mode and less heat is generated in SOFC mode (see Figure 6.7). Increased heat generation in SOEC mode, shown as a 10°C larger air temperature increase, is particularly notable because it occurs despite increased roundtrip efficiency. Shifting from air to oxygen implies operating the SOFC much more efficiently, and the SOEC slightly less efficiently, leading to a more beneficial thermal characteristic and improved overall stack roundtrip

efficiency.

The system implications of storing oxidant are significant. Specifically, this configuration modification requires an additional pressurized storage tank and compression (and possibly expansion) turbo-machinery. Ultimately the benefit of using an oxidant with higher oxygen content is determined by the tradeoff between the stack efficiency and thermal benefit against the increased capital cost and auxiliary power of the compressor. Pressurizing the ReSOC stack may be synergistic with storing oxidant because the pressure ratio between the stack and storage tanks is reduced. While pressurized stacks are presently considered less feasible at the distributed scale, this configuration may be competitive in applications where energy density and efficiency are favored over cost.

6.2.5 Fuel-channel product recycle

Recycling the fuel-channel products is a common operating strategy for internal reforming SOFCs to provide the steam content required for methane reforming (i.e., anode-gas recycle). SOEC systems also use recycle so that some hydrogen is present at the fuel-channel inlet to keep from damaging the PEN materials with the otherwise highly oxidized feedstock (i.e., H_2O and CO_2). This recycle is achieved by means of a stream-split downstream of the stack and a high temperature ejector to mix the recycled stream with fresh product. In a ReSOC system the implications of product recycle are not obvious and warrants further exploration. Product recycle — and the recycle ratio defined as the ratio of mass flow in the recycle stream to mass flow discharged from the stack (see Figure 6.8) — can influence system performance through the electrical characteristic, thermal characteristic, and local gas compositions. The effects of recycle also vary between the two operating modes, providing unique benefits and/or tradeoffs.

Here the impact of fuel-channel recycle is analyzed in terms of the roundtrip efficiency and heat generation metrics as in the previous sections of this chapter. The base case parameters in Table 6.1 are used in this simulation, although the utilization and gas composition parameters are applied differently. Specifically, the fuel utilization of 60% is set based on

136
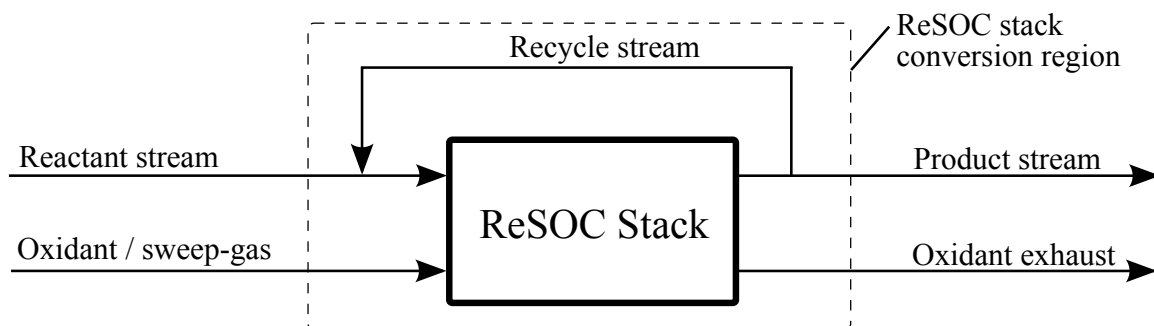
Figure 6.8: Schematic of the ReSOC stack with fuel-channel product recycle.

the composition at the inlet and outlet of the "ReSOC stack conversion region" shown in Figure 6.8, which encompasses the stack conversion and recycle processes. As a result, the fuel utilization in the stack, or "per pass" utilization, is lower than the system fuel utilization. The gas compositions are also held constant at the inlet to the "conversion region", meaning that the composition entering the fuel-channel is affected by the recycle ratio.

The air temperature increase and cell voltage are plotted as a function of recycle ratio in Figure 6.9. First, consider varying the recycle ratio at constant current density. As recycle ratio increases, the cell voltage decreases in SOFC mode and increases in SOEC mode indicating decreased roundtrip efficiency. These voltage trends are attributed to dilution of the tanked feedstock gases by the recycle stream and the associated effect on the local open-circuit voltage. In other words, the fuel cell operates less efficiently when the fuel feedstock is premixed with exhaust species. Another trend shown in Figure 6.9 is that the air temperature increase in each operating mode is higher when recycle is employed; although, this trend is a direct cause of the reduced operating efficiency. When the cell is operated at constant voltage in each mode (i.e., constant roundtrip efficiency), the air temperature increase is mostly constant with recycle ratio. The lower air temperature increase at high recycle ratio in SOEC mode is attributed to a small drop in methane production caused by the interactions of species conversion and local cell temperature. Ultimately, this analysis suggests that recycling gas streams exhausted from the fuel channel has the effect of lowering the roundtrip efficiency. Any thermal management benefit (i.e., increased air temperature
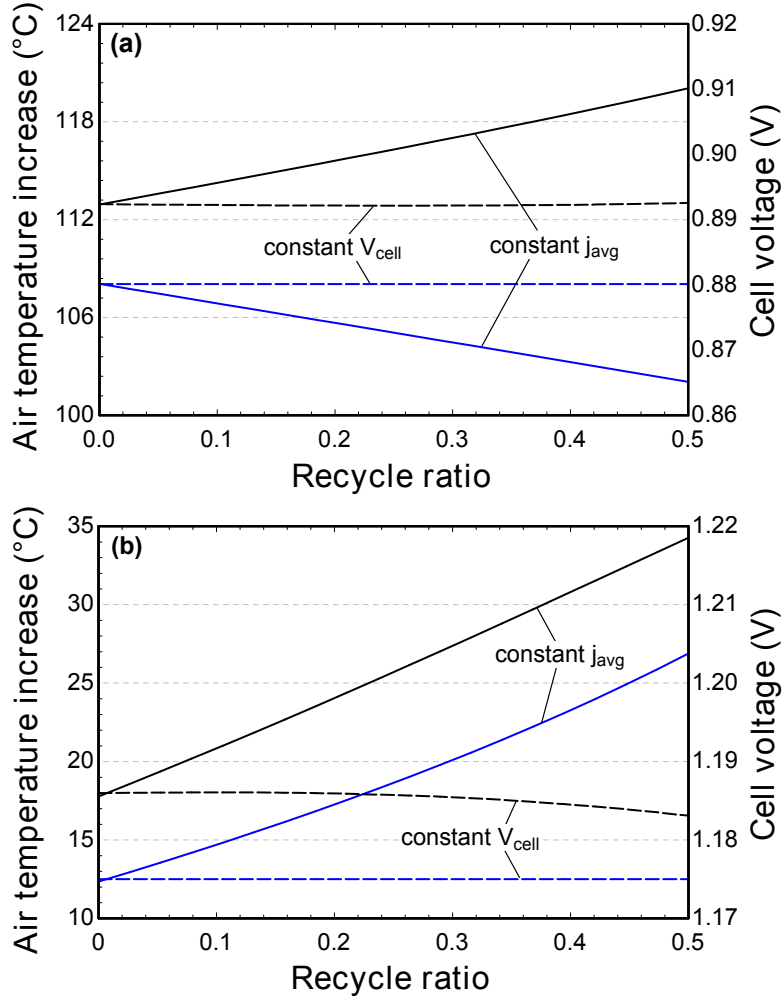
Figure 6.9: Air temperature increase and cell voltage vs. fuel-channel recycle ratio for (a) SOFC and (b) SOEC modes at constant cell voltage or constant current density.

rise in SOEC mode), is solely attributed to decreased efficiency, so recycle is not expected to benefit system performance.

The negative impact of fuel-channel recycle on electrical efficiency discussed above is common to SOFC systems [171], but this penalty is overcome when considering system operation because of the reduced boiler load needed to achieve a given steam-to-carbon ratio, for example. Next we will consider the potential impact of recycle on reactant preheating in a ReSOC system. In ReSOC systems where water is stored as a liquid, the roundtrip efficiency is limited by the energetic cost to generate steam in SOEC mode (see Chapters
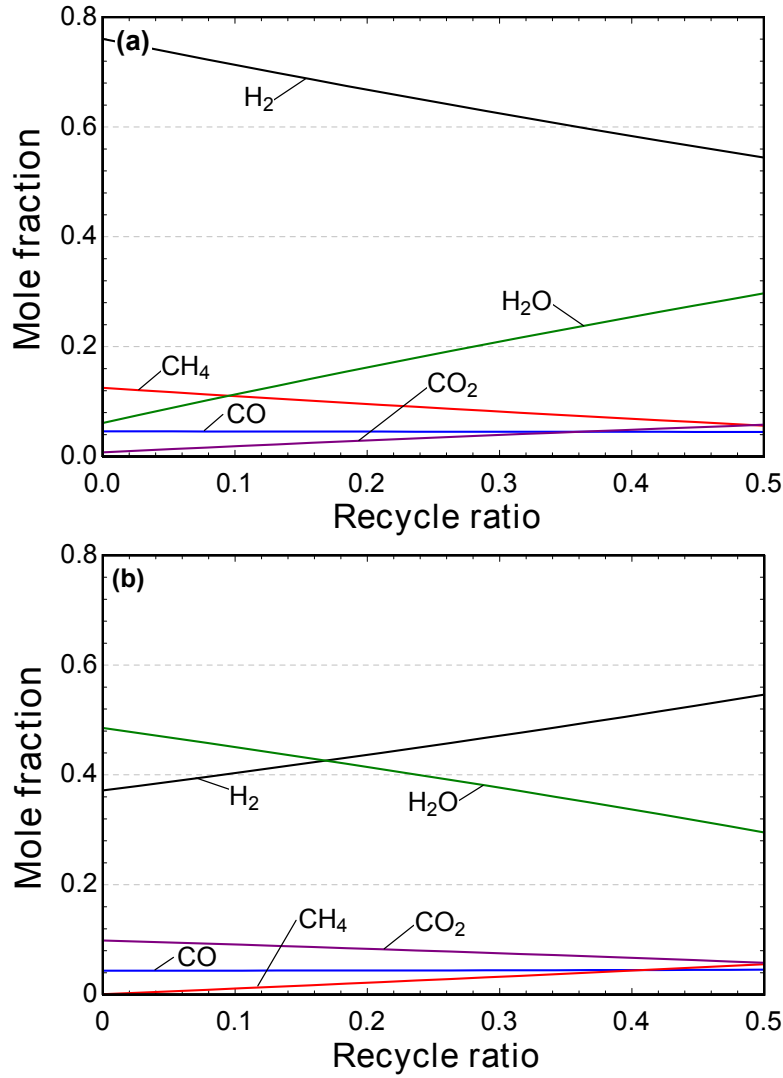
Figure 6.10: Composition entering the fuel-channel vs. fuel-channel recycle ratio in (a) SOFC and (b) SOEC modes with constant composition entering the "conversion region".

7 and 8). Reducing this evaporation load through product recycle might benefit system performance. The following example considers a possible approach for realizing this benefit, but in the end it is not achievable because of carbon deposition constraints in the electrolysis cell.

In a ReSOC system, the composition entering the "conversion region" in either operating mode is equal to the tanked compositions. This fresh reactant composition is mostly constant with fuel-channel recycle, because the products generated in the fuel-channel are only mildly

affected by the recycle ratio. Thus, the preheating (and steam generation) loads are also relatively constant with recycle. However, the reactant composition that enters the ReSOC stack after mixing with the recycle stream does vary with recycle ratio as indicated for both SOFC and SOEC modes in Figure 6.10. Focusing first on the SOFC mode fuel-channel inlet composition, it is clear that higher proportion of steam and lower proportion of fuel species enter the stack as recycle ratio increases. One approach to increasing system efficiency might be to utilize fuel-channel recycle in SOFC mode and operate the system with more carbon-species (i.e., lower HTCR) or less oxygen in the stored fuel. A lower hydrogen-to-carbon ratio would further reduce the evaporator load in SOEC mode as described in Chapter 8, allowing higher stack and system efficiency. This benefit of fuel-channel recycle appears promising when considering SOFC mode, but problems arise when accounting for the reversibility conditions and SOEC mode limitations. Specifically, because the fuel composition consumed in SOFC mode must be generated from the SOEC mode stack, the produced fuel composition is constrained by carbon deposition.

Fuel-channel recycle has been shown to decrease electrical efficiency and does not impact the thermal management or system preheating loads. Additional benefits of recycle that are not realized in this simplified stack-level analysis may become apparent through system-level analysis; however, because no benefit is expected from the arguments shown here, fuel-channel recycle is not considered in the system simulations presented in the following chapters.

6.2.6 Stack operating pressure

Stack pressurization is an effective strategy to increase ReSOC electrical efficiency by lowering the activation and concentration polarization losses. Furthermore, increasing the stack pressure has a major influence on methanation and reforming chemistry, and therefore on the stack thermal behavior. The stack modeling results given here quantify the roundtrip stack efficiency and air temperature increase (i.e., waste-heat generation) for intermediate pressurization (up to 10 bar). The impact of pressurization on the individual ohmic, activa-

tion, and concentration polarizations is also given. While pressurization increases methane formation, it is also shown that a different H-C-O composition is necessary to realize this benefit.
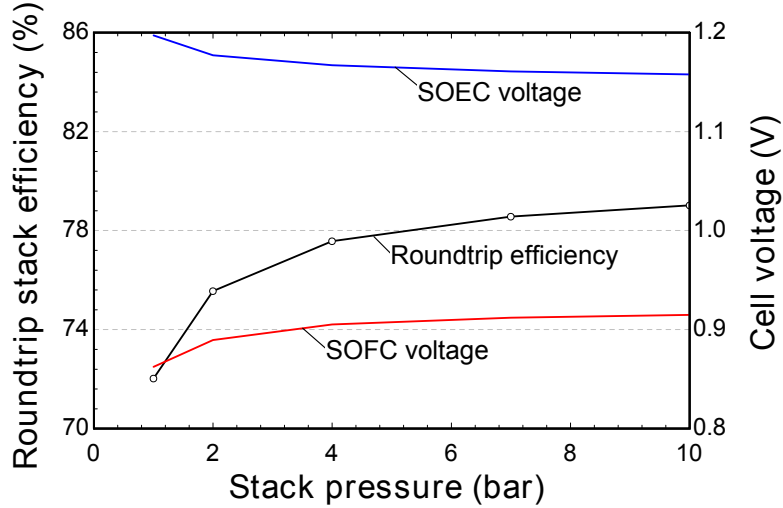
Figure 6.11: Roundtrip stack efficiency and cell voltages vs. stack pressure.

The roundtrip stack efficiency increases with pressurization because of lower overpotential in both SOFC and SOEC operating modes. In fact, Figure 6.11 shows a 7 %-point increase in roundtrip stack efficiency between ambient pressure and 10 bar stack operation at constant current density. The increased efficiency results from a 53 mV increase in SOFC mode voltage and a 39 mV decrease in SOEC mode voltage. The effect of pressurization is logarithmic as has been shown elsewhere [59, 138]. In the model equations, the logarithmic characteristic with pressurization is attributed to the Nernst and Butler-Volmer equations. Thus, the benefit of pressurized operation on electrical performance is most prominent below 5 bar.

To further understand the impact of stack pressure on electrical performance, Figure 6.12 shows the change in the individual area specific resistance contributions in both operating modes with varying pressure. The ASR terms are averaged over the length of the cell. The ohmic resistance is the primary contribution to total stack ASR, which encompasses both serial resistance in the MEA and losses from cell-stacking which are invariant with pressure. Small variations in ohmic ASR with pressure result from changes in the axial cell temperature

profile and associated impact on local electrolyte conductivity. The activation resistances at each electrode degrade logarithmically with increased stack pressure. This behavior captures the increased reactant partial pressure and associated increase in exchange current density at the fuel and oxygen electrodes. The fuel-electrode activation losses are strongly influenced by operating pressure, decreasing by 80% from 1–10 bar. It should be noted that pressurized cell data was not available for this model calibration and the exchange current density formulation and parameters were taken from different ReSOC models (see 5.1.3).
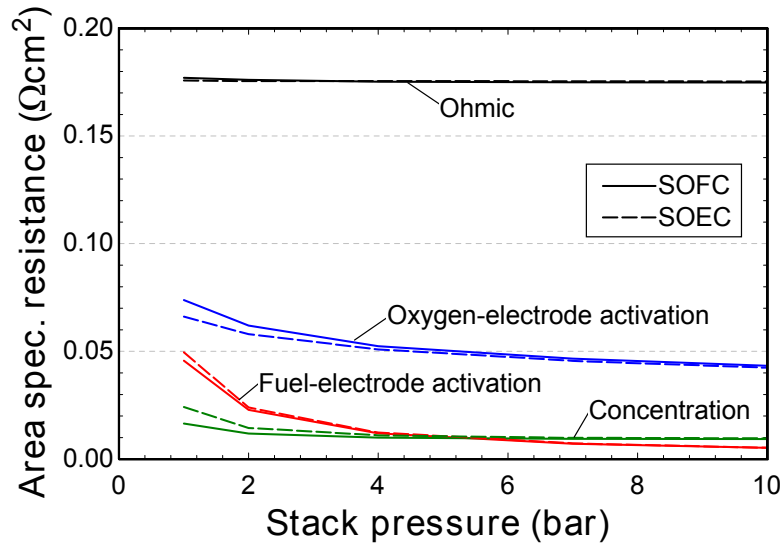
Figure 6.12: Stack area specific resistance vs. stack pressure.

Figure 6.12 shows a decreasing concentration polarization with elevated stack pressure. This is attributed to increased reactant partial pressure and diffusion transport to the active sites at both electrodes. The activation and concentration polarization resistances show some discrepancy between SOFC and SOEC modes at ambient pressure, where the SOFC mode shows higher oxygen-electrode activation but lower fuel-electrode activation and concentration losses. However, at elevated pressure, the polarization resistances converge between the two operating modes.

The increased electrical efficiency suggests that pressurized stack operation is beneficial to system performance, but the thermal behavior must also be considered, here quantified

through the air temperature increase. This analysis also highlights the interdependence of stack operating parameters, specifically the pressure and composition (parameterized by the hydrogen-to-carbon ratio). As pressure increases, the carbon deposition boundary suggests a more carbonaceous reactant mixture can be used without suffering coking. Figure 6.13 shows the air temperature increase as a function of pressure for two cases: (i) constant hydrogen-to-carbon ratio as indicated by the basecase in Table 6.1, and (ii) variable hydrogen-to-carbon ratio to take advantage of the increased carbon tolerance at elevated pressure suggested by the thermodynamic deposition boundary.
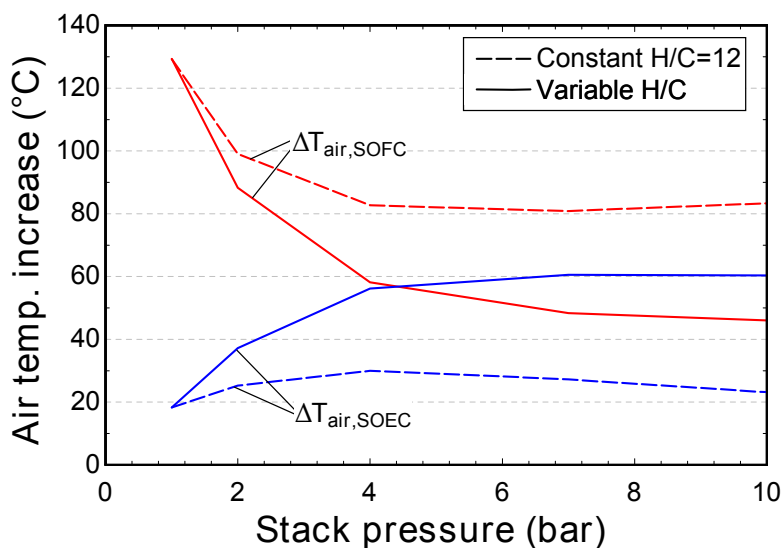
Figure 6.13: Air temperature increase vs. stack pressure for constant HTCR of 12 (dashed) and pressure-dependent HTCR as set by the carbon deposition boundary (solid).

The constant HTCR result in Figure 6.13 shows a slight improvement in SOEC mode air temperature increase at low pressure, but then a decrease indicating less waste heat availability at high pressure. As pressure increases, methanation initially increases, but is quickly limited by the stoichiometry of the baseline H-C-O ratios. At higher pressure, the increased efficiency leads to lower waste heat generation and lower air temperature increase. The SOFC mode air temperature increase at constant HTCR is lower at elevated pressure due to the combined effects of increased efficiency and higher rate of internal reforming (caused by increased SOEC mode methane generation).

The real benefit of pressurization on thermal performance is realized when the composition is also changed along with stack pressure. Figure 6.14 shows the minimum HTCR as a function of pressure as dictated by the carbon deposition boundary (all compositions include oxygen content of 5%). The allowable HTCR decreases from the baseline value of 12 at ambient pressure to 6.2 at 10 bar.

By using a variable reactant composition, the effect of pressure on air temperature increase is more significant. Figure 6.13 shows that the SOEC mode air temperature increases continually with increased pressure for the variable HTCR case (even despite increased electrical efficiency). The SOFC mode air temperature increase also drops more rapidly when the composition is varied. At pressures greater than 4 bar the air temperature increase in SOEC mode exceeds that of SOEC mode, indicating that the internal reforming in the SOFC causes the stack to be more endothermic than the SOEC. This behavior is directly associated with the increased methane formation when higher pressure and lower HTCR are used. In Figure 6.14, the constant HTCR case reaches a maximum methane content < 20 mol.% at 10 bar, while the variable HTCR case has methane content exceeding 40 mol.%.
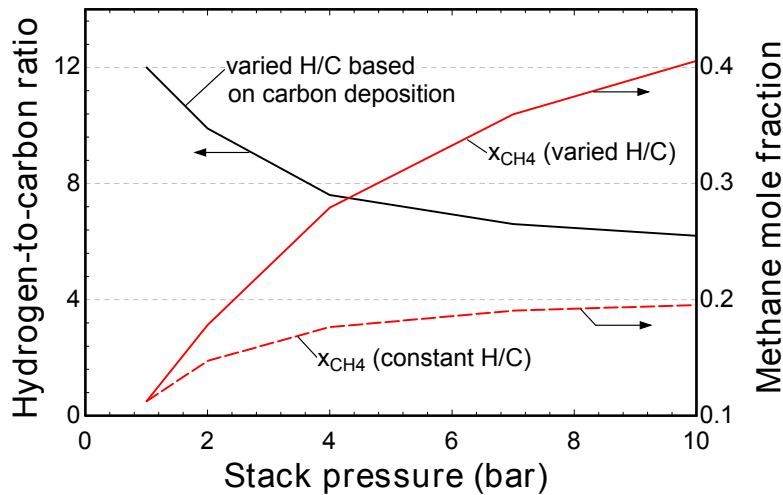
Figure 6.14: Hydrogen-to-carbon ratio and fuel methane content vs. stack pressure for constant HTCR of 12 (solid) and pressure-dependent HTCR as set by the carbon deposition boundary (dashed).

Similar to the electrical efficiency, the impact of pressurization on the allowable HTCR, methane content, and air temperature increase are logarithmic, and the largest benefit is observed at pressures below 5 bar. However, with the combined effects of lower HTCR and higher pressure, the methane content in the variable H/C case continue to increase significantly up to 10 bar (see Figure 6.14).

6.2.7 Stack operating temperature

The results presented thus far show that high roundtrip stack efficiency is achieved using projected stack performance of current button-cells at 650°C. There is benefit to further reducing the cell operating temperature, but requires improved cell performance. The present cells show a nearly 100% increase in cell resistance moving from 650°C to 600°C (see Section 5.1). Lower operating temperature allows increased methane formation in SOEC mode, benefiting thermal management and energy density.

Model simulations show that at nominal stack temperature of 600°C, the methane formed in SOEC mode is 19% (versus 13% at 650°C) with an optimal HTCR of 9.9 and fuel oxygen content of 5%. Other operating conditions include inlet fuel temperature of 550°C, 60% fuel utilization, and 100°C air temperature increase. For these conditions, the target 80% efficiency is achieved in conjunction with exothermic electrolysis operation. The excess air ratios are 3.6 and 1.3 in SOFC and SOEC modes, respectively, suggesting that the air flows may be serviced by the same equipment (3x difference between operating modes). However, achieving this efficiency with present stack performance projections requires a low current density of 0.2 A/cm^2.

If cell and stack improvements lead to stack resistance below 0.2 Ωcm^2 at 600°C, the high efficiency can be achieved at practical current densities. It is likely that both cell and stack improvements will contribute to this target, as the resistance attributed to cell stacking is currently a significant proportion of total stack losses.

6.3 Conclusions from the stack modeling studies

Stack operation of a reversible solid oxide cell system is analyzed using a calibrated computational model. High performance, intermediate temperature button cells made from LSGM-electrolyte material set show area specific resistance below 0.20 Ωcm^2 at 650°C. The reported cell performance meets target roundtrip efficiencies of 80% at practical operating current densities (0.48 A/cm^2), but additional losses expected from cell-stacking and system BOP must be minimized. Improving cell performance at 600°C will benefit system performance through increased methane formation. The cell heat generation, particularly in electrolysis mode, is an important system constraint and is influenced by current density, reactant composition, and flow configuration. Parametric analysis of these operating parameters reveals tradeoffs between efficiency, thermal management, and durability.

Stack heat generation in SOEC mode is maximized for intermediate hydrogen-to-carbon ratio of 12.6, and is also improved by using highly reduced fuel mixtures. Operating co-flow in SOFC mode and counter-flow in SOEC mode improves thermal performance by optimizing methane production. However, counter-flow operation in both modes optimizes roundtrip efficiency performance. The specific flow configuration implementation may require switching flow direction in either the fuel or oxygen channel. Switching fuel-flow direction stabilizes the local gas composition between operating modes, but the local temperature may cycle up to 50°C. Increasing the oxygen content of the oxidant / sweep-gas significantly increases cell electrical and thermal performance, but system challenges and parasitic load associated with oxidant storage may outweigh the benefit. Because the unique conditions of reversible systems include near-equilibrated reactant compositions, severe temperature gradients and cell temperature profiles are greatly mitigated compared with typical internal reforming, methane-fueled SOFC applications.

To generalize the results, electrolysis heat generation is increased either by increased methane production or reduced efficiency. Operating modifications that shift efficiency benefit from SOEC to SOFC mode can improve both roundtrip stack efficiency and thermal

performance (e.g., increasing oxidant oxygen content or using highly reduced fuel compositions). While these results are important in informing stack operation, the tradeoffs must also be considered within the context of a full system.

CHAPTER 7

SYSTEM CONFIGURATIONS: ANALYSIS OF A DISTRIBUTED SCALE SYSTEM

The objective of this chapter is to determine favorable system configurations and operating conditions for stand-alone reversible solid oxide cell systems by evaluating the technical performance for distributed scale energy storage applications (approx. 100 kW / 1 MWh). This objective is achieved by simulating roundtrip operation of a ReSOC system through steady-state computational modeling with a physically based ReSOC stack model and thermodynamic system component models. The stack model is calibrated to high performance intermediate temperature magnesium- and strontium-doped lanthanum gallate (LSGM)-electrolyte cells, as described in Chapter 5 and operated at 600℃. Various system configurations are evaluated based on roundtrip efficiency and tanked energy density.

A series of system configurations are presented starting with the stored-vapor case, in which tanked reactants are stored at elevated temperature to maintain vapor phase of stored water. As will be shown, this system suffers from relatively low energy density, but achieves high efficiency, particularly with the inclusion of an expansion turbine to recuperate losses from compressing gas to tanks pressure. Next, an alternate approach is considered in which water is condensed out of the gas streams and stored in a separate reservoir prior to compression. This approach enables lower temperature and higher energy density storage for more economical tank sizing. The efficiency of this water separation configuration is limited by the energetic requirement to re-boil reactant water. Within each configuration, parametric studies reveal the impact of key operating conditions such as fuel utilization, current density, and tank pressure. The different systems are compared based on their efficiency and energy density performance metrics, including a discussion of the implications of transient tanked storage and projected improvements in ReSOC stack performance.

7.1 Stored vapor system results

The stored vapor system schematic and statepoint data for SOFC and SOEC modes are shown in Figure 7.1. This system includes heat exchangers to preheat reactants and cool stack products, and compressors to pump stack products back to the storage tanks. The reactant species are preheated from the storage tank temperature (fixed to 50℃ above saturation) to the stack inlet temperature, which requires a thermal load of 7-9 kW depending on the operating mode. The gas streams are heated and electrochemically converted in the stack which operates at sufficiently high overpotentials to be net exothermic. Thus, the hot fuel and air channel tail-gases can be used to recuperatively preheat the incoming reactant streams. Additional preheating is provided from hot gases downstream of the fuel compressors. The stack inlet reactant gas temperatures are 50℃ and 72℃ below nominal stack temperature in SOFC and SOEC modes, respectively. The lower stack inlet temperature in SOEC mode ensures that the pinch temperature is met in the fuel preheater due to the higher heat capacitance rate of the cold-side gas. A different preheating strategy of using an electric heater is discussed in Section 7.1.2, but ultimately is not considered feasible under the present operating conditions. The fuel heat exchanger serves two important functions: to preheat reactant gases and to cool product gases for compression. Because of the imbalance in flow rates and heat of compression, the fuel preheat does not lower the stack tail-gas enough to achieve a sufficiently low compressor inlet temperature. Thus, pre-compressor cooling and inter-stage cooling using system airflow as a heat sink lowers compression temperature to a minimum compressor inlet temperature of 50℃ above saturation.

The air preheater and intercooling processes increase the ambient air temperature from 25℃ to an inlet ReSOC oxygen channel temperature of 460℃ (SOFC) or 544℃ (SOEC) as shown in Figure 7.1. The air flowrate and stack-inlet temperature are selected such that a nominal stack temperature (e.g., 600℃) is achieved with a specified air temperature rise of 150℃ (SOFC) and 50℃ (SOEC) across the air electrode side of the stack. Despite the internal chemical reactions balancing the thermal load between operating modes, the stack

149
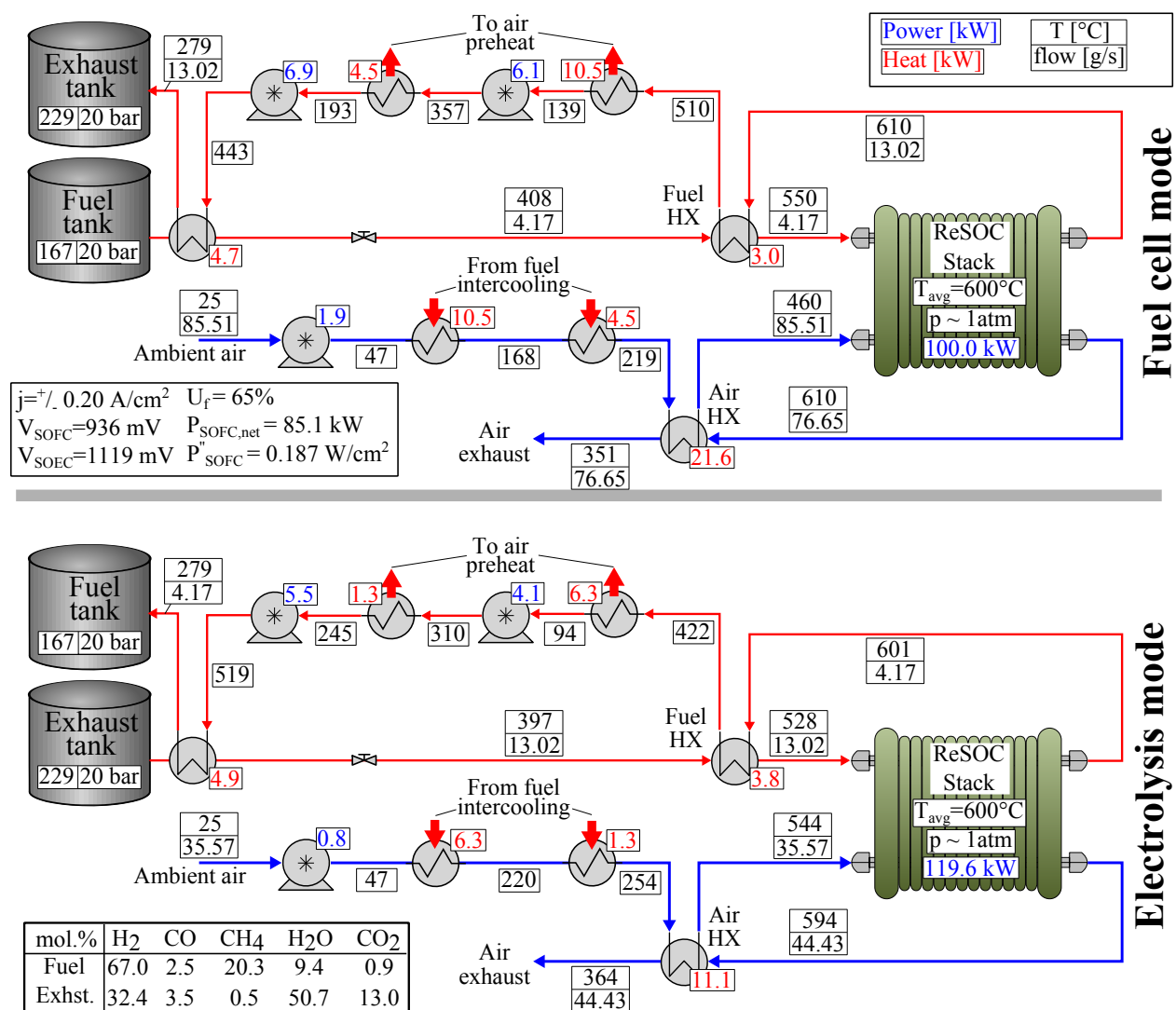
Figure 7.1: Statepoint data and system schematic for the distributed scale stored vapor system.

is more exothermic in SOFC mode. Thus, the air temperature rise in SOFC mode is higher compared to SOEC mode resulting in more similar air flowrates and exhaust temperatures (350°–365°C).

The stack and system efficiencies for the stored vapor system are 83.6% and 65.4%, respectively, indicating that a significant efficiency penalty is incurred from compression parasitics. In each operating mode, the fuel compressor load is 7–12 times larger than the air blower load due to the much higher pressure ratio. However, the preheat load is higher

on the air-side due to the higher flowrate of air compared to fuel and exhaust. The thermal or electric loads on the BOP are similar enough between SOFC and SOEC modes that the system may be dual-mode operated using the same components, favorably reducing system capital cost; although system simulation with specified hardware is required to validate this design approach.

The volumetric energy density is 18.9 kWh/m^3 for the stored vapor system. For an 8 hour operating duration at 100 kW stack discharge power, the fuel and exhaust tank volumes are 14.3 and 21.6 m^3, respectively as calculated by Equation 5.24. The temperature of the compressed fuel and exhaust streams enter their respective storage tanks above the tank temperature. The elevated gas inlet temperature allows for heat loss to the environment through the tank insulation, but additional heat may need to be removed from the stream prior to tanking to account for compression heat within the rigid tank. In any case, higher fidelity analysis to explore the transient effects of storage with specified tank geometry and materials is necessary to complete this element of the system design.

Improving system efficiency requires reducing the auxiliary power loads. The performance impacts of operating conditions, including fuel utilization and current density, and the addition of a fuel expander are considered for the stored vapor system next.

7.1.1 Fuel utilization parameter study

A consequence of the relatively low fuel utilization (65%) given in the Figure 7.1 results is that a significant fraction of the reactants and products transported through the system are not used in the electrochemical conversion. On the other hand, heat evolution in the ReSOC stack is strongly influenced by fuel utilization, resulting in either more exothermic SOFC operation or more endothermic SOEC operation with increasing fuel utilization. The reader is referred to Section 4.4 for a discussion on the influence of utilization on stack thermal characteristic.

Stack and system efficiency are plotted as a function of fuel utilization in Figure 7.2(a) at a fixed current density of 0.20 A/cm^2, meaning that fuel utilization is increased by reducing
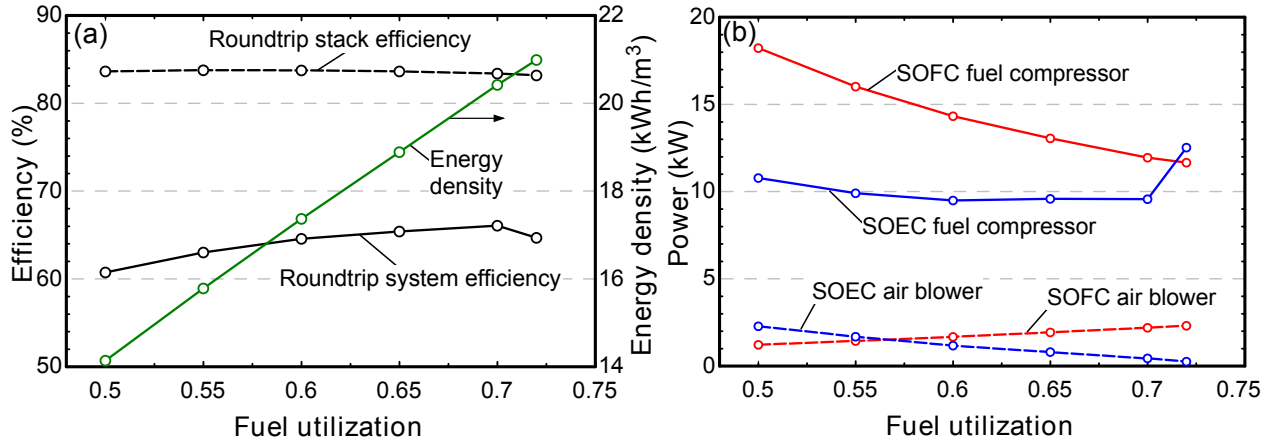
Figure 7.2: (a) Efficiency, energy density, and (b) auxiliary power load for varying fuel utilization in the stored vapor system at nominal stack temperature of 600°C, current density of 0.20 A/cm^2, and tank pressure of 20 bar.

the reactant flow. Roundtrip system efficiency increases with increased fuel utilization because the fuel compressor loads are lower relative to stack power. Stack efficiency is relatively constant with fuel utilization, but experiences a slightly negative effect from increasing reactant depletion in the fuel and oxygen channels. A limiting condition occurs near 72% fuel utilization where the SOEC mode stack shifts from exothermic to thermoneutral operation. Figure 7.2(b) shows the electricity consumption by the fuel and air pumps. The SOEC mode air blower load drops to zero at 72% utilization, indicating that no cooling airflow is required (i.e., thermoneutral point reached). The opposite trend is seen in SOFC mode where the low air blower parasitic power at low utilization results from the stack being more endothermic (efficient) and thus requiring less cooling airflow.

The fuel compressor load decreases significantly with fuel utilization in SOFC mode. In SOEC mode, the fuel compressor load decreases slightly because of competing effects between lower gas flows and higher inlet compressor temperatures due to the lower available airstream heat capacitance rate which provides intercooling. Lack of intercooling leads to a rapid increase in SOEC compressor power and associated decrease in system efficiency as the SOEC mode approaches thermoneutral operation. Using an alternate intercooling heat sink (e.g., ambient air or process water) can mitigate the decreased roundtrip efficiency at 72%

fuel utilization, but the energy deficit in SOEC mode prevents further efficiency improvement within the present system design. Increasing utilization to around 70% maximizes roundtrip efficiency, but also imbalances the air-side BOP load between SOFC and SOEC modes, potentially making it difficult to use the same set of BOP components in both modes. Energy density increases with increased fuel utilization as shown in Figure 7.2(a) because a lesser volume of fuel and exhaust must be stored for equivalent energy capacity. The storage conditions (T, p, x_i) do not vary significantly with fuel utilization, so the change in energy density is solely attributed to achieving equivalent energy capacity with a lesser amount of gas stored.

7.1.2 Current density parameter study

The system efficiency is improved by operating the stack more efficiently (i.e., at lower current density), but the ultimate merit of this design condition is best informed through an economic analysis that judiciously weights low power density stack operation, capital cost associated with system thermal management, and operating costs (electrical energy, O&M). At lower current density, the stack generates less waste heat and therefore preheating process streams with reasonable pinch temperatures is problematic. Figure 7.3 shows the roundtrip efficiency for varied current density for the stored vapor system. Improvement to 66.8% system efficiency is achieved at 0.15 A/cm². However, at lower current density the system efficiency degrades because much less cooling airflow is available for compressor intercooling in SOEC mode as the stack approaches the thermoneutral point at about 0.10 A/cm².

An alternate operating strategy might consider operating at voltages below the thermoneutral voltage and supplying the deficit thermal energy in the SOEC stack with, for example, an electric heater integrated with the stack to preheat reactant gases or otherwise maintain stack temperature. The electric heater allows the SOEC stack to operate under endothermic conditions, but the power supplied to the heater must be included in the efficiency definition as auxiliary power. The SOEC stack efficiency is constant with current density if the stack is at or below the thermoneutral voltage. However, a roundtrip efficiency
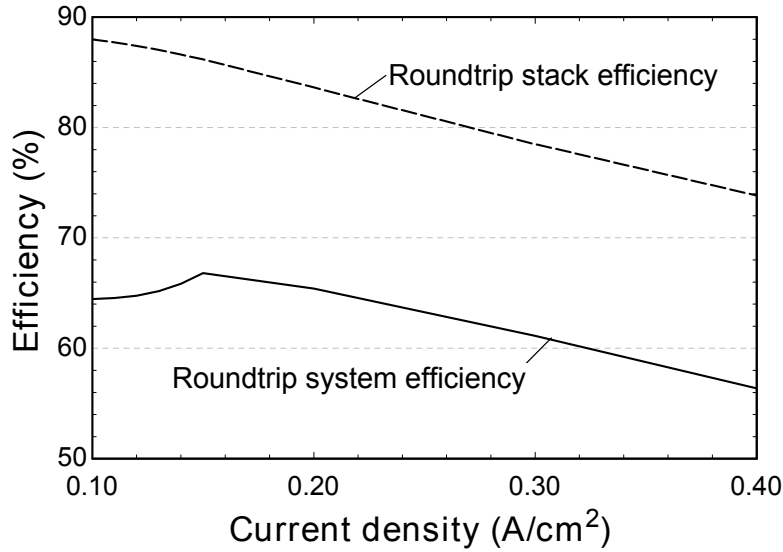
Figure 7.3: Efficiency vs. current density for the stored vapor system at nominal stack temperature of 600°C, fuel utilization of 65%, and tank pressure of 20 bar.

benefit may be realized due to a higher operating voltage in SOFC mode, which is required to satisfy the charge balance constraint with equal charge/discharge durations. Ultimately, this strategy is not considered in the present work because the thermoneutral voltage is reached in SOEC mode at low overpotential (< 50 mV), so operating at even lower power density values is not considered economically feasible. The electric heater approach may be more realistically considered in steam-hydrogen systems where reaching the thermoneutral voltage requires high overpotential.

7.1.3 Expansion turbine system configuration

Another method for system performance improvement is integrating a fuel expansion turbine to recover energy as reactant streams are discharged from pressurized tanks. For the conditions in Figure 7.1, including an 80% isentropic efficiency turbine in place of the tank discharge valve in both operating modes increases system efficiency to 73.7% an 8.5-percentage point increase. Small-scale (1-10 kW) scroll expanders developed for PEM fuel cell systems and experimental organic Rankine cycles suggest that high efficiency expansion is viable at the proposed scale [173].

154
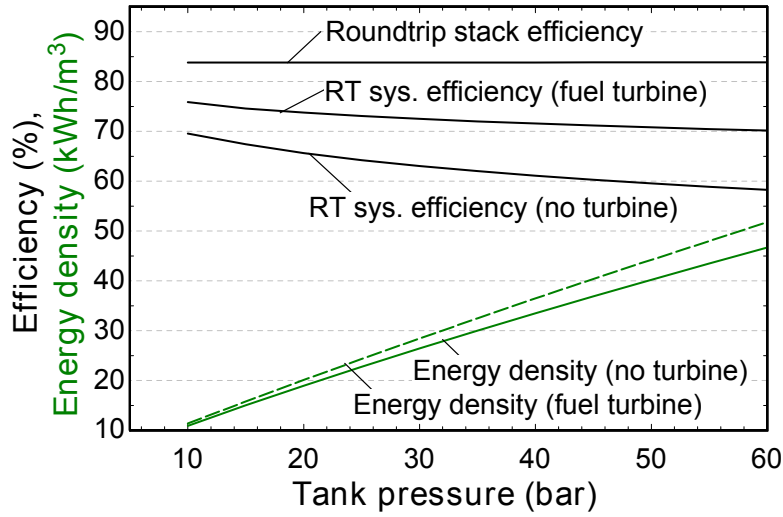
Figure 7.4: Efficiency and energy density vs. tank pressure for the stored vapor system with and without an expander at nominal stack temperature of 600°C, fuel utilization of 65%, and current density of 0.20 A/cm^2.

The system efficiency and tank energy density are shown as a function of tank pressure in Figure 7.4 (recall that this nominal tank pressure is approximately half of the maximum tank pressure). Using a turbine expander increases the system efficiency, particularly at high tank pressure. Furthermore, the energy density increases significantly with increased storage pressure and the turbine configuration enables higher storage pressure while maintaining >70% roundtrip efficiency. The energy density trend shown in Figure 7.4 is explained because less volume is required to store the required quantity of gas at high pressure. In fact, the stored compositions do not deviate from those shown in Figure 7.1 as storage pressure increases. The compositions in the tanks are not chemically altered between the stack fuel-channel outlet and storage tank, meaning that they are not in chemical equilibrium at the storage conditions. The composition is expected to remain stable over the time-scales of roundtrip storage (e.g., days to weeks) when uncatalyzed. The energy density improves slightly when a turbine is included in the system because the system roundtrip efficiency is higher and therefore less gas must be stored for equivalent energy discharge capacity. That is, because the net power generation in SOFC mode is higher due to the added turbine, more

155

energy can be extracted from a fixed amount of stored fuel.

7.2 Water separation system results

Separating water from the fuel and exhaust gas streams prior to storage benefits system efficiency by reducing the compressor flowrate and temperature; and it also benefits energy density by reducing the mass and temperature of the stored gaseous reactants. These benefits come at the expense of needing to supply thermal energy to re-boil reactant water, which particularly impacts the process thermal management in electrolysis mode where steam is a major reactant.

The statepoint data and system configuration for the water separation case are shown in Figure 7.5. The reactant heating load increases from the stored vapor case to 15.3 and 33.9 kW in SOFC and SOEC mode, respectively, because of the lower storage temperature and additional boiler load. Operating conditions are selected to satisfy the increased thermal load while maintaining high stack efficiency. For example, an ejector is included to recycle air sweep-gas exhausted from the stack in SOEC mode. Mixing the recycled gas with fresh air achieves the stack inlet temperature setpoint such that 16.3 kW can be extracted from the high temperature air exhaust for boiling and water superheat. The remaining boiler load is satisfied by hot gas exhausted from the stack fuel channel. Most of the fuel preheat is provided by the hot compressor exhaust gas (5.1 kW) at 343°C so that the higher quality fuel exhaust can be utilized for water superheat at 461°C.

Despite these operating modifications, the stack must operate less efficiently compared to the stored vapor system to overcome the increased preheating requirements. Stack efficiency of nearly 80% is achieved with an operating current density of 0.27 A/cm². However, the auxiliary power load is also lower relative to the stored vapor case as a consequence of lower flowrate and lower temperature at the compressor inlet. The system efficiency is 65.1%, which is slightly lower than the stored vapor basecase shown in Figure 7.1. Because the stack efficiency is limited by the need to generate enough waste heat for the preheating load, the stack cannot be operated more efficiently, for example as shown in the stored vapor case

results of Figure 7.3.

The system concept employing water separation achieves a tank energy density of 36.8 kWh/m³ (95% higher than storing vapor). Both fuel and exhaust tanks are set to ambient temperature for storage, which allows higher energy density and mitigates the need to maintain high tank temperature during operation (as in the stored vapor case). Tank inlet gases are at an elevated temperature of 121-135℃, which may increase storage temperature if heat loss through the tank walls is not sufficient. The saturation temperature is higher at
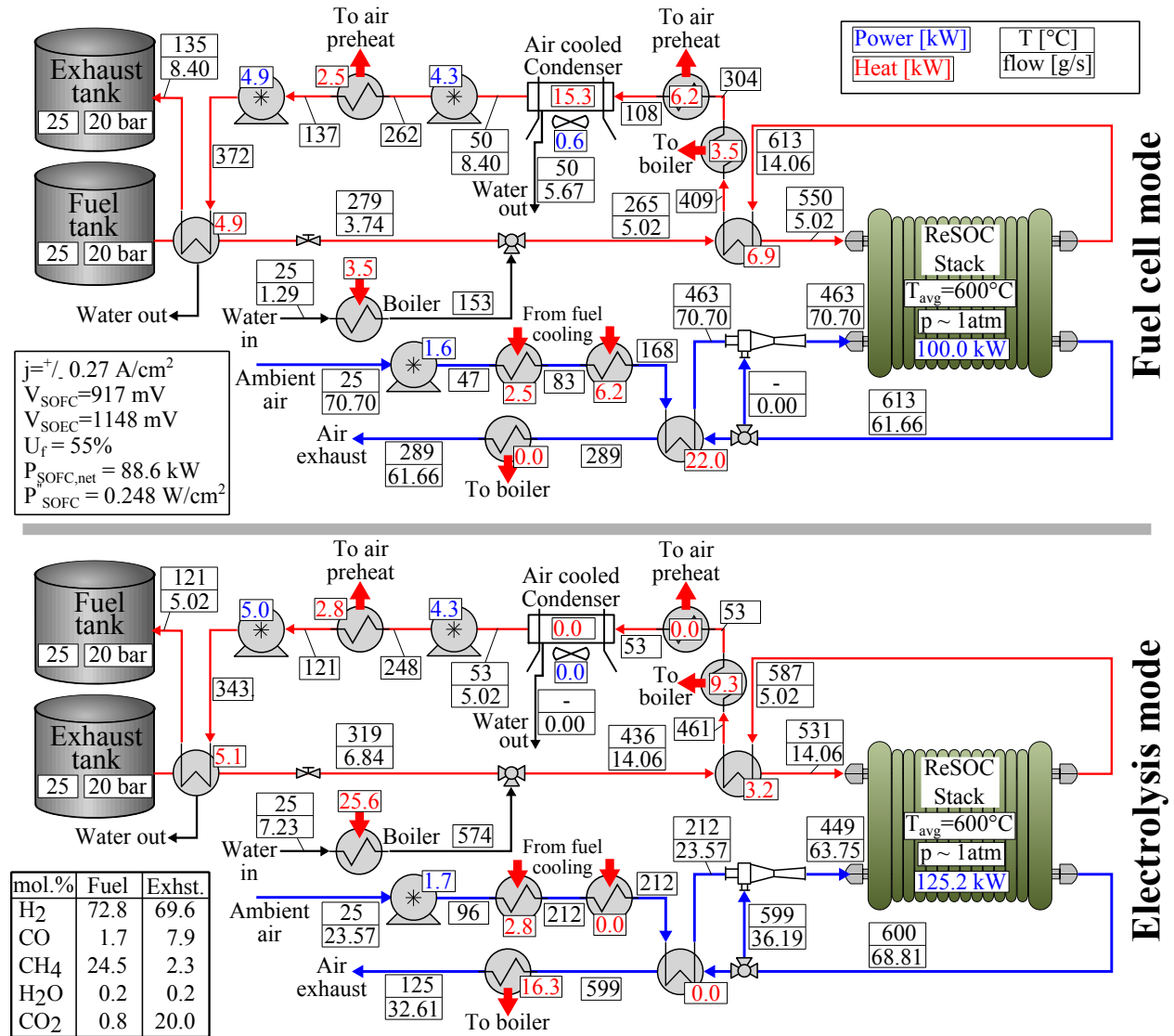
Figure 7.5: Statepoint data and system schematic for the distributed scale water separation system.

the elevated storage pressure compared to the ambient pressure condenser. Thus, additional water condensation will occur as tanked gases cool to ambient temperature. This water may condense in the storage tank or be removed with a condenser prior to tanking. For the results presented in Figure 7.5, the water is assumed to condense in the storage tanks, meaning that more water must be re-boiled than was condensed in the opposite operating mode. This approach also requires intermittent blowdown of the liquid accumulated in the tanks.

The difference in preheating loads between operating modes results in a significant imbalance of the thermal load on some components. Specifically, the boiler load differs by a factor of 7, while the condenser and air preheater are each only used in one operating mode. This imbalance in thermal loads may require bypass lines when selecting specific BOP hardware.

Including an expansion turbine in the water separation system improves roundtrip efficiency to 68.3%; although the turbine is only used in SOFC operating mode. Because efficiency is limited by SOEC mode heat generation, extracting enthalpy from the preheat gas streams with a turbine requires operating the stack at lower efficiency (e.g., by increasing current density) such that the system efficiency is ultimately lowered.

7.3 System configuration comparison

Performance of the stored vapor and water separation system configurations are summarized in Table 7.1. The highest roundtrip efficiency of 73.7% is obtained using the stored vapor configuration with a fuel expander. The energy density of the system increases by 120% if the tank pressure is increased to a nominal 50 bar, with an associated decrease in system efficiency of 2.9 percentage points.

Comparing the stored vapor and water separation systems without a fuel expander, the water separation system has slightly lower roundtrip efficiency, but almost twice the energy storage capacity for a given size tank at 20 bar storage pressure. However, including a turbine in the water separation system does not have as much benefit as in the stored vapor system because less gas is expanded from the pressurized storage tank and the turbine is

158

Table 7.1: Summary of distributed scale system performance for different configurations.

Configuration	η_{system} (%)	η_{stack} (%)	j (A/cm^2)	p_{tank} (bar)	ϵ_{st} (kWh/m^3)	HX UA (W/K)
Stored vapor	65.4	83.6	0.20	20	18.9	439
Stored vapor + fuel expander	73.7	83.8	0.20	20	20.1	589
Stored vapor + fuel expander	70.8	83.8	0.20	50	44.2	594
Water separation	65.1	79.9	0.27	20	36.8	1443
Water separation + fuel expander	68.3	79.9	0.27	20	38.4	1475
Water separation + fuel expander	65.5	79.9	0.27	50	89.2	1428

only used in SOFC mode in the water separation system. The water separation system with a turbine and an average 50 bar storage pressure achieves the highest energy density of 89.2 kWh/m^3.

In general, the stored vapor approach has higher roundtrip system efficiency, while the water separation approach has higher energy density. The system design challenges in the stored vapor case are focused on reducing the auxiliary power load of the fuel compressors by, for example, increasing fuel utilization or lowering the compression temperature. Utilizing a fuel expander in the stored vapor case is instrumental in maintaining high efficiency at elevated storage pressure. In contrast, the challenges in achieving high efficiency in the water separation system concept relate to operating the stack as efficiently as possible while still satisfying the preheating load (i.e., boiler load) in SOEC mode. Thus, configuration and operating condition modifications that increase heat generation in SOEC mode without lower stack efficiency are beneficial, for example lowering stack temperature or increasing stack pressure which consequently increase the extent of internal methanation.

The total system overall heat transfer coefficients (HX UA) are calculated from the log mean temperature difference and heat transfer in each heat exchange component and reported in Table 7.1. In general, the water separation systems have a UA value about 3 times greater than the stored vapor systems, indicating increased system cost. The difference is primarily attributed to the additional boiler and condenser in the water separation system.

In fact, in the water separation systems, the condenser and boiler account for about 46% and 18%, respectively, of the total system UA. System UA increases when a fuel expander is included in the stored vapor system mostly because an additional heat exchanger is included to preheat fuel gases after turbine expansion using the hot air exhaust. Alternatively, the water separation system configuration has no additional heat exchangers when a fuel expander is included, and changes to the total UA are attributed to small variations in heat exchanger loads and approach temperature differences.

7.4   Influence of lower stack ASR on system performance

Improvements in cell-stack performance by lowering the effective stack ASR can affect the system in a number of ways. The calibrated cell model used in the simulations has an ASR of about 0.40 Ωcm^2 at 600°C, and the resistance decreases to about 0.20 Ωcm^2 at 650°C. Improving the cell performance at 600°C will allow the stack to operate at a higher power density while still achieving the system efficiencies reported in Table 7.1. The previous system results show that system efficiency is limited by energetic preheating requirements, meaning that improving the cell performance will not enable roundtrip efficiencies higher than those already presented. However, system cost will certainly be affected by ASR improvements. Figure 7.6 shows the SOFC mode power density vs. ASR for the stored vapor + fuel expander configuration. For the conditions considered in this study at a current density of 0.20 A/cm^2, present day button-cell performance achieves a power density of 0.18 W/cm^2 when operating on carbonaceous reactants. The power density increases to 0.39 W/cm^2 at 0.40 A/cm^2 for an improved ASR of 0.20 Ωcm^2. Economically viable current densities for full-scale ReSOC systems will likely require stack-level ASRs very near these performance levels.

7.5   Implications of tanked storage

The steady state results presented herein reveal useful tradeoffs between efficiency and energy density within different system configurations. However, energy storage is inherently a dynamic process and the implications of tanked storage must be considered in system design
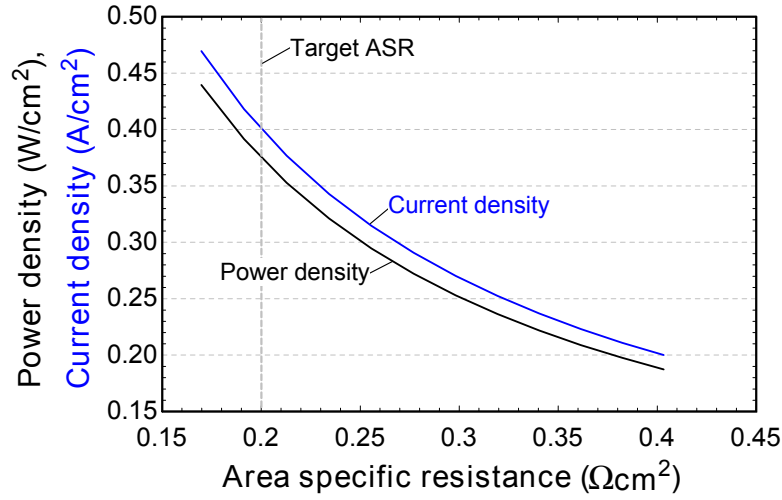
Figure 7.6: Power density and current density vs. area specific resistance for projected improvements in cell-stack performance at constant efficiency of 73.7% for the "stored vapor + fuel expander" configuration with nominal stack temperature of 600°C and fuel utilization of 65%.

and analysis. This section discusses some implications of tank property variation during filling and evacuating, the interdependency of thermal management and compression, and elevated temperature storage for the stored vapor system.

For rigid tanks, temperature variation associated with pressure change during filling and evacuation will change system performance by influencing BOP operation and tank conditions. As the tank is discharged, temperature and pressure decrease, increasing the preheating load to achieve a given stack inlet temperature and eventually condensing the water vapor present in the gas mixture. Satisfying the increased thermal load may require a lower stack efficiency to increase stack waste heat generation. Alternatively, the opposite tank (i.e., that being filled) will increase in temperature, so thermally integrating the two storage tanks may mitigate the temperature variations. The tank property variations are particularly impactful in the stored vapor system approach where pressure variations affect dewpoint temperature. For the water separation systems, heat exchange with the environment may stabilize tank temperatures and declaring tank geometry and material properties is necessary to inform this design.

Another potential challenge for the systems considered in this study is that they utilize compression heat to preheat reactant streams. Under transient operation, the compression heat will vary with tank pressure. For example, when the system is initially discharging from a fully-charged state, the exhaust tank will have low pressure and little compression heat is available for preheating. The deficit heat may require lower efficiency stack operation. The auxiliary power from compressors and turbines will also vary with state of charge. Preliminary analysis indicates that the roundtrip efficiency of systems with turbine expansion improves slightly when considered over a full charge/discharge cycle compared to the steady state efficiency at nominal storage pressures as presented here. However, the integration of preheating with compression heat and tank pressure variation indicates that the roundtrip efficiency will depend on system state of charge and depth of discharge.

A variable volume storage tank will solve many of the issues discussed in this section by maintaining relatively constant tank pressure during operation. One considered approach to variable volume tanking is a "floating piston" tank where a rigid vessel is separated into two compartments by a movable partition, creating distinct fuel and exhaust chambers. This arrangement mitigates many problems associated with individual rigid tanks and also increases energy density by reducing the total tank volume [109, 174].

7.6 Conclusions from the system configuration study

In this chapter, stand-alone energy storage systems utilizing reversible solid oxide cells were conceptualized and analyzed for 100 kW-scale distributed applications. System modeling is used to calculate efficiency and energy density metrics using a calibrated ReSOC model based on intermediate temperature LSGM-electrolyte data at 600℃. The system results compare "stored vapor" and "water separation" strategies, which are distinguished by the phase of the H_2O constituent during tanked storage. The stored vapor system achieves higher roundtrip system efficiency of 73.7% compared to 68.3% in the water separation case. The water separation case is limited by the thermal load required to re-boil water in SOEC mode. A fuel expander is necessary to achieve high roundtrip efficiency, particularly at el-

evated storage pressure in the stored vapor system. The energy density is higher in the water separation system as a result of the lower quantity of stored gas and lower storage temperature. Energy density of 89.2 kWh/m^3 is achieved in the water separation case for a nominal storage pressure of 50 bar compared to 44.2 kWh/m^3 at the same storage pressure for the stored vapor case.

The effects of improvement in ReSOC cell-stack performance and transient tanked storage on system efficiency are also discussed. Improved cell performance does not allow increased roundtrip system efficiency because roundtrip efficiency is limited by energetic preheating loads. However, reducing present day cell resistance from about 0.40 to 0.20 Ωcm^2 at 600°C will increase power density from 0.18 to 0.39 W/cm^2 for fixed system efficiency. System simulations during transient charge/discharge operation must be explored to address unresolved design decisions related to the variation in tank properties during filling and evacuation. The tank design will affect system efficiency because of the interdependence with preheating and turbomachinery loads.

CHAPTER 8

STACK AND SYSTEM OPERATING CONDITIONS: ANALYSIS OF A BULK-SCALE

SYSTEM

The previous chapter compared different ReSOC system configurations for distributed applications. While those systems can be envisioned as an initial market penetration it is also interesting and informative to consider the possibility of ReSOC energy storage systems for bulk-scale applications. In this chapter, a viable system configuration is presented for intermediate- (> 10 MWh) and large-scale (GWh) energy storage applications. The systems suitable for large application scales have increased complexity compared to the distributed-scale systems shown previously. The increased application scale and increased importance to maximize system efficiency when larger amounts of energy are being converted necessitate increased turbomachinery and consequently more complex system integration. A result of the increased system complexity is that stack operating conditions have a greater impact on system performance through the integrated BOP. Thus, this chapter explores the impact of key operating conditions on system efficiency and draws additional conclusions relevant to operating ReSOC systems in large-scale applications. Roundtrip system efficiency estimates are generated from computational modeling using performance on par with state-of-the-art steam-hydrogen fueled ReSOCs.

8.1 Calculation methodology

For this operating condition study, some modifications have been made to the ReSOC stack model and modeling methodology which require additional explanation.

8.1.1 Stack model modifications

The stack model used to generate model results in this chapter differs slightly from that presented in Chapter 5. Specifically, because of the wide range of operating conditions ex-

plored here, a single calibrated electrochemical characteristic will strongly weight the results toward the optimized operating temperature (e.g., high temperature for a YSZ-electrolyte cell, intermediate temperature for an LSGM-electrolyte cell). The electrochemical characteristic is modified here to assume a constant ASR value of 0.20 Ω cm^2 and the cell voltage is calculated as:

$$V_{\text{cell}} = E_N(T, p, x_i) - ASR * j \tag{8.1}$$

where E_N is calculated as in Equation 2.7. The model includes discretized mass and energy balances on the cell channel as described in Section 5.1, and Equation 8.1 simply replaces Equation 5.1.

8.1.2 Model parameter selection

The selected current density and fuel composition are important model parameters that depend on the stack temperature and pressure. As noted previously, it is desirable to operate with high concentrations of carbonaceous species (i.e., low hydrogen-to-carbon ratio) for stack and system thermal management, for example, using methane. However, at these operating temperatures (>550℃), carbon containing reactant gases can deposit coke on electrode surface, reducing performance. For this study, the thermodynamic carbon deposition limit is used to select reactant compositions that are expected to avoid coke formation.

The current density is selected to ensure that enough waste heat is generated by the stack to meet the process gas heating requirements including reactant preheat and steam evaporation. The waste heat generated within the cell stack due to resistive losses is a nonlinear function of the operating current density and is a direct result of stack inefficiency. Operating the stack efficiently enough to maintain high roundtrip efficiency while also generating enough waste heat for gas processing can be a challenge. In many stationary energy storage applications, high system efficiency is valued over high power density (i.e., high current density). Ultimately the balance between these performance parameters requires considering economic impact.

Practically, the minimum current density is determined based on the thermal requirements in SOEC mode because a large quantity of steam must be generated and the electrochemical reduction reactions are endothermic. These endothermic processes are offset by heat generated in the stack from both methanation of generated fuel species and resistive heating associated with stack polarizations. If, for example, less heat is generated from the methanation reaction because of the selected fuel constituents or stack conditions (T, p), then a greater operating current density is required to provide the needed thermal energy. The "discharging" (SOFC) mode is exothermic for all but very low current densities.

Selecting the current density in each mode of operation also requires considering the operating durations. For example, if the charge duration is twice as long as the discharge duration, then the discharge current density must be twice as large as the charging current density to return the system to its original state of charge. For this study, the charge and discharge duration are assumed to be equal, such that the current density is equal in both modes and is set to the minimum value that allows exothermic "charging" (SOEC) mode.

In the following modeling results, the fuel utilization parameter (see Equation 2.4) is used to describe the extent of electrochemical conversion in both operating modes. This implies that the SOFC mode operating conditions (e.g., fuel flow) satisfy the prescribed fuel utilization, and the SOEC mode conditions are such that the fuel flow rate generates a fuel mixture suitable for sustaining repeated charge/discharge cycles. Said differently, the charging mode parameters are set to return the system to its original state of charge following system discharge at the prescribed fuel utilization. The reactant utilization could alternatively be used in place of the fuel utilization parameter, but was not considered in the present study.

8.2 System modeling results and discussion

The following modeling results describe the technical performance of a 10 MW stack discharge power ReSOC system by reporting the efficiency and energy density at different operating conditions. First, a base case system is presented including a discussion of the

selected system BOP configuration applicable for bulk-scale applications. Next, parametric studies of stack pressure, stack temperature, fuel utilization, and operating duration are reported and discussed.

8.2.1 Base case results

The base case system operating parameters include a nominal stack temperature of 650℃, stack pressure of 20 bar, and fuel utilization of 90%. Other relevant operating parameters for the base case are listed in Table 8.1 along with the ranges explored in the following parametric studies. The electric power from the ReSOC stack and system components in both modes of operation are shown in Figure 8.1. Nevertheless, the efficiency results presented in this paper are considered to be scale-independent because the stack performance is estimated by extrapolating from a channel-level cell model and the BOP performance is set by isentropic efficiency specifications. The statepoint data and gas mixture compositions for the base case system are listed in Table 8.2 and Table 8.3.

Table 8.1: Model parameters for the bulk-scale system base case and parametric studies.

Operating parameter	Base value	(Parametric study range)
Stack pressure	20 bar	(5-150)
Average stack temperature	650℃	(500-800)
Fuel utilization	90%	(55-90)
Hydrogen-to-carbon ratio	6.19	(5-10)
Average current density	0.695A/cm^2	(0.55-1.15)
Charge/discharge duration ratio	1.0	(0.5-2.5)
Area specific resistance	0.20 Ωcm^2	
Storage tank temperature	25℃	
Storage tank pressure	160 bar	
SOFC mode oxidant recycle ratio	60-65%	
SOEC mode oxidant recycle ratio	50-70%	
Minimum SOFC excess air ratio	1.5 stoichs	
Oxidant channel temp. increase	150℃	
Fuel channel inlet temp.	100℃ less stack temp.	
Compressor isentropic efficiency	88%	
Turbine isentropic efficiency	90%	
Ejector efficiency	20%	

Table 8.2: Statepoint data for the base case system shown in Figure 8.1.

State point	Flow (kg/s)	T (°C)	p (bar)	Composition
			SOFC mode	
1	25.8	25	160.0	Fuel (stored)
2	32.3	145	20.0	Fuel + steam
3	32.3	550	20.0	Fuel + steam
4	128.5	615	20.0	Exhaust + steam
5	63.5	50	20.0	Exhaust (stored)
6	63.5	139	160.0	Exhaust (stored)
7	523.9	25	1.0	21% O2 / 79% N2
8	523.9	288	20.38	21% O2 / 79% N2
9	1284.3	517	20.0	12% O2 / 88% N2
10	1188.0	667	19.97	5% O2 / 95% N2
11	760.4	667	19.97	5% O2 / 95% N2
12	427.6	667	19.97	5% O2 / 93% N2
13	427.6	100	1.1	5% O2 / 95% N2
			SOEC mode	
1	26.0	25	160.0	Exhaust (stored)
2	128.5	207	20.0	Exhaust + steam
3	128.5	550	20.0	Exhaust + steam
4	32.3	618	20.0	Fuel + steam
5	26.0	50	20.0	Fuel (stored)
6	26.0	162	160.0	Fuel (stored)
7	227.6	25	1.0	21% O2 / 79% N2
8	227.6	112	20.93	21% O2 / 79% N2
9	802.7	506	20.0	36% O2 / 64% N2
10	898.9	656	19.97	43% O2 / 57% N2
11	575.0	656	19.97	43% O2 / 57% N2
12	323.8	656	19.97	43% O2 / 57% N2
13	323.8	87	1.1	43% O2 / 57% N2

Table 8.3: Gas compositions represented in the base case system.

Gas composition mole fractions (%)					
	H_2	CO	CH_4	H_2O	CO_2
Exhaust (stored)	23.6	3.4	2.0	<0.1	71.0
Exhaust + steam	8.2	1.2	0.7	65.4	24.6
Fuel (stored)	38.2	0.5	60.9	<0.1	0.5
Fuel + steam	33.1	0.4	52.8	13.3	0.4
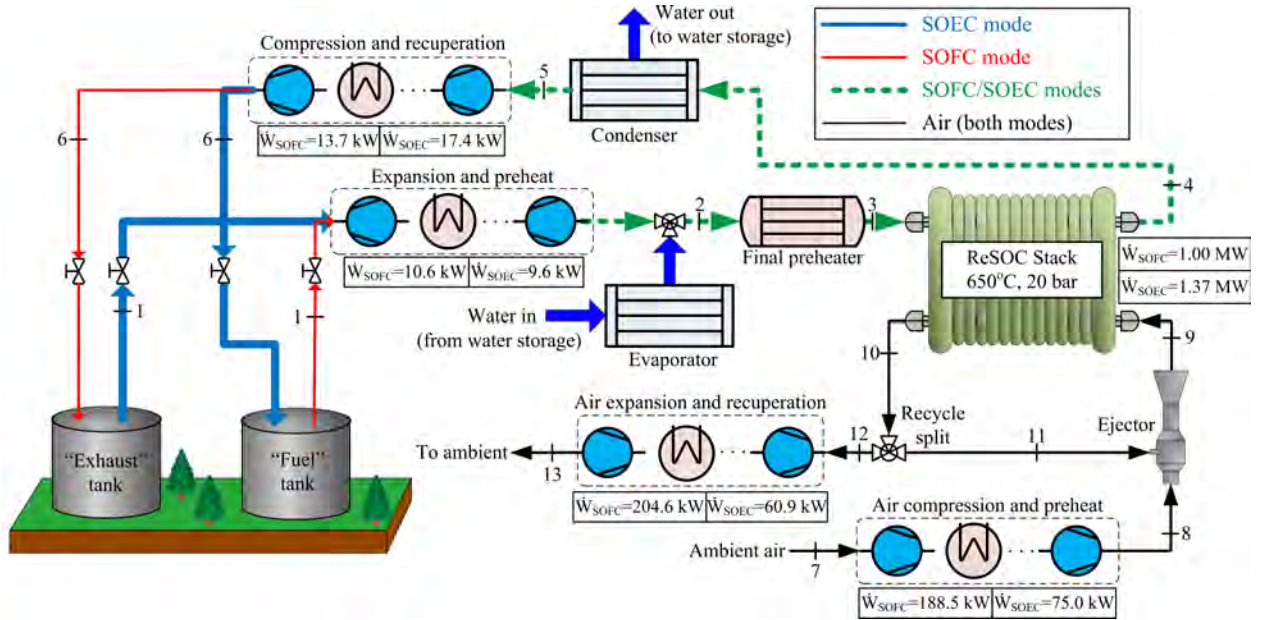
Figure 8.1: Basecase system schematic for bulk-scale applications with component electric power loads in both SOFC and SOEC modes (see Table 8.1, Table 8.2 and Table 8.3 for operating conditions, statepoint data, and gas compositions, respectively).

The base case system stores electricity with dc roundtrip stack and system efficiencies of 72.8% and 72.6%, respectively. It is notable that the system efficiency is nearly as large as the stack efficiency, indicating that most of the power consumed during compression is recuperated in the expansion processes. This configuration is similar to an SOFC-gas turbine hybrid system, but differs because stack tail-gases are not combusted such that a smaller fraction of the compressor power is recuperated from expansion. The ensuing parametric studies show that some net power is generated from the BOP under certain operating conditions. In the base case system, for example, the air expansion process in SOFC mode produces 205 kW while air compression consumes only 189 kW. Net power is generated by the air turbomachinery in SOFC mode but not in SOEC mode. The reason for this difference can be explained by the thermal interactions of the BOP components. For example, in SOEC mode the main reactant is H_2O which leads to a high evaporation heat load and the air exhausted from the stack is the primary heat source for this evaporation process. Therefore, relatively less power is generated from the SOEC mode air expansion

169

compared to SOFC mode because the expansion temperatures are lower after heat is provided to the evaporator.

The power loads on the air turbomachinery are an order of magnitude larger than the fuel expansion/compression processes because of high air flowrates. Thus, system performance is more drastically impacted by the air BOP components than fuel BOP components, which is a useful conclusion in understanding the parametric study results. Also, the power requirement of the air expansion/compression in SOFC mode is about 2.5-3.5 times larger than that for SOEC mode. This is because the SOFC mode stack operates more exothermically and thus requires more cooling airflow, despite significant internal methanation in SOEC mode.

The following parametric studies consider the effect of ReSOC stack temperature, pressure, fuel utilization, and operating duration on system efficiency. These parameters are significant because they impact stack thermal management, including the kinetic and thermodynamic effect on methane formation and steam-methane reforming. System operation is also affected by these parameters, for example, by the influences on heat exchanger preheating and recuperation duties, and compressor and turbine power consumption and generation.

8.2.2 Stack pressure parametric study

The operating pressure of the ReSOC stack has a significant impact on the system efficiency. Importantly, stack pressure also affects the minimum current density required to satisfy gas processing thermal loads, and the reactant composition which is expected to mitigate carbon deposition. Figure 8.2 shows the fuel composition in terms of the minimum molar hydrogen-to-carbon ratio allowed and average stack current density as a function of ReSOC operating pressure at a fixed average stack temperature of 650°C, fuel utilization of 90%, and storage pressure of 160 bar. A plot of the minimum HTCR needed to avoid carbon deposition (see Figure 8.2) shows that increasing stack operating pressure enables higher concentrations of carbonaceous species in the fuel and exhaust compositions.

A certain amount of stack waste heat is essential to meet the heating load required by reactant gas processing in the stack periphery. As the ReSOC stack pressure increases, more

Figure 8.2: Minimum current density required for exothermic SOEC mode operation (left) and minimum hydrogen-to-carbon ratio as dictated by the carbon deposition boundary (right) vs. stack pressure.

heat is generated from the methanation reaction in charging (SOEC) mode; therefore less heat is required from stack inefficiency (i.e., resistive heating) and a lower current density can be used. Figure 8.2 shows the current density as a function of stack pressure, where the current density is relatively low at high pressure and increases sharply at lower pressure to overcome the heating deficit caused by lower conversion of the exothermic methanation reaction. There are two primary reasons for higher conversion of the methanation reaction at higher pressure: (1) the HTCR of the fuel composition decreases, approaching closer to the stoichiometric ratio for methane (i.e., H/C=4), and (2) improved reaction kinetics of methanation.

The optimum roundtrip system efficiency is achieved based on a trade-off between stack efficiency and auxiliary power. As shown in Figure 8.3, the roundtrip stack efficiency increases with increased stack pressure because the current density required for exothermic SOEC mode operation decreases (see also Figure 8.2). However, the increased stack efficiency is counterbalanced by increased auxiliary power consumption at high stack pressure.

Figure 8.3: Roundtrip stack and system efficiency (left), net BOP power produced ($\dot{W}_{BOP}$) relative to stack power ($\dot{W}_{stack}$) (right), and stored methane mole fraction (top) vs. stack pressure.

The right-axis in Figure 8.3 shows the net auxiliary power generated in each mode as a fraction of the stack electric power where negative values imply that more power is required by compression processes than is generated by the turbines. At lower stack pressure, the SOFC mode auxiliary components produce net power because the turbine expansion of air exhausted from the stack produces more power than is required to compress air to the stack operating pressure. Yet, the benefit of net energy generation from the auxiliary components is overcome by a rapid decline in stack efficiency at low stack pressure. The competing trends of stack efficiency and auxiliary power result in an optimal system efficiency of 72.5% at a stack pressure of about 20 bar. The reason the SOFC mode auxiliary power generation increases with decreased stack pressure is that the air does not need to be compressed to as great a pressure and the exhausted air from the stack can be expanded at higher temperatures while still performing the required heating processes.

Another consideration when determining the most suitable stack pressure is the affect it has on the composition of the stored gases. The top horizontal axis of Figure 8.3 shows

the mole fraction of stored methane in the fuel tank where the remaining stored gas is primarily hydrogen. As stack pressure increases, the amount of stored methane increases due to increased methanation in SOEC mode. Higher purities of produced methane can be achieved at high stack pressure with limited efficiency loss which allows for increased energy storage density and the possibility of coupling such an energy storage system with existing natural gas infrastructure.

It is an important result that the system efficiency is significantly influenced by the system BOP when turbomachinery is employed because the desirable operating conditions expected from only analysis of the ReSOC stack differ from the operating conditions that achieve optimal system efficiency. Furthermore, the optimal system configuration must, in addition to efficiency, also consider cost, dynamic operation, and control.

8.2.3 Stack temperature parametric study

The average stack temperature impacts roundtrip efficiency; however, as shown in the previous parametric study, much of this impact can be understood by considering the effect of stack operating temperature on the hydrogen-to-carbon ratio of the reactant gas mixture and average operating current density. Figure 8.4 illustrates how the current density and HTCR of the reactant mixtures vary with changes in average stack temperature. The HTCR is set based on the thermodynamic carbon deposition limit and increases with increased temperature. The required average current density to meet process thermal loads decreases with increasing stack temperature in the low temperature range primarily because the exhaust airflow used to supply heat to the evaporator in charging (SOEC) mode exits the stack at a lower temperature, therefore necessitating more heat generation in the stack to satisfy pinch-point temperatures. A minimum current density is reached at an average stack temperature of about 680°C. At higher temperatures the required current density increases because more waste heat is required from the stack at higher temperatures where the exothermic methanation reaction has lower equilibrium conversion.
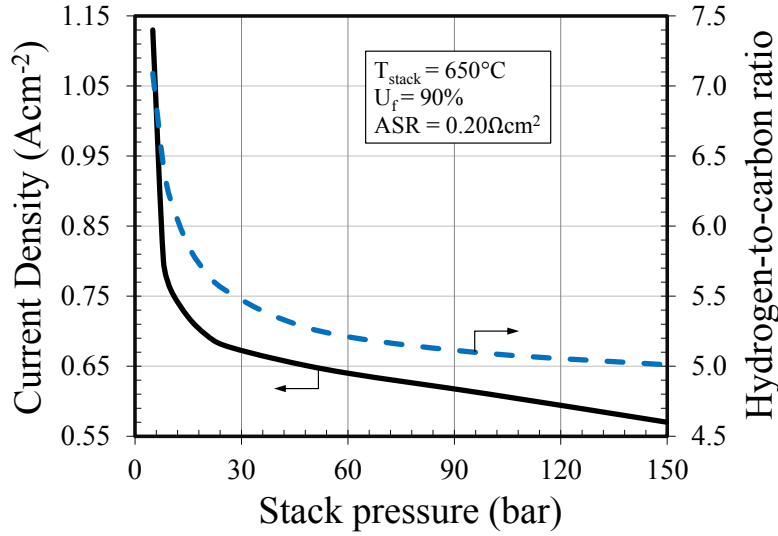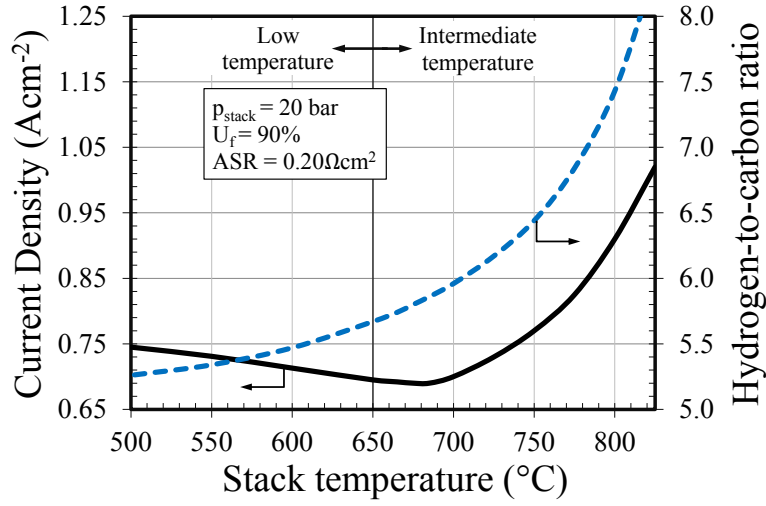
Figure 8.4: Minimum current density required for exothermic SOEC mode operation (left) and minimum hydrogen-to-carbon ratio as dictated by the carbon deposition boundary (right) vs. stack temperature.

Figure 8.5 shows the stack and system roundtrip efficiencies as a function of average stack temperature. System efficiency is maximized at an intermediate operating temperature of about 680°C and is primarily influenced by the stack efficiency and discharge mode auxiliary power. The stack efficiency increases slightly with increased stack temperature at lower temperatures and then drops off sharply at temperatures above 700°C in accordance with the increased current density (see also Figure 8.4). Recall that cell ASR has been fixed (i.e., the temperature dependence removed) so that the plots shown here are a direct result of the influence of changes in reaction energies and BOP power, and are decoupled from changes in cell resistance. Nevertheless, previous work has shown cell performance for operating temperatures below 650°C to be on par with the total cell resistance of 0.20 Ωcm^2 assumed in the present study [54, 175].

The SOFC (discharge) mode BOP power shifts from consuming net power at lower temperatures to producing net power at higher temperatures. The net auxiliary power generation in SOFC mode increases with increased average stack temperature primarily because the excess air exhausted from the stack is at a higher temperature such that more power is
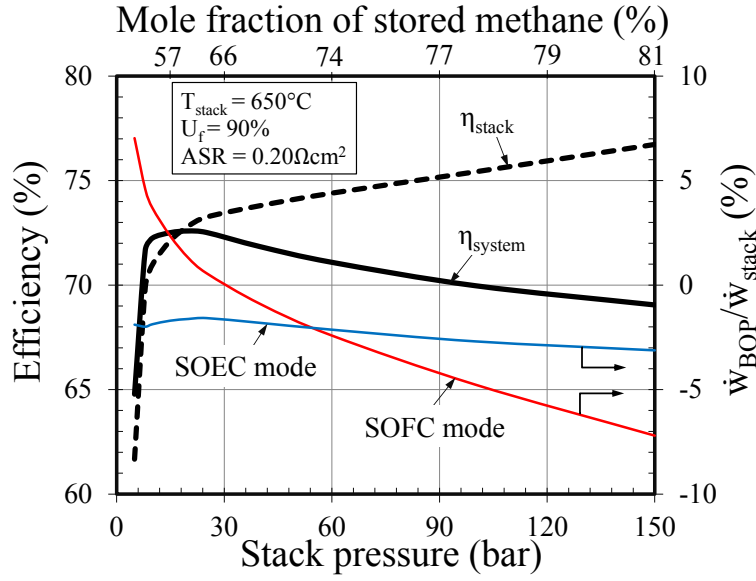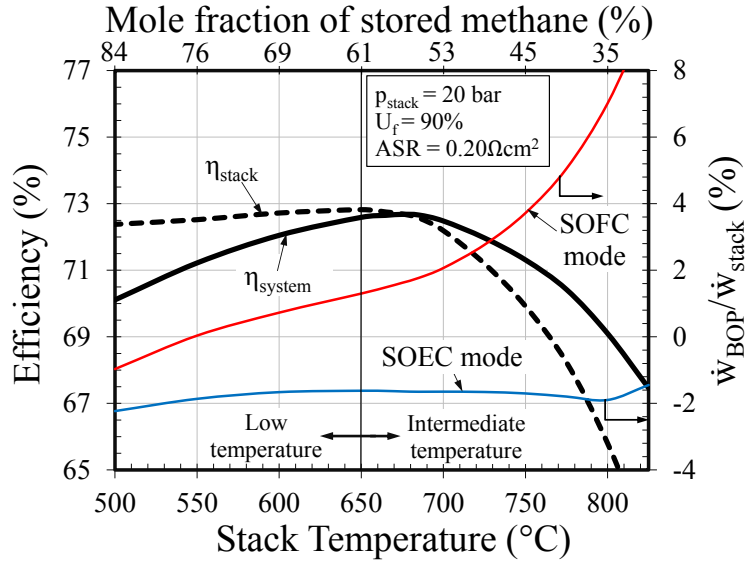
Figure 8.5: Roundtrip stack and system efficiency (left), net BOP power produced ($\dot{W}_{BOP}$) relative to stack power ($\dot{W}_{stack}$) (right), and stored methane mole fraction (top) vs. stack temperature.

generated from expanding it to ambient pressure. One conclusion from these results indicates that low temperature cell operation (<650°C) is not necessarily a materials requirement for ReSOC energy storage systems configured in this way, so long as the stack pressure is sufficiently high. Additionally, the optimum associated with roundtrip efficiency is relatively shallow, changing by only 5% across a large temperature range.

The methane content in the stored gas mixture is a strong function of stack temperature as shown by the top axis of Figure 8.5. Greater than 80% methane content is achieved at stack temperature below 550°C, although that value drops to 55% at optimal efficiency at 680°C. This trend exemplifies a distinct tradeoff between efficiency and stored energy density and such tradeoffs must ultimately be informed by economic optimization analysis.

8.2.4 Fuel utilization parametric study

In the present study, lowering the fuel utilization implies oxidizing the stored fuel species to a lesser extent. In other words, the H-C-O composition of the fuel tank remains fixed as dictated by the carbon deposition boundary and at higher fuel utilization the exhaust tank

contains a more oxidized gas mixture. The stored fuel and fuel + steam compositions are only slightly impacted by changing the fuel utilization and are similar to compositions from the base case system (see Table 8.3).

The stack efficiency is affected by the fuel utilization parameter through the open-circuit voltage which is a function of the bulk composition; however, this affect is minor, particularly compared with changes in stack efficiency from current density variation. Finally, it should be noted that unlike typical SOFC systems, lowering the fuel utilization in the present system does not directly correspond to reduced system efficiency. This is because the proposed system is closed and the denominator of the efficiency definitions is the power input to the system, rather than rate of energy input from fuel. Lower fuel utilization, however, requires storing a larger proportion of unused fuel species, negatively impacting energy density.

Figure 8.6: Roundtrip stack and system efficiency (left) and net BOP power produced ($\dot{W}_{BOP}$) relative to stack power ($\dot{W}_{stack}$) (right) vs. fuel utilization.

The fuel utilization changes the thermal operating characteristic of the ReSOC such that for higher fuel utilization, more waste heat must be generated from the ReSOC stack for exothermic operation in SOEC mode. This necessitates an increased current density with increased fuel utilization (not shown). The causal relationship between fuel utilization and stack thermal behavior depends on both stoichiometric constraints and Nernst potential

effects, which are explained in Chapter 4. Figure 8.6 shows the stack and system efficiencies as a function of fuel utilization. Stack efficiency increases with decreased fuel utilization because the stack can operate more efficiently (i.e., lower current density) while still satisfy system thermal loads.

The roundtrip system efficiency is affected by the fuel utilization both because of the effect on stack efficiency and the impact on the BOP performance due to transporting a different proportion of unreacted species throughout the system and different cooling airflow requirements. The stack efficiency increases with decreased fuel utilization (see Figure 8.6). However, the parasitic losses from the BOP increase with decreased utilization such that the roundtrip system efficiency is maximized to nearly 74% at about 70% fuel utilization. It is clear from these results that the roundtrip system efficiency is only mildly affected by changes in fuel utilization.

Figure 8.6 also shows the ratio of net BOP power generated to stack electric power in each mode as a function of fuel utilization. The SOEC mode net BOP power is relatively constant with fuel utilization. The cooling airflow in SOEC mode is mostly independent of fuel utilization because any reduction in heat generation from the internal chemical reactions is subsidized with increased current density to satisfy the required system heating loads. Thus, with similar airflows, and stack temperature and pressure, the air turbomachinery loads are nearly independent of fuel utilization. Alternatively, based on the changed thermal characteristic of the ReSOC stack with fuel utilization in SOFC mode, the BOP net power increases with increased utilization. This is because less heat is generated in the SOFC mode stack when it is operated more efficiently such that the excess oxidant exhausted from the stack is expanded at a lower temperature after fulfilling the required system heating processes. As a result, less power is recuperated from the air turbine. The fuel utilization also affects the reactant and product turbomachinery, but the flowrate of the air is significantly higher, such that the air turbomachinery dominate the BOP performance.

The stack pressure and fuel utilization studies show a common trend in that increased stack efficiency correlates with increased parasitic BOP power in SOFC mode due to the decreased excess heat generation from the stack. In short, these studies illustrate the competing trends between stack efficiency and BOP power consumption that lead to optimal system efficiency operating points.

8.2.5   Operating duration parametric study

Specific energy storage applications often prescribe charge/discharge durations based on the operating requirements. For example, certain applications may require approximately equal charge/discharge durations (e.g., voltage regulation), while others can have a significantly longer duration to charge and then discharge rapidly (e.g., peak shaving). A non-unity charge/discharge ratio implies a different magnitude current density in each mode of operation so that the system is able to operate continuously without being eventually depleted of fuel or exhaust species. The system is reversible when Equation 5.18 is satisfied, so a longer operating duration in one mode implies a proportionally lower current density.
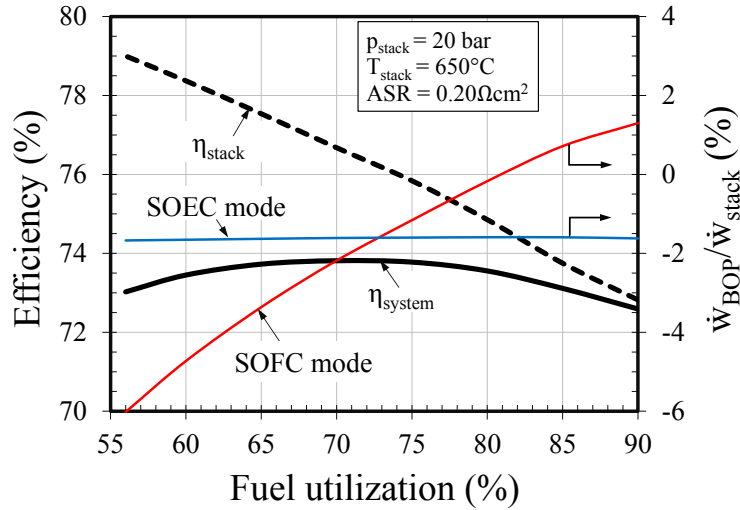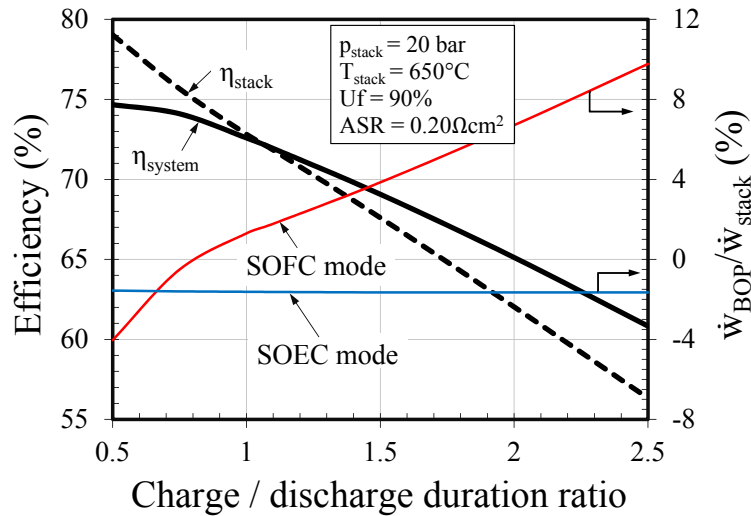

Figure 8.7: Roundtrip stack and system efficiency (left) and net BOP power produced ($\dot{W}_{\mathrm{BOP}}$) relative to stack power ($\dot{W}_{\mathrm{stack}}$) (right) vs. charge/discharge duration ratio.

For this study, the current density in charging (SOEC) mode is set to ensure exothermic operation, so increasing the charge/discharge ratio implies operating the discharge (SOFC) mode at higher current density (i.e., less efficiently). Less efficient SOFC mode operation results in lower roundtrip stack efficiency as shown in Figure 8.7 where stack efficiency decreases with increased charge/discharge ratio. However, as was observed in the previous parametric studies, when the SOFC mode stack operates less efficiently, there is higher net power generation from the BOP. Thus, the system efficiency degrades less rapidly than the stack efficiency with increased charge/discharge ratio. Furthermore, the system efficiency does not improve as rapidly for charge/discharge ratios <1 because of the increased net power consumption from the SOFC mode BOP. This result indicates the proposed system achieves higher efficiency for energy storage applications with lower charge/discharge ratios. Although, >65% efficiency is still achieved for charge/discharge ratio of 2.0.

8.2.6 Reactant composition parametric study

Practical ReSOC-based energy storage systems will need to operate at hydrogen-to-carbon ratios in the fuel gas mixture that are sufficiently far from thermodynamically established carbon deposition limits. Since the minimum HTCR established from chemical equilibrium is not entirely accurate in predicting the coking behavior in ReSOCs, the HTCR must be in excess of the minimum value. Figure 8.8 shows the HTCR and average current density as a function of the percent-increase from the minimum hydrogen-to-carbon ratio that mitigates carbon deposition. That is, 0% increase implies that the fuel composition within the stack will pass exactly tangential to the carbon deposition limit and higher percent-increase includes a factor of safety similar to increasing the steam-to-carbon ratio. The current density increases with increased percent-increase because more waste heat is required for exothermic operation in SOEC mode. More waste heat is required because additional steam must be evaporated to achieve a higher HTCR, and less heat is generated from the methanation reaction in the SOEC stack for fuel compositions with higher HTCR. Similar to the pressure variation study, the current density is directly related to the fuel

179

compositions HTCR.
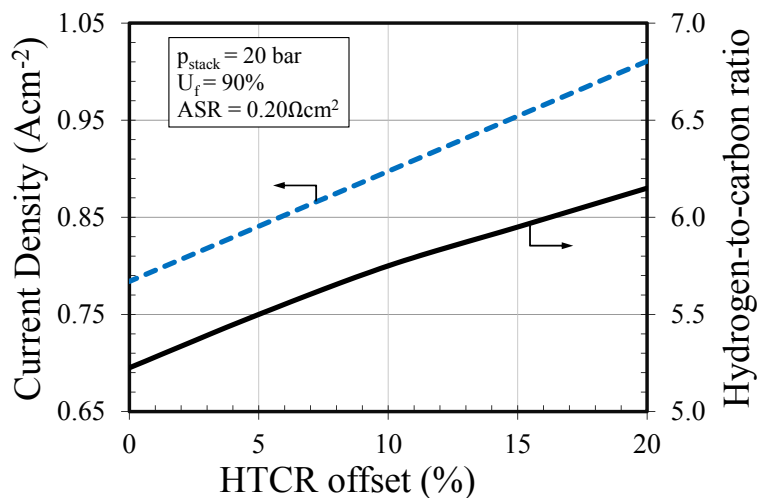
Figure 8.8: Minimum current density required for exothermic SOEC mode operation (left) and minimum hydrogen-to-carbon ratio as dictated by the carbon deposition boundary (right) vs. percentage hydrogen-to-carbon ratio offset from the carbon deposition boundary.

The HTCR is important to consider in avoiding detrimental operating conditions within the ReSOC stack and it is necessary to explore the effect of this parameter on roundtrip efficiency and energy density. Figure 8.9 shows the stack and system roundtrip efficiencies as a function of percent-increase from the limiting HTCR. Both the stack and system efficiency improve as the composition approaches the thermodynamic coking limit (i.e., 0% increase). This behavior presents a distinct tradeoff between high roundtrip efficiency and operating under conditions where carbon deposition is more likely to occur. Notably, as the percent-offset increases, the system efficiency does not degrade as rapidly as the stack efficiency. The system efficiency is affected by both the stack efficiency and the auxiliary power requirements. As seen in Figure 8.9, the auxiliary components generate net power in discharge (SOFC) mode due to the efficient expansion of high temperature excess air exhausted from the stack. The net power generated from these auxiliary components increases as the fuel composition moves away from the coking boundary because the current density also increases with percent-increase (see Figure 8.8) meaning that more waste heat is generated

in the SOFC stack. The additional waste heat requires increased airflow to act as a heat-sink in the stack and the increased airflow results in increased net power production from the turbomachinery. The SOEC mode net auxiliary power remains relatively constant because the excess waste heat generated from inefficiencies in the SOEC stack at higher current density is offset by reduced heat generated from the methanation reaction; therefore, the net excess heat from the stack is nearly constant and balance of plant operation is relatively unchanged.
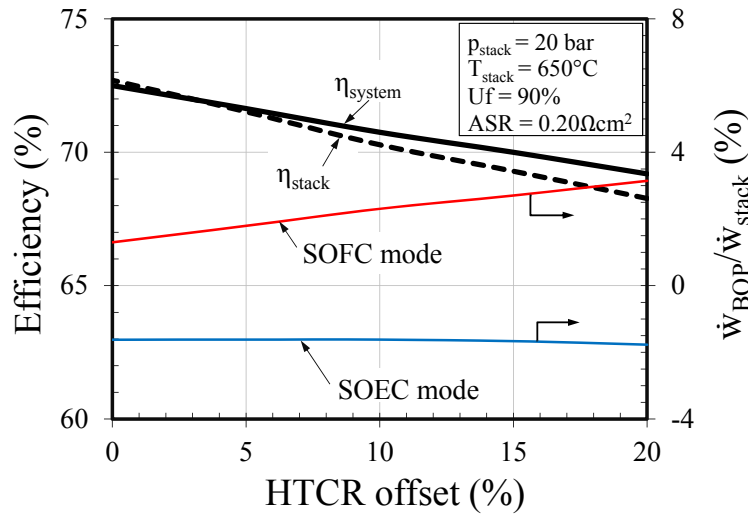
Figure 8.9: Roundtrip stack and system efficiency (left) and net BOP power produced ($\dot{W}_{\mathrm{BOP}}$) relative to stack power ($\dot{W}_{\mathrm{stack}}$) (right) vs. percentage hydrogen-to-carbon ratio offset from the carbon deposition boundary.

These results show a distinct performance reduction when the fuel composition is set further from the carbon deposition boundary. Specifically, the system efficiency and energy density are reduced by 5% and 10%, respectively for a 20% increase in the hydrogen-to-carbon ratio of the fuel.

8.3 Conclusions from the operating conditions study

Throughout this chapter, a bulk-scale ReSOC energy storage system has been analyzed to estimate achievable roundtrip efficiencies and to examine the influence of stack temperature, pressure, and fuel utilization on system efficiency. >70% roundtrip storage efficiencies were

achieved for the proposed system. Steady-state system modeling results indicate that system efficiency is maximized at intermediate ReSOC stack operating conditions of about 680°C, 20 bar, and 70% fuel utilization based on the trade-off between stack efficiency and balance of plant power consumption. The auxiliary power generation has a significant effect on system efficiency, and it is important to note that the nature of this impact could change for alternately configured ReSOC systems, potentially shifting or eliminating the optimal efficiency points. It is promising, however, that the initial results suggest optimal behavior at intermediate operating conditions such that extreme operation (i.e., low temperature, high pressure) are not necessarily required for efficient bulk-scale energy storage.

Several system challenges have been revealed, which motivate further study of this promising system. One challenge is that the roundtrip efficiency is strongly influenced by system thermal integration. Specifically, the stack efficiency is constrained by the system heating requirements such that the stack efficiency cannot be arbitrarily increased by lower current density operation within the present system configuration. Another challenge is the difference in gas flowrates (i.e., air, fuel, and exhaust streams) processed by the BOP in each mode of operation. Assessing the feasibility of utilizing the same BOP components in both operating modes requires system simulation and may ultimately require system configuration modifications. Finally, the parametric studies highlight a distinct tradeoff between system efficiency and energy density of storage. The stack temperature and pressure for optimal system efficiency correspond with sub-optimal stored methane content (< 60 mol%), which reduces storage energy density and may present additional challenges associated with tanking of hydrogen-rich gases.

CHAPTER 9

SYSTEM COSTING AND ECONOMICS

Minimizing the capital and operating costs of an energy storage technology are critical to wide-spread adoption. In this chapter, economic analysis of a reversible solid oxide cell system is presented. First, a bulk-scale system is considered which follows from the technical modeling results in Chapter 8. Specifically, this analysis considers a 250 MW / 500 GWh energy storage system in which the storage of dry fuel and exhaust gases is in underground geological features and the water is separately stored in an above ground reservoir. The basecase system described in Section 8.2.1 is scaled up to estimate the performance and system component size. The costing methodology is described, followed by a detailed breakdown of the system capital and operating costs. Second, the cost of a 100 kW / 1 MWh distributed scale system from Chapter 7 is estimated. The distributed scale analysis considers the economic impact of above ground tank storage and component cost scaling. This analysis, while preliminary, provides an additional tool for evaluating the efficiency and energy density tradeoffs in the distributed scale system configuration comparison. Economic evaluation at the two application scales is important because the 100 kW system has greater chance of market penetration preceding production scales to support a 250 MW ReSOC system. Because of the vast difference in application scale, the two system costing procedures include some different assumptions, particularly for ReSOC cost. Finally, cost metrics estimated in this chapter are compared against competing energy storage technologies and published cost metrics.

9.1   Methodology and assumptions

Determining the capital cost of the ReSOC energy storage system is accomplished by estimating the cost of individual system components from literature. These components

183

include: ReSOC stack, recuperative heat exchangers, gas compressors and expanders, evaporator, condenser, underground storage cavern or storage tanks, water reservoir, feedwater system, accessory electric plant, instrumentation and control, piping and valves, site improvement, and building structures. Where cost scaling is required, the following equation is used:

$$C = C_0(S/S_0)^n \tag{9.1}$$

where n is a scaling exponent, C and C_0 are the component installed cost and reference cost, and S and S_0 are the component scale and reference scale.

One metric for estimating energy storage cost is the simple formula used in Reference [18] which is based on the capital cost, energy capacity, roundtrip efficiency, and number of cycles:

$$\text{Storage cost} = \frac{\text{Capital cost}}{\text{Energy capacity} \cdot \# \text{ of cycles} \cdot \eta_{\text{RT,system}}} \tag{9.2}$$

To compare with published cost targets, system capital and levelized costs are also estimated in this work. The levelized cost calculations assume an interest rate of 5% and the annual expenses are calculated based on an annuity loan with a 20 year system lieftime and 5 year stack lifetime. The annualized cost contribution of each component is calculated based on the installed capital cost by:

$$\text{Annualized cost} = C \left[\frac{i}{1 - (1+i)^{-n}} \right] \tag{9.3}$$

where i is the interest rate and n is the component lifetime.

Solid oxide cell durability concerns have been a key challenge in commercialization of the technology, although long duration demonstrations have been achieved up to 50,000 hours in fuel cell operation at 650°C [176]. Electrolysis mode operation suffers higher degradation rates, although the technology is less mature and durability improvement is expected to reach levels of SOFC [29, 169, 176, 177]. Thus, a 5 year ReSOC stack lifetime is suitable for this preliminary analysis.

In the following subsections, each component cost is explained including the assumptions and final cost used for the bulk-scale (250 MW / 500 GWh) and distributed-scale (100 kW / 1 MWh) ReSOC systems. Because of the vast capacity discrepancy, different sources are used for each application scale. This bottom-up calculation methodology has an expected accuracy of ± 30% [178].

9.1.1 Bulk-scale system component costing

The system component and operating costs for the bulk-scale system are determined from previous studies and adjusted for the present system scale and inflation as in Jensen, et al. [86]. All costs for the bulk-scale system are given in 2013 prices adjusted using the US Consumer Price Index [179]. The system cost is summarized in Table 9.1. The system cost varies slightly from that determined by Jensen, et al. [86] because the present analysis uses specific values (e.g., flowrates, compositions) directly from the system simulation to refine some estimates in the previous study.

ReSOC stack

The cost of ReSOCs is uncertain because the technology is not yet commercialized and is projected to depend significantly on production scale. However, because of the physical and operational similarities between ReSOCs and SOFCs, projected costs for SOFCs are used here. A 2007 study estimated system cost for a 3.1 MW stationary hybrid SOFC system with a 2 MW SOFC stack to be 419–499 $/kW given annual SOFC production of 250 MW [180]. Adjusting for inflation, the stack cost contribution is 139-203 $/kW. A different study modeled an integrated gasification fuel cell plant and assumed a cost of 108 $M for a pressurized (19 bar) 221 MW SOFC stack [181]. Adjusted for inflation, this is equivalent to 489 $/kW. Finally, another study considering production volume of 500 MW/year estimated the cost of an SOFC stack in a 362 kW stationary system to be 165 $/kW [182]. In this dissertation, a cost of 200 $/kW is assumed as a baseline cost for the bulk-scale system with balance of stack and stack assembly costs equal to 2.2 and 5.7 $/kW, respectively. For the

bulk-scale ReSOC energy storage system, production volume must be very large to sustain a single 250 MW plant leading to lower stack cost per kW.

Air compressor and expander

The air compressor and expander cost are estimated from the report by Thijjsen [180], where a cost of 148 $/kW is assumed for the rotating equipment. Scaling up to the 250 MW ReSOC system and adjusting for inflation provides a total cost for the compressor and expander of 42 M$ (168 $/kW).

"Fuel" / "exhaust" compressor and expander

The fuel-side turbomachinery cost is estimated by scaling relative to the air-side turbomachinery based on the gas flowrate. Assuming that both the fuel- and air-side components are sized based on maximum molar flowrate, the fuel-side components require only 13% the capacity of the air-side. Specifically, the maximum airflow occurs during SOFC mode operation, while the maximum fuel-side flow is associated with the "fuel" composition which is compressed in SOEC mode and expanded in SOFC mode. Thus, the compressor and expander cost is estimated to 5.5 M$.

Recuperative heat exchangers

The recuperative heat exchangers are estimated to 32$/kW based on a 2007 study [180]. Adjusting for inflation and linearly scaling to the 250 MW ReSOC system, these components contribute 9.1 M$ to the total system cost.

Feedwater and miscellaneous balance of plant systems

A study of fossil fueled power plants by the Department of Energy [183] estimated the cost for an 809 ton/hr feedwater system including a demineralized water storage tank, condensate pumps, aerator, intermediate and high pressure feedwater pumps, boiler, service air

compressors, instrument air dryers, closed cycle cooling heat exchangers, closed cycle cooling water pumps, raw water pumps, filtered water pumps, makeup water demineralizer, water makeup and pretreating. The cost for the entire system including equipment, materials, and labor was 31 M\$; however, the ReSOC system requires feedwater at 46 ton/hr. Using a scaling exponent of 0.7 [184], the total cost for a 250 MW ReSOC system is 4.2 M\$.

Evaporator

The evaporator cost is estimated from a Department of Energy study [183] including a 694 ton/hr heat recovergy steam generator system with a cost of 51.5 M\$. The 46 ton/hr steam generator required for a 250 MW ReSOC system is calculated to be 7.7 M\$ assuming a scaling factor of 0.7 [184].

Condenser

An 810 ton/hr condenser used in a 298 MW steam turbine system [183] had an estimated cost of 7.0 M\$, which includes equipment, materials, labor, and auxiliaries. Furthermore, steam piping has an estimated cost of 10.6 M\$. The maximum capacity of the condenser unit in the 250 MW ReSOC system is 122 ton/hr leading to a total cost of 4.7 M\$ with a scaling exponent of 0.7.

Methane cavern

Natural gas storage in underground caverns (such as, depleted gas reservoirs, aquifers, and salt caverns), is an established and cost-effective method for seasonal storage [185, 186]. A salt cavern storage facility in Lille Torup, Denmark stores approximately 120 million Nm^3 per cavern, where 70 million Nm^3 of the gas is accessible and the remainder acts as a pressure buffer and is referred to as a "cushion gas". The caverns operate between 150 and 200 bar. The capital expense of one of the 500-800,000 m^3 (geometric volume) storage caverns at the Lille Torup storage facility is approximately 36 M\$. For the bulk-scale storage sys-

tem, cavern pressure is assumed to be 160 bar. The volumetric energy density of the stored fuel is 72% that of natural gas (i.e., for 58% methane and 40% hydrogen), leading to an energy density of 4.2 GJ/m^3 at 160 bar and 60°C. Thus, an energy capacity of >500 GWh is achieved with a single cavern and the cost is selected as 36 M\$ (144 \$/kW). The storage capacity of 500 GWh and power rating of 250 MW suggest that the discharge duration is >2000 hours, or nearly 3 months. This scale of energy storage is suitable for seasonal energy storage applications.

Carbon dioxide cavern

Storing carbon dioxide in salt caverns is a relatively new process. Furthermore, this implementation may be complicated because the "exhaust" gas used in the system simulation is a mixture that includes some hydrogen (24%) and carbon monoxide (3%). To account for the uncertainty, process contingency of 40% and project contingency of 50% are included in the final cost [187]. The molar quantity of stored CO_2-rich exhaust is 81% less than the volume of stored fuel. Meanwhile, the exhaust has 1.6 times higher volumetric density compared with the fuel mixture. Accounting for the above differences, the cost of the CO_2 cavern is estimated as 36 M\$ · 0.8 · 140% · 150% / 1.6 = 37.8 M\$.

Water reservoir

A 75,000 m^3 water pit for thermal energy storage was constructed in Marstal, Denmark in 2012 at a cost of 50.4 \$/m^3 [188]. For the 250 MW system, a maximum water volume of 81,000 m^3 is generated from oxidizing the stored fuel when the system is completely discharged, so the water reservoir cost is taken as 4.1 M\$.

Accessory electric plant

An accessory electric plant is required to interface the ReSOC electrical energy storage system with the electric grid. Previous estimates for accessory electric plan and power condi-

tioning include 31 M\$ (123 \$/kW) for a 250 MW fuel cell plant [181] and 0.2 M\$ (57 \$/kW) for a 3.1 MW SOFC system [180]. In this study 80 \$/kW is assumed for a total cost of 20 M\$.

Instrumentation and control

Previous studies assumed instrumentation and control cost of 41 \$/kW for a 250 MW SOFC system [181] and 34.1 \$/kW for a 3.1 MW hybrid SOFC system [180]. Here 37 \$/kW is assumed for a total cost of 9.25 M\$.

Miscellaneous costs

Piping and valves, site improvement, and buildings and structures costs are also included in this comprehensive costing analysis. Piping and valves are estimated to cost 34 \$/kW for a total cost of 8.5 M\$ [180]. Site improvement is estimated based on the 250 MW IGFC plant [181] for a total cost of 8 M\$ (32 \$/kW). The same study is used to estimate building cost equaling 8 M\$ (32 \$/kW).

Labor expenses

Labor expenses for the bulk-scale system are estimated based on a 555 MW IGCC plant in Reference [183] which required 16 jobs. Because the ReSOC system considered here is approximately half the size of the IGCC plant, 8 jobs are assumed. The annual labor expense is taken from References [181, 183] to be 0.43 M\$ per job for a total labor cost of 3.4 M\$ per year.

Maintenance, materials, water, and chemicals

Variable operating costs are considered to include makeup water, maintenance materials, and chemicals. These costs are estimated as 0.71 ¢/kWh [181]. The total yearly cost is estimated by assuming the plant operates for 5400 hours per year. This value is determined by considering a case-study of energy arbitrage on the Danish electricity spot market [86].

Table 9.1: System component cost and total plant cost summary for a 250 MW / 500 GWh ReSOC system.

Item	Installed capital cost (M$)	($/kW)	Annualized cost (M$/year)
CH_4 cavern	36	144	2.89
CO_2 cavern	37.8	151.2	3.03
H_2O reservoir	4.1	16.4	0.33
250 MW ReSOC (5 yr. life)	50	200	11.55
Balance of stack	0.55	2.2	0.13
Stack assembly	1.425	5.7	0.33
Air compression/expansion	42	168	3.37
Fuel compression/expansion	5.45	21.8	0.44
Recuperative heat exchangers	9	36	0.72
Feed water and misc. BOP systems	4.2	16.8	0.34
Evaporator	7.7	30.8	0.62
Condenser	4.7	18.8	0.38
Power conditioning	20	80	1.60
Instrumentation and control	9.25	37	0.74
Piping and valves	8.5	34	0.68
Improvement to site	8	32	0.64
Building and structures	8	32	0.64
Labor expenses	–	–	3.40
Variable operating cost	–	–	9.6
Total	256.7	1026.7	41.39

Multiplying the annual hours of operation by the nominal plant power capacity determines the annual expense to be 9.6 M$.

9.1.2 Distributed-scale system component costing

The capital and annualized cost of distributed-scale (100 kW/1 MWh) ReSOC systems is evaluated by scaling component cost from several sources as described here. Component costs for the distributed-scale system are adjusted to 2012 prices using the Chemical Engineering Plant Cost Index (CEPCI).

ReSOC stack

James, et al. [189] presented a detailed costing of SOFC stacks and systems for 1-100 kWe systems over a range of annual production scales. The study considers common YSZ-electrolyte SOFCs produced by tape-casting and screen printing methods. The LSGM-electrolyte cells chosen for this study require mostly conventional manufacturing methods suitable for commercial production (e.g., tape-casting, screen-printing). The increased cost of LSGM compared to YSZ is a small problem because the electrolyte material cost is only considered to comprise about 1% of the total assembled ReSOC stack cost [189]. Ultimately the stack cost is selected to 0.0874 $/cm^2, based on a production volume of 10,000 systems per annum, and a 30% contingency to account for uncertainty in material cost and manufacturing. By selecting the cell active area as the representative scale, the relatively low and varying power densities in the distributed scale system are included in the cost comparison. As in the bulk-scale system, the stack is assumed to be replaced every 5 years, while the other system components have an assumed life of 20 years.

Storage tanks

The gaseous storage tanks for the distributed scale system vary in volume from about 4–20 m^3. Baseline carbon steel tank costs were scaled based on the tank volume using correlation charts in Perry's Chemical Engineers' Handbook [190]. Adjustment factors in Reference [178] suggest a materials factor of 2.0 for stainless-steel tanks and pressurization factor of 3.0, which are applied to the baseline cost. The required water storage in the water separation systems is approximately 55-gallons with a tank cost of 491$ [178].

Heat exchanger components

Cost of the various heat exchangers in the distributed scale systems are determined by scaling according to the heat transfer area with a scaling exponent of 0.6. Heat transfer area is determined from the system modeling results assuming a fixed overall heat transfer

coefficient of 25 W/m-K. The correlation used to determine heat transfer cost is taken from Shirazi, et al. [191] as $C = 2290(A_{\mathrm{HX}})^{0.6}$, where A_{HX} is the heat transfer surface area in m^2. The air-cooled condenser used in the water separation systems is priced from a correlation in Reference [192] based on the heat transfer area as $C = 70000(A_{\mathrm{cond}}/280)^{0.8}$. The inflation-adjusted price agrees well with the values for air-cooled heat exchangers in [178].

Turbomachinery

Turbomachinery in the distributed-scale system include blowers, compressors, and expanders. The blower cost is determined based on correlations to the volume flow in Reference [178]. Compressors to deliver stack product gases to the pressurized storage tanks are sized from Reference [192] based on the compressor load as $C = 450000(\dot{W}_{\mathrm{comp}}/1000)^{0.9}$, where $\dot{W}_{\mathrm{comp}}$ is the compressor power in kW. Two compressors are required by each system for the multi-stage process. Small-scale expander cost is taken from Reference [192] with a fixed value of \$1600 for 5–30 kW power rating. Recycle ejector cost is lumped with the turbomachinery and estimated by linear scaling from a 5 kW SOFC system in Reference [171] for a final cost of \$1650.

Miscellaneous costs

Miscellaneous costs include power electronics, valves, and piping. Power electronics are estimated from 100 kWe SOFC systems in Reference [189] to a cost of \$1420. Valves and piping are scaled from Reference [171] at a reported cost of 74 \$/kW$_{\mathrm{gross}}$.

9.2 Cost of bulk-scale energy storage

The individual component and variable costs are tabulated in Table 9.1 indicating a total plant installed cost of 256.7 M\$ for the 250 MW / 500 GWh ReSOC system. In the considered application, the storage system has energy capacity to charge and discharge seasonally (i.e., 2000 hour charge and discharge duration). Therefore, the number of roundtrip cycles over the 20 year system life is estimated as 20 years / 4000 hours = 44 cycles, or about one roundtrip

cycle per year. The energy capacity is taken as 500 GWh and efficiency is assumed to be 70% based on the results in Chapter 8. These assumptions result in a storage cost of 1.7 ¢/kWh for the bulk-scale system as calculated by Equation 9.2. This energy-capacity normalized cost is very favorable compared to other storage technologies. Figure 9.1 illustrates that ReSOC system performance compares favorably with pumped hydro and CAES based on energy capacity and storage cost. In fact, pumped hydro storage is the only technology with storage cost lower then the ReSOC system.
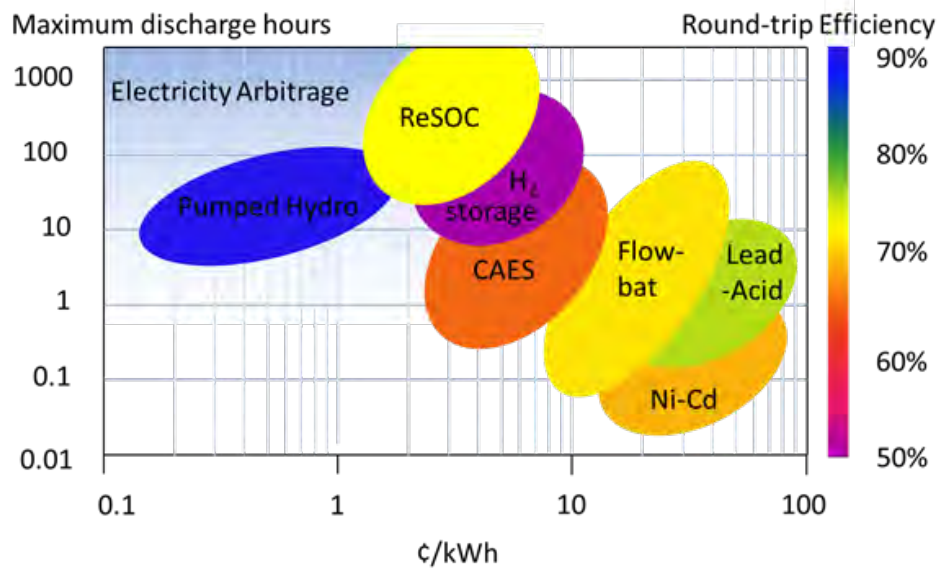
Figure 9.1: Comparison of bulk-scale ReSOC system performance with other energy storage technologies performance reported in literature [7, 18].

The specific application of seasonal storage considered in this economic analysis indicates economically competitive performance. It is also reasonable to assume that low cost storage can be achieved for shorter duration energy-time shift. Specifically, if a charge/discharge duration of 8 hours is assumed for the 250 MW system, only 2 GWh of energy capacity is used. The cycle count of the system also increases in this application (i.e., 20 years / 16 hours = 11,000 cycles, or about 2700 cycles/stack life). Applying these values to Equation 9.2 results in the same storage cost of 1.7 ¢/kWh achieved for the high energy-capacity system. This calculation is predicated on two key assumptions: (1) system cost is equivalent between

2 GWh and 500 GWh systems and (2) ReSOC stacks are durable for >5000 cycles (i.e., in line with the DOE targets given in Section 2.1.2). The storage cost will account for a lower portion of the total system cost if the storage capacity is reduced by a factor of 250. Above ground tanks might be more economically employed at this scale [193]. Durable galvanic cycling of ReSOCs has been demonstrated for >1000 hours and 1000 cycles when the cycle duration is 1-hour (i.e., 30 minutes in each mode) or 12-hour, although the degradation rate increases significantly when the current density increases from 0.5–1.5 A/cm^2 [60]. Favorably, the optimal system results shown in Chapter 8 were at an operating current density near 0.70 A/cm^2. While these results are promising, more research in cycle-induced degradation (or activation) is required to definitively achieve the cycle life targets of 5000 hours.

The capital cost of the ReSOC system is 0.51 $/kWh based on the 256.7 M$ value reported in Table 9.1 and an energy capacity of 500 GWh. This suggests that the system capital cost is well below the DOE target of 150 $/kWh [1]. However, contrary to that presented in Equation 9.2, this capital cost metric is not normalized by the efficiency or cycle count. Therefore, a system that has a lower energy capacity and higher cycle life will be penalized. For example, consider the 250 MW / 2 GWh system theorized above with 8 hour discharge capacity. If the storage capacity is scaled linearly and other component costs are equivalent to those in Table 9.1, the system installed capital cost is reduced to 183.5 M$ for a normalized capital cost of 91.8 $/kWh. This indicates that the system capital cost is very sensitive to the energy capacity and the extremely low cost of the seasonal storage system results from the storage contributing a small portion of the total system cost.

The annualized system cost is also calculated (see Table 9.1) and the cost distribution of the various components and operating expenses are given in Figure 9.2. The key contributing factors to the system cost are the ReSOC stack (28%), O&M cost (23%), and storage caverns (14%). The storage costs only make up 14% of the total system cost meaning that increasing the storage system energy-capacity can be achieved with relatively little system cost increase. Specifically, doubling the capacity of the storage caverns increases the system levelized cost
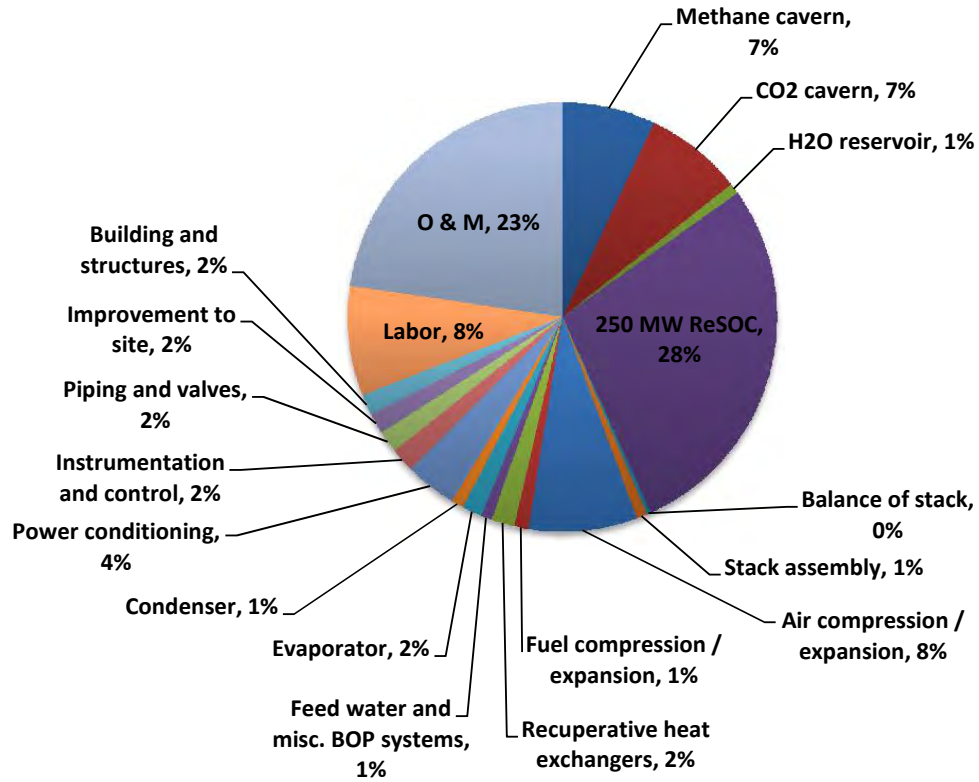
Figure 9.2: Annualized component cost breakdown of system component and operating costs for a 250 MW ReSOC system.

by 21%. The system levelized cost is estimated by dividing the annualized cost by the estimated energy storage over a year (i.e., 5400 hours · 250 MW and about 1 cycle per year). This results in a levelized cost of 3.1¢/kWh-cycle, which compares favorably with the long-term DOE target of 10 ¢/kWh-cycle [1].

9.3 Cost of a distributed-scale energy storage

The cost of energy storage calculated by Equation 9.2 is reported in Figure 9.3 for the six distributed scale system configurations modeled in Chapter 7. The baseline stored vapor system is most expensive with a capital cost of 403 $/kW and cost of storage of 11 ¢/kWh. The economic analysis reveals that cost of energy storage decreases substantially with increased energy density due to lower cost of tank storage, but the cost is also influenced by roundtrip efficiency, stack power density, and complexity of the heat exchanger network.

For the stored vapor system, the cost of storage is reduced by 9% when a fuel expander is included because the increased roundtrip efficiency overcomes small capital cost increase from an additional heat exchanger and cost of the fuel expander. Increasing the storage pressure to 50 bar further reduces system cost because of the smaller tanks required for equivalent energy capacity. The baseline water separation system has 11% lower cost than the baseline stored vapor system, indicating that the increased complexity and size of the heat exchangers and lower roundtrip efficiency are overcome by reduced capital investment in large storage tanks and reduced stack cost due to increased power density. Similar to the stored vapor systems, the cost of the water separation system decreases with inclusion of a turbine and increased tank pressure. Ultimately the lowest cost system is that with water separation and high tank pressure, which has a relatively low roundtrip efficiency of 65.5% (see Table 7.1). The energy storage costs reported in Figure 9.3 are on par with flow battery systems and exceed conventional battery storage (see Figure 9.1)
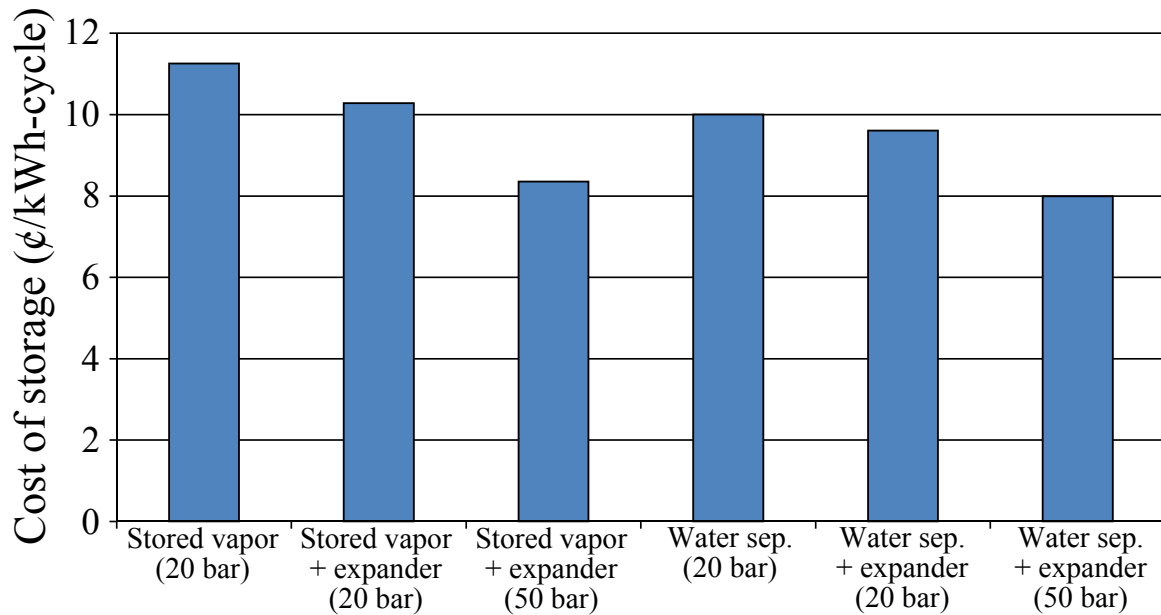
Figure 9.3: Energy storage cost for several distributed scale systems detailed in Chapter 7.

The component annualized cost breakdown for the highest and lowest cost systems is given in Figure 9.4. Greater than half of the cost of the baseline stored vapor system

is attributed to the relatively low energy density gaseous storage tanks. the bulk of the remaining cost, 34.4% is attributed to the ReSOC stack and the cost of the relatively simple system BOP is small. Alternatively, the majority expense in the lowest cost system is attributed to the ReSOC stack. This system includes separate storage of water and dry gases and 50 bar storage tanks, leading to a 5 times reduction in tank volume. The reduction in tank cost from increased energy density and ReSOC stack cost from increased power density overcome the increased heat exchanger cost associated primarily with the air cooled condenser. Thus, this preliminary system costing analysis motivates future studies to focus on increasing energy density of storage to mitigate the high cost of storage tanks.
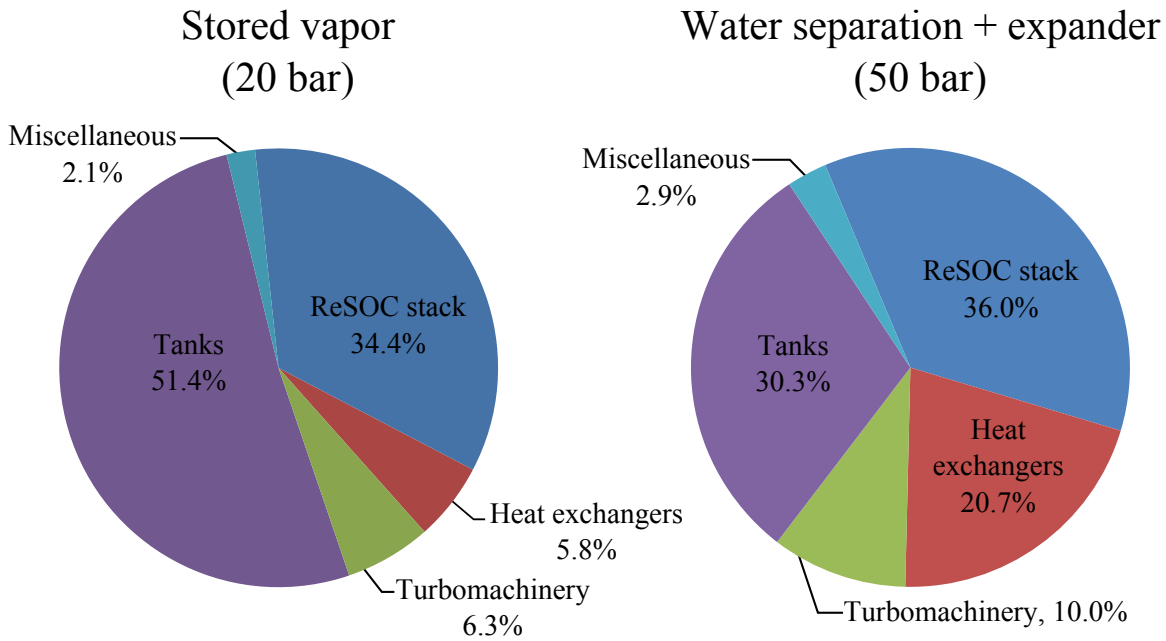
Figure 9.4: Annualized component cost breakdown for the highest and lowest cost distributed-scale systems.

The results given here show system cost when the system operation is intended to optimize roundtrip efficiency. However, this analysis also indicates that the higher stack power density in the water separation systems lead to lower cost of energy storage. This suggests that the operating conditions to achieve optimal efficiency may be distinct from the lowest cost operating strategy.

The distributed scale system has high capital cost compared to the published targets and application-derived cost requirements outlined in Section 2.1.2. The capital cost target from the Department of Energy of 150 $/kWh is not met be any of the distributed scale systems here, which range from 287–403 $/kWh. Furthermore, the application derived target of 1340 $/kW for the distributed-scale system is exceeded by 4–6 times with the systems given here (4800–6670 $/kW). Similar to the bulk-scale, ReSOC systems are more favorable when compared with economic metrics normalized by energy capacity, rather than power capacity. Further analysis is required to quantify the levelized cost of the distributed-scale systems to include O&M and labor costs.

9.4 Conclusions from the economic analysis

The economic results generated here using a bottom-up costing methodology suggest that ReSOC storage systems can be economically viable for bulk-scale seasonal applications. The costing methodology relies on many assumptions that should be reconsidered in future analyses as ReSOC system design progresses to include specific hardware selection and system simulation. A 250 MW / 500 GWh system is estimated to have capital cost of 257 M$ (1026.7 $/kW). The levelized cost is estimated to be 3.1 ¢/kWh and storage cost as calculated as in Yang et al. [18] to be 1.7 ¢/kWh. The bulk-scale ReSOC system is estimated to be less expensive than all competing energy storage technologies except pumped hydro.

However, considering bulk-scale ReSOC system cost against power-capacity normalized metrics is less favorable. The 20 year life-cycle cost is 2840 $/kW, which is over three times higher than the desired cost based on energy storage application benefit of 820 $/kW (see Reference [8] as well as Section 2.1.2). The discrepancy in economic favorability based on the metrics described here is a consequence of the seasonal energy storage application and the relatively low contribution of energy capacity to total system cost.

Economics of the distributed-scale system are presented to distinguish between the technical tradeoffs associated with efficiency, energy density, and system complexity. The results here indicate that maximizing energy density is key to minimizing system cost because of the

large contribution of storage tanks to total system cost. The present systems do not meet the established capital cost targets, suggesting that future designs should aim to reduce capital expense without sacrificing technical performance.

It is important to note that the costing analysis in this work was applied following a thorough technical analysis, meaning that the system design was not intended to optimize economic performance. Future work might be able to approach the economic targets even with present day technology by re-directing the system design effort toward cost minimization.

CHAPTER 10

CONCLUSIONS

Conclusions from the individual modeling studies presented in Chapters 4 and 6–9 are given at the end of each chapter. Here, those results and conclusion are again summarized and broader conclusions drawn from the culmination of these results. The results in this dissertation have shown that ReSOC energy storage systems should be considered a promising solution to future energy storage needs, although much work is still required before these systems are ready for product development and implementation. This chapter also includes a discussion of future research efforts that will continue advancing ReSOC systems toward commercialization.

10.1 Summary of the work completed

The thermodynamics of a ReSOC system have been thoroughly analyzed and a methodology developed to predict theoretical roundtrip performance sensitive to variations in temperature, pressure, reactant composition, and utilization. This analysis is critical to understanding the performance impact of stack operating conditions on ReSOC energy storage systems. An intermediate temperature cell model was developed and calibrated to represent performance of a promising LSGM material set. The cell characteristic shows low resistance and high power density at temperatures below 650℃. The electrochemical model was calibrated to capture performance to temperature and reactant composition. The electrochemical model is applied to a channel-level ReSOC model which is based on conservation equations to capture the effects of reactant dilution, flow configuration, and operating pressure. The cell model was employed to characterize performance impact of various cell operating parameters including current density, flow configuration, reactant composition, and oxidant composition. This analysis included quantifying roundtrip efficiency and thermal characteristics, which are both critical to system design and operation.

The calibrated ReSOC model was also coupled with thermodynamic balance of plant component models to simulate steady-state roundtrip operation of ReSOC energy storage systems. The methodology to accurately represent performance of these novel system was also explained and implemented. The system modeling capabilities were applied to two different application scales (100 kW and >10 MW) to estimate roundtrip efficiency and energy density performance metrics. The distributed scale analysis focused on exploring different system configurations, including the design decision to either store a high temperature gas that maintains H_2O in a vapor phase, or condense water for separate storage. Use of a small-scale expansion turbine was also considered to recuperate energy lost in compressing gases to storage pressure. System operating conditions including tank storage pressure, current density, and fuel utilization were also explored.

A large scale system was analyzed for technical and economic performance. A system configuration for the bulk-scale was designed with application constraints including highly pressurized gaseous storage and ambient air used as the oxidant / sweep-gas. Stack and system operating conditions including stack temperature, stack pressure, reactant composition, fuel utilization, and charge/discharge duration were parametrically analyzed to determine the impact on bulk-scale system efficiency. Finally, the economics of the bulk-sale system were estimated based on system capital cost and cost of energy storage metrics. The economic and technical performance was compared with current energy storage technologies.

10.2   Roundtrip efficiency conclusions

The roundtrip efficiency is the primary performance metric considered in this work and was considered at the thermodynamic level (Chapter 4), the stack level (Chapter 6), and at two different system scales (Chapters 7 & 8). Thus, this work has shown the efficiency impact attributed to various effects; in other words, quantified the energetic limitations on roundtrip efficiency, considered the impact of practical stack operation and capabilities with current cell technology, and estimated the losses from integrating the stack into a system to include the impact of auxiliary BOP loads. Each progression in this analysis reveals

areas where efficiency may be improved through targeting the specific cause of efficiency loss. The targeted roundtrip efficiency of 80% given in the objectives was not achieved through this work. In fact, the maximum efficiencies shown for the distributed and bulk-scale system implementations were both around 74% (although this efficiency was achieved with significantly different system configurations and operating conditions). Ultimately, the system implementation and cell technology are both factors limiting roundtrip energy storage efficiency. In the remainder of this section, the efficiency results are summarized and analyzed together with the goal of highlighting where efficiency gains are possible in future systems.

The thermodynamic analysis predicted that 100% reversibility (i.e., theoretical roundtrip efficiency) is achievable at the stack level with carefully tuned operating conditions. This ideal case is achieved at conditions where the thermoneutral and reversible voltages are equal. This approach of lowering the thermoneutral voltage allows higher energetic efficiency compared to steam-hydrogen reversible fuel cell systems which have a limited theoretical efficiency of about 85% for high temperature electrochemical cells (>500°C). Furthermore, it shows that the ideal case observed in the thermoneutral methane red-ox cycle is achievable while overcoming the practical limitations of methane related to high reactant conversion and carbon deposition. However, if reactant water evaporation is included in the energetic calculation, then this irrecoverable energy (i.e., low-grade water condensation) loss results in about 10% roundtrip efficiency penalty. It is shown that the operating parameters adjusted to achieve the ideal thermodynamic conditions are highly interconnected such that an infinite possibility of operating conditions combinations can achieve 100% theoretical roundtrip efficiency — although operating ranges, especially temperature, must match ranges of high stack efficiency. The relevant stack operating conditions include stack temperature, pressure, reactant composition and reactant utilization. From an energetic perspective, either an intermediate temperature and ambient pressure stack, or a high pressure and high temperature stack can potential result in favorable operating conditions. Stack pressurization

202

strongly influences methane formation, so even relatively low pressurization (i.e., < 10 bar) can have a major impact on the theoretical efficiency.

Progressing from the thermodynamic analysis to the calibrated stack model indicates a significant efficiency penalty. In particular, the stack modeling results indicate that at reasonable current density (0.5 A/cm^2), the roundtrip stack efficiency is below 75% based on present stack performance. This relatively low efficiency suggests that improved stack performance (i.e., lower area specific resistance and resistance associated with cell-stacking) is critical to achieve high roundtrip efficiency at economically viable stack power density. Adjusting stack operating conditions so that more methane is formed in electrolysis mode is favorable to heat generation and therefore system efficiency. Desirable operating modifications include operating the electrolysis mode stack in counter-flow, operating at optimal hydrogen-to-carbon ratios (i.e., about H/C=12.6 for the 650℃ and ambient pressure stack), and producing a highly reduced (i.e., low oxygen content) fuel composition in the electrolysis mode. It should be noted that the temperature and pressure used throughout the stack modeling study in Chapter 6 are not optimal from an energetic standpoint, meaning that the theoretical roundtrip efficiency is limited. Increasing the pressure and/or reducing the cell temperature are critical to implementing practical systems, but lower temperature operation (e.g., 600℃) is not practical with current cell technology. Modifying the cell operating condition to understand the system performance with improved cells is considered in the system modeling studies summarized next.

The distributed scale system study analyzed different configurations for a 100 kW discharge power rating system with an ambient pressure stack operated at 600℃. The resulting roundtrip system efficiency is shown to be highly dependent on configuration, particularly on the design decision to either operating the storage tanks at elevated temperature to maintain vapor phase of all stored species (e.g., steam), or to condense water out of the storage system and store the remaining gases at ambient temperature, but suffer the increased energetic cost of reactant preheating. The stored vapor approach results in the highest roundtrip efficiency

of nearly 74%, while the system that condense steam for storage achieves roundtrip efficiency of 68%. Further optimizing the operating conditions, particularly pressurizing the stack, may result in higher efficiencies; although the ambient pressure systems considered here are considered more feasible than pressurized systems at the distributed scale. Furthermore, the stack operating temperature of 600°C is an operating target set by these system studies, and suitably low resistance has not yet been achieved at this low temperature with present cells. The efficiency penalty associated with system balance of plant for these systems is primarily attributed to the compressor load to pump stack tail-gases into their respective storage tanks. This auxiliary power load is responsible for about 30-40% of the total roundtrip efficiency loss, while the remainder is attributed to conversion losses in the stack.

The bulk scale system configuration is constrained by high gas storage pressures (160 bar) and using ambient pressure air as oxidant / sweep-gas. Other constraints on this system are that water must be separated from the reactant and product streams before storage and high utilization is required so that stored gases are of relatively high purity. These constraints result in a relatively complex system balance of plant to mitigate efficiency losses, including multiple thermally integrated compression and expansion stages and operating at intermediate stack pressures in between ambient and storage pressure. The benefit of this complex system is that system BOP losses are severely reduced, and under certain conditions net electricity is generated from the BOP components. The optimal roundtrip efficiency is nearly 74% and was shown to be highly dependent on the balance of plant operation; however, it should be noted that formal optimization was not performed here and the "optimal" efficiency is determined by individual stack parameter variation. The optimal roundtrip efficiency in the bulk-scale system arises due to tradeoffs between losses in the stack and the BOP. Thus, within the constraints of this system design significant efficiency improvements are not expected. The primary limitation on roundtrip efficiency is the energetic requirement to evaporate reactant water in electrolysis mode. This load ultimately limits the stack efficiency because a certain amount of waste heat generation is

required for steam generation.

Taken together, these studies conclude that the roundtrip efficiency is ultimately limited by both cell and system performance. The stack modeling results show that lower resistance is required at the thermodynamically favorable conditions (i.e., lower temperature), however high performance can be achieved under pressurized conditions with current cell technology. At the system level, efficiency improvement may be realized through configuration and operating condition modifications. The modeling methodologies and configurations presented throughout this dissertation provide a basis for future optimization and system simulation efforts.

10.3 System configuration conclusions

An equivalent roundtrip system efficiency was achieved in both the distributed and bulk-scale studies (i.e., about 74%), although the system configurations and operating conditions vary significantly between these two cases. Here, the two systems are compared to consider the tradeoffs of the two approaches.

The high roundtrip system efficiency in the distributed scale system requires maintaining stored reactants in the vapor phase. On the other hand, the bulk-scale system achieves the same efficiency when water is condensed and stored separately from the other reactants species. If water is stored separately in both systems, the bulk scale system has roundtrip efficiency 6 percentage-points higher than the distributed scale system. The difference in this performance is attributed to use of a pressurized stack in the bulk-scale system and a more complex balance of plant. In the bulk-scale system, balance of plant power has a small net effect on system efficiency because the power expended in the compressors is almost entirely recovered in expansion of gases from either the pressurized storage tank (fuel/exhaust) or the pressurized stack (air channel exhaust). The increased capital cost required in the more complex bulk-scale system allows higher energy density of storage and energy capacity suitable for seasonal energy storage applications.

10.4   System cost conclusions

The costing analysis revealed that reversible solid oxide cells systems can be competitive for bulk-scale seasonal energy storage applications, although the smaller scale systems are shown to exceed the cost targets. The bulk-scale system has an estimated energy storage cost of 2.6 ¢/kWh for a 250 MW and 500 GWh system. This system application is designed for seasonal energy storage with gaseous storage in geological caverns providing and energy capacity to fulfill the nominal discharge power for nearly 3 months. When compared to other energy storage technologies, only pumped hydro storage has lower cost, which suggests that these ReSOC energy storage systems should be considered an important component of bulk-scale energy storage in the future. The primary contributions to system cost include the ReSOC stack, underground cavernous storage, and operating expenses. The analysis uses capital cost value for the ReSOC assuming high production volume capable of satisfying such large scale systems (200 \$/kW), so this production capacity is a prerequisite to achieving the reported cost. Further reductions in ReSOC cost, or increases in durability, can contribute to lower total system cost.

The distributed scale systems have energy storage cost of 8–11¢/kWh which is similar to the cost of red-ox flow batteries and exceeds conventional batteries [18]. However, the capital cost and application-derived benefits are not met with the systems analyzed in this work.

10.5   Cell-stack performance targets

One objective of this work was to set performance targets for cell and materials development for specific operating ranges that benefit system operation. The results indicate that lower stack resistance is required for successful implementation at the desired operating temperature. The distributed-scale system analysis shows that an overall stack resistance of $0.20~\Omega\text{cm}^2$ should be targeted to achieve high system efficiency at economically viable power density (i.e., about $0.40~\text{W/cm}^2$). Furthermore, this low stack resistance should be achieved

at a cell temperature of 600℃ for successful implementation of the ambient pressure stack, distributed-scale system.

The operating conditions found to be optimal for the bulk-scale system match well with current intermediate temperature ReSOCs (i.e., 680℃ and 20 bar). Furthermore, laboratory cell performance achieves the targeted cell performance at these conditions (see Section 5.1.4), although the impact of cell-stacking increase overall stack resistance dramatically (see Section 5.1.6). Mitigating the increased resistance associated with cell-stacking is critical to implementing such ReSOC systems with present cell technology.

10.6   Future work

I will conclude this dissertation with a brief discussion to help guide future researchers with my knowledge of ReSOC energy storage systems. Future research efforts should focus in two categories: higher fidelity system simulation and alternative system configurations analysis.

Higher fidelity system simulation is an important extension of the work presented in this dissertation. The modeling results here rely on thermodynamic system component models. This approach helps to provide a general idea of system operation, but does not capture the influence of, for example, off-design performance associated with part-load and dual-mode operation. Future work must also address the complications of dynamic system operation. Dynamic operation in a ReSOC energy storage system is somewhat distinct from, for example, SOFC power systems. In other words, even if the power supplied or consumed by the ReSOC is constant in time, the impacts of tank storage introduce time dependent properties to the BOP and stack. In addition to the inherent system dynamics associated with tanked storage, system performance under dynamic external load must be explored. Most energy storage applications require some degree of system load following, and the capabilities of ReSOC systems for this purpose have not yet been addressed.

A wealth of system configurations exist which have not been comprehensively evaluated in this work. The discussion in Section 2.5 outlines various design considerations, although

not every trade off presented in Section 2.5 was addressed in this work. Furthermore, other work has suggested different thermal management strategies, reactant storage configurations, and system integration approaches. In my opinion, the most promising configurations that should be explored in extending the present work include the following: (1) Inclusion of auxiliary methanation and reforming reactors to drastically increase the methane content of the stored gas. This has been initially explored elsewhere [95], and should continue to be considered in future research. In particular, this approach may be synergistic with utilizing the natural gas network as a storage medium to mitigate the challenges and high cost of tank storage. In other words, this approach would involve using the ideas presented in this dissertation to achieve increased roundtrip efficiency with the power-to-gas systems [107]. (2) System integration with heat sources from other industrial processes. The approach of coupling nuclear [32] or solar-thermal [111] with reversible fuel cell systems has been described previously. These approaches can also be explored in conjunction with the ReSOC operating strategies explored in this work. Flexible thermal management through either tuning ReSOC operating conditions (as in this work) or utilizing an external heat source (as elsewhere) will increase the robustness of these systems for different operating applications. Furthermore, performance benefit is possible for the systems presented in this dissertation by supplying relatively low grade heat for steam generation.

Finally, within any of the future studies, optimization can help to establish the best system performance. This work has shown the high degree of operating parameter interdependency, particularly with regard to stack operating conditions. Many opportunities exists for system optimization including system BOP configuration, stack operating conditions, and reactant compositions.

REFERENCES CITED

[1] Grid energy storage. Technical report, US Department of Energy, 2013.

[2] Ronald M Dell and David AJ Rand. Energy storagea key technology for global energy sustainability. *Journal of Power Sources*, 100(1):2–17, 2001.

[3] Josep M Guerrero, Frede Blaabjerg, Toshko Zhelev, Kas Hemmes, Eric Monmasson, Samir Jemei, Maria P Comech, Ramón Granadino, and Juan I Frau. Distributed generation: toward a new energy paradigm. *IEEE Industrial Electronics Magazine*, pages 52–64, 2010.

[4] Kas Hemmes, Josep M Guerrero, and Toshko Zhelev. Highly efficient distributed generation and high-capacity energy storage. *Chemical Engineering and Processing: Process Intensification*, 51:18–31, 2012.

[5] David Lindley. Smart grids: The energy storage problem. *Nature News*, 463(7277): 18–20, 2010.

[6] Abbas A Akhil, Georgianne Huff, Aileen B Currier, Benjamin C Kaun, Dan M Rastler, Stella Bingqing Chen, Andrew L Cotter, Dale T Bradshaw, and William D Gauntlett. Doe/epri 2013 electricity storage handbook in collaboration with nreca. *ed: Albuquerque, NM: Sandia National Laboratories*, 2013.

[7] Bruce Dunn, Haresh Kamath, and Jean-Marie Tarascon. Electrical energy storage for the grid: a battery of choices. *Science*, 334(6058):928–935, 2011.

[8] Jim Eyer and Garth Corey. Energy storage for the electricity grid: Benefits and market potential assessment guide. *Sandia National Laboratories*, pages 69–73, 2010.

[9] Elliot Hinds and Jonathan Boyer-Dry. The emergence of an electric energy storage market. *The Electricity Journal*, 27(2):6–13, 2014.

[10] S Eckroad and I Gyuk. Epri-doe handbook of energy storage for transmission & distribution applications. *Electric Power Research Institute, Inc*, 2003.

[11] California Senate Bill XI-2, April 12 2011.

[12] Colorado House Bill 10-1001, 2010.

[13] Energy strategy 2050 - from coal, oil and gas to green energy. The Danish ministry of Climate and Energy, Copenhange, DK, 2011.

[14] European union directive 2009/28/ec, 2009.

[15] John Baker. New technology and possible advances in energy storage. *Energy Policy*, 36(12):4368–4373, 2008.

[16] Hussein Ibrahim, Adrian Ilinca, and Jean Perron. Energy storage systemscharacteristics and comparisons. *Renewable and sustainable energy reviews*, 12(5):1221–1250, 2008.

[17] Ioannis Hadjipaschalis, Andreas Poullikkas, and Venizelos Efthimiou. Overview of current and future energy storage technologies for electric power applications. *Renewable and Sustainable Energy Reviews*, 13(6):1513–1522, 2009.

[18] Zhenguo Yang, Jianlu Zhang, Michael CW Kintner-Meyer, Xiaochuan Lu, Daiwon Choi, John P Lemmon, and Jun Liu. Electrochemical energy storage for green grid. *Chemical reviews*, 111(5):3577–3613, 2011.

[19] Electricity storage association, 2011. Accessed: 2015-2-13.

[20] SJ Peighambardoust, S Rowshanzamir, and M Amjadi. Review of the proton exchange membranes for fuel cell applications. *International Journal of Hydrogen Energy*, 35(17): 9349–9384, 2010.

[21] Laetitia Dubau, Luis Castanheira, Frédéric Maillard, Marian Chatenet, Olivier Lottin, Gaël Maranzana, Jérôme Dillet, Adrien Lamibrac, Jean-Christophe Perrin, Eddy Moukheiber, et al. A review of pem fuel cell durability: materials degradation, local heterogeneities of aging and possible mitigation strategies. *Wiley Interdisciplinary Reviews: Energy and Environment*, 3(6):540–560, 2014.

[22] Martin Miller and A Bazylak. A review of polymer electrolyte membrane fuel cell stack testing. *Journal of Power Sources*, 196(2):601–613, 2011.

[23] M Secanell, J Wishart, and P Dobson. Computational design and optimization of fuel cells and fuel cell systems: a review. *Journal of Power Sources*, 196(8):3690–3704, 2011.

[24] Yun Wang, Ken S Chen, Jeffrey Mishler, Sung Chan Cho, and Xavier Cordobes Adroher. A review of polymer electrolyte membrane fuel cells: technology, applications, and needs on fundamental research. *Applied Energy*, 88(4):981–1007, 2011.

[25] Eric D Wachsman and Kang Taek Lee. Lowering the temperature of solid oxide fuel cells. *Science*, 334(6058):935–939, 2011.

[26] Nima Shaigan, Wei Qu, Douglas G Ivey, and Weixing Chen. A review of recent progress in coatings, surface modifications and alloy developments for solid oxide fuel cell ferritic stainless steel interconnects. *Journal of Power Sources*, 195(6):1529–1542, 2010.

[27] Cheng-Chieh Chao, Ching-Mei Hsu, Yi Cui, and Fritz B Prinz. Improved solid oxide fuel cell performance with nanostructured electrolytes. *ACS nano*, 5(7):5692–5696, 2011.

[28] Sune Dalgaard Ebbesen, Søren Højgaard Jensen, Anne Hauch, and Mogens Bjerg Mogensen. High temperature electrolysis in alkaline cells, solid proton conducting cells, and solid oxide cells. *Chemical reviews*, 114(21):10697–10734, 2014.

[29] Sune Dalgaard Ebbesen, Jens Høgh, Karsten Agersted Nielsen, Jens Ulrik Nielsen, and Mogens Mogensen. Durable soc stacks for production of hydrogen and synthesis gas by high temperature electrolysis. *International Journal of Hydrogen Energy*, 36(13):7363–7373, 2011.

[30] SH Jensen and Mogens Bjerg Mogensen. Perspectives of high temperature electrolysis using soec. In *19th World Energy Congress 2004*, 2004.

[31] MA Laguna-Bercero. Recent advances in high temperature electrolysis using solid oxide fuel cells: A review. *Journal of Power Sources*, 203:4–16, 2012.

[32] JE OBrien. Thermodynamic considerations for thermal water splitting processes and high-temperature electrolysis. In *2008 ASME International Congress and Exposition, paper# IMECE2008-68880, Boston*, 2008.

[33] D Stolten, D Krieg, Detlef Stolten, and Thomas Grube. Alkaline electrolysis-introduction and overview. *Hydrogen and Fuel Cells-Fundamentals, Technologies and Applications. Editor: D Stolten. Wiley-VCH, Weinheim*, 2010.

[34] Lars Yde, Cecilia Kristin Kjartansdóttir, Frank Allebrod, Mogens Bjerg Mogensen, Per Møller, Lisbeth R Hilbert, Peter Tommy Nielsen, Troels Mathiesen, Jørgen Jensen, Lars Andersen, et al. 2nd generation alkaline electrolysis: Final report. Technical report, Århus University Business and Social Science–Centre for Energy Technologies, 2013.

[35] Kai Zeng and Dongke Zhang. Recent progress in alkaline water electrolysis for hydrogen production and applications. *Progress in Energy and Combustion Science*, 36(3):307–326, 2010.

[36] AS Arico, S Siracusano, N Briguglio, V Baglio, A Di Blasi, and V Antonucci. Polymer electrolyte membrane water electrolysis: status of technologies and potential applications in combination with renewable power sources. *Journal of Applied Electrochemistry*, 43(2):107–118, 2013.

[37] Hiroshi Ito, Tetsuhiko Maeda, Akihiro Nakano, and Hiroyasu Takenaka. Properties of nafion membranes under pem water electrolysis conditions. *international journal of hydrogen energy*, 36(17):10527–10540, 2011.

[38] Proton onsite, www.protonproton.com.

[39] Giner, inc., www.ginerinc.com.

[40] Hydrogenics, www.hydrogenics.com.

[41] Teledyne energy systems, inc. teledyneenergysystems.com.

[42] Office of energy efficiency & renewable energy, March 2015. URL `http://energy.gov/eere/fuelcells/`.

[43] Christopher Graves, Sune D Ebbesen, and Mogens Mogensen. Co-electrolysis of co 2 and h 2 o in solid oxide cells: performance and durability. *Solid State Ionics*, 192(1):398–403, 2011.

[44] Xiufu Sun, Ming Chen, Per Hjalmarsson, Sune Dalgaard Ebbesen, So?ren Ho?jgaard Jensen, Mogens Mogensen, and Peter Vang Hendriksen. Performance and durability of solid oxide electrolysis cells for syngas production. *ECS Transactions*, 41(33):77–85, 2012.

[45] Michael Keane, Manoj K Mahapatra, Atul Verma, and Prabhakar Singh. Lsm–ysz interactions and anode delamination in solid oxide electrolysis cells. *international journal of hydrogen energy*, 37(22):16776–16785, 2012.

[46] RK Akikur, R Saidur, HW Ping, and KR Ullah. Performance analysis of a cogeneration system using solar energy and sofc technology. *Energy Conversion and Management*, 79:415–430, 2014.

[47] Alexander Buttler, Roman Koltun, Romano Wolf, and Hartmut Spliethoff. A detailed techno-economic analysis of heat integration in high temperature electrolysis for efficient hydrogen production. *International Journal of Hydrogen Energy*, 40(1):38–50, 2015.

[48] Nguyen Q Minh. Development of reversible solid oxide fuel cells (rsofcs) and stacks. *ECS Transactions*, 35(1):2897–2904, 2011.

[49] Connor J Moyer, Neal P Sullivan, Huayang Zhu, and Robert J Kee. Polarization characteristics and chemistry in reversible tubular solid-oxide cells operating on mixtures of h2, co, h2o, and co2. *Journal of The Electrochemical Society*, 158(2):B117–B131, 2011.

[50] Nansheng Xu, Xue Li, Xuan Zhao, John B Goodenough, and Kevin Huang. A novel solid oxide redox flow battery for grid energy storage. *Energy Environ. Sci.*, 4(12): 4942–4946, 2011.

[51] Gareth A Hughes, Kyle Yakal-Kremski, Ann V Call, and Scott A Barnett. Durability testing of solid oxide cell electrodes with current switching. *Journal of The Electrochemical Society*, 159(12):F858–F863, 2012.

[52] K Choy, W Bai, S Charojrochkul, and BCH Steele. The development of intermediate-temperature solid oxide fuel cells for the next millennium. *Journal of Power Sources*, 71(1):361–369, 1998.

[53] John B Goodenough. Oxide-ion electrolytes. *Annual review of materials research*, 33 (1):91–128, 2003.

[54] Zhongliang Zhan, Da Han, Tianzhi Wu, Xiaofeng Ye, Shaorong Wang, Tinglian Wen, Sungmee Cho, and Scott A Barnett. A solid oxide cell yielding high power density below 600 c. *RSC Advances*, 2(10):4075–4078, 2012.

[55] James E O'Brien, Michael G McKellar, Carl M Stoots, J Stephen Herring, and Grant L Hawkes. Parametric study of large-scale production of syngas via high-temperature co-electrolysis. *International Journal of Hydrogen Energy*, 34(9):4216–4226, 2009.

[56] Xiufu Sun, Ming Chen, Søren Højgaard Jensen, Sune Dalgaard Ebbesen, Christopher Graves, and Mogens Mogensen. Thermodynamic analysis of synthetic hydrocarbon fuel production in pressurized solid oxide electrolysis cells. *international journal of hydrogen energy*, 37(22):17101–17110, 2012.

[57] Moritz Henke, Caroline Willich, Christina Westner, Florian Leucht, Robert Leibinger, Josef Kallo, and K Andreas Friedrich. Effect of pressure variation on power density and efficiency of solid oxide fuel cells. *Electrochimica Acta*, 66:158–163, 2012.

[58] Xiongwen Zhang, SH Chan, Guojun Li, HK Ho, Jun Li, and Zhenping Feng. A review of integration strategies for solid oxide fuel cells. *Journal of Power Sources*, 195(3): 685–702, 2010.

[59] Søren Højgaard Jensen, Xiufu Sun, Sune Dalgaard Ebbesen, Ruth Knibbe, and Mogens Mogensen. Hydrogen and synthetic fuel production using pressurized solid oxide electrolysis cells. *International journal of hydrogen energy*, 35(18):9544–9549, 2010.

[60] Gareth A Hughes, Kyle Yakal-Kremski, and Scott A Barnett. Life testing of lsm–ysz composite electrodes under reversing-current operation. *Phys. Chem. Chem. Phys.*, 15 (40):17257–17262, 2013.

[61] David J Bents. High temperature solid oxide regenerative fuel cell for solar photovoltaic energy storage. In *IECEC'87; Proceedings of the Twenty-second Intersociety Energy Conversion Engineering Conference*, volume 1, pages 808–817, 1987.

[62] WL Becker, RJ Braun, M Penev, and M Melaina. Design and technoeconomic performance analysis of a 1mw solid oxide fuel cell polygeneration system for combined production of heat, hydrogen, and power. *Journal of Power Sources*, 200:34–44, 2012.

[63] Thomas A Adams, Jake Nease, David Tucker, and Paul I Barton. Energy conversion with solid oxide fuel cell systems: a review of concepts and outlooks for the short-and long-term. *Industrial & Engineering Chemistry Research*, 52(9):3089–3111, 2012.

[64] Priscilla Caliandro, Laurence Tock, Adriano V Ensinas, and François Marechal. Thermo-economic optimization of a solid oxide fuel cell–gas turbine system fuelled with gasified lignocellulosic biomass. *Energy Conversion and Management*, 85:764–773, 2014.

[65] Marta Gandiglio, Andrea Lanzini, Pierluigi Leone, Massimo Santarelli, and Romano Borchiellini. Thermoeconomic analysis of large solid oxide fuel cell plants: Atmospheric vs. pressurized performance. *Energy*, 55:142–155, 2013.

[66] WL Becker, RJ Braun, M Penev, and M Melaina. Production of fischer–tropsch liquid fuels from high temperature solid oxide co-electrolysis units. *Energy*, 47(1):99–115, 2012.

[67] Jun Udagawa, P Aguiar, and NP Brandon. Hydrogen production through steam electrolysis: model-based dynamic behaviour of a cathode-supported intermediate temperature solid oxide electrolysis cell. *Journal of Power Sources*, 180(1):46–55, 2008.

[68] UB Pal and SC Singhal. Electrochemical vapor deposition of yttria-stabilized zirconia films. *Journal of the Electrochemical Society*, 137(9):2937–2941, 1990.

[69] M Brown, S Primdahl, and M Mogensen. Structure/performance relations for ni/yttria-stabilized zirconia anodes for solid oxide fuel cells. *Journal of the Electrochemical Society*, 147(2):475–485, 2000.

[70] Ho-Sung Noh, Kyung Joong Yoon, Byung-Kook Kim, Hae-June Je, Hae-Weon Lee, Jong-Ho Lee, and Ji-Won Son. The potential and challenges of thin-film electrolyte and nanostructured electrode for yttria-stabilized zirconia-base anode-supported solid oxide fuel cells. *Journal of Power Sources*, 247:105–111, 2014.

[71] Tatsumi Ishihara, Nitiphong Jirathiwathanakul, and Hao Zhong. Intermediate temperature solid oxide electrolysis cell using lagao 3 based perovskite electrolyte. *Energy & Environmental Science*, 3(5):665–672, 2010.

[72] JW Stevenson, TR Armstrong, DE McCready, LR Pederson, and WJ Weber. Processing and electrical properties of alkaline earth-doped lanthanum gallate. *Journal of the Electrochemical Society*, 144(10):3613–3620, 1997.

[73] Zhongliang Zhan, David M Bierschenk, J Scott Cronin, and Scott A Barnett. A reduced temperature solid oxide fuel cell with nanostructured anodes. *Energy & Environmental Science*, 4(10):3951–3954, 2011.

[74] Zhan Gao, Elizabeth C Miller, and Scott A Barnett. A high power density intermediate-temperature solid oxide fuel cell with thin (la0. 9sr0. 1) 0.98 (ga0. 8mg0. 2) o3-δ electrolyte and nano-scale anode. *Advanced Functional Materials*, 24(36):5703–5709, 2014.

[75] Nguyen Q Minh. Solid oxide fuel cell technologyfeatures and applications. *Solid State Ionics*, 174(1):271–277, 2004.

[76] Jim Eyer. Electric utility transmission and distribution upgrade deferral benefits from modular electricity storage. *Sandia National Laboratories, Albuquerque*, 2009.

[77] National renewable energy laboratory. (2012). renewable electricity futures study. hand, m.m.; baldwin, s.; demeo, e.; reilly, j.m.; mai, t.; arent, d.; porro, g.; meshek, m.; sandor, d. eds. 4 vols. nrel/tp-6a20-52409. golden, co: National renewable energy laboratory.

[78] TMI Mahlia, TJ Saktisahdan, A Jannifar, MH Hasan, and HSC Matseelar. A review of available methods and development on energy storage; technology update. *Renewable and Sustainable Energy Reviews*, 33:532–545, 2014.

[79] Martin Stotzer, Ines Hauer, Marc Richter, and Zbigniew A. Styczynski. Potential of demand side integration to maximize use of renewable energy sources in germany. *Applied Energy*, 146(0):344 – 352, 2015. ISSN 0306-2619. doi: http://dx.doi.org/10.1016/j.apenergy.2015.02.015.

[80] Sebastian Gottwalt, Wolfgang Ketter, Carsten Block, John Collins, and Christof Weinhardt. Demand side managementa simulation of household behavior under variable prices. *Energy Policy*, 39(12):8163–8174, 2011.

[81] Goran Strbac. Demand side management: Benefits and challenges. *Energy policy*, 36 (12):4419–4426, 2008.

[82] P Finn, C Fitzpatrick, and David Connolly. Demand side management of electric car charging: Benefits for consumer and grid. *Energy*, 42(1):358–363, 2012.

[83] Gregor P Henze, Clemens Felsmann, and Gottfried Knabe. Evaluation of optimal control for active and passive building thermal storage. *International Journal of Thermal Sciences*, 43(2):173–183, 2004.

[84] Yuan Tian and Chang-Ying Zhao. A review of solar collectors and thermal energy storage in solar thermal applications. *Applied Energy*, 104:538–553, 2013.

[85] Smart grid system resport. Technical report, Office of Electricity Delivery and Energy Reliability, US Department of Energy, 2009.

[86] S. Jensen. A novel method for electrochemical electricity storage utilizing underground storage of methane and carbon dioxide. *Submitted to Energy and Environmental Science*, 2015.

[87] Sune Dalgaard Ebbesen and Mogens Mogensen. Electrolysis of carbon dioxide in solid oxide electrolysis cells. *Journal of Power Sources*, 193(1):349–358, 2009.

[88] K Sasaki and Y Teraoka. Equilibria in fuel cell gases ii. the cho ternary diagrams. *Journal of The Electrochemical Society*, 150(7):A885–A888, 2003.

[89] GHJ Broers and BW Treijtel. Carbon deposition boundaries and other constant parameter curves, in the triangular representation of c? h? o equilibria, with applications to fuel cells. *Advanced Energy Conversion*, 5(4):365–382, 1965.

[90] EJ Cairns and AD Tevebaugh. Cho gas phase compositions in equilibrium with carbon, and carbon deposition boundaries at one atmosphere. *Journal of Chemical & Engineering Data*, 9(3):453–462, 1964.

[91] Engineering equation solver (v9.710), www.fchart.com/ees.

[92] P Kazempoor and RJ Braun. Model validation and performance analysis of regenerative solid oxide cells for energy storage applications: Reversible operation. *International Journal of Hydrogen Energy*, 39(11):5955–5971, 2014.

[93] Guobao Chen, Huamin Zhang, Jinbing Cheng, Yuanwei Ma, and Hexiang Zhong. A novel membrane electrode assembly for improving the efficiency of the unitized regenerative fuel cell. *Electrochemistry communications*, 10(9):1373–1376, 2008.

[94] Zhongliang Zhan, Worawarit Kobsiriphat, James R Wilson, Manoj Pillai, Ilwon Kim, and Scott A Barnett. Syngas production by coelectrolysis of co2/h2o: the basis for a renewable energy cycle. *Energy & Fuels*, 23(6):3089–3096, 2009.

[95] A. Monti. Methanation reactors in resoc systems for increased energy density. Master's thesis, Technica de Torino, 2015.

[96] Laurence O Williams. *Hydrogen power: an introduction to hydrogen energy and its applications.* Elsevier, 1980.

[97] JBS Haldane. Daedalus or science and the future. In *Kegan, Paul, Trench, Trubner and Company Ltd., London*, 1924.

[98] RA Erren and WH Campbell. Hydrogengen from off-peak power – a possible commercial fuel. *Chemical Trade Journal*, 92:238–239, 1933.

[99] H Dittmann and RW Schulte. Cell for storing electrical energy by electrolysis of water and for recovering the water by electrochemically recombining the hydrogen and oxygen formed by the electrolysis, 1970.

[100] H Niederreither. Method of producing, storing, and distributing electrical energy by operating gas batteries, particularly oxy-hydrogen gas batteries and electrolyzers, 1937.

[101] Eugene Findl, Harvey A Frank, Martin G Klein, and Bernard M Wilner. Electrolytically regenerative hydrogen-oxygen fuel cell, 1970.

[102] G Ross and WC Hall. Fuel cell, 1945.

[103] Alfred J Cavallo. Energy storage technologies for utility scale intermittent renewable energy systems. *Journal of solar energy engineering*, 123(4):387–389, 2001.

[104] A Doddathimmaiah and J Andrews. Theory, modelling and performance measurement of unitised regenerative fuel cells. *international journal of hydrogen energy*, 34(19): 8157–8170, 2009.

[105] E Varkaraki, N Lymberopoulos, E Zoulias, D Guichardot, and G Poli. Hydrogen-based uninterruptible power supply. *International journal of hydrogen energy*, 32(10): 1589–1596, 2007.

[106] Christopher P Garcia, Bei-jiann Chang, Donald W Johnson, David J Bents, Vincent J Scullin, Ian J Jakupca, Vincent J Scullin, and Ian J Jakupca. Round trip energy efficiency of nasa glenn regenerative fuel cell system. 2006.

[107] Sebastian Schiebahn, Thomas Grube, Martin Robinius, Vanessa Tietze, Bhunesh Kumar, and Detlef Stolten. Power to gas: Technological overview, systems analysis and economic assessment for a case study in germany. *International Journal of Hydrogen Energy*, 2015.

[108] MS Hsu. Solid oxide electrochemical energy converter, 1984.

[109] Robert J Braun, Robert J Kee, and Scott Barnett. High efficiency, reversible flow battery system for energy storage, January 28 2014. US Patent 8,637,197.

[110] Nigel Brandon, Anthony Kucernak, and Vladimir Yufit. Regenerative fuel cells, September 19 2011. US Patent App. 13/825,199.

[111] Gong Zhang and Arun KS Iyengar. High temperature fuel cell/electrolyzer system with energy storage media and auxiliaries outside the fuel cell power generator, February 18 2013. US Patent App. 13/769,610.

[112] James Frederick McElroy and John E Finn. Sorfc system and method with an exothermic net electrolysis reaction, April 10 2007. US Patent 7,201,979.

[113] KR Sridhar and Matthias Gottmann. Combined energy storage and fuel generation with reversible fuel cells, April 29 2008. US Patent 7,364,810.

[114] Jie Guan, Badri Ramamurthi, Jim Ruud, Jinki Hong, Patrick Riley, and Nguyen Minh. High performance flexible reversible solid oxide fuel cell. *GE Global Research Center Final Report for DOE Cooperative Agreement DE-FC36-04GO-14351*, 2006.

[115] James F McElroy, Darren B Hickey, and Fred Mitlitsky. Optimization and demonstration of a solid oxide regenerative fuel cell system. Technical report, Ion America Corporation, 2004.

[116] David M Bierschenk, James R Wilson, and Scott A Barnett. High efficiency electrical energy storage using a methane–oxygen solid oxide cell. *Energy & Environmental Science*, 4(3):944–951, 2011.

[117] Jiancong Ren, Stephen R Gamble, AJ Roscoe, John TS Irvine, and Graeme Burt. Modeling a reversible solid oxide fuel cell as a storage device within ac power networks. *Fuel Cells*, 12(5):773–786, 2012.

[118] Masahiro Shiraki, Hisataka Yakabe, and Hiroyuki Uchida. Efficiency calculations for sofc/soec reversible system and evaluations of performances of button-size anode-supported cell. *ECS Transactions*, 57(1):3261–3267, 2013.

[119] Easa I Al-Musleh, Dharik S Mallapragada, and Rakesh Agrawal. Continuous power supply from a baseload renewable power plant. *Applied Energy*, 122:83–93, 2014.

[120] Hanaâ Er-rbib and Chakib Bouallou. Modeling and simulation of co methanation process for renewable electricity storage. *Energy*, 75:81–88, 2014.

[121] Xuan Zhao, Yunhui Gong, Xue Li, Nansheng Xu, and Kevin Huang. Cyclic durability of a solid oxide fe-air redox battery operated at 650 c. *Journal of The Electrochemical Society*, 160(10):A1716–A1719, 2013.

[122] Xuan Zhao, Yunhui Gong, Xue Li, Nansheng Xu, and Kevin Huang. Performance of solid oxide iron-air battery operated at 550 c. *Journal of The Electrochemical Society*, 160(8):A1241–A1247, 2013.

[123] Xuan Zhao, Nansheng Xu, Xue Li, Yunhui Gong, and Kevin Huang. Energy storage characteristics of a new rechargeable solid oxide iron–air battery. *RSC Advances*, 2 (27):10163–10166, 2012.

[124] Meng Guo, Xuan Zhao, Ralph E White, and Kevin Huang. A multi-physics model for solid oxide iron-air redox flow battery: Simulation of discharge behavior at high current density. *Journal of The Electrochemical Society*, 160(11):A2085–A2092, 2013.

[125] Xiaoyu Zhang, James E O'Brien, Robert C O'Brien, and Gregory K Housley. Durability evaluation of reversible solid oxide cells. *Journal of Power Sources*, 242:566–574, 2013.

[126] Gareth Allen Hughes. *Improving the Efficiency and Durability of Reversible Solid Oxide Cells for Energy Storage*. PhD thesis, NORTHWESTERN UNIVERSITY, 2014.

[127] Karen Wonsyld, Lone Bech, Jens Ulrik Nielsen, and Claus Friis Pedersen. Operational robustness studies of solid oxide electrolysis stacks. *Journal of Energy and Power Engineering*, 9:128–140, 2015.

[128] Daniel JL Brett, Alan Atkinson, Nigel P Brandon, and Stephen J Skinner. Intermediate temperature solid oxide fuel cells. *Chemical Society Reviews*, 37(8):1568–1578, 2008.

[129] Zongping Shao, Wei Zhou, and Zhonghua Zhu. Advanced synthesis of materials for intermediate-temperature solid oxide fuel cells. *Progress in Materials Science*, 57(4): 804–874, 2012.

[130] Jianbing Huang, Fucheng Xie, Cheng Wang, and Zongqiang Mao. Development of solid oxide fuel cell materials for intermediate-to-low temperature operation. *international journal of hydrogen energy*, 37(1):877–883, 2012.

[131] Jing Di, Mingming Chen, Chengyang Wang, Jiaming Zheng, Liangdong Fan, and Bin Zhu. Samarium doped ceria–(li/na) 2 co 3 composite electrolyte and its electrochemical properties in low temperature solid oxide fuel cell. *Journal of Power Sources*, 195(15): 4695–4699, 2010.

[132] Zuo Ning, Zhang Milin, Xie Fucheng, Wang Cheng, Liu Zhixiang, and Mao Zongqiang. Fabrication and characterization of anode support low-temperature solid oxide fuel cell based on the samaria-doped ceria electrolyte. *International Journal of Hydrogen Energy*, 37(1):797–801, 2012.

[133] MA Laguna-Bercero, SJ Skinner, and JA Kilner. Performance of solid oxide electrolysis cells based on scandia stabilised zirconia. *Journal of Power Sources*, 192(1):126–131, 2009.

[134] S Hashimoto, H Nishino, Y Liu, K Asano, M Mori, Y Funahashi, and Y Fujishiro. Effects of pressurization on cell performance of a microtubular sofc with sc-doped zirconia electrolyte. *Journal of the Electrochemical Society*, 155(6):B587–B591, 2008.

[135] Kurtis P Recknagle, Emily M Ryan, Brian J Koeppel, Lenna A Mahoney, and Moe A Khaleel. Modeling of electrochemistry and steam–methane reforming performance for simulating pressurized solid oxide fuel cell stacks. *Journal of Power Sources*, 195(19): 6637–6644, 2010.

[136] Stephanie Seidler, Moritz Henke, Josef Kallo, Wolfgang G Bessler, Uwe Maier, and K Andreas Friedrich. Pressurized solid oxide fuel cells: experimental studies and modeling. *Journal of Power Sources*, 196(17):7195–7202, 2011.

[137] Li Zhou, Mojie Cheng, Baolian Yi, Yonglai Dong, You Cong, and Weishen Yang. Performance of an anode-supported tubular solid oxide fuel cell (sofc) under pressurized conditions. *Electrochimica Acta*, 53(16):5195–5198, 2008.

[138] M Henke, J Kallo, KA Friedrich, and WG Bessler. Influence of pressurisation on sofc performance and durability: a theoretical study. *Fuel Cells*, 11(4):581–591, 2011.

[139] Devin Todd, Maximilian Schwager, and Walter Mérida. Thermodynamics of high-temperature, high-pressure water electrolysis. *Journal of Power Sources*, 269:424–429, 2014.

[140] Zhenwei Wang, Masashi Mori, and Takuto Araki. Steam electrolysis performance of intermediate-temperature solid oxide electrolysis cell and efficiency of hydrogen production system at 300 nm 3 h- 1. *international journal of hydrogen energy*, 35(10): 4451–4458, 2010.

[141] Sriram Gopalan, Mohsen Mosleh, Joseph J Hartvigsen, and Robert D McConnell. Analysis of self-sustaining recuperative solid oxide electrolysis systems. *Journal of Power Sources*, 185(2):1328–1333, 2008.

[142] Christopher Graves, Sune D Ebbesen, Mogens Mogensen, and Klaus S Lackner. Sustainable hydrocarbon fuels by recycling co 2 and h 2 o with renewable or nuclear energy. *Renewable and Sustainable Energy Reviews*, 15(1):1–23, 2011.

[143] P Kazempoor and RJ Braun. Model validation and performance analysis of regenerative solid oxide cells: Electrolytic operation. *International Journal of Hydrogen Energy*, 39(6):2669–2684, 2014.

[144] K Eguchi, H Kojo, T Takeguchi, R Kikuchi, and K Sasaki. Fuel flexibility in power generation by solid oxide fuel cells. *Solid State Ionics*, 152:411–416, 2002.

[145] K Sasaki and Y Teraoka. Equilibria in fuel cell gases i. equilibrium compositions and reforming conditions. *Journal of The Electrochemical Society*, 150(7):A878–A884, 2003.

[146] CH Wendel, Z Gao, SA Barnett, and RJ Braun. Modeling and experimental performance of an intermediate temperature reversible solid oxide cell for high-efficiency, distributed-scale electrical energy storage. *Journal of power sources, in press*, 2015.

[147] Patricia Aguiar, CS Adjiman, and Nigel P Brandon. Anode-supported intermediate temperature direct internal reforming solid oxide fuel cell. i: model-based steady-state performance. *Journal of Power Sources*, 138(1):120–136, 2004.

[148] RJ Braun, SA Klein, and DT Reindl. Evaluation of system configurations for solid oxide fuel cell-based micro-combined heat and power generators in residential applications. *Journal of Power Sources*, 158(2):1290–1305, 2006.

[149] J Udagawa, P Aguiar, and NP Brandon. Hydrogen production through steam electrolysis: Model-based steady state performance of a cathode-supported intermediate temperature solid oxide electrolysis cell. *Journal of Power Sources*, 166(1):127–136, 2007.

[150] EC Miller, Z Gao, and SA Barnett. Fabrication of solid oxide fuel cells with a thin (la0. 9sr0. 1) 0.98 (ga0. 8mg0. 2) o3–δ electrolyte on a sr0. 8la0. 2tio3 support. *Fuel Cells*, 13(6):1060–1067, 2013.

[151] Feng Zhao and Anil V Virkar. Dependence of polarization in anode-supported solid oxide fuel cells on various cell parameters. *Journal of power sources*, 141(1):79–95, 2005.

[152] Huayang Zhu and Robert J Kee. A general mathematical model for analyzing the performance of fuel-cell membrane-electrode assemblies. *Journal of Power Sources*, 117(1):61–74, 2003.

[153] H Timmermann, W Sawady, R Reimert, and E Ivers-Tiffée. Kinetics of (reversible) internal reforming of methane in solid oxide fuel cells under stationary and apu conditions. *Journal of Power Sources*, 195(1):214–222, 2010.

[154] N Liu, M Shi, C Wang, YP Yuan, P Majewski, and F Aldinger. Microstructure and ionic conductivity of sr-and mg-doped lagao3. *Journal of materials science*, 41(13): 4205–4213, 2006.

[155] Olga A Marina, Nathan L Canfield, and Jeff W Stevenson. Thermal, electrical, and electrocatalytical properties of lanthanum-doped strontium titanate. *Solid State Ionics*, 149(1):21–28, 2002.

[156] S Hashimoto, L Kindermann, PH Larsen, FW Poulsen, and M Mogensen. Conductivity and expansion at high temperature in sr0. 7la0. 3tio3- α prepared under reducing atmosphere. *Journal of electroceramics*, 16(2):103–107, 2006.

[157] IA Raj, AS Nesaraj, M Kumar, F Tietz, HP Buchkremer, and D Stöver. On the suitability of la0. 60sr0. 40co0. 20fe0. 80o3 cathode for the intermediate temperature solid oxide fuel cell (itsofc). *J. New Mater. Electrochem. Syst*, 7(2):145–151, 2004.

[158] Ryan P O'Hayre, Suk-Won Cha, Whitney Colella, and Fritz B Prinz. *Fuel cell fundamentals*. John Wiley & Sons New York, 2006.

[159] E Achenbach. Three-dimensional and time-dependent simulation of a planar solid oxide fuel cell stack. *Journal of Power Sources*, 49(1):333–348, 1994.

[160] P Kazempoor, V Dorer, and F Ommi. Modelling and performance evaluation of solid oxide fuel cell for building integrated co-and polygeneration. *Fuel Cells*, 10(6):1074–1094, 2010.

[161] S Campanari and P Iora. Definition and sensitivity analysis of a finite volume sofc model for a tubular cell geometry. *Journal of Power Sources*, 132(1):113–126, 2004.

[162] Xuejiao Liu, Xie Meng, Da Han, Hao Wu, Fanrong Zeng, and Zhongliang Zhan. Impregnated nickel anodes for reduced-temperature solid oxide fuel cells based on thin electrolytes of doped lagao 3. *Journal of Power Sources*, 222:92–96, 2013.

[163] Daniel Marinha, Laurent Dessemond, and Elisabeth Djurado. Electrochemical investigation of oxygen reduction reaction on la 0.6 sr 0.4 co 0.2 fe 0.8 o 3- δ cathodes deposited by electrostatic spray deposition. *Journal of Power Sources*, 197:80–87, 2012.

[164] Jan Pawel Stempien, Meng Ni, Qiang Sun, and Siew Hwa Chan. Thermodynamic analysis of combined solid oxide electrolyzer and fischer–tropsch processes. *Energy*, 2015.

[165] J Aicart, M Petitjean, J Laurencin, L Tallobre, and L Dessemond. Accurate predictions of h 2 o and co 2 co-electrolysis outlet compositions in operation. *International Journal of Hydrogen Energy*, 40(8):3134–3148, 2015.

[166] Frank P Incropera. *Fundamentals of heat and mass transfer*. John Wiley & Sons, 2011.

[167] Bruce E Poling, John M Prausnitz, and John P O'connell. *The properties of gases and liquids*, volume 5. McGraw-Hill New York, 2001.

[168] Process systems enterprise, gproms, http://www.psenterprise.com/gproms.html.

[169] Ming Chen, Jens Valdemar Thorvald Høgh, Jens Ulrik Nielsen, Janet Jonna Bentzen, Sune Dalgaard Ebbesen, and Peter Vang Hendriksen. High temperature co-electrolysis of steam and co2 in an soc stack: Performance and durability. *Fuel Cells*, 13(4):638–645, 2013.

[170] RG Cunningham and RJ Dopkin. Jet breakup and mixing throat lengths for the liquid jet gas pump. *Journal of fluids engineering*, 96(3):216–226, 1974.

[171] Robert J Braun. *Optimal Design and Operation of Solid Oxide Fuel Cell Systems for Small-scale Stationary Applications*. PhD thesis, University of Wisconsin-Madison, 2002.

[172] Yu Luo, Yixiang Shi, Wenying Li, and Ningsheng Cai. Comprehensive modeling of tubular solid oxide electrolysis cell for co-electrolysis of steam and carbon dioxide. *Energy*, 70:420–434, 2014.

[173] Air squared, inc. http://airsquared.com/. Accessed: 2015-02-13.

[174] C Wendel and R Braun. Modeling and design of a novel solid oxide flow battery system for grid-energy storage. In *10th European SOFC Form*, pages 80–90, 2012.

[175] Toshio Suzuki, Toshiaki Yamaguchi, Koichi Hamamoto, Yoshinobu Fujishiro, Masanobu Awano, and Nigel Sammes. A functional layer for direct use of hydrocarbon fuel in low temperature solid-oxide fuel cells. *Energy Environ. Sci.*, 4(3):940–943, 2011.

[176] N. Christiansen. Development of next generation metal based sofc technology. EU FP7211940, 2012.

[177] Arata Nakajo, Fabian Mueller, Jacob Brouwer, Daniel Favrat, et al. Mechanical reliability and durability of sofc stacks. part i: Modelling of the effect of operating conditions and design alternatives on the reliability. *international journal of hydrogen energy*, 37(11):9249–9268, 2012.

[178] Klaus D Timmerhaus, Max S Peters, and RE West. Plant design and economics for chemical engineers. *Chemical Engineering Series*, 1991.

[179] Us consumer price index, 2015. URL `www.inflationdata.com`.

[180] J. Thijssen. The impact of scale-up and production volume on sofc manufacturing cost. Technical report, National Energy Technology Laboratory, 2007.

[181] Integrated gasification fuel cell performance and cost assessment. Technical report, National Energy Technology Laboratory, US DOE, 2009.

[182] Joshua Warren, Sujit Das, and Wei Zhang. Manufacturing process modeling of 100-400 kwe combined heat and power stationary fuel cell systems. In *ASME 2012 10th International Conference on Fuel Cell Science, Engineering and Technology collocated with the ASME 2012 6th International Conference on Energy Sustainability*, pages 25–34. American Society of Mechanical Engineers, 2012.

[183] Cost and performance baseline for fossil energy plants. Technical report, National Energy Technology Laboratory, US DOE, 2007.

[184] Quality guidelines for energy system studies: Capital cost scaling methodology. Technical report, National Energy Technology Laboratory, 2013.

[185] A.H. Pedersen. Evaluation of underground storage of co2, o2, and h2. Technical report, DONG Energy A/S, 2013.

[186] Donald L Katz, M Rasin Tek, et al. Overview on underground storage of natural gas. *Journal of Petroleum Technology*, 33(06):943–951, 1981.

[187] Carbon capture and sequestration systems analysis guidelines. Technical report, National Energy Technology Laboratory, US DOE, 2009.

[188] Thomas Schmidt, Dirk Mangold, A Sorensen, and Niels From. Large-scale heat storage. In *IRES 2011 6th International Renewable Energy Storage Conference, Eurosolar, Berlin, Germany*, 2011.

[189] Brian D James, Andrew B Spisak, and Whitney G Colella. Manufacturing cost analysis of stationary fuel cell systems. *Strategic Analysis Inc. Arlington VA, September*, 2012.

[190] Don W Green et al. Perrys chemical engineers handbook. *McGrawHill, New York*, 2, 2008.

[191] Ali Shirazi, Mehdi Aminyavari, Behzad Najafi, Fabio Rinaldi, and Majid Razaghi. Thermal–economic–environmental analysis and multi-objective optimization of an internal-reforming solid oxide fuel cell–gas turbine hybrid system. *international journal of hydrogen energy*, 37(24):19111–19124, 2012.

[192] Robert F Boehm. *Design analysis of thermal systems.* Wiley New York, 1987.

[193] Tage Petersen, Brian Elmegaard, and Allan Schrøder Pedersen. Adiabatic liquid piston compressed air energy storage. Technical report, Danish Technological Institute, 2013.